TECHNICAL REPORT STANDARD TITLE PAGE

1. Report No. FHWA/RD-86/164	2. Government Accession No.	3. PB87-212783
4. Title and Subtitle ROLLOVER POTENTIAL OF VEHICLES ON EMBANKMENTS, SIDESLOPES AND OTHER ROADSIDE FEATURES.		5. Report Date August 1986
		6. Performing Organization Code Y10
7. Author(s) N.J. DeLeys and L.O. Parada		8. Performing Organization Report No. 7204-2
9. Performing Organization Name and Address Calspan Corporation P.O. Box 400 Buffalo, N.Y. 14225		10. Work Unit No. FCP
		11. Contract or Grant No. DTFH61-83-C-00060
12. Sponsoring Agency Name and Address Office of Safety and Traffic Operations R&D Federal Highway Administration U.S. Department of Transportation 6300 Georgetown Pike McLean, Virginia 22101		13. Type of Report and Period Covered Final Report September 1983-August 1986
		14. Sponsoring Agency Code

15. Supplementary Notes
FHWA COTR: C.P. Brinkman (HSR-30)

16. Abstract

The objective of this research program was to study the interaction of vehicles with various roadside features to determine critical roadside-feature design criteria based on the potential for inducing vehicle rollover. Results of a review of accident data analyses reported in the literature are presented to indicate the general state of knowledge of rollover accidents. Among the findings are that: (1) different classes of vehicles based on use and/or size exhibit distinct differences in rollover tendencies, and (2) the existing accident data base lacks the information necessary to define the roadside-feature geometry and other conditions that caused vehicle rollover. Full-scale tests with an instrumented automobile were performed to verify the HVOSM (Highway-Vehicle-Object Simulation Model) as modified to improve its utility for studying vehicle off-road traversals. The HVOSM was then used to predict the dynamic responses of representative small and large cars encountering different roadside-feature configurations, including both tracking and nontracking departures from the roadway. It is concluded that the side-slope of fill embankments should be no steeper than 3:1, and preferably flatter, for fill heights greater than 3 ft (0.9 m) to reduce the likelihood of small-car-rollover. It is recommended that consideration be given to revising the present AASHTO design criteria for barrier warrants accordingly. It is also shown that the rounding of slope breaks currently recommended by AASHTO further reduces the rollover hazard.

17. Key Words HVOSM, Computer Simulation, Rollover Accidents, Roadside-Feature Design, Highway Safety	18. Distribution Statement No original distribution by the sponsoring agency. This document is available to the public only through the National Technical Information Service, Springfield, Virginia 22161.

19. Security Classif. (of this report)	20. Security Classif. (of this page)	21. No. of Pages	22. Price
Unclassified	Unclassified	246	

Form DOT F 1700.7 (8-69)

METRIC (SI*) CONVERSION FACTORS

APPROXIMATE CONVERSIONS TO SI UNITS

Symbol	When You Know	Multiply By	To Find	Symbol
		LENGTH		
in	inches	2.54	millimetres	mm
ft	feet	0.3048	metres	m
yd	yards	0.914	metres	m
mi	miles	1.61	kilometres	km
		AREA		
in^2	square inches	645.2	millimetres squared	mm^2
ft^2	square feet	0.0929	metres squared	m^2
yd^2	square yards	0.836	metres squared	m^2
mi^2	square miles	2.59	kilometres squared	km^2
ac	acres	0.395	hectares	ha
		MASS (weight)		
oz	ounces	28.35	grams	g
lb	pounds	0.454	kilograms	kg
T	short tons (2000 lb)	0.907	megagrams	Mg
		VOLUME		
fl oz	fluid ounces	29.57	millilitres	mL
gal	gallons	3.785	litres	L
ft^3	cubic feet	0.0328	metres cubed	m^3
yd^3	cubic yards	0.0765	metres cubed	m^3

NOTE: Volumes greater than 1000 L shall be shown in m^3.

TEMPERATURE (exact)

Symbol	When You Know	Multiply By	To Find	Symbol
°F	Fahrenheit temperature	5/9 (after subtracting 32)	Celsius temperature	°C

* SI is the symbol for the International System of Measurements

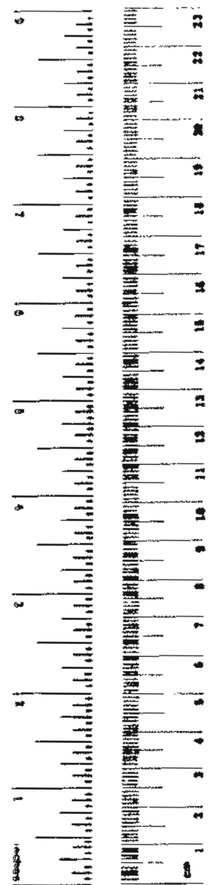

APPROXIMATE CONVERSIONS TO SI UNITS

Symbol	When You Know	Multiply By	To Find	Symbol
		LENGTH		
mm	millimetres	0.039	inches	in
m	metres	3.28	feet	ft
m	metres	1.09	yards	yd
km	kilometres	0.621	miles	mi
		AREA		
mm^2	millimetres squared	0.0016	square inches	in^2
m^2	metres squared	10.764	square feet	ft^2
km^2	kilometres squared	0.39	square miles	mi^2
ha	hectores (10 000 m^2)	2.53	acres	ac
		MASS (weight)		
g	grams	0.0353	ounces	oz
kg	kilograms	2.205	pounds	lb
Mg	megagrams (1 000 kg)	1.103	short tons	T
		VOLUME		
mL	millilitres	0.034	fluid ounces	fl oz
L	litres	0.264	gallons	gal
m^3	metres cubed	35.315	cubic feet	ft^3
m^3	metres cubed	1.308	cubic yards	yd^3

TEMPERATURE (exact)

Symbol	When You Know	Multiply By	To Find	Symbol
°C	Celsius temperature	9/5 (then add 32)	Fahrenheit temperature	°F

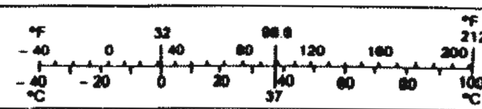

These factors conform to the requirement of FHWA Order 5190.1A.

TABLE OF CONTENTS

TABLE OF CONTENTS (cont.)

LIST OF ILLUSTRATIONS

LIST OF ILLUSTRATIONS (cont.)

LIST OF ILLUSTRATIONS (cont.)

LIST OF TABLES

LIST OF TABLES (cont.)

LIST OF TABLES (cont.)

Section 1
INTRODUCTION

PURPOSE AND SCOPE OF PROGRAM

Accident studies have revealed that rollover of vehicles that accidentally leave the roadway is not only a frequent event, particularly in single-vehicle accidents, but also the most hazardous in terms of the frequency and severity of injuries to vehicle occupants. In addition, these studies show that small, lightweight automobiles are more prone to overturn in an accident than are large, heavy cars. In view of these facts, the trend toward increasing use of small, lightweight vehicles in recent years gives rise to concerns regarding whether the existing guidelines for the design of roadside features are appropriate or require modification to reduce the rollover potential of these newer-type vehicles during encroachments on the roadside.

The objective of this research program was to study the interaction of vehicles with various roadside features to determine critical roadside-feature design criteria based on the potential for inducing vehicle rollover. The HVOSM (Highway-Vehicle-Object Simulation Model) computer program was used to determine the dynamic responses of representative small and large cars traversing various sideslope, fill-embankment, and ditch configurations. Both tracking and nontracking departures from the roadway were simulated. Prior to the simulation study, full-scale tests with an instrumented Volkswagen Rabbit automobile were performed to verify the HVOSM, which had been modified to incorporate several revisions and extensions developed by McHenry Consultants, Inc. (MCI) to improve the application of HVOSM to rollover situations.

CONTENT AND ORGANIZATION OF REPORT

This report consists of six principal sections and three appendices. The background of the rollover problem is discussed in Section 2, which contains results of a reveiw of the literature to obtain data and information useful to the present study. Section 3 describes modifications and extensions developed by MCI which were implemented in a special version of the HVOSM. Several of the extensions to the model were not used in this study; however, brief descriptions of them are included for completeness. Section 4 contains descriptions of the full-scale tests performed and the results of simulations of the tests to assess the accuracy of the model predictions. The methodology and results of the HVOSM simulations of vehicles traversing roadside features is discussed in Section 5. Conclusions and recommendations based on the findings of the study are given in Section 6.

Appendix A presents the HVOSM input data sets used to simulate each of the full-scale tests described in Section 4. Instructions for supplying input to the modified computer program are given in Appendix B, which shows the data that must be provided in the various fields of each data card. Appendix C provides a functional description of the HVOSM extensions.

Section 2

LITERATURE REVIEW AND ACCIDENT DATA ANALYSIS

SUMMARY

This section provides information pertaining to vehicle rollover accidents gathered from a review and analysis of existing literature and available data. The overall objective of this task was to determine the general state of knowledge of rollover accidents, particularly with regard to the frequency of occurrence for various classes of vehicles, the severity of such accidents in producing injuries to the vehicle occupants, and the identification of possible causative factors related to roadside features encountered by the vehicles as well as conditions at which vehicles depart from the roadway.

The search for literature dealing with rollover accidents revealed a relatively large number of potential information sources. However, many of the documents examined were found to contain little or no information useful to this study. During the course of the study, it also became clear that certain types of information sought either were nôt available or would be difficult to extract from existing accident data files. Hence, little attempt was made to generate new information from further analysis of the data files beyond that already reported in the literature, since such attempts were deemed unlikely to prove very worthwhile.

The information presented herein was obtained from the documents referenced and is divided into five main subject areas, or subsections: (1) vehicle classifications, (2) frequency of rollover accidents, (3) vehicle roadway-departure conditions, (4) occupant-injury frequency and severity, and (5) roadside features (those involved in rollover, and non-rollover, accidents). The section concludes with a discussion of the principal findings of the task.

VEHICLE CLASSIFICATIONS

The tendency of a vehicle to overturn is affected by numerous characteristics of the vehicle design, including the height of the center of gravity, wheel tread, moment of inertia, properties of the tires and suspension, etc. Because these characteristics vary widely within and among all types of vehicles, there is no single theoretically relevant variable or combinations of such variables that can be simply and reliably used to classify vehicles according to their different rollover propensities.

The review of the literature showed that classifications based on vehicle use and/or size have exhibited distinct differences among classes in their rollover rates. Classifications mainly used to group vehicles by type or use include passenger cars, pickup trucks, utility vehicles, vans, and light and heavy trucks. Passenger cars in particular are often further subdivided by weight ranges or by the size categories described as subcompact, compact, intermediate, and full-size automobiles. A major drawback of using "subcompact," "compact," etc., for classifying cars is the lack of adequate definitions of such terms. Indeed, since the advent of "down sizing" of automobiles in recent years, the meaning has changed, so, for example, a car now described as "full size" may well correspond in actual size (or weight) to one that formerly was considered an "intermediate" size. To provide a frame of reference, the approximate wheelbases corresponding to these size classifications, as given by the Motor Vehicle Manufacturers Association (MVMA) for cars manufactured in the early 1970s, are listed in Table 1[1]. Also shown in Table 1 are the values of the estimated average weight of vehicles in each category as determined in a study of the relationship between accident involvement rate and car size reported by Evans.[2]

---

1. "1975 Model Year Passenger Car and Truck Accident Investigations Manual," Motor Vehicle Manufacturers Association of the United States, Inc.
2. Evans, Leonard, "Accident Involvement Rate and Car Size," General Motors Research Laboratories, Report No. GMR-4453, August 1, 1983.

Table 1. Size/wheelbase/weight relationships for vehicles manufactured in early 1970s.[1,2]

Size classification	Approximate wheelbase range, in.	Estimated average weight, lb
Subcompact	94 to 101	1,998
Compact	102 to 111	2,796
Intermediate	112 to 118	3,510
Standard (Full-Size)	119 or over	4,324

1 in. = 2.54 cm
1 lb = 0.4535 kg

Toward the objective of further identifying appropriate vehicle classes for differentiating among vehicles in their tendency to roll over, an analysis was made to determine if the weight of passenger cars is highly correlated with other design variables that might be more directly related to rollover propensity but for which information is not available in the automated accident data files. Variables considered for which data were readily available include:

(1) Tread (track) width -- The ratio of this variable to CG height is theoretically related to vehicle static roll stability. Since limited data indicate rather little variation among automobiles in their CG heights, track width was expected to have a strong relation to rollover tendencies.

(2) Wheelbase -- This variable was thought possibly related to tendencies for control loss and, thus, indirectly to rollover tendencies.

(3) Overall height -- This variable is probably correlated with CG height and, thus, to rollover tendencies.

(4) Curb weight -- This variable would relate to rollover tendencies through its relation to roll moment of inertia and to the energy required to produce rollover.

All four variables were expected to intercorrelate through the common dimension of vehicle size. To examine their correlations, a systematic sample of vehicle makes and models was drawn from MVMA listings of 1980 passenger cars. The sample included all major models of all U.S. manufacturers plus the major imported cars. Care was taken to avoid inclusion of two models of a manufacturer when those models were identical on the variables examined.

The intercorrelations among the variables are shown in Figure 1. It can be seen that wheelbase, average tread width, and curb weight are highly interrelated, especially among the American cars. Overall height is related to the other variables, but to a lesser degree. It can also be seen that the intercorrelations are generally greater among American cars than among the foreign ones. From these results, it may be concluded that classes based on wheelbase, average tread width, or curb weight would be very similar. Consequently, one would expect that rollover rates of passenger cars would correlate about equally well with any of these classificatory variables, in terms of both dispersion (i.e., the difference in rollover rates between the classes with the highest and lowest rates, which is a measure of the classification's ability to distinguish vehicles with the greatest and least rollover propensity) and the degree of monotonicity as indicated by the rank-order correlation between the levels of the classificatory variable and the rollover rates of the classes.

FREQUENCY OF ROLLOVER ACCIDENTS

Overview of Independent Analyses

Several reports examined contain information on the frequency of rollover accidents determined from analyses of various accident data files, such as the National Accident Sampling System (NASS), the National Crash Severity Study (NCSS), the Fatal Accident Reporting System (FARS), and accident data records maintained by different states. Although not always directly comparable because of differences in case selection criteria and the methods of classifying vehicles, the results of these studies all show that the frequency of rollover varies considerably for different vehicle types.

The available data indicate that rollover is an event mainly associated with single-vehicle accidents (SVAs). For example, from analysis of over 2300 single-vehicle and multiple-vehicle accidents of passenger cars in a Collision

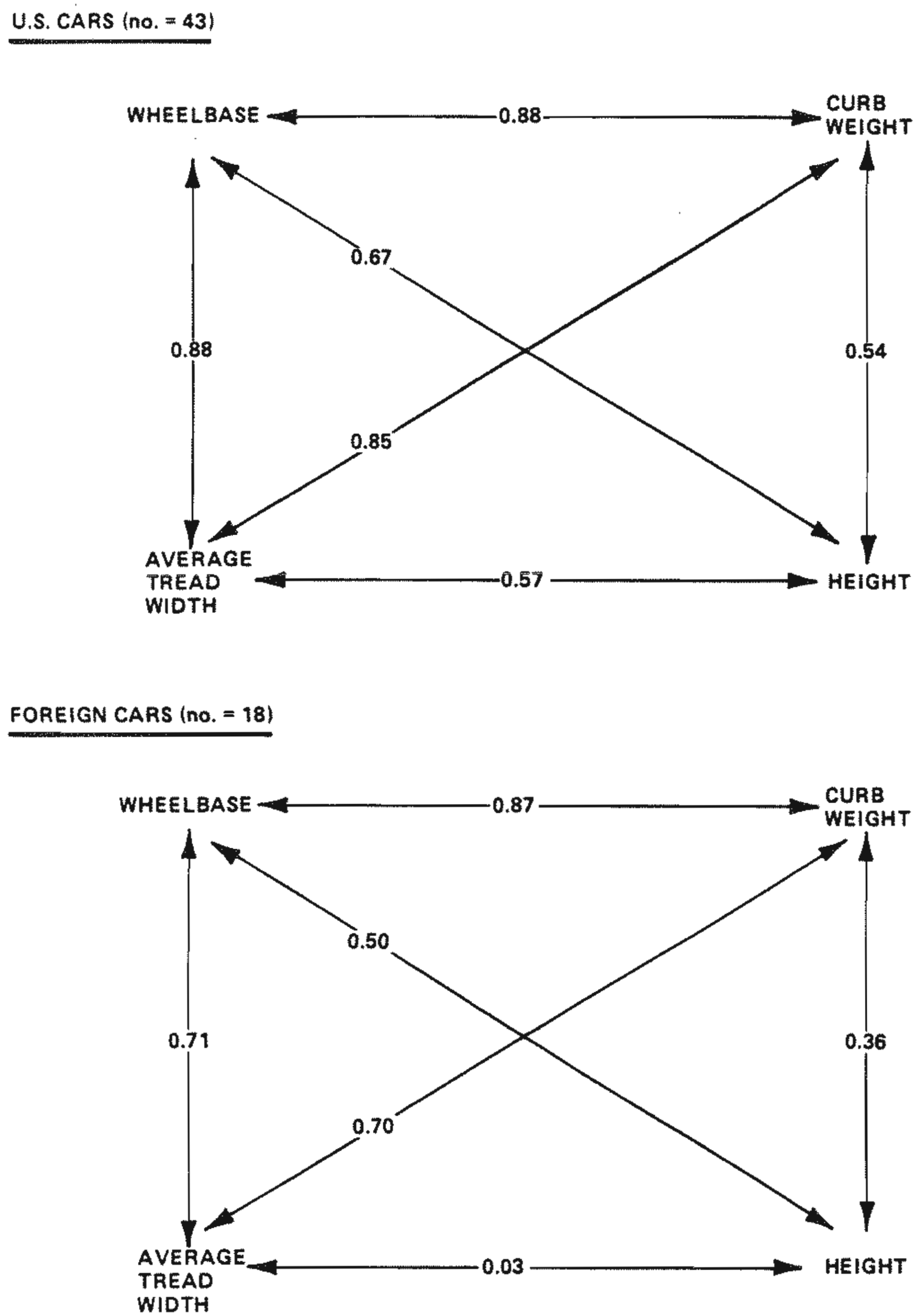

Figure 1. Correlations among key vehicle variables for 1980 model year passenger cars.

Performance and Injury Report (CPIR) file at the University of Michigan, Huelke et al.[3] determined that : (1) nearly 29% of all accidents in the sample were SVAs, (2) about 10% of all accidents involved rollover, (3) rollover occurred in 29% of the SVAs, compared to only 3% of the multiple-vehicle accidents, and (4) 79% of all rollover accidents were SVAs. The latter value is slightly lower than the finding of McGuigan and Bondy,[4] who reported that 87.5% of the rollover accidents on the NCSS post-March 1978 file are SVAs. Results from a study of accidents occurring in North Carolina during 1973 to 1978 reported by Reinfurt et al.[5] also show that the percentages of rollovers in single-vehicle crashes were much higher than in multiple-vehicle crashes. Their data indicate that the rollover frequency of passenger cars and pickup trucks was 60 times greater in single-vehicle accidents than in multiple-vehicle crashes, and 20 times greater for utility vehicles. Similar large differences between the rollover frequencies for the two types of accidents were found in the study performed by Snyder et al.[6]

Results obtained by different researchers who determined the rollover (R.O.) frequencies of different classes of vehicles from analyses of various accident data files are presented separately in Tables 2 through 8. In comparing these results, it is important to bear in mind that rollover frequency values vary, depending on the accident data base. For example, the rollover rate for a given vehicle class expressed as a percentage of all accidents is considerably different (lower) than when computed on the basis of, for example, only single-vehicle accidents (SVAs), or perhaps only single-vehicle fatal crashes. Note also that several of the analyses considered only

---

3. Huelke, Donald F., Marsh, Joseph C., and Sherman, Harold W., "Analysis of Rollover Factors and Injury Causation," in Proceedings of the 16th Conference of the American Association for Automotive Medicine, October 1972.
4. McGuigan, R. and Bondy, N., "A Descriptive Study of Rollover Crashes," National Highway Traffic Safety Administration, unpublished report, July 1980.
5. Reinfurt, D.W., Li, L.K., and Popkin, C.L., "Rollover and Serious Driver Injury Differences Among Utility Vehicles, Pickup Trucks, and Passenger Car Groups," in Proceedings of the 26th Annual Conference of the American Association for Automotive Medicine, October 1982.
6. Snyder, R.G., McDole, T.L., Ladd, W.M., and Minahan, D.J., "On-Road Crash Experience of Utility Vehicles," University of Michigan Highway Safety Research Institute, Report No. UM-HSRI-80-14, February 1980.

those accidents in which rollover was the first (or first harmful) event for determining rollover frequencies.

Table 2. Incidence of rollover in all passenger car accidents (CPIR).[3]

Car size	No. of accidents	No. R.O.	% R.O.
Mini	245	39	16
Compact	764	99	13
Intermediate	547	60	11
Standard	697	42	6
Luxury	77	4	5
All Sizes	2,330	244	10.47

Table 3. Incidence of rollover as first harmful event (Michigan data, 1976).*[6]

Vehicle type	% R.O. in all crashes	% R.O. in SVAs
Utility Vehicles	12.7 (11.7)	39 (38.5)
Pickup or Panel Trucks	2.9	
Straight Trucks	3.1	
Passenger Cars	1.1 (1.6)	7 (12.3)
Sports Car	3.5	
Compact	2.3	
Intermediate	1.4	
Full Size	0.6	
All Vehicles	1.7	

*Values for combined data from five states are shown in parentheses.

Table 4. Incidence of rollover in SVAs (North Carolina - P.D. over $200).[5]

Vehicle type	R.O. rate/10,000 registrations	% R.O.
Utility Vehicles	55.5	36.6
Pickup Trucks	11.8	18.7
Passenger Cars	15.1	12.6
Subcompact	33.8	20.0
Compact	20.2	13.5
Intermediate	8.9	8.1
Full Size	3.6	5.0

Table 5. Incidence of rollover in fatal SVAs (FARS 1978-79, 1972-78 model years).[5]

Vehicle type	No. fatal SVAs	Fatal SVAs/ 10,000 registrations	% R.O.
Utility Vehicles	633	3.1	83
Pickup Trucks	2,556	1.3	64
Passenger Cars	10,145	0.8	47
Subcompact	3,596	1.1	56
Compact	2,458	0.9	45
Intermediate	2,668	0.7	41
Full Size	1,423	0.5	35

Table 6. Incidence of rollover as first event in SVAs.[7]

Vehicle type	No. SVAs	No. R.O.	% R.O.
Utility Vehicles	187	76	40.6
Heavy Trucks	788	290	36.8
Vans, Motor Homes	285	91	31.9
Light Trucks	1,338	348	26.0
Passenger Cars	5,223	711	13.6
Sports, Subcompact	1,124	252	22.4
Compact	1,255	191	15.2
Intermediate	1,203	126	10.5
Full Size	1,641	142	8.7
All Vehicles	7,821	1,516	19.4

Note: The overall rollover rate (i.e., regardless of whether first-event) of all vehicles combined was 47.9%. Thus, a majority (59.5%) of the rollovers were not first events.

Table 7. Incidence of rollover as first harmful event based on 1978-1979 data (% of SVAs).[8]

Vehicle type	NASS 1978-79 ave.	FARS 1978-79 ave.
Straight trucks	42.1	32.3
Pickup Trucks	20.1	28.7
Combination Trucks	17.9	34.0
Vans	11.2	23.0
Passenger Cars	6.6	17.1

---

7. Perchonok, K., Ranney, T., Baum, S., Morris, D., and Eppich, J., "Hazardous Effects of Highway Features and Roadside Objects," Calspan Field Services, Inc., Report No. ZR-5564-V-2, September 1978.
8. Malliaris, A.C., Nicholson, R.M., Hedlund, J.H., and Scheiner, S.R., "Problems In Crash Avoidance and In Crash Avoidance Research," Society of Automotive Engineers, Inc., Paper No. 830560, March 1983.

Table 8. Rollover rate in SVAs of light and heavy cars (%).[8]

	NASS 1978-79 ave.	NCSS 1978	FARS 1978-79 ave.
Light-Car (3,500 lb or less) SVAs	11.6	22.2	46.4
Heavy-Car (over 3,500 lb) SVAs	3.4	10.7	36.2
All Cars	8.3	17.4	43.1

1 lb = 0.4535 kg

Calspan examined the data contained in the NASS accident data files for the most recent years for which data were available (1979 through 1981) to determine the relationship between the type of vehicle and its propensity to roll over. Table 9 shows the proportion of single-vehicle crashes which involved a rollover as the first harmful event; the vehicles are ordered by type in the same general manner used for Tables 3 through 7. To more clearly show the relationship of rollover to weight, however, passenger cars were also subdivided into seven weight classes; and, to provide a more complete overview of rollovers, counts were made of <u>any</u> rollover by a crashed vehicle, regardless of whether or not the rollover was the first harmful event. (The majority--59%--of the rollovers were <u>not</u> first harmful events.) The results of these analyses are presented in Table 10.

Table 9. Incidence of rollover as first harmful event based on 1979-1981 data (% of SVAs).

Vehicle type	No. SVAs	% R.O.
Utility Vehicles	86	38.4
Pickup Trucks	503	19.3
Vans	119	13.5
Station Wagons	811	7.9
Passenger Cars	1,637	7.1
3,500 lb or less	1,015	10.0
over 3,500 lb	622	2.3
All Vehicle Types	3,156	10.33

1 lb = 0.4535 kg

Table 10. Incidence of any rollover, regardless of whether first harmful event (% SVAs).

Vehicle type	Location of first harmful event				% R.O. on and off roadway combined
	On roadway		Off roadway		
	No. SVAs	% R.O.	No. SVAs	% R.O.	
Utility Vehicles	24	79.2	65	60.0	65.2
Pickup Trucks	76	34.2	430	40.7	39.7
Vans	33	18.2	86	34.9	30.3
Station Wagons	143	6.3	668	23.2	20.2
Passenger Cars	302	7.6	1,346	24.6	21.5
2,000 lb or less	33	24.2	105	49.5	43.5
2,100-2,500 lb	31	22.6	204	35.3	33.6
2,600-3,000 lb	30	13.3	227	30.8	28.8
3,100-3,500 lb	69	2.9	323	21.1	17.9
3,600-4,000 lb	67	3.0	264	15.2	12.7
4,100-4,500 lb	51	0.0	167	12.6	9.6
4,600 lb or more	21	0.0	56	14.3	10.4
All Vehicle Types	578	14.4	2,595	28.1	25.6

1 lb = 0.4535 kg

Comparison of Results

Examination of the data presented in Tables 2 through 10 shows a consistency among all of the study findings with regard to the rank ordering of the different vehicle classes by rollover rate. Utility-type vehicles clearly are identified as having the highest frequency of rollover in accidents and are about three times as likely to overturn as passenger cars considered as a whole. Of interest in the results shown in Table 10 is the finding that, in contrast with those of the other vehicle types, the rollover frequency of utility vehicles is higher for accidents in which the first harmful event occurred on the road, rather than off the roadway. This suggests that utility vehicles are inherently less stable and more susceptible to roll moments generated on the roadway, as in swerving maneuvers. With all the other vehicles, it may be posited that rollovers depend more on the tripping or flipping forces that are generated in traversing embankments, ditches, and other roadside terrain irregularities or in impacts with objects such as culverts, trees, rocks, and posts.

Although the tabulated data show differences in the strength of the trend of rollover frequency in relation to the size of passenger cars, the results of the various studies are consistent without exception in indicating that rollover tendencies decrease systematically with vehicle weight (or size). The curves of Figure 2, which are plots of the data presented in Table 10, show this most clearly. The relationships tend to be curvilinear, flattening out at weights above 3,500 lb (1,587 kg). This suggests either that the basic relationship with weight is curvilinear or that, at the upper weight ranges, another key variable is stabilizing in its values. However, inspections of the relationships with wheelbase, tread width, or vehicle height did not indicate that either of these stabilizes in the upper weight range. Another possible explanation is that the interrelationships among weight, wheelbase, and tread width, or some other unknown relevant variable, produce a cumulative effect on rollover tendencies in the lower weight ranges, i.e., in those ranges, two or more factors combine to produce the exaggerated rollover tendencies.

Malliaris et al.,[8] who separated the car population into two groups, i.e., those weighing 3,500 lb (1,587 kg) or less (lighter cars) and those weighing more than 3,500 lb (heavier cars), also shows that lighter cars have a higher relative rate (percentage of car involvements in accidents divided by percentage of car registrations). To provide a comparison with the relative rates of involvement reported by Malliaris, similar rates were computed from data given by Reinfurt et al.[5] by assuming that the subcompact and compact car sizes could be lumped to represent the "lighter car" group and that the intermediate and full size cars together constituted the "heavier car" category. Tables 11 and 12 compare the Malliaris and Reinfurt data obtained from analysis of FARS data files for all single-vehicle accidents (Table 11) and for single-vehicle rollover accidents (Table 12). It may be seen from these tables that the values for the relative rates of involvement calculated from the Reinfurt data agree quite closely with those reported by Malliaris and likewise indicate that the accident involvement per registered vehicle is higher for small cars than for larger ones.

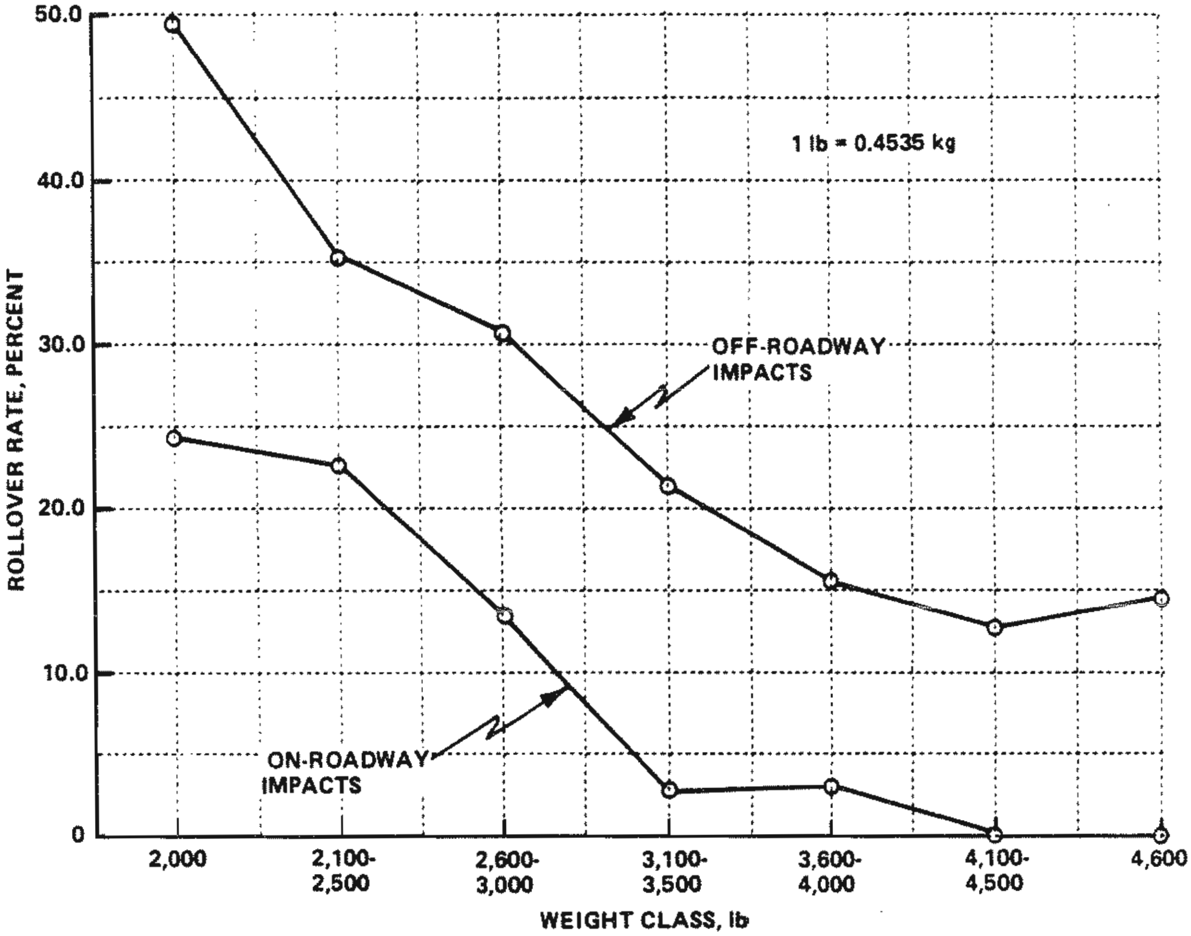

Figure 2. Passenger car rollover rates by weight class.

Table 11. Comparison of involvement rates for all fatal SVAs.[8,5]

Car size	% Car involvements		% Car registrations		Relative rate of involvement	
	Malliaris	Reinfurt	Malliaris	Reinfurt	Malliaris	Reinfurt
Lighter	67.6	59.7	49.1	47.3	1.38	1.26
Heavier	32.4	40.3	50.9	52.7	0.64	0.76

Table 12. Comparison of involvement rates for fatal SVAs with rollover.[8,5]

Car size	% Car involvements		% Car registrations		Relative rate of involvement	
	Malliaris	Reinfurt	Malliaris	Reinfurt	Malliaris	Reinfurt
Lighter	72.8	66.2	49.1	47.3	1.48	1.40
Heavier	27.2	33.8	50.9	52.7	0.53	0.64

In a similar manner, the data of Table 10 were used to determine if certain car sizes are overrepresented in rollover accidents by comparing the proportion of all single-vehicle accidents that occurred with cars of each weight class with the corresponding proportion of accidents that involved rollover. The results are presented in Table 13 and show that cars weighing 3,000 lb (1,360 kg) or less are overrepresented. This is particularly true for the lightest car weight class, which comprised 8.4% of all cars in the sample but accounted for 17% of all rollovers.

Table 13. Comparison of passenger car relative rollover involvement rates (SVAs) (NASS 1979, 1980, 1981 combined).

Car weight, lb	Proportion of all accidents		Proportion of all rollovers		Relative rollover involvement rate
	No.	%	No.	%	
2,000 or less	138	8.4	60	16.9	2.01
2,100-2,500	235	14.2	79	22.3	1.57
2,600-3,000	257	15.6	74	20.9	1.34
3,100-3,500	392	23.8	70	19.8	0.83
3,600-4,000	331	20.1	42	11.9	0.59
4,100-4,500	218	13.2	21	5.9	0.45
4,600 or more	77	4.7	8	2.3	0.49
Total	1,648	100.0	354	100.0	1.00

1 lb = 0.4535 kg

VEHICLE ROADWAY-DEPARTURE CONDITIONS

As might be expected, data from studies of accidents show that most off-road accidents are preceded by the vehicle's skidding out of control. From an analysis of the NCSS post-March 1978 accident data file, McGuigan and Bondy[4] reported that 85.7% of the vehicles in rollover accidents were sliding (including moving essentially forward with locked wheels) at the start of rollover. Approximately 48% of the vehicles were rotated at an angle of 90 degrees to the direction of travel (i.e., skidding broadside) at initiation of rollover, and another 36% were moving at a slip angle of $\pm$60 degrees. However, it is reported that only 30% of the vehicles were spinning at the start of rollover.

Perchonok et al.[7] determined the attitude of vehicles upon departing from the road in terms of whether they were tracking (as indicated by coincident front and rear wheel paths) or nontracking. In the latter case, the implication is that the vehicle was either spinning or skidding with a sideways component of velocity and, hence, was likely to have been out of control. Of 6,745 accidents for which the initial departure attitude could be ascertained (no data on the magnitudes of the slip angles are given in the report), 30.7% involved nontracking vehicles. Nearly one-fourth (23.9%) of the vehicles that departed on the right side of the road were not tracking, compared to 43.2% for left-side departures. While the percentage of vehicles that were nontracking is considerably lower than the findings of McGuigan and Bondy, it is noted that the rate determined by Perchonok et al. is based on all single-vehicle accidents, whereas the McGuigan and Bondy results are with reference to only rollover accidents.

The study by Perchonok et al. revealed the importance of the attitude of the vehicle in its effect on the type of event that occurred during the initial departure from the road. They found that vehicles were much more likely to "get away" without any impact if they were tracking. Also, nontracking vehicles were far more likely to experience rollover. Among nontracking vehicles, the proportion of (first-event) rollovers (30%) was two to three times greater than for vehicles that were tracking when they left the roadway.

Malliaris *et al.*[8] analyzed information contained in the NCSS 1978 automated accident file to obtain the estimates shown in Table 14 regarding the behavior of cars before the accidents. The condition "Going Straight" means that the car apparently was under control by the driver and was not undergoing any maneuver such as turning, changing lanes, or passing--or, in the case of car-to-vehicle collisions, was not stopped in traffic, slowing, parked, etc.--all of which are included in the "Other" category. "Out of Control" means that the driver was not in control of the car, which was either skidding or spinning.

Table 14. Frequency of pre-crash conditions of cars (%).[8]

Pre-crash condition	Single-car accidents	Car-to-vehicle collisions	All accidents
Going Straight	40.0	47.5	46.3
Out of Control	49.5	11.7	18.2
Other	10.5	40.8	35.5
	100.0	100.0	100.0

It may be noted that skidding or spinning out of control is the leading pre-crash condition for single-car accidents. Tables 15 and 16 show the distribution of single-vehicle accidents according to the pre-crash condition (with "Out of Control" subdivided into three groups) and the resulting type of impact for cars (Table 15) and for light trucks and vans (Table 16) involved in single-vehicle accidents.

Table 15. Pre-crash condition and resulting type of impact in passenger car SVAs (%).

Pre-crash condition		Resulting type of impact				
		Frontal	Side	Rollover	All other	All
	Straight	29.0	3.5	4.5	3.0	40.0
No Control	Skid Sideways	8.5	10.5	9.1	1.1	29.2
No Control	Skid Front	13.4	1.0	1.1	0.9	16.4
No Control	Spin	1.0	1.6	0.7	0.6	3.9
	Other	8.0	0.5	0.9	1.1	10.5
	All	59.9	17.1	16.3	6.7	100.0

Table 16. Pre-crash condition and resulting type of impact in light truck and van SVAs (%).

Pre-crash condition		Resulting type of impact				
		Frontal	Side	Rollover	All other	All
	Straight	28.3	2.5	7.8	2.6	41.2
No Control	Skid Sideways	7.3	7.4	17.4	2.2	34.3
No Control	Skid Front	10.4	1.2	2.3	0.7	14.6
No Control	Spin	0.0	0.3	3.1	0.0	3.4
	Other	2.9	0.0	2.7	0.8	6.4
	All	48.9	11.4	33.3	6.3	99.9

It is of interest to note that, in about 25% of the single-vehicle rollover accidents, both for cars and for light trucks and vans, the vehicles were going straight without loss of control (or, at least, the driver presumably had the option to control even though he may not have exercised the option). Also, it may be seen that more than half of the vehicles were skidding sideways prior to rolling over, and that relatively few were spinning, which compares favorably with the findings of McGuigan and Bondy[4] discussed earlier.

Results of further analyses to compare the relative rates of pre-crash conditions of light (3,500 lb (1,587 kg) or less) and heavy (over 3,500 lb) cars in single-vehicle accidents are also reported by Malliaris _et al._[8] These relative rates, which, for each pre-crash condition, is the percentage of all involvements divided by the percentage of the total car registrations represented by each weight group, are shown in Table 17.

Table 17. Relative rates of pre-crash conditions of light and heavy cars in SVAs (NCSS)[8]

Pre-crash condition	Relative rate of involvement	
	Lighter cars	Heavier cars
Straight	1.24	0.81
Skid Sideways	1.43	0.65
Skid Front	1.15	0.88
Spin	1.33	0.73
Other	1.28	0.77
All	1.29	0.76

Table 17 indicates overinvolvement of lighter cars for all of the pre-crash conditions and, particularly, for skidding sideways and spinning out of control, which are the conditions most likely to induce rollover. Based on these findings, the authors conclude that, "It is in fact this mode of losing control that leads the lighter cars to roll over so overwhelmingly more often than heavier cars."

Some information on the speeds and path angles at which vehicles accidentally depart from the roadway was also gleaned from the reports reviewed. Wright and Zador report that the average departure angle at 48 rollover crash sites examined in Georgia was 9.6 degrees.[9] The data of Perchonok et al.[7] show that the distribution of vehicle departure angles is slightly different for divided and undivided highways, but is mostly affected by whether the vehicle traversed a lane adjacent to the one in which it was traveling prior to departure. Overall, 88% of the accident vehicles were traveling in the right-most lane, and, of these, 67% departed on the right side. The distribution of departure angles for vehicles departing to the right from the right-hand lane of both divided and undivided roads combined is depicted in Figure 3. The curve shows that the median departure angle was 10 degrees, and that nearly 70% of the vehicles left the road at an angle of 15 degrees or less. The calculated mean angle for all departure is 13.9 degrees. For the subset of accidents in which rollover was the first event, the median departure angle was 15 degrees, or 5 degrees higher than median angle for all accidents.

On the average, the mean departure angle of vehicles that crossed over a lane prior to leaving the road was about 8 degrees larger than those which departed on the same side of the road as the lane in which they were traveling. The overall mean departure angle of tracking vehicles (right and left departures combined) was 14.3 degrees, compared to 22.8 degrees for non-tracking vehicles.

---

9. Wright, P.H. and Zador, P., "A Study of Fatal Rollover Crashes in Georgia," Insurance Institute for Highway Safety, unnumbered report, November 1980.

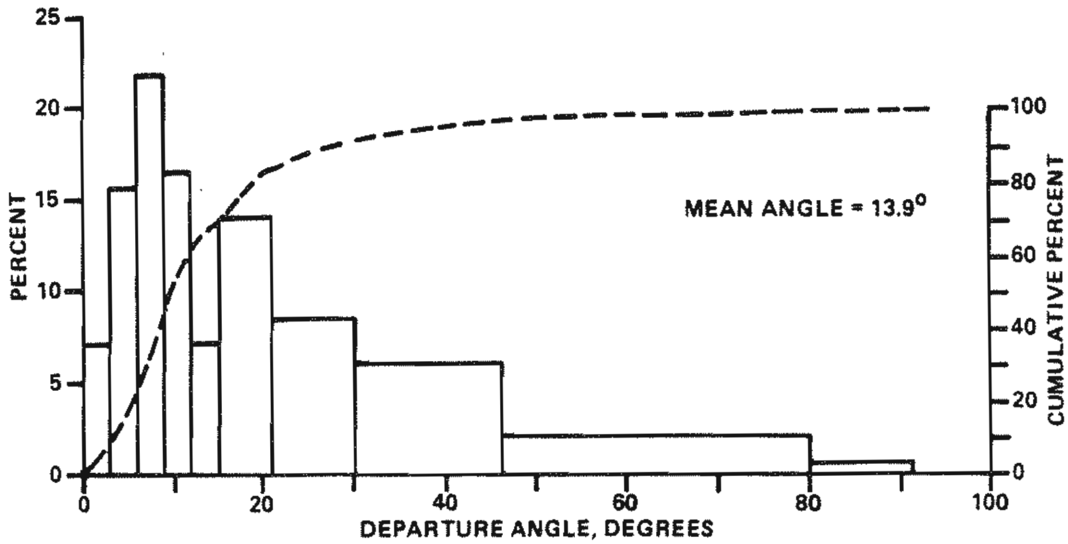

Figure 3. Distribution of departure angles for right-side departures from right lane.

Similar departure-angle results were obtained in an analysis by Viner[10] of data obtained from two sources: (1) 1982 NASS Longitudinal Barrier Special Study (289 observations, first impact with a guardrail or median barrier) and (2) "Analysis of Investigated Accidents," FHWA contract DOT-FH-11-9253, Southwest Research Institute (SWRI), October 1983 (203 observations, police-reported single-vehicle accidents of all types). Figure 4 compares plotted distributions of departure angle (reported as impact angle in the case of the NASS data) for the two sets of data. From the distributions shown, mean departure angles were calculated as 17 degrees for the NASS data and 15 degrees for the SWRI data, both of which are slightly higher than the 13.9 degrees shown by Figure 3. Viner notes that some error was introduced in developing the SWRI distribution of Figure 4, because the data used were available for only 5-degree increments of departure angle; SWRI reported a median departure angle of 18.7 degrees. (Also of interest is that SWRI reported this value to be 2 degrees lower than the median <u>impact</u> angle calculated from analysis of their data.) <u>Yaw</u>-angle distributions determined by Viner from the same two sets of data, depicted in Figure 5, are in surprisingly good agreement and show that, in half of the police-reported (NASS and SWRI) accidents studied, the vehicle was yawed at impact.

---

10. Personal communication from John G. Viner, FHWA Office of Safety and Traffic Operations R&D, 1985, on tentative findings of FHWA staff study 21T1-554, "Clinical Analysis of Roadside Accidents."

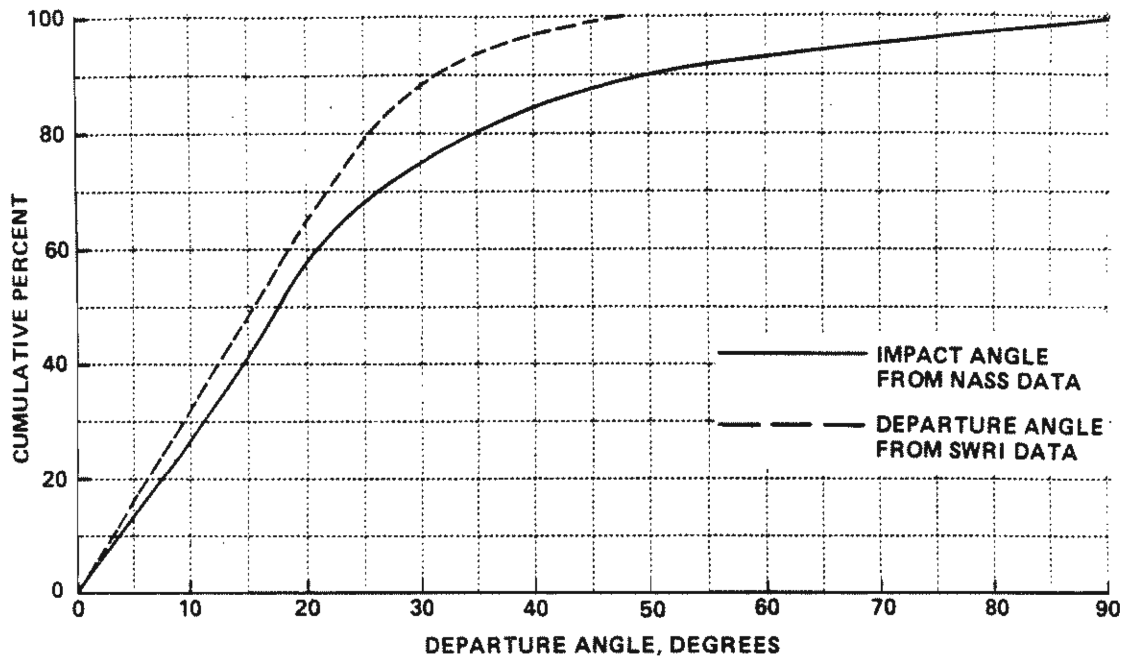

Figure 4. Comparison of departure-angle distributions from two accident data bases.

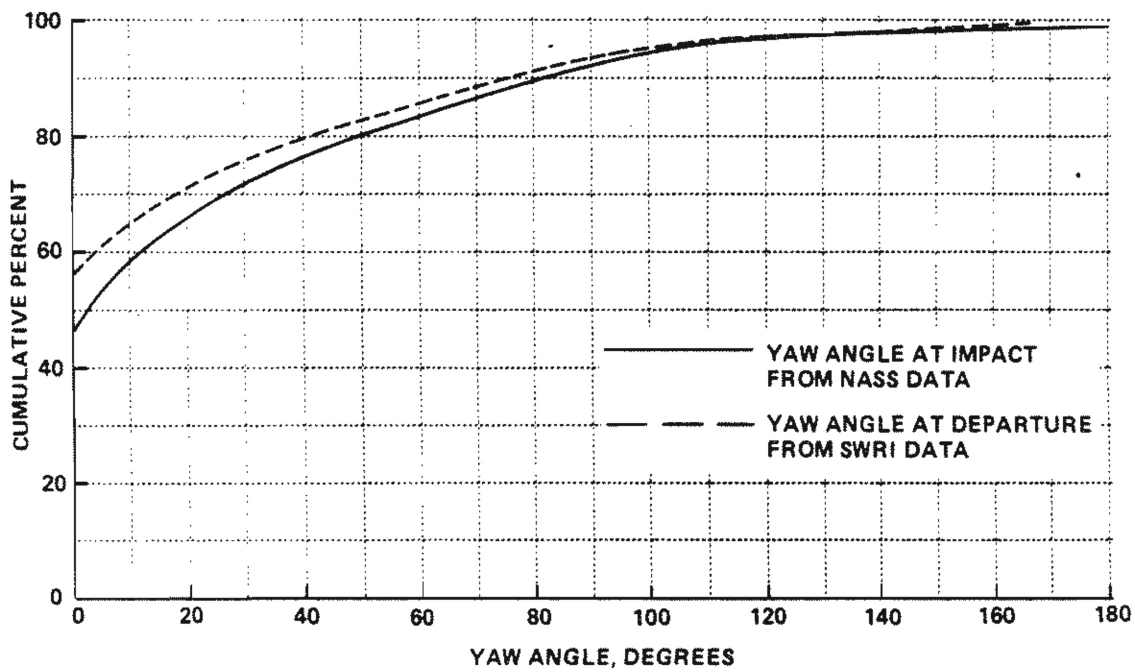

Figure 5. Comparison of yaw-angle distributions from two accident data bases.

With regard to crash speeds, Huelke _et al._[3] give the results shown in Table 18, which were obtained from an analysis of over 2,300 car accidents in a CPIR data file.

Table 18. Car speed prior to impact.[3]

Speed range, mi/h	No. of accidents	Rollovers No.	Rollovers %	Percent of all rollovers	Cumulative %
1-10	178	4	2	1.9	1.9
11-20	157	2	1	1.0	2.9
21-30	341	9	3	4.4	7.3
31-40	405	37	9	18.0	25.3
41-50	361	55	15	26.7	52.0
51-60	195	41	21	19.9	71.9
61-70	157	33	21	16.0	87.9
71-80	38	9	24	4.4	92.3
81-90	25	10	40	4.9	97.2
91-100	10	6	60	2.9	100.1
Total	1,867	206	11	100.1	

1 mi/h = 1.609 km/h

Not surprisingly, Table 18 shows that the likelihood of rollover increases with increasing speed prior to impact. About one-quarter of the rollover crashes occurred at speeds below 40 mi/h (64.4 km/h), and over half of the rollovers in the sample involved vehicles traveling 50 mi/h (80.5 km/h) or less. These data also indicate that the median speed of vehicles in rollover accidents was somewhat higher than the median speed of all crashes.

From a study of rollover accidents of British cars and light vans, Mackay and Tampen[11] obtained the distribution of estimated crash speeds shown in Table 19. Compared to the findings of Huelke _et al._[3] these data show that more rollovers occurred at the lower speed ranges, with nearly 83% of the vehicles overturning at speeds below 50 mi/h (80.5 km/h).

11. Mackay, G.M. and Tampen, I.D., "Field Studies of Rollover Performance," Society of Automotive Engineers, Inc., Paper 700417, 1970.

Table 19. Estimated speeds of rollover.[11]

Estimated speed, mi/h	Rollover No.	Rollover %	Cumulative %
0-10	2	2.3	2.3
10-20	13	14.9	17.2
20-30	18	20.7	37.9
30-40	22	25.3	63.2
40-50	17	19.5	82.7
50-60	8	9.2	91.9
60-70	6	6.9	98.8
70-80	1	1.2	100.0
Total	87	100.0	

1 mi/h = 1.609 km/h

The report by Perchonok et al.[7] provides data on the estimated speed of the vehicle for the primary impact of each accident. In multi-impact accidents, the primary impact was the one thought to have resulted in the highest change of velocity (delta V) and, therefore, was most likely to have caused injury to the occupants. Although the primary impact speeds are not necessarily the same as those at which the vehicles departed from the highway, the data are nonetheless useful in providing some insight as to the minimum departure speeds, since most vehicles probably decelerated (rather than accelerated) along the path to the point of impact. The distribution of speed for primary impacts (46% were rollovers and 54% were nonrollover impacts) is given in Table 20, which shows that most of the impacts occurred in the 21-30 mi/h (33.8-48.3 km/h) speed range, and that 87% of the vehicles were traveling at 40 mi/h (64.4 km/h) or less. On the average, the speed was slightly higher when the primary impact was a rollover, rather than a nonrollover, crash.

Table 20. Distribution of primary impact speeds.

Impact speed, mi/h	Primary impacts No.	Primary impacts %	Cum. %
0-10	683	8.9	8.9
11-20	1,861	24.2	33.1
21-30	2,731	35.6	68.7
31-40	1,429	18.6	87.3
41-50	679	8.8	96.1
51-60	219	2.9	99.0
over 60	79	1.0	100.0
Total	7,681	100.0	

1 mi/h = 1.609 km/h

OCCUPANT-INJURY FREQUENCY AND SEVERITY

Data on the frequency and severity of injuries to occupants of crash vehicles indicate that rollovers tend to be more severe than other types of accidents. Viner[12] reported that overturn was the leading cause of roadside fatalities in 1981, accounting for 33.8% of the fatalities on all roads and 44.7% of those on the Interstate system. From an analysis of single-vehicle police-reported accidents in Texas in 1981, it was found that 2.32% of overturn accidents resulted in driver fatality, as compared to 1.21% for nonrollovers--a ratio of nearly 2 to 1.

McGuigan and Bondy[4] report a severe injury rate (AIS (Accident Injury Scale) of 3 or more) of 11.5% for occupants of rollover vehicles, compared to 4.1% for the occupants of vehicles that did not overturn, from analysis of the NCSS post-March 1978 data file. They also observed, in examining FARS 1978 data, that 53% of all occupants in fatal rollover accidents were killed, as opposed to 41.6% of the vehicle occupants in non-rollover fatal accidents. Table 21 shows, from the FARS data, the percentages of occupants killed by vehicle type.

Table 21. Frequency of occupants killed in rollovers of different type vehicles (FARS 1978).[4]

Vehicle type	% Rollover occupants killed	Killed rollover occupants as % of all killed for vehicle type
Passenger Cars	55.6	23
Light Trucks	50.9	39
Vans	41.8	39
Multiple-purpose Vehicles	48.6	61
All Vehicle Types	53.5	26.4

Table 21 indicates that, although the percentage of occupants who are killed in rollover accidents of multi-purpose vehicles is lower than for passenger cars, rollover is a relatively more serious problem for the former,

---

12. Viner, John G., "Implications of Small Cars on Roadside Safety," in Proceedings of the 27th Annual Conference of the American Association of Automotive Medicine, October 1983.

since it accounts of 61% of all fatalities that occur to multi-purpose vehicle occupants, in contrast with 23% of all those killed in passenger cars.

In the study by Reinfurt et al.,[5] it was determined that the rates for serious (A) and fatal (K) driver injuries in single-vehicle rollover crashes per 10,000 registered vehicles was much higher for drivers of utility vehicles (10.0), compared to passenger cars (2.0). Among passenger cars, the serious-injury rates decreased with increasing car size, with an approximately fivefold difference (4.1 vs. 0.8) between subcompact and full-size cars. Thus, accident data show not only that small cars roll over more frequently than larger ones, but also that the consequences are more severe.

Ejection is a leading cause of serious and fatal injuries in rollover accidents. McGuigan and Bondy[4] report that 40% of the occupants of passenger cars that overturned were ejected, and 53% of those who were killed were ejected. The latter value is somewhat lower than the four-out-of-six (67%) fatal ejection rate cited by Huelke et al.,[3] who determined the distribution of injury severity for passenger-car rollovers and for all accidents shown in Table 22.

Table 22. Overall occupant injury severity.[3]

Injury severity AIS	Rollover	All accidents
0 - No Injury	15.3	23.9
1 - Minor	44.6	46.6
2 - Moderate	12.8	11.9
3 - Severe (Not Life-threatening)	7.8	6.0
4 - Serious (Survival Probable)	1.4	2.0
5 - Critical (Survival Uncertain)	2.5	1.7
6-9 Fatal	15.6	7.9
	100.0%	100.0%

Table 22 shows that the distribution of injuries at the lower injury levels is approximately the same in rollovers as in all vehicle collisions. However, almost 16% of the occupants were fatally injured in rollovers which is nearly twice that for all accidents.

The injury severity of 89 rollover accidents of British passenger cars and light vans (147 occupants) as reported by Mackay and Tampen[11] is presented in Table 23. It may be seen that this distribution more nearly corresponds to the results of Huelke for all accidents rather than the distribution for rollovers. (Note that Tables 22 and 23 cannot be directly compared, since the former is based on the total number of occupants involved in the accidents, whereas Table 23 shows the distribution of rollover accidents according to the level of injury sustained by the most severely injured occupant.) This may be a reflection of the observation noted earlier that the vehicle speeds in rollover crashes estimated by Mackay and Tampen were lower than those reported by Huelke et al.

Table 23. Injury severity for rollover accidents.[11]

Injury severity	No. of accidents	%
None	26	29.2
Minor	33	37.1
Moderate	14	15.7
Severe	10	11.2
Fatal	6	6.8
Total	89	100.0

Data on the most severe injury sustained by any occupant of the accident vehicle are given in the report by Perchonok et al.[7] Injuries were classified by three levels of severity: none, nonfatal, and fatal. The frequency of the most severe injury to an occupant in all rollover and nonrollover accidents is shown in Table 24. The data show that occupants were injured in two-thirds of the rollover accidents and in slightly less than half of the nonrollover crashes. Also, the fatality rate of rollovers was nearly double that for nonrollover impacts. That rollovers in general are shown to be more hazardous than other types of accidents is in keeping with the findings of other studies using different accident data bases.

Table 24. Distribution of the most severe injury level in rollover and nonrollover accidents.[7]

Impact type	Injury			Total	Injured*		% Killed
	None	Nonfatal	Fatal		No.	%	
Rollover	1,189	2,134	235	3,558	2,369	66.6	6.6
Nonrollover	2,160	1,914	146	4,220	2,060	48.8	3.5
Overall	3,349	4,048	381	7,778	4,429	56.9	4.9

*Includes both fatal and nonfatal injuries

As part of a study of factors influencing injury, Perchonok et al.[7] analyzed accidents on ditch and fill cut-type roads to determine if there were differences in injury experience. It is well to point out that while the presence of a ditch or fill is implied, neither of these features may necessarily have affected the outcome of the accident. For example, in some accidents on roads with a ditch, the vehicles may have safely traversed the ditch, or perhaps not even have encountered it at all. The results of the analyses show little difference in the frequency of injuries or fatalities for the two road types. No relationship between the likelihood of injury and the sideslope of either ditches or fills is evidenced by the results, but, for fills, there is an indication of higher injury and fatality rates on slopes steeper than 3:1. Analysis of the effects of fill height and ditch depth does show a tendency of increased injury rate with increasing height or depth. The trend is apparent for increases of fill height from 1 to 5 ft (0.3 to 1.5 m), and, for ditches, there was the general effect of a higher injury rate for depths greater than 2 ft (0.6 m).

ROADSIDE FEATURES

Although many analyses of accident data have shown, not surprisingly, that the vast majority of rollovers occur off the road, most reports contain little or no detailed information concerning the location and shape of the roadside terrain features that caused the vehicles to overturn, or even whether rollover was the result of a prior impact with an object. From their analysis of NCSS data, McGuigan and Bondy[4] determined that 72% of the rollover accidents were initiated off the roadway. Slightly more than half of the rollovers occurred without a prior impact, and, of the accidents for which there was an impact prior to overturning, the impact was judged to have initiated overturning in 59% of them. Also, from the FARS 1978 accident data file, they found that collision with a fixed object was the "first harmful event" in 51% of the fatal single-vehicle rollover accidents. The frequency of impact with the three terrain features included in the list of fixed objects struck given in the report is shown in Table 25, where it may be noted that embankments and ditches together were the objects struck in 36% of the accidents of all types of vehicles (passenger cars, light trucks, vans, and utility vehicles).

Table 25. Object struck as first harmful event in single-vehicle fatal rollover accidents (FARS 1978).[4]

Object struck	No. of accidents (all vehicle types)	% of all fixed object impacts
Embankment	673	18.3
Culvert/Ditch	652	17.8
Curb or Wall	232	6.3
All Other Objects	2,117	57.6
Total	3,674	100.0

From the analysis of data collected in a field study of 151 rollover crash sites in New Mexico, Hall and Zador[13] observed that a comparatively small object was the most probable cause of overturning. These objects included curbs, edge dropoffs, ditches, and soft soil. Among their findings were: 85% of the vehicles overturned within 27 ft (8.2 m) of the roadway; only 18% of the crash sites had slopes greater than 3:1, and there was evidence to clearly indicate that vehicles which departed the road had serious difficulty in traversing front slopes of 4:1; and over half of the fatal rollover crashes occurred on embankments less than 4 ft (1.2 m) high. In a similar study of rollover accident sites in Georgia, Wright and Zador[9] found that about 90% of the rollovers were precipitated within 30 ft (9.1 m) of the pavement edge. Elongated hazards, such as ditches and embankments, were found more likely to be present at sites of rollover accidents than at locations of fixed-object crashes.

Results reported by Malliaris _et al._[8] and Huelke _et al._[3] are in substantial agreement with the findings discussed above. The former study showed that over 80% of the rollovers were initiated off the road. Curbs are cited as the tripping source of vehicles in 10% of the cases, whereas ditches, embankments, and drop-offs constituted the majority of the rest. Of 200 rollover accidents selected from a CPIR automated file for detailed review in the study by Huelke, 97% occurred off the roadway, and 60% of those case vehicles struck another object or vehicle before overturning. In only four accidents

---

13. Hall, J.W. and Zador, P., "A Survey of Single Vehicle Fatal Rollover Crash Sites in New Mexico," Insurance Institute for Highway Safety, unnumbered report, November 1980.

was there an indication that rollover occurred without tripping (e.g., hitting a curb, or wheels digging into soft earth) or vaulting over an embankment.

Klein _et al._[14] performed a study of roadway disturbances most likely to be encountered and to cause an accident, as determined from accident data and a survey of drivers. Approximately 4% of all accidents were found to have as a causal factor a "road defect," which includes dips, bumps, shoulder drop-off, holes, washboard, loose gravel, etc. A shoulder drop-off was rated as the most hazardous disturbance in terms of the likelihood of causing loss of control. However, shoulder drop-offs are seen to be a relatively infrequent causal factor of rollover accidents, since, according to the authors, they "appear to be involved in 1 to 3 percent of all passenger car accidents on dry roads with unimpaired drivers."

From analyses examining the effects of the character of the roadside on the locations and of types of events that occurred in accidents, Perchonok _et al._[7] found that 20% of all (7972) first events occurred on the shoulder. Of 1,528 accidents for which rollover was the first event, only 3.5% occurred on, or were initiated on, the shoulder. The most frequent type of first event on the shoulder was a "no impact" departure. In 60% of the 1,412 accidents in which there was no impact during the initial departure, the vehicles did not encroach on the roadside beyond the shoulder. No systematic relationship between shoulder width and event type was found in the results of the analyses.

In studying the effects of side slopes, Perchonok _et al._ distinguished between two road types that are referred to as ditch cut or fill type roads. Table 26 shows the frequency of the type of event (rollover, nonroll impact, or no impact) that occurred in the first departure from these types of roads. (Accidents also occurred on roads with rock cuts, retaining walls, hillsides, etc., but the limited numbers of observations precluded meaningful analyses.)

---

14. Klein, R.H., Johnson, W.A., and Szostak, H.T., "Influence of Roadway Disturbances on Vehicle Handling," Volumes 1-3, Systems Technology, Inc., Report Nos. DOT HS-802-210,-211,-212, February 1977.

Table 26. Event type for fill and ditch cut type roads (first event).[7]

Road type	Rollover		Nonroll impact		No impact		% roll for:	
	No.	%	No.	%	No.	%	Impacts	NOS*
Fill	971	23.1	2497	59.5	731	17.4	28.0	57.1
Ditch	404	16.1	1609	64.0	500	19.9	20.1	44.7

*No object struck

The data show ditch cut roads had relatively fewer rollovers, more nonroll impacts, and slightly more frequent nonimpacts. Although the term "ditch cut" implies that ditches were present on that type of road, the roadside on an unknown number of roads built on fill also included a ditch. The extent to which rollovers resulted from encounters with a ditch is not reported, but it is stated that there were a total of 660 nonroll impacts with ditches. As indicated by the last two columns of Table 26, the frequency of rollover was higher for the fill type of road, regardless of whether computed on the basis of all impacts or only those accidents in which there was no object struck (NOS).

Analysis of the objects struck in nonroll impacts showed that collisions with ditches, embankments, and culverts were much more frequent on ditch cut roads than on fill type roads, whereas guardrail impacts were overrepresented for roads built on fill. Upon removing the nonroll impacts with these objects characteristically associated with each type of road, the proportion of nonroll impacts was essentially equal for the two road types. Moreover, the proportion of rollovers for fill type roads was still greater than for ditch cut roads. Thus, it was concluded that the lesser likelihood of rolling over on ditch cut roads was not due to more nonroll impacts, but appears to result from the direct effect on rollover of differences between the general terrain contours associated with these two types of road construction.

The analyses of side slopes included examination of the effects of the steepness of the slope as well as the height/depth of fills/ditches on event type. Table 27 shows the distribution of event type as a function of side slope for both fills and ditches. (It is tacitly assumed that, for ditches, the slope pertains to the terrain between the road and the ditch and, in general, not to the side of the ditch itself.) The proportion of rollovers on fill slopes show no consistent relationship with slope, but the likelihood of nonrollover impacts increased, and the proportion of no impacts decreased, with increasing slope. Thus, for accidents in which there were no objects struck, the proportion of rollovers increased with increases of the side slope. Note that the highest proportion of rollovers occurred on 3:1 slopes; on steeper slopes, the frequency of nonroll impacts increased sharply. Also, even on the shallowest of slopes, less than one-quarter of the vehicles were able to "get away" without rolling over or colliding with an object.

Table 27. First event type by slope for fill and ditch cut type roads.

Slope	Rollover		Nonroll impact		No impact		Total		% Roll for:	
	No.	%	No.	%	No.	%	No.	%	Impacts	NOS*
Fill										
6:1, or flatter	256	22.4	645	56.4	242	21.2	1,143	100.0	28.4	51.4
4:1	167	22.8	425	57.9	142	19.2	734	100.0	28.2	54.0
3:1	177	25.7	410	59.4	103	14.9	690	100.0	30.2	63.2
2:1	196	19.6	669	67.0	133	13.3	998	100.0	22.7	59.6
1:1	28	24.3	77	67.0	10	8.7	115	100.0	26.7	73.7
Ditch Cut										
6:1, or flatter	125	20.6	351	57.9	130	21.5	606	100.0	26.3	49.0
4:1	86	18.8	273	59.7	98	21.4	457	100.0	24.0	46.7
3:1	43	10.7	277	69.1	81	20.2	401	100.0	13.4	34.7
2:1	53	10.1	388	74.0	83	15.8	524	100.0	12.0	39.0
1:1	21	10.4	155	76.7	26	12.9	202	100.0	11.9	44.7

*No object struck

The effect of sideslope on ditch cut roads is seen to be somewhat different. As with fill slopes, the proportion of nonroll impacts increased, and the proportion of no impacts decreased, with increasing slope. Surprisingly, however, a decrease in the relative frequency of rollovers with increased slope is clearly evident, and the highest proportion of rollovers occurred on slopes of 6:1 or flatter. The frequency of rollovers dropped sharply on 3:1 slopes, primarily because relatively many more accidents involved nonroll impacts, which increased almost 20% from shallow to steep ditch slopes.

The distribution of the type of event that occurred in the initial departure as a function of the height of fill and depth of ditch is shown in Table 28. The data show that the proportion of rollovers increased with increases of both fill height and ditch depth. For fills, the frequency of rollovers increased most rapidly as the height increased from 3 ft (0.9 m) to the 4-5 ft (1.2-1.5 m) range. The results for ditches are similar in that the major increase in the proportion of rollovers is also seen to occur when the depth increased from 3 ft (0.9 m) to the 4-5 ft (1.2-1.5 m) range. No orderly trends in the results were found when the combined effect of side slope and the height/depth of fills/ditches on event type was examined.

Table 28. First event type by height of fill or depth of ditch.[7]

Height, ft	Rollover		Nonroll impact		No impact		Total		% Roll for:	
	No.	%	No.	%	No.	%	No.	%	Impacts	NOS*
Fill										
1	40	15.1	172	64.9	53	20.0	265	100.0	18.9	43.0
2	54	15.2	243	68.3	59	16.6	356	100.0	18.2	47.8
3	64	19.1	195	58.2	76	22.7	335	100.0	24.7	45.7
4-5	211	27.2	415	53.4	151	19.4	777	100.0	33.7	58.3
6-10	134	23.3	339	59.1	101	17.6	574	100.0	28.3	57.0
11-20	91	26.4	210	60.9	44	12.8	345	100.0	30.2	67.4
20+	58	24.6	149	63.1	29	12.3	236	100.0	28.0	66.7
Ditch										
1	49	11.7	307	73.3	63	15.0	419	100.0	13.8	43.8
2	78	11.5	441	65.2	157	23.2	676	100.0	15.0	33.2
3	50	12.5	273	68.4	76	19.0	399	100.0	15.5	39.7
4-5	108	25.1	243	56.5	79	18.4	430	100.0	30.8	57.8
6+	19	14.6	89	68.5	22	16.9	130	100.0	17.6	46.3

*No object struck   1 ft = 0.3048 m

Unfortunately, information regarding the terrain features and geometry where rollovers were initiated is not given in the report. Thus, for example, whether rollovers occurred mostly on the side slope, at break points such as at the toe of the slopes, or as a result of encounters with objects such as ditches, embankments, culverts, field approaches (raised driveways), etc., cannot be established. However, to the extent that they are equally likely to induce vehicle rollover, the frequencies with which various terrain features are struck in nonrollover accidents may be indicative of their relative rate of involvement in rollover accidents. Table 29 gives the distribution of terrain objects struck in nonrollover accidents. These data indicate that embankments, ditches, and culverts are features most frequently encountered, and that they together account for nearly three-fourths of the terrain objects struck in nonrollover accidents. Moreover, the high percentage of primary impacts for these features, compared to the other terrain objects struck, suggests that impacts with them are likely to be more severe.

Table 29. Terrain objects struck in nonrollover impacts.[7]

Object	All impacts		Primary impacts	
	No.	%	No.	%
Embankment	773	30.6	413	53.4
Ditch	642	25.4	374	58.3
Culvert	436	17.2	239	54.8
Ground	224	8.9	156	69.6
Field Approach	220	8.7	75	34.1
River, Pond, etc.	51	2.0	24	47.1
Snowbank	38	1.5	8	21.1
Curb	35	1.4	6	17.1
Other, Unknown	108	4.3	14	13.0
Total	2,527	100.0	1309	100.0

Of value to the prssent study is the information given in the report regarding the location of certain terrain features with respect to the edge of the road. The lateral distance to terrain features struck in primary nonrollover impacts is shown in Table 30. From this table, it may be seen that 66% of the ditches, 73% of the embankments, 78% of the culverts, and 69% of the field approaches were no more than 20 ft (6.1 m) from the road. The 13 to 20 ft (4 to 6.1 m) lateral distance interval was the median range for all of the features except culverts, for which the median distance was in the 7 to 12 ft (2.1 to 3.7 m) range.

Table 30. Lateral distance to terrain objects struck in primary nonrollover impacts.

Lateral distance, ft	Terrain object						Field approach	
	Ditch		Embankment		Culvert			
	No.	%	No.	%	No.	%	No.	%
0-6	36	9.8	74	18.0	35	14.9	5	6.8
7-12	97	26.3	120	29.2	86	36.6	17	23.3
13-20	110	29.8	107	26.0	61	26.0	28	38.4
21-40	86	23.3	88	21.4	41	17.5	21	28.8
41-60	20	5.4	11	2.7	6	2.5	2	2.7
over 60	20	5.4	11	2.7	6	2.5	0	0.0
	369	100.0	411	100.0	235	100.0	73	100.0

1 ft = 0.3048 m

Information reported by Perchonok et al.[7] concerning rollovers in relation to borders and border offset distances is also of interest. A border was defined to be a generally nontraversable obstacle which extended at least through 50% of the vehicle's off-road path. The most frequent type of border was a "natural object," such as trees and brush; roughly one-half of the borders were of this type. The next most frequent type of border was "terrain"; this classification accounted for over one-third of the borders and included ditches, embankments, water, etc. Other border types included permanent barriers such as guardrails, fixed objects (primarily fences, but also buildings), and road structures such as bridge side rails and overpass supports.

Table 31 shows the distribution of rollovers (first-event) by lateral distance and border offset. Note that two-thirds of all of the rollovers occurred at lateral distances less than the border offset, and that the proportion of rollovers that occurred in that region increased with increasing border offset. On the whole, one-third of the impacts occurring between the road and the border were rollovers, and two-thirds were nonrollover impacts. Whether these results are characteristic of terrain borders in particular is not known, but it suggests that rollover may be caused as often by the effect of slopes, surface irregularities, and the firmness of "traversable" roadside terrain as by encounters with generally "nontraversable" terrain features.

Table 31. Distribution of rollovers (first-event) by lateral distance and border offset.

Border offset, ft	Rollover lateral distance					
	Less than border offset		Equal to border offset		Greater than border offset	
	No.	%	No.	%	No.	%
0-10	-	-	29	50	29	50
11-20	45	39.1	52	45.2	18	15.7
21-30	49	62.8	23	29.5	6	7.7
31-40	37	80.4	5	10.9	4	8.7
41-60	42	82.4	9	19.6	0	0
61-100	16	88.9	2	11.1	0	0
over 100	171	98.3	3	1.7	-	-
	360	66.7	123	22.8	57	10.5

1 ft = 0.3048 m

PRINCIPAL FINDINGS

The major findings derived from the review of the literature are briefly summarized below.

- Rollover is a relatively frequent occurrence, particularly in single-vehicle accidents.

- Classifications of vehicles based on use and/or size exhibit . distinct differences in the rollover rates among classes.

- Utility vehicles have been identified as a class having the highest rollover frequency (40 to 60% rollover rate) and are about three to five times more likely to overturn than passenger cars considered as a whole.

- For passenger cars, the rollover rate decreases with increasing car size; the weight, wheelbase, and tread width appear to be equally appropriate as classificatory variables, since they are all highly interrelated.

- In most (50 to 80%) of the rollover accidents, the vehicles were skidding out of control at a large yaw angle prior to overturning.

- About half of all accidental departures from the roadway occurred at path angles greater than 15 degrees, and the majority of vehicles were estimated to have been traveling at speeds less than 40 to 50 mi/h (64 to 80 km/h).

- The vast majority of rollovers occur within 30 ft (9.1 m) of the roadway, and relatively few occur or are initiated on the shoulder.

- Embankments, ditches, and culverts are the roadside terrain features cited as being most frequently involved in overturn accidents, though detailed information on the geometry of the terrain and/or whether rollover was caused by the wheels contacting a small obstacle or digging into soft soil so as to trip the vehicle is generally lacking in accident data files.

- The likelihood of rollover increases with the steepness and height of sideslopes and the depth of ditches. Available data indicate that rollover frequency increases sharply for fill/ditch heights/depths greater than 3 ft (0.9 m).

- Rollover accidents are severe in terms of the frequency and severity of injuries to the vehicle occupants. The fatality rate of occupants of rollover vehicles is approximately twice that for occupants of vehicles in nonrollover impacts. Ejection is the leading cause of serious and fatal injuries, accounting for more than half of the fatalities incurred in rollover accidents.

Section 3

HVOSM MODIFICATIONS AND EXTENSIONS

SUMMARY

The simulation aspect of this research project required several analytical refinements and computer-program extensions to improve the application of HVOSM to rollover situations. McHenry Consultants, Inc. (MCI), retained as a consultant throughout this project, had incorporated several specific program modifications in a proprietary (MCI) version of HVOSM to achieve more realistic simulations of actual rollover accidents. Those MCI modifications, and additional modifications, were implemented in the HVOSM program at Calspan for use in this study.

Portions of this revised version of HVOSM are still in developmental stages. Many of the new enhancements were developed in response to needs that arose during previous research efforts. As a result of this functional implementation, the program code is essentially a "working copy" and, hence, contains variables redefined from previous options and dummy variables for uncompleted extensions. Certain options previously available in the HVOSM-RD2 version[15] have been removed; these include the sprung-mass/barrier-impact simulation and the road-roughness simulation.

Outlines of the MCI modifications are provided in this section for convenience; for more detailed discussions of the related topics, the reader is referred to the references noted throughout this section. For the new options, functional descriptions of input, output, and intermediate variables are given in Appendix C. For revised or extended computer routines, input variables are defined in Appendix C. For extensions that produce additional printed output, output variables are described in Appendix C.

---

15. Segal, D.J., "Highway-Vehicle-Object Simulation Model--1976," Volumes 1 through 4, Report No. FHWA-RD-76-162, -163, -164, and -165, February 1976.

DEFORMABLE-SOIL MODEL

Tire sinkage into soft soil can produce motion-resistance forces greater than those associated with pavement. As a consequence, vehicle rollover occurs more frequently on unpaved surfaces.

The related MCI modifications of HVOSM are based on analytical relationships developed by Bekker[16,17] for a rigid wheel in homogeneous soil. The selection of rigid, as opposed to elastic, wheel relationships was made in consideration of: (1) the relatively cumbersome nature of Bekker's motion-resistance relationships for elastic wheels, and (2) the fact that the predicted magnitude of the motion-resistance forces for elastic wheels tends to be independent of inflation pressure in the range above 25 psi (172,369 Pa).

The specific analytical approach of the MCI modifications consists of the following sequence of calculations:

(1) extent of tire sinkage (limited to one-sixth of the wheel diameter),

(2) sideslip angle of tire,

(3) projected area of the tire/soil interface at the existing conditions of sinkage and sideslip,

(4) motion-resistance force for a tracking wheel adjusted for the projected area of the sideslipping wheel, and

(5) addition of the resultant plowing force components to the rigid-surface circumferential and side forces of the tire.

---

16. Bekker, M.G., Off-the-Road Locomotion, University of Michigan Press, Ann Arbor, MI, 1960.
17. Bekker, M.G., Introduction to Terrain-Vehicle Systems, University of Michigan Press, Ann Arbor, MI, 1969.

The sinkage, Z, of a vehicle wheel i and the resulting motion resistance force for a tracking wheel are approximated by Bekker's equations for a rigid wheel as follows:

tire sinkage,
$$Z_i = \left[\frac{3 F'_{Ri}}{(3-n)(k_c + t_w k_\phi) \sqrt{2 h_i}} \right]^{\left(\frac{2}{2n+1}\right)} \tag{1}$$

motion-resistance force,
$$F_{mR_i} = \frac{(3 F'_{Ri})^{\epsilon}}{(3-n)^{\epsilon} (n+1) (k_c + t_w k_\phi)^{\left(\frac{1}{2n+1}\right)} (2 h_i)^{\epsilon/2}} \tag{2}$$

where:

F'_{Ri}	=	tire normal load
n	=	exponent of soil deformation
k_c	=	modulus of soil deformation due to cohesive components
k_ϕ	=	modulus of soil deformation due to frictional components
t_w	=	tire tread width
h_i	=	tire rolling radius
ϵ	=	$\frac{2n+2}{2n+1}$

It is logical to expect that the resistance force due to plowing of the soil is related to the vertical tire/soil-interface area and would be maximum when the wheel is moving broadside at a 90-degree slip angle. The effect of a sideslipping tire is accounted for in the model by assuming that the motion resistance increases in proportion to the increase of the projected vertical tire/soil-contact area in the direction of motion. The tire/soil-interface areas for the contacts by the front and sidewall of the tire are illustrated in Figure 6.

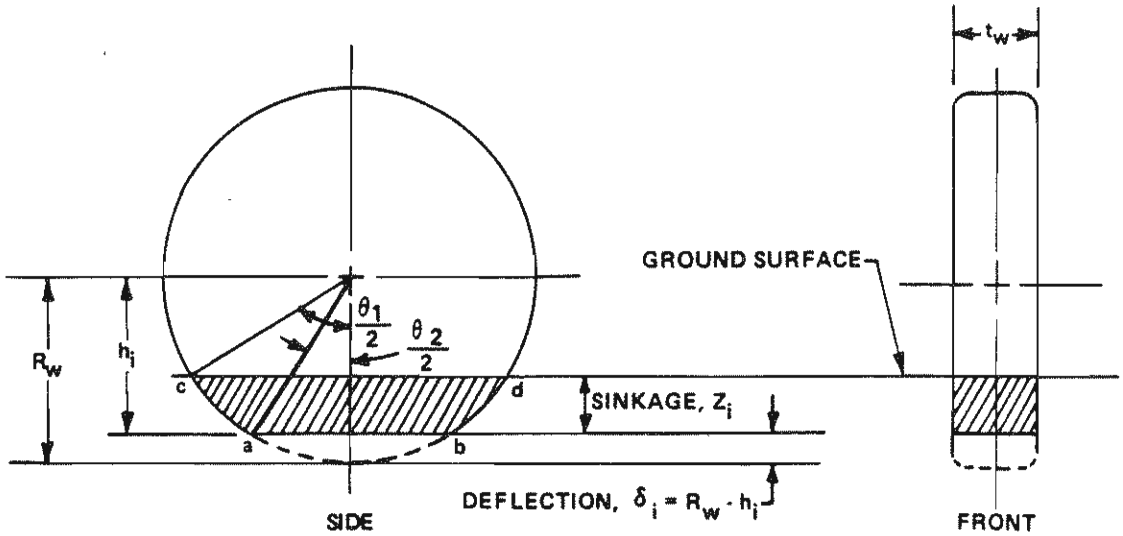

Figure 6. Tire/soil interface areas.

For a deflected tire that has sunk Z_i inches into the soil, the area of the tire sidewall in contact with the ground is determined by subtracting the area of the segment associated with the chord ab from the area of the segment formed by the chord cd for an undeflected tire of radius R_w, i.e.:

$$A_\Delta = A_{cd} - A_{ab}$$

$$A_{cd} = \frac{1}{2} R_w^2 (\theta_1 - \sin\theta_1) \tag{3}$$

where $\theta_1 = 2\cos^{-1}\left[(h_i - Z_i)/R_w\right]$

R_w = undeflected wheel radius

h_i = rolling radius

Z_i = sinkage

$$A_{ab} = \frac{1}{2} R_w^2 (\theta_2 - \sin\theta_2) \tag{4}$$

where:

$$\theta_2 = 2\cos^{-1}(h_i/R_w)$$

Thus,

$$A_\Delta = \frac{1}{2} R_w^2 \left[(\theta_1 - \sin\theta_1) - (\theta_2 - \sin\theta_2)\right] \tag{5}$$

The frontal tire/ground-contact area is:

$$A_f = t_w \, (Z_i) \tag{6}$$

The projected tire/soil-interface area in the direction of motion, A_p, for a tire sideslipping at an angle of α degrees is:

$$A_p = \left| A_f \cos\alpha \right| + \left| A_s \sin\alpha \right| \tag{7}$$

The motion-resistance force calculated from equation (2) is multiplied by the ratio A_p/A_f to determine the resultant soil plow force for the sideslipping tire:

$$F_{plow_i} = F_{MRi} \left(\frac{A_{pi}}{A_{f_i}} \right) \tag{8}$$

The components of the resultant soil plow force in the x and y directions of the wheel coordinate system are:

$$F_{plow\,x_i} = -F_{plow_i} \cos\alpha_i \left(\mathrm{sgn}\, U_{G_i} \right) \tag{9}$$

$$F_{plow\,y_i} = F_{plow_i} \sin\alpha_i \left(\mathrm{sgn}\, F_{S_i} \right) \tag{10}$$

where: U_{G_i} = wheel center forward velocity in the direction parallel to the tire-rigid terrain contact plane

F_{S_i} = tire side force in the tire/terrain contact patch plane perpendicular to the line of intersection of the wheel plane and the ground plane

These tire/soil plow force components are added to the rigid-surface circumferential and side forces of the tire, respectively, in the equations that resolve the tire forces into components along the vehicle-fixed axes.

TIRE MODEL

Purpose of Modifications

The 1976 version of the HVOSM tire model was revised to: (1) reduce the elastic rebound of the tires in the "hardening" spring phase of radial loading, (2) calculate normal load independent of the side force, and (3) assure saturation for an overloaded tire at a sideslip angle of 60 degrees. A detailed discussion of each modification follows.

Simulation of Energy Dissipation for Large Radial Deflections

The HVOSM represents the radial load-deflection characteristic of a tire as a "hardening" spring, as depicted in Figure 7. The hardening spring is used to represent forces generated during excessive radial deflections of the tire and to prevent the wheel center from penetrating the terrain. The hardening-spring simulation is accomplished by use of a rate-increasing factor, λ_T, which is applied whenever the tire deflection is excessive (i.e., $>\sigma_T$).

Several application runs of the HVOSM by MCI in which the tire deflection went into the range of the hardening spring (i.e., deflection$\gg\sigma_T$) were found to produce excessive elastic rebound of the tire. This excessive rebound does not appear to be representative of the real world in cases where energy is dissipated in deforming the rim of the wheel. Therefore, the logic was revised to reduce the elastic rebound of the tires in the hardening phase of radial loading. Energy dissipation of the hardening spring is simulated by implementing logic that applies the rate-increasing factor (λ_T) only during compression of the tire. This modification produces "plastic" load-deflection properties for the hardening phase of the deflection, as depicted in Figure 8.

The tire radial force is controlled by the following logic implemented in subroutine GCP:

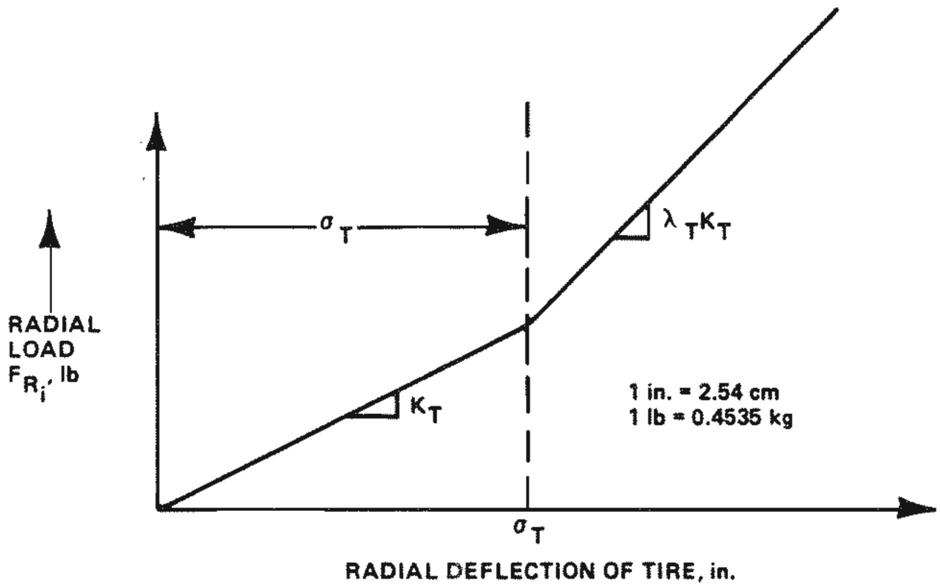

Figure 7. Radial load-deflection characteristic of a tire (1976 version).

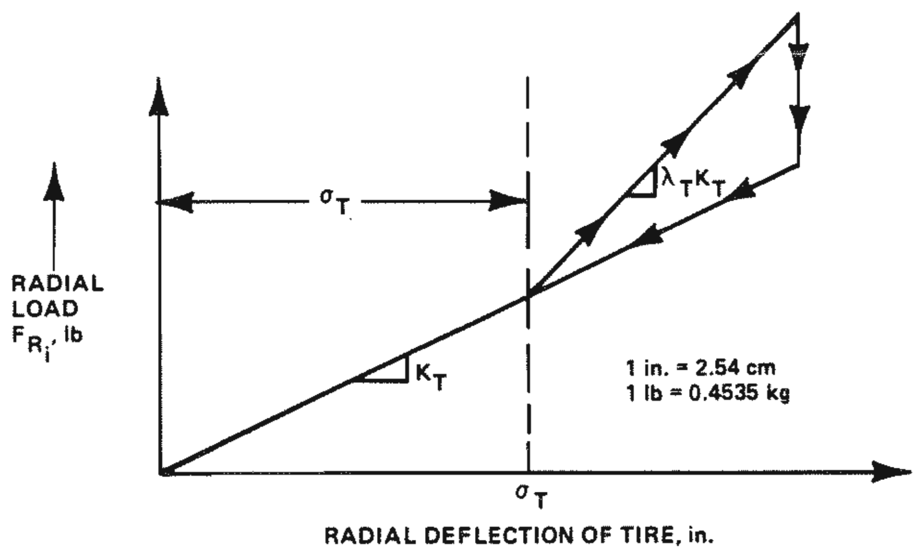

Figure 8. Modified radial load-deflection characteristic of a tire.

$$F_{R_i} = \begin{cases} 0, \ for \ (R_W - h_i) = 0 \\ K_T \ (R_W - h_i), \ for \ 0 < (R_W - h_i) < \sigma_T \\ K_T \left[\lambda_T (R_W - h_i) - (\lambda_T - 1) \ \sigma_T\right], for \ \sigma_T \leqslant (R_W - h_i) \\ K_T \ (R_W - h_i) \ for \ \sigma_T \leqslant (R_W - h_i) \\ \qquad and \ (R_W - h_i) < (R_W - h_i)_{LAST} \end{cases} \tag{11}$$

Calculation of Normal Load

The expression for the calculation of tire loading perpendicular to the local terrain was revised to make the normal load (F'_R) independent of the side force (F_S) as follows:

Previous: $$F'_R = (F_R - F_S \ \sin \phi_{CG}) \ \sec \phi_{CG} \tag{12}$$

Revised: $$F'_R = \begin{cases} F_R \ \sec \ \phi_{CG} & for \ \phi_{CG} < 84.3^\circ \\ F_R \times 10 & \phi_{CG} \geqslant 84.3^\circ \end{cases} \tag{13}$$

where:

F'_R	=	Tire normal load
F_R	=	Tire radial load
F_S	=	Tire side force
ϕ_{CG}	=	Tire camber angle relative to tire/terrain contact plane

The previous analytical approach was based on the assumption that the tire load deflection was directional, in the plane of the wheel, and that the component of F_S that acted along the wheel plane altered the radial force and, therefore, the normal force. However, difficulties were encountered by MCI in achieving realistic predictions of rollover responses which appeared related to the increases in the tire normal load caused by the combination of a large camber angle and the resulting side force. The need for the modification becomes apparent at large roll angles, where the original relationship clearly can produce unrealistically large values of normal load when the side force is negative and the camber angle approaches 90 degrees.

Since the tire exerts a resultant force, F'_R , perpendicular to the terrain contact patch, the assumption that the side force, F_S , in the plane of the contact patch can alter the magnitude of the normal force appears unfounded (see Figure 9). Therefore, the equation for the calculation of the tire normal force (F'_R) was revised to make the normal load independent of the side force.

Calculation of Side Forces for Overloaded Tires

The general analytical approach for the calculation of side forces in the HVOSM tire model was to adapt the approach of Radt and Milliken[18] (i.e., application of a nondimensional slip-angle variable and "friction circle" concept) with modifications to approximate the effects of camber and load changes. (For more detailed discussions, refer to the work of McHenry _et al._[19] and McHenry[20].)

The resulting equation governing the side-force characteristics for the entire range of slip and camber angles is (Figure 10):

$$f(\bar{\beta}_i) = \frac{F_{S_i}}{(F_{S_i})_{max}} = \bar{\beta}_i - \frac{1}{3}\bar{\beta}_i\,|\bar{\beta}_i| + \frac{1}{27}\bar{\beta}_i^3 \tag{14}$$

and

$$\bar{\beta}_i = \left(\frac{A_1 F'_{R_i}(F'_{R_i} - A_2) - A_0 A_2}{A_2 (F_{S_i})_{max}}\right) \cdot \times \left(\arctan\frac{v_{G_i}}{|u_{G_i}|} - (1\ \mathrm{sgn}\ u_{G_i})\,\psi'_i + \beta'_i\right) \tag{15}$$

18. Radt, H.S. and Milliken, W.F., "Motions of Skidding Automobiles," Society of Automotive Engineers, Inc., Paper No. 205A, June 1960.
19. McHenry, R.R., DeLeys, N.J., and Segal, D.J., "Determination of Physical Criteria for Roadside Energy Conversion Systems," Calspan Corporation, Report No. VJ-2251-V-1, Contract No. CPR-11-3988, July 1967.
20. McHenry, R.R., "An Analysis of the Dynamics of Automobiles During Simultaneous Cornering and Ride Motions," Institute of Mechanical Engineers, Paper No. 3, Symposium--Handling of Vehicles under Emergency Conditions, 1969.

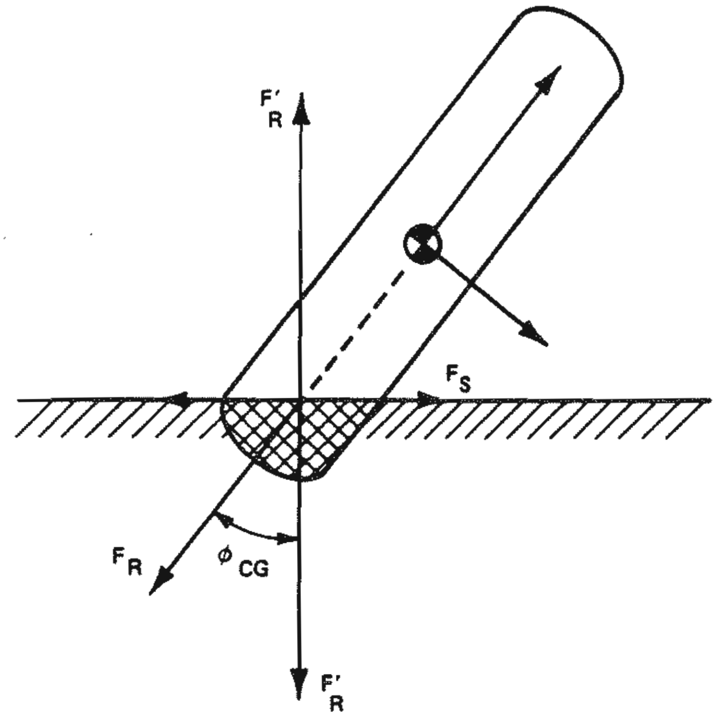

Figure 9. Tire loading normal to the ground contact patch.

$$f(\bar{\beta}) = \begin{cases} \bar{\beta} - \frac{1}{3}\bar{\beta}|\bar{\beta}| + \frac{1}{27}\bar{\beta}^3, & \text{for } |\bar{\beta}| < 3 \\ 1, & \text{for } 3 \leqslant |\bar{\beta}| \end{cases}$$

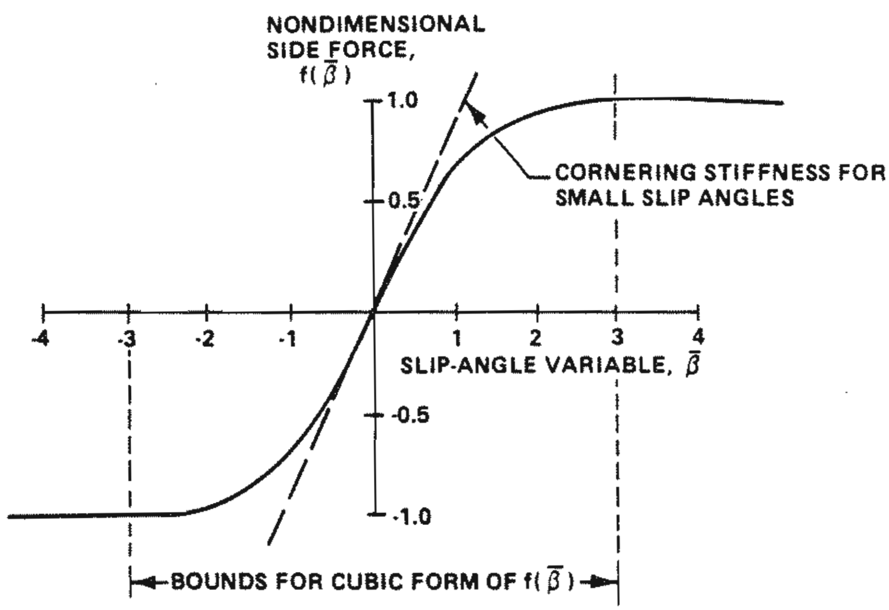

Figure 10. Nondimensional tire side-force curve.

For tire loading in excess of $\Omega_T A_2$, the fitted parabolic curves governing the small-angle cornering and camber stiffness are abandoned, and the side-force properties in the original form of HVOSM were treated as being independent of tire loading. The logic for the side-force properties during tire overload was intended to avoid an artificial reversal of the slip-angle forces (i.e., the fitted parabolic relationships are not limited to positive values; see Figure 11).

The equation governing the side-force characteristics for the overload conditions (i.e., $F'_{R_i} > \Omega_2 A_2$) is as follows:

$$\bar{\beta}_i = \left[\frac{A_1 A_2 \Omega_T(\Omega_T - 1) - A_0}{\sqrt{\mu^2 (F'_{R_i})^2 - F^2_{C_i}}} \right] \left[\arctan \frac{v_{G_i}}{|u_{G_i}|} + \beta'_i - (1 \operatorname{sgn} u_{G_i}) \psi'_i \right] \qquad (16)$$

where:

$$\beta'_i = \left[\frac{A_2 A_3 \Omega_T (A_4 - \Omega_T A_2)}{A_4 \left[A_1 A_2 \Omega_T (\Omega_T - 1) - A_0 \right]} \right] \left[\phi_{CG_i} - \frac{2}{\pi} \phi_{CG_i} \left| \phi_{CG_i} \right| \right] \qquad (17)$$

MCI encountered problems with the overload-condition logic in simulations of vehicle rollovers in which overloaded tires did not develop the full friction force at a slip angle of 90 degrees. For slip angles in the range of 20 to 90 degrees, the actual side-force characteristics are not known, but the full friction force logically must be developed somewhere between 20 and 90 degrees.

The problem with achieving saturation for an overloaded tire at large slip angles is related to the variation of the effective cornering stiffness for small slip angles. As the normal load increases beyond $A_2/2$, the effective cornering stiffness decreases; therefore, it takes a greater slip angle to achieve saturation (i.e., for $f(\bar{\beta})$ to equal 1.0), and saturation may not occur by 90 degrees. Figure 12 shows the tire carpet plot of a sample tire used to demonstrate the tire side-force revisions; however, it does not represent the tires used on the vehicles in this study. Note in Figure 12, which is based on the original form of the HVOSM tire model, that, at 7,400 lb

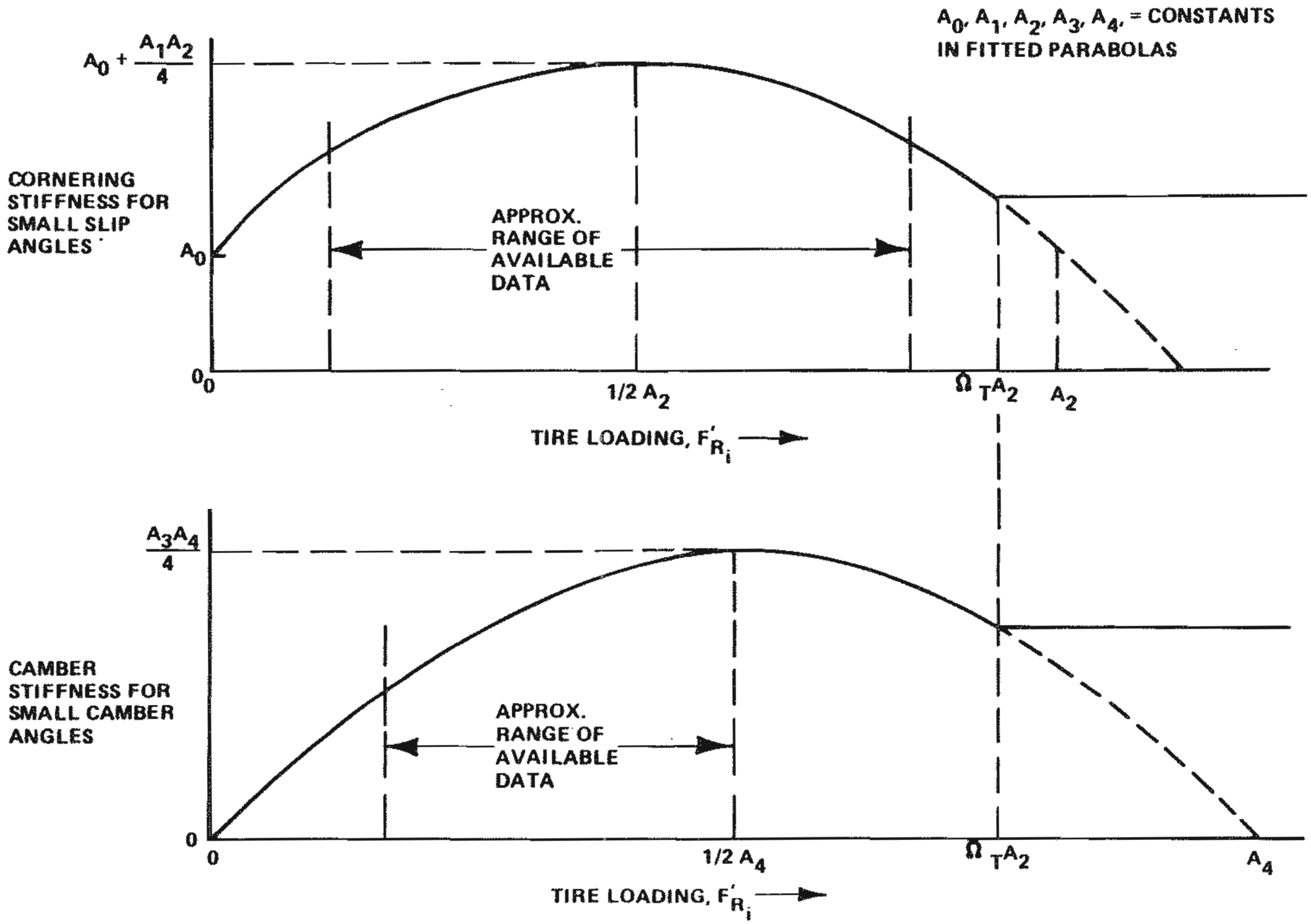

Figure 11. Simulated variation of small-angle cornering and camber stiffness with loading normal to tire/terrain contact patch.

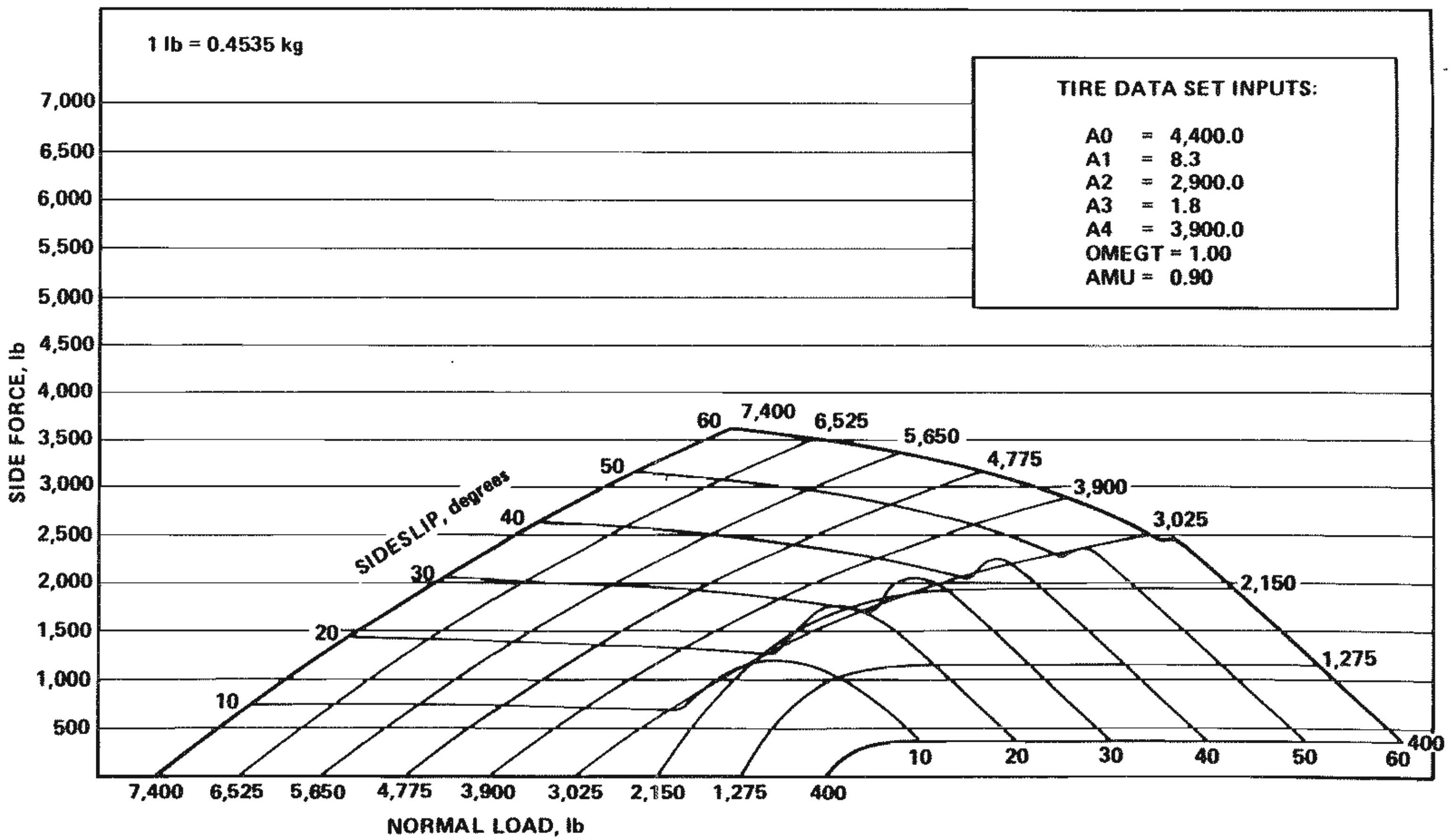

Figure 12. Tire carpet plot of sample tire data (1976 version of model).

(3,356 kg) of normal load and a 60-degree sideslip angle, only 3,600 lb (1,633 kg) of side force is developed (i.e., only a 54% utilization of the available friction).

Intuitively, it would appear that, for slip angles greater than 60 degrees, the full saturation of the tire side forces must be achieved (i.e., tires begin marking, indicating saturation, at approximately 20 degrees of sideslip). Therefore, modifications were made to the HVOSM tire model to assure saturation for an overloaded tire at a sideslip angle of 60 degrees.

The equations for the revised logic are as follows:

Let the sideslip angle for wheel i (equal to the terms in the second bracket of equation (16)) be designated as β_i. If the sideslip angle is greater than 30 degrees and the nondimensional slip-angle variable $\bar{\beta}_i$ is not saturated (i.e., $\bar{\beta}_i < 3.0$), the following adjustment to $\bar{\beta}_i$ is made:

$$\bar{\beta}_i = \left[0.5236 \left| \frac{\bar{\beta}_i}{\beta_i} \right| + \left(3.1 - 0.5236 \left| \frac{\bar{\beta}_i}{\beta_i} \right| \right) \left(\frac{|\beta_i| - 0.5236}{0.5236} \right) \right] \operatorname{sgn} \bar{\beta}_i \tag{18}$$

If the absolute value of the adjusted $\bar{\beta}_i$ is less than the absolute value of the unadjusted $\bar{\beta}_i$, the latter is taken as the current value for $\bar{\beta}_i$. This procedure assures that the side force saturates at 60 degrees of sideslip, using a transition zone between 30 and 60 degrees to avoid step discontinuities.

Figure 13 illustrates results obtained with the modified version of the HVOSM tire model for the same sample data set used in Figure 12 and shows that full tire saturation is made to occur at 60 degrees of sideslip. The adjustment of the tire side forces in the sideslip-angle range between 30 degrees and 60 degrees reflects a simplistic approach toward achieving full saturation by 60 degrees of sideslip. However, until a wider range of real-world tire data becomes available for sideslips greater than 30 degrees and loads greater than 2,500 lb (1,134 kg), a more elaborate and sophisticated form of transition cannot be justified.

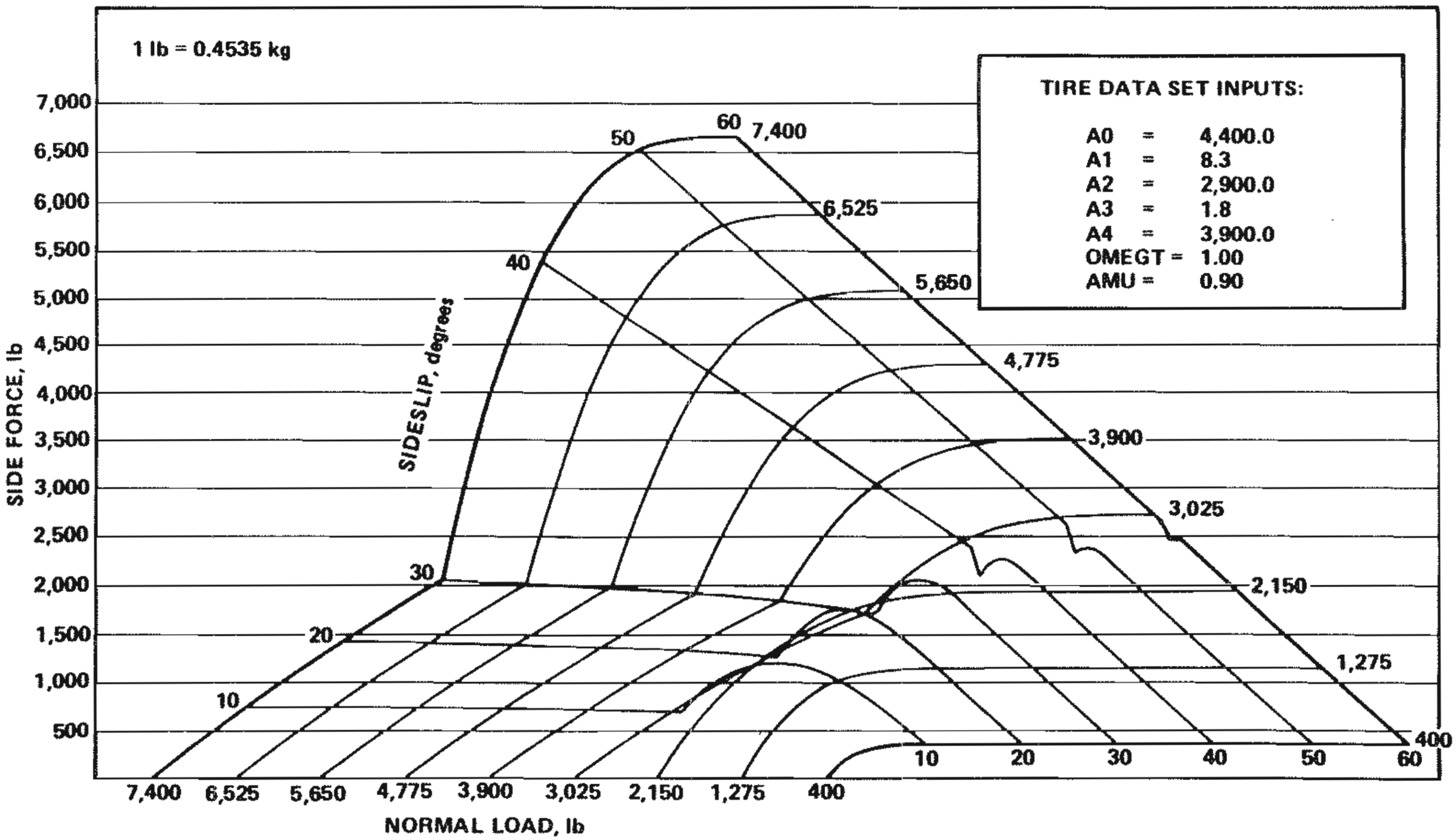

Figure 13. Tire carpet plot of sample tire data (revised model).

TIRE-SIDEWALL CONTACT MODEL

The curb-impact option in the computer program was extended by MCI to include the ability to simulate tire-sidewall contact forces[21]. This modification was prompted by a recent HVOSM simulation study of curb impacts.[22] The simulation results compared reasonably well with actual data for high-speed, large-approach-angle configurations but were considered unacceptable for low-speed, shallow-approach-angle conditions.

The HVOSM simulation of tire forces during curb contacts has remained unchanged since 1967[19] with the minor exception that the maximum number of curb slopes was extended from three to six in 1974.[23] Each vehicle tire is represented by a single, thin disc that generates forces primarily in the plane of the wheel. The thin-disc representation of a tire generates forces perpendicular to the wheel plane (i.e., side forces) only through the mechanisms of (1) combined slip and camber angles and (2) components of the tire load normal to the local terrain. The points of application of side forces determine the corresponding moments about the kingpin axes that act on the simulated steering system of the vehicle.

An important aspect of a shallow-angle traversal of a pavement/shoulder dropoff is the relatively large side force required to overcome the contact force produced by scrubbing of the tire sidewall on the pavement edge. (See Figure 14.) When the pavement edge is mounted, the sudden release of the scrubbing contact force creates an unbalanced side force toward the roadway and also tends to increase the already excessive steer angle by removing resistance to driver-input torque applied at the steering wheel. The existing form of HVOSM was extended to include an approximation of the indicated scrubbing contact force and of steering-wheel torque inputs, as opposed to position inputs, by the driver.

---

21. McHenry, B.G., "Final Report on the Investigation of Pavement/Shoulder Dropoffs," Contract No. DTFH61-80-C-00146, November 1982.
22. McHenry, R.R., McHenry, B.G., and Glennon, J.C., "Follow-up HVOSM Studies of Highway Curb Impacts," Contract No. DOT-FH-11-9575, March 1981.
23. Olson, R.M. et al., "Effect of Curb Geometry and Location on Vehicle Behavior," Transportation Research Board, National Cooperative Highway Research Program, Report No. 150, Washington, 1974.

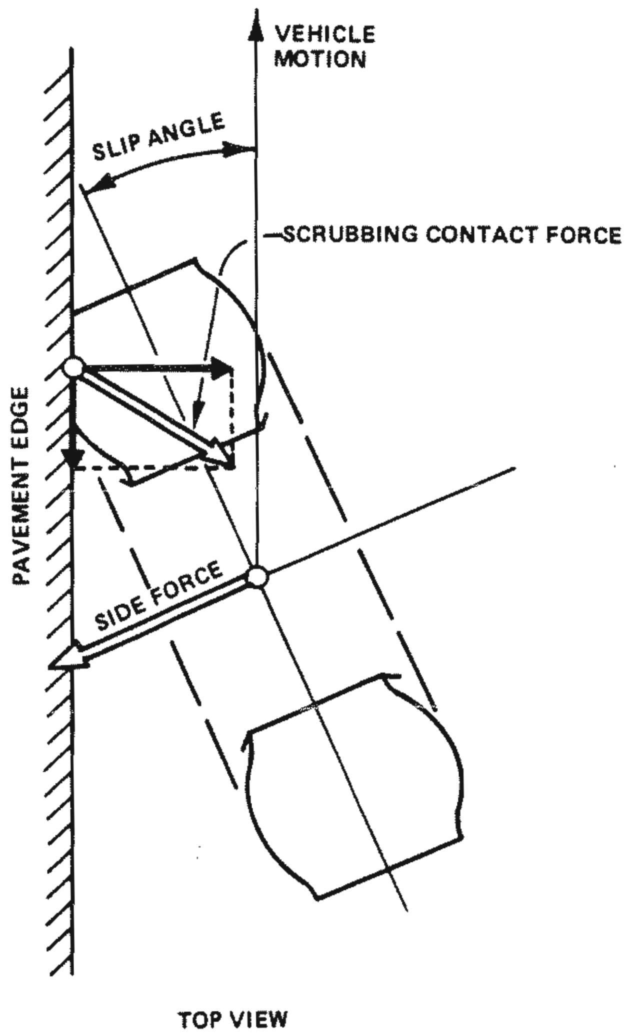

Figure 14. Scrubbing contact in shallow-angle approach to a pavement edge.

The existing thin-disc representation of the tire is illustrated by the left-hand portion of Figure 15. Tire forces are represented by a series of radial springs distributed at 4-degree intervals around the tire. The elastic forces generated in these springs are scanned and summed at fixed intervals by the computer program. The tire sidewall contact forces are approximated in a similar manner through the use of discrete points (or "springs"), with elastic lateral load-deflection proporties, on the tire sidewalls adjacent to the existing radial springs. The positions of these lateral springs are illustrated in the right-hand portion of Figure 15 and in Figure 16.

The analytical approach used by MCI was selected with a view toward minimizing the extent of related programming changes. The explanation of this approach is necessarily presented in the terminology used in HVOSM. These terms are briefly defined and described here; for a more detailed discussion, the reader is referred to the documentation of the program development.[24]

The analysis of tire contact forces in curb impacts uses three coordinate systems: a space-fixed coordinate system; a vehicle-fixed coordinate system; and a wheel-fixed coordinate system. For example, in the space-fixed coordinate system, the x-axis represents distance along the roadway (positive forward), the y-axis represents distance across the roadway (positive to the right), and the z-axis represents elevation (positive downward). In the HVOSM program, the matrix $\|A_j\|$ is used to transform the coordinates of a point j on the circumference of wheel i into the vehicle-fixed coordinate system. This matrix corresponds to the sequence ϕ_i , ψ_i , θ_j , where:

ϕ_i = camber angle of wheel i ,
ψ_i = steer angle of wheel i, and
θ_j = angular position of point j .

24. McHenry, R.R. and Deleys, N.J., "Automotive Dynamics--A Computer Simulation of Three-Dimensional Motions for Use in Studies of Braking Systems and of the Driving Task," Calspan Corporation, Report No. VJ-2251-V-7, Contract No. CPR-11-3988, August 1970.

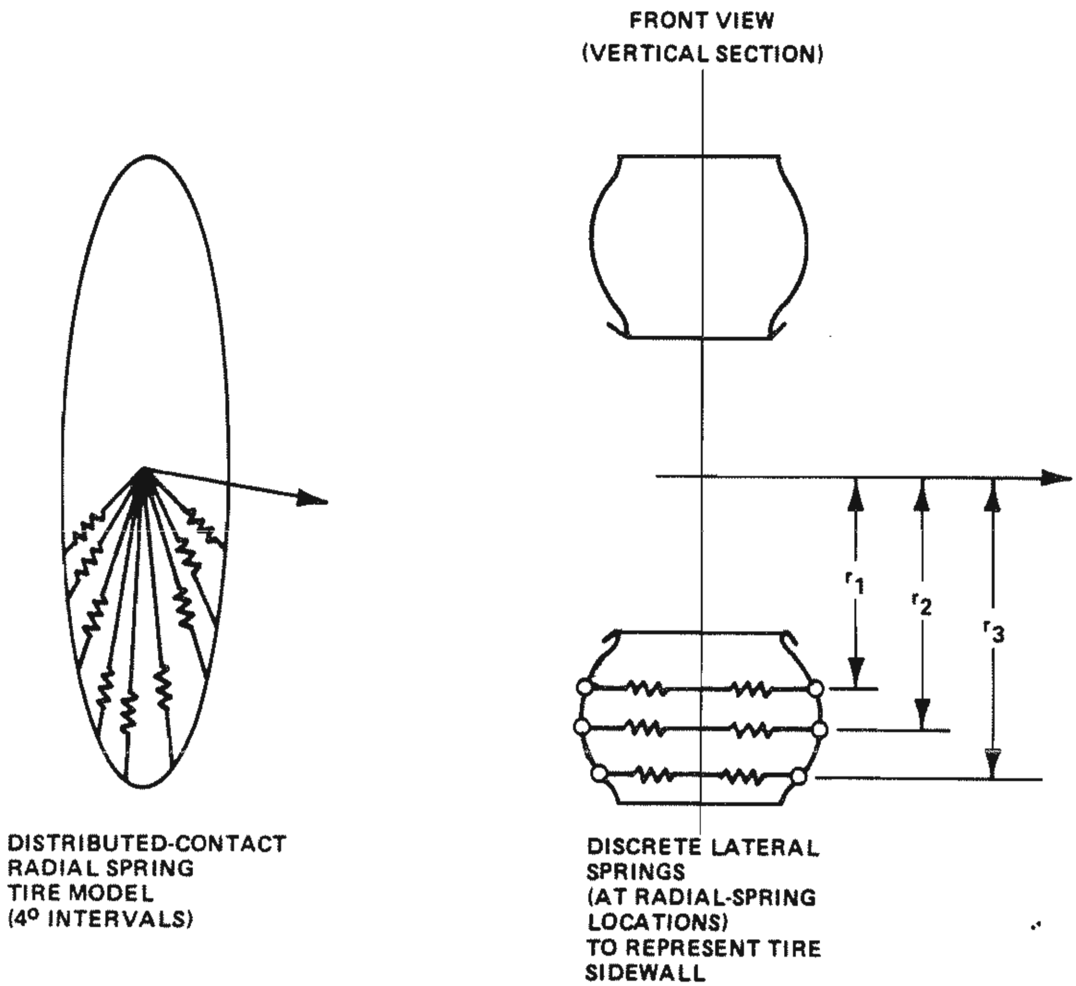

Figure 15. Tire models for generating radial and sidewall contact forces.

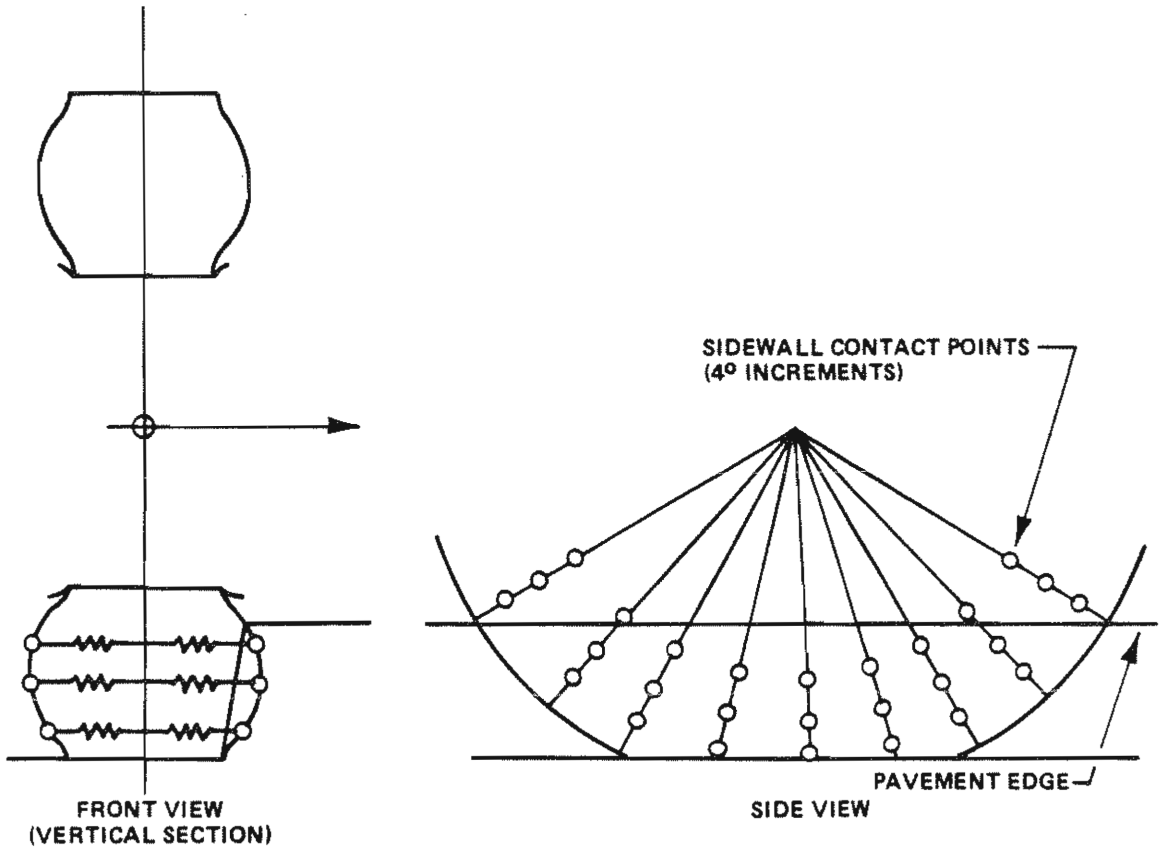

Figure 16. Sidewall contact with pavement edge.

Similarly, a matrix $\| A \|$ is used to transform the vehicle-fixed coordinates of $\| A_j \|$ into space-fixed coordinates. A matrix $\| B \|$ is defined as $\| A \| \cdot \| A_j \|$ and used to transform points on the circumference of wheel i directly into the space-fixed coordinate system. Thus, the space coordinates of point on the periphery of the wheel disc are obtained as:

$$\begin{Vmatrix} X'_j \\ Y'_j \\ Z'_j \end{Vmatrix} = \begin{Vmatrix} X'_i \\ Y'_i \\ Z'_i \end{Vmatrix} + \| B \| \cdot \begin{Vmatrix} 0 \\ 0 \\ h'_j \end{Vmatrix} \tag{19}$$

where: X'_i, Y'_i, Z'_i = the coordinates in space of the center of wheel i,

h'_j = the radial distance, in the wheel plane, to the point of interest.

Equation (19) is used in the existing model to determine what portion of the tire is in contact with the ground.

A determination of the portion of the sidewall in contact with the pavement/shoulder dropoff can be obtained from additional solutions of equation (19) with the following substitutions in the column matrix for the wheel:

$$\begin{Vmatrix} X'_j \\ Y'_j \\ Z'_j \end{Vmatrix} = \begin{Vmatrix} X'_i \\ Y'_i \\ Z'_i \end{Vmatrix} + \| B \| \cdot \begin{Vmatrix} 0 \\ y_n \\ r_n \end{Vmatrix} \tag{20}$$

where: n = the number of points defining the sidewall, and

y_n = one-half of the tire width at radius r_n.

If the tire sidewall is in contact with the dropoff (Figure 16), the components of the sidewall contact forces that are generated are calculated by the equations presented below.

The force occurring in a sidewall-spring contact is defined as:

$$FTSWP = \frac{-\delta_{SW}\,(SWKST)\ \text{sign}(YSW - YWP)}{B_{22}\ \sin\phi_{c_i} - B_{32}\ \cos\phi_{c_i}} \tag{21}$$

where: $\delta_{SW} = \begin{cases} WSIGT & \text{for } |YSW - YWP| \geq WSIGT \\ |YSW - YWP| & \phantom{\text{for }} |YSW - YWP| < WSIGT \end{cases}$

$WSIGT$	=	sidewall point deflection at which saturation occurs (input)
YSW	=	distance from wheel centerline to sidewall point
YWP	=	calculated distance from wheel centerline to the curb face
B_{22}, B_{32}	=	components of B matrix defined above
ϕ_{c_i}	=	i^{th} curb slope angle
$SWKST$	=	sidewall point load-deflection rate

The X, Y, and Z components of the sidewall/curb face contact force in space-fixed coordinates are determined by:

$$\begin{aligned} F_{X_{SWP}} &= -\,FTSWP\ (AMU)\,(AMUC)\,(SWMU) \\ F_{Y_{SWP}} &= FTSWP\,(\sin\phi_{c_i}) \\ F_{Z_{SWP}} &= -\,FTSWP\,(\cos\phi_{c_i}) \end{aligned} \tag{22}$$

where: AMU	=	tire/terrain friction coefficient
AMUC	=	curb friction-coefficient multiplier
SWMU	=	sidewall point friction-coefficient multiplier

Finally, these forces are translated to vehicle-fixed coordinates:

$$\begin{bmatrix} F_{X_{SWU}} \\ F_{Y_{SWU}} \\ F_{Z_{SWU}} \end{bmatrix} = \begin{bmatrix} A^T \end{bmatrix} \begin{bmatrix} F_{X_{SWP}} \\ F_{Y_{SWP}} \\ F_{Z_{SWP}} \end{bmatrix} \tag{23}$$

The forces and moments on wheel i that are produced by the individual contact points are added directly to the existing summations in subroutines TIRFRC, UMOMNT, and DAUX in the equations of motion for the steering system and for the vehicle equations of motion.

During the implementation of the tire-sidewall contact option, a developmental version of a variable-torque path-following (VTPF) driver model was also incorporated into the HVOSM.[21]

Prior to this addition, the simulation of impacts with curb-like obstacles (i.e., pavement/shoulder dropoffs) could be performed only in a "hands-off" steering mode. The use of either the input steer tables or path-following driver model was abandoned, and a steering-system degree-of-freedom routine was activated once a simulated tire came into contact with a curb. The steering-system degree-of-freedom routine included the simulation of external forces, such as aligning torques and the effects of terrain irregularities (i.e., curbs), in the determination of the front-wheel steer activity.

The VTPF was incorporated into HVOSM to give the user an alternative to the "hands-off" steering mode. The VTPF driver model utilizes the enhancements made to the vehicle-dynamics driver model, including:

(1) A "wagon-tongue" type of guidance algorithm which calculates a driver-applied front-wheel steering torque proportional to the path error at a point on a forward extension of the x-axis of the vehicle, relative to the desired path.

(2) An interface within HVOSM to convert the variable inputs of standard roadway geometric path descriptors to a second-order polynomial definition of the desired path.

(3) Inclusion of a variable input "neuro-muscular" filter within the HVOSM driver model which permits the simulation of first-order effects of the neurological and muscular systems of a human driver.

(4) A varible input damping term and closed-loop amplitude limits on the steering-system activity.

A discussion of the above modifications is presented later in this section in the subsection entitled "Driver Model."

The calculated torque from the VTPF driver model is included in the steering-system degree-of-freeom routine to create a path-following mode. The incorporation of this VTPF output into the routine permits simulation of maneuvers such as those used in a pavement/shoulder dropoff, where the driver inputs corrective torque to the steering system during the obstacle contact and the return to the lane of travel. Difficulties were encountered in applications of the VTPF by MCI to evaluate its performance which led to a decision to abandon further attempts to develop this form of closed-loop control.

SPRUNG-MASS GROUND CONTACT MODEL

To simulate terrain contacts by the sprung mass, the terrain-table interpolation routine used for tire contacts has been adapted to detect ground interference of up to 39 points on the sprung mass that may be specified.

Deflections of the vehicle structure are assumed to occur in directions that are perpendicular to the local terrain at the locations of the individual contacts. A coefficient of restitution is applied to the structural deflections to permit the achievement of equilibrium under conditions of static loading. The resultant velocities tangential to the terrain contacts are calculated for the individual points, and friction forces opposing the motions are applied. Load-deflection properties of the points can be either uniform or individually specified.

The rationale for the described analytical approach is based on impulse-momentum considerations. The contact forces prior to the final rest position are generally of a sufficiently short duration to be considered impulsive. Therefore, the specific load-deflection properties of the points are not of critical importance to the generation of appropriate linear and angular impulse magnitudes, as long as realistic geometry for the applied impulsive forces is produced by the point coordinates. Note that the simulated points retain their deformed positions for use in secondary contacts. Subroutine SFORCE first transforms the deflected and undeflected points from vehicle-fixed to space-fixed coordinates. Subroutine INTRP5 is called to find the elevation, slope, and pitch of the terrain at the body point locations in the space-fixed reference frame. If a point is below the ground surface, the deflection is calculated from:

$$\delta_{HP_i} = \frac{Z_{HP_i} - Z_{GHP_i}}{\cos\theta_{GHP_i} \, \cos\phi_{GHP_i}} \tag{24}$$

where: Z_{HP_i} = elevation of body point i

Z_{GHP_i} = terrain elevation at body point i

θ_{GHP_i} = terrain pitch angle at body point i

ϕ_{GHP_i} = terrain camber angle at body point i

If the deflection is greater than the previous maximum deflection for this point, the resultant normal force is calculated:

$$F_{NST_i} = K_{ST_i} \times (\delta_{HP_i}) \tag{25}$$

where: K_{ST_i} = omnidirectional stiffness for body point i

The resultant normal force is adjusted if the deflection is in the restitution range (i.e., if the deflection is within 90% of the previous maximum deflection):

$$F_{NST_i} = 10\, K_{ST_i} \left[\delta_{HP_i} - 0.9 (\delta_{HP_i})_{max} \right] \tag{26}$$

The space-fixed location of the deflected point in the ground plane is determined from:

$$X_{ST_{ip}} = X_{HP_i} - \delta_{HP_i} \cos\phi_{GHP_i} \sin\theta_{GHP_i} \tag{27}$$

$$Y_{ST_{ip}} = Y_{HP_i} + \delta_{HP_i} \sin\phi_{GHP_i} \tag{28}$$

$$Z_{ST_{ip}} = Z_{HP_i} - \delta_{HP_i} \cos\phi_{GHP_i} \cos\theta_{GHP_i} \tag{29}$$

where the assumptions are made that the structure deflects in a direction normal to the ground, and that the ground does not deflect.

After the deflection and normal forces are calculated for each point, the normal forces are summed:

$$\sum F_{NST} = \sum_i F_{NST_i} \tag{30}$$

and the locations of the deflected points are transformed back to vehicle-fixed coordinates:

$$\begin{bmatrix} X_{ST_i} \\ Y_{ST_i} \\ Z_{ST_i} \end{bmatrix} = \begin{bmatrix} A^T \end{bmatrix} \begin{bmatrix} X_{ST_{i_P}} - X'_c \\ Y_{ST_{i_P}} - Y'_c \\ Z_{ST_{i_P}} - Z'_c \end{bmatrix} \tag{31}$$

where A^T is the transpose of the matrix to transform from vehicle-fixed to space-fixed axes. If the sum of the normal forces ($\sum F_{NST}$) is greater than zero, the resultant forces and moments acting on the vehicle are calculated in subroutine RESFRC.

The velocity components of each of the body points are determined and transformed to space-fixed coordinates:

$$\begin{bmatrix} U'_{ST_i} \\ V'_{ST_i} \\ Z'_{ST_i} \end{bmatrix} = \begin{bmatrix} A \end{bmatrix} \begin{bmatrix} U - R(Y_{ST_i}) + Q(Z_{ST_i}) \\ V + R(X_{ST_i}) - P(Z_{ST_i}) \\ W + P(Y_{ST_i}) - Q(X_{ST_i}) \end{bmatrix} \tag{32}$$

The velocity components in the ground plane of each point are calculated from:

$$\begin{bmatrix} V_{GHP_X} \\ \\ V_{GHP_Y} \end{bmatrix} = \begin{bmatrix} \cos\theta_{GHP_i} & 0 & -\sin\theta_{GHP_i} \\ & & \\ \sin\theta_{GHP_i}\,\sin\phi_{GHP_i} & \cos\phi_{GHP_i} & \cos\theta_{GHP_i}\,\sin\phi_{GHP_i} \end{bmatrix} \begin{bmatrix} U'_{ST_i} \\ V'_{ST_i} \\ W'_{ST_i} \end{bmatrix} \tag{33}$$

If the resultant velocity $\left(V_{GHP} = \sqrt{V_{GHP_X}^2 + V_{GHP_Y}^2} \right)$ is greater than 2.5, the resultant friction force is:

$$a = \mu_{HP_i} \times F_{NST_i} \tag{34}$$

where μ_{HP_i} = nominal body/ground contact-friction coefficient

If velocity v_{GHP} is less than the input value ϵ_{HP} (friction nullband), the magnitude of the resultant friction force is adjusted:

$$a = \mu_{HP_i} \times F_{NST_i} \left[\frac{\epsilon_{HP} - v_{GHP}}{\epsilon_{HP}} \right] \tag{35}$$

The resultant space-fixed body-point forces are calculated using equations (36) and (37):

Let
$$a' = - \frac{a}{v_{GHP}} \tag{36}$$

$$\begin{bmatrix} F_{XP_i} \\ F_{YP_i} \\ F_{ZP_i} \end{bmatrix} = \begin{bmatrix} F_{NST_i} & a' v_{GHP_X} & a' v_{GHP_Y} \end{bmatrix} \begin{bmatrix} \cos\phi_{GHP_i} \sin\theta_{GHP_i} & \cos\theta_{GHP_i} & \sin\phi_{GHP_i} \sin\theta_{GHP_i} \\ \sin\phi_{GHP_i} & 0 & \cos\phi_{GHP_i} \\ \cos\theta_{GHP_i} \cos\phi_{GHP_i} & \sin\theta_{GHP_i} & \cos\theta_{GHP_i} \sin\phi_{GHP_i} \end{bmatrix} \tag{37}$$

and then transformed to vehicle-fixed axes:

$$\begin{bmatrix} F_{X_i} \\ F_{Y_i} \\ F_{Z_i} \end{bmatrix} = \begin{bmatrix} A \end{bmatrix}^T \begin{bmatrix} F_{XP_i} \\ F_{YP_i} \\ F_{ZP_i} \end{bmatrix} \tag{38}$$

Finally, the vehicle-fixed body-point forces as well as the calculated moments are summed:

$$\begin{aligned} \Sigma F_{XS} &= \sum_i F_{X_i} \\ \Sigma F_{YS} &= \Sigma F_{Y_i} \\ \Sigma F_{ZS} &= \sum_i F_{Z_i} \end{aligned} \tag{39}$$

$$\begin{aligned} \Sigma N_{\phi S} &= \sum_i (F_{Z_i} \; Y_{ST_i} - F_{Y_i} \; Z_{ST_i}) \\ \Sigma N_{\theta S} &= \sum_i (F_{X_i} \; Z_{ST_i} - F_{Z_i} \; X_{ST_i}) \\ \Sigma N_{\psi S} &= \sum_i (F_{Y_i} \; X_{ST_i} - F_{X_i} \; Y_{ST_i}) \end{aligned} \tag{40}$$

Path-Following Option

New routines were furnished by MCI to incorporate a "wagon-tongue" type of steering control and the definition of a desired path in the current version of the computer program.[25] The "wagon-tongue" algorithm calculates a front-wheel steer angle that is directly proportional to the error of a point on a forward projection of the vehicle x-axis relative to the desired path. The minimum distance from the projected point to the desired path is calculated in subroutine PROBE. If the absolute value of the distance, $|\epsilon_i|$, is less than or equal to the input value P_{min} (the nullband for the error correction), the steer angle is determined by:

$$\psi_F = -K_Q \left[\frac{\epsilon_i - \epsilon_{i\,(LAST)}}{D_{PRB}} \right] \tag{41}$$

where: K_Q = steer velocity damping term

ϵ_i = error or distance from desired path

D_{PRB} = time between probe samples

For $|\epsilon_i| > P_{min}$:

$$\psi_F = -K_P \left(|\epsilon_i| - P_{min} \right) \mathrm{sgn}(\epsilon_i) - K_Q \left[\frac{\epsilon_i - \epsilon_{i\,(LAST)}}{D_{PRB}} \right] \tag{42}$$

where K_P = steer correction factor.

If the new steer angle, ψ_F, increases and results in a comfort factor that exceeds the maximum acceptable comfort factor, the steer angle is reset to its previous value, i.e., if

$$\begin{aligned} |CMF_{A1}| &> P_{max} \\ \psi_F &= \psi_{F\,LAST} \,. \end{aligned} \tag{43}$$

---

25. Glennon, J.C., McHenry, B.G., and Neuman, T.R., "HVOSM Studies of Highway Cross Slope Design," Contract No. DOT-FH-11-9575, October 1983.

This check prevents any increase in the steer angle if the comfort factor becomes too high.

A path-generating routine to create a desired path of X,Y data pairs from standard roadway geometric descriptors was added to HVOSM as an enhancement of the current driver model. Subroutine SETD produces a Degree of Curve set from a gross description of the desired path such that a set of equally spaced points describing the path may be computed. The Degree of Curve information is passed to subroutine PATH, which initializes the first X,Y data point and computes the initial tangent from a specified heading angle. Subroutine PATHG is then called to evaluate the path descriptors from the recursion relations described below. For a given arbitrary point and the path descriptors, subroutine PROBE determines the sector in which the point lies, computes the minimum distance to the desired curve, and computes the point of closest approach. The output subroutine PTHOUT produces a printout of the calculated path descriptors as well as important variables of the selected driver-model options.

The path generated is defined as a curved roadway consisting of a sequence of straight-line segments and circular arcs where the continuity of the tangent has been preserved at the junction of the various segments.

The basic geometry of two adjoining segments is shown in Figure 17, where:

X_n, Y_n	=	location of point n on the roadway,
ψ_n	=	direction of path (tangent) at point n,
θ_n	=	direction of chord, directed toward point $n+1$,
ϕ_n	=	subtended angle of arc from point n to point $n+1$,
Δ_n	=	length of chord from point n to point $n+1$,
r_n	=	radius of curvature of path from point n to point $n+1$,
D_n	=	Degree of Curve, defining arc from point n to point $n+1$.

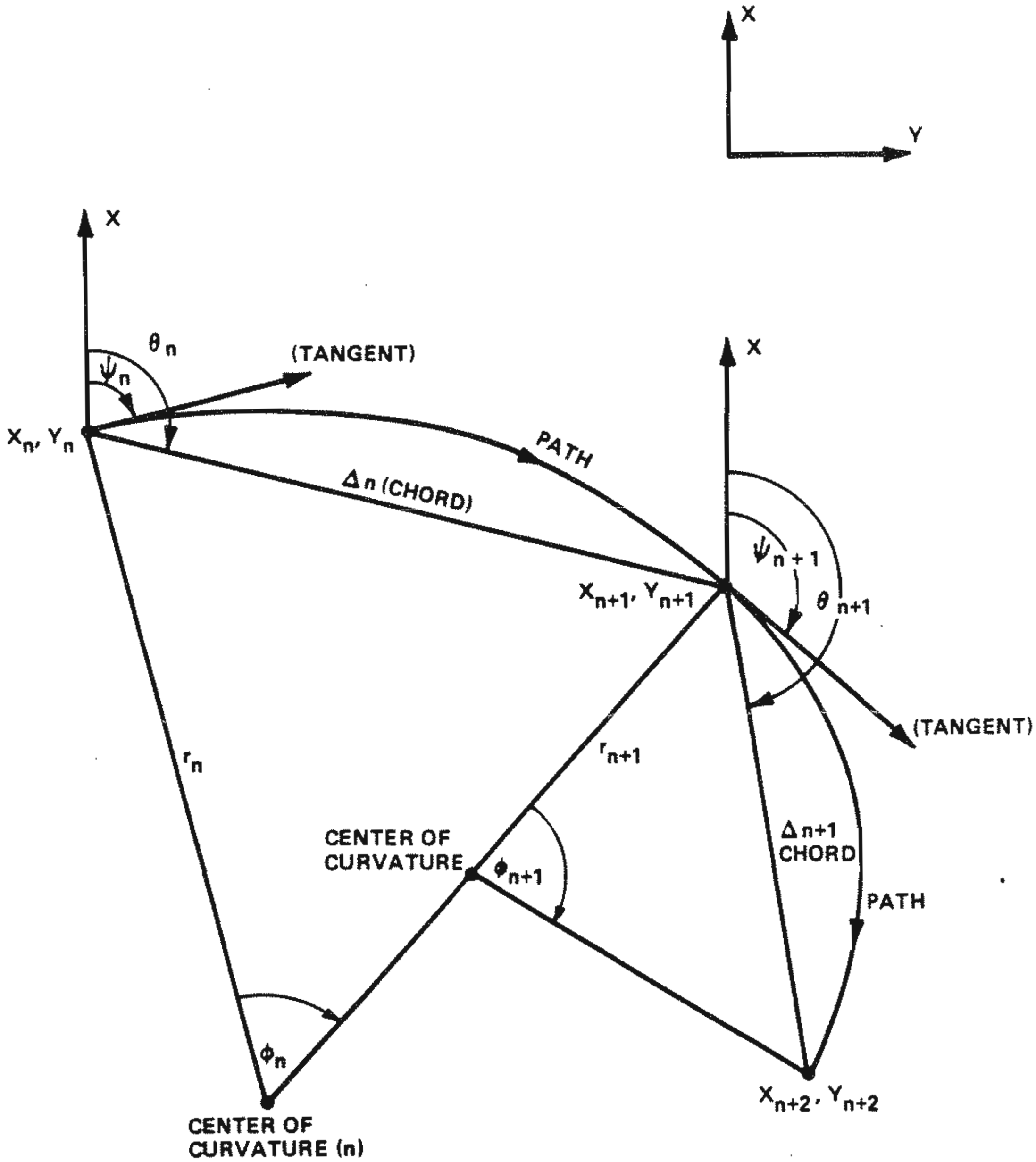

Figure 17. Basic geometry of two adjoining segments.

It is noted that the center of curvature for the arc from point $n+1$ to point $n+2$ lies on the line from point $n+1$ to the center of curvature of the arc from point n to point $n+1$. This assures that the tangent vector to the path is continuous at points where the Degree of Curve changes.

The Degree of Curve is the angle subtended at the center of curvature by an arc 100 ft (30.5 m) in length. The radius of curvature, r_n, is determined from the Degree of Curve, D_n, by:

$$\frac{1}{r_n} = \frac{(\pi \times D_n)}{(180 \times 100)} = \frac{D_n}{5729.58} \tag{44}$$

The subtended angle ϕ_n equals:

$$\phi_n = \frac{2 \times \sin^{-1}(\pi \times D_n \times \Delta_n)}{2 \times 180 \times 100} = \frac{\sin^{-1}(\pi \times D_n \times \Delta_n)}{18{,}000} \tag{45}$$

From the geometry of Figure 17, we have the following relations:

$$\theta_n = \psi_n + \frac{\phi_n}{2} \tag{46}$$

$$X_{n+1} = X_n + \Delta_n \times \cos\theta_n \tag{47}$$

$$Y_{n+1} = Y_n + \Delta_n \times \sin\theta_n \tag{48}$$

$$\psi_{n+1} = \psi_n + \phi_n \tag{49}$$

The unit tangent vector at point n has the components:

$$\left[\cos\psi_n \, , \; \sin\psi_n\right]$$

Note that the recursion relations are valid for a Degree of Curve of zero. Equation (45) yields a zero value for ϕ_n when D_n is zero; in this case, equation (46) shows that $\theta_n = \psi_n$, and equation (49) shows that $\psi_{n+1} = \psi_n$. These relations are valid for a straight-line path from point n to point $n+1$. For convenience, a sign convention is adopted for the Degree of Curve: A positive value of D_n will produce a positive ϕ_n and, hence, an increasing value of ψ (equation (49)), resulting in a clockwise rotation of the path. A negative value of D_n will produce a counterclockwise rotation of the path (a decreasing value of ψ). That is, a positive value of D_n is assigned to produce a clockwise (to-the-right) curve, and a negative value is assigned to produce a counterclockwise (to-the-left) curve.

A roadway consisting of a series of arcs and/or straight-line segments with a continuous tangent for a smooth transition may be defined by specifying the parameters that follow.

Initial position and heading:

$[X_1, Y_1]$	=	starting point
ψ_1	=	direction of path at starting point (tangent vector)

For each segment for values of n from 1 to $N-1$:

N	=	total number of points ($N-1$) segments,
Δ_n	=	chord length from point n to point $n+1$, and
D_n	=	Degree of Curve for section of path from point n to point $n+1$: D_n is positive if the turn is to the right, D_n is zero for a straight-line segment, and D_n is negative for a turn to the left.

The recursion relations given by equations (45) through (49) may be used to compute the values of all of the parameters describing the geometry. The complete definition of the path may be retained for later use by saving the following:

$[X_n, Y_n]$	=	position of point n ($n=1$ to N)
$[U_n, V_n]$	=	unit tangent at point n ($n=1$ to N)
D_n	=	Degree of Curve for segment from point n to point $n+1$ ($n=1$ to $N-1$).

It is sometimes convenient to assign a value of zero to D_N, which has the effect of extrapolating the path as a straight line from the last point (N) to any point in the direction of the tangent to point N .

To establish the vector geometry of the path, consider the geometry shown in Figure 18, which illustrates the segment of a path from point n to point $n+1$.

Define the following:

T_n	=	the unit tangent (to the path) vector at point n,
N_n	=	the unit normal (to the path) vector at point n,
Z_n	=	a vector from point n to an arbitrary point in the plane of the path,
r_n	=	the radius of curvature of the segment of the path,
d_n	=	the distance (smallest) of the point Z from the path, defined so that, if d_n is positive, the point Z is to the right of the path when the path is traversed in the sense of the tangent vector T, and
D_n	=	the Degree of Curve of the segment.

We then have:

T_n	has the components $[u_n, v_n]$.
N_n	has the components $[-v_n\ u_n]$ and is directed toward the right of the path as it is traversed in the direction of the tangent.
Z_n	has the components $[X-X_n, Y-Y_n]$, where X and Y are the location of Z in the basic reference system.

To determine the distance of an arbitrary point from the path, refer to Figure 18, which shows that the vector from the center of curvature to the point Z is given by:

$$Z_n - r_n N_n \tag{50}$$

The minimum distance to the desired path, since it is a circular arc, is the distance from the point Z to the point of intersection of the vector $Z_n - r_n N_n$ with the arc. Thus:

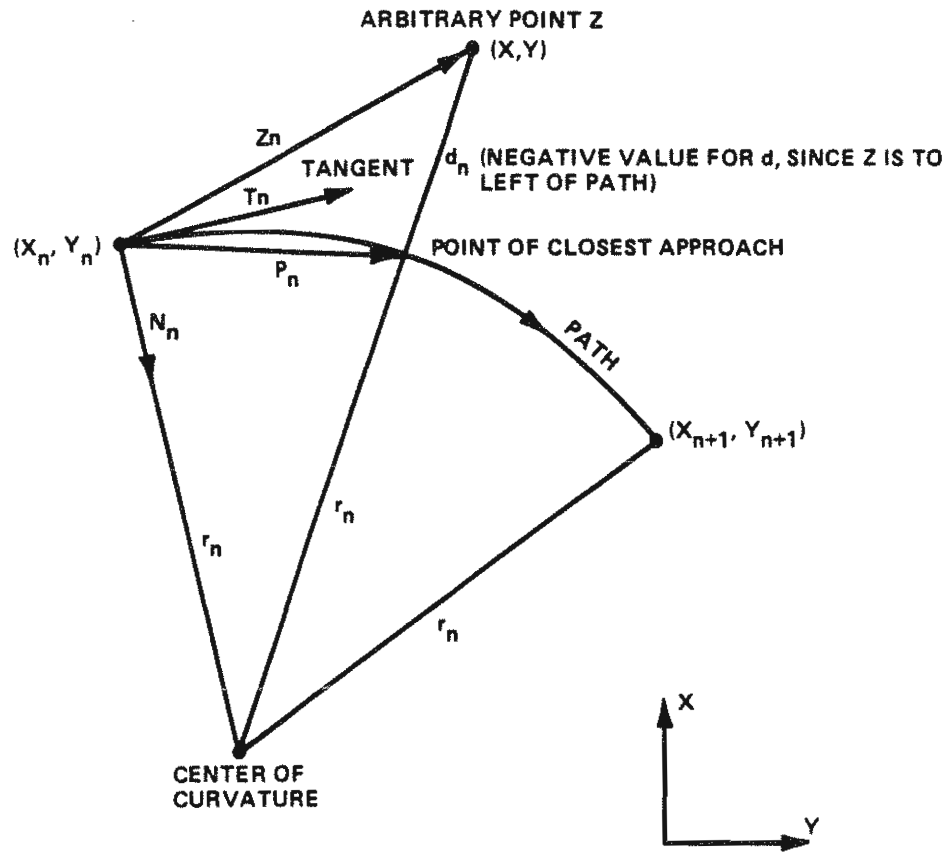

Figure 18. Vector geometry of segment of path from point n to point n+1.

$$d_n = r_n - \left| Z_n - r_n N_n \right| \tag{51}$$

where $|Q|$ indicates the magnitude of a vector Q. Rewriting equation (44) as:

$$\frac{1}{2 r_n} = a = \frac{\pi D_n}{36000} \tag{52}$$

(note that a has the same sign as D_n)

and letting

$$b = N_n \cdot Z_n - a \times Z_n \cdot Z_n \tag{53}$$

where $\cdot$ represents the vector dot product, then d_n is given by

$$d_n = \frac{b}{0.5 + \sqrt{0.25 - ab}} \tag{54}$$

Equation (54) is an exact equation and, thus, is valid even when the Degree of Curve is zero--i.e., when

$$D_n = 0 \;, \quad d_n = b = N_n \cdot Z_n \;.$$

To determine the location of the point of closest approach, P_n, on the arc:

$$P_n = \frac{Z_n - d_n N_n}{1 - 2 a d_n} \tag{55}$$

This formula for P_n is valid as long as Z_n is in the half plane containing the point n. The dividing line of the plane is the line passing through the center of curvature and parallel to the tangent. The formula is valid for all Z_n when the Degree of Curve is zero (the center of curvature is at infinity).

To determine the sector containing an arbitrary point, refer to Figure 19. Using the same notation as employed previously for Figure 18, we see that:

If the dot product $Z_n \cdot T_n$ is positive, the point Z is to the right of the boundary line defined by the normal N_n to the path.

If the dot product $Z_n \cdot T_n$ is negative, the point Z is to the left of the boundary line defined by the normal N_n to the path.

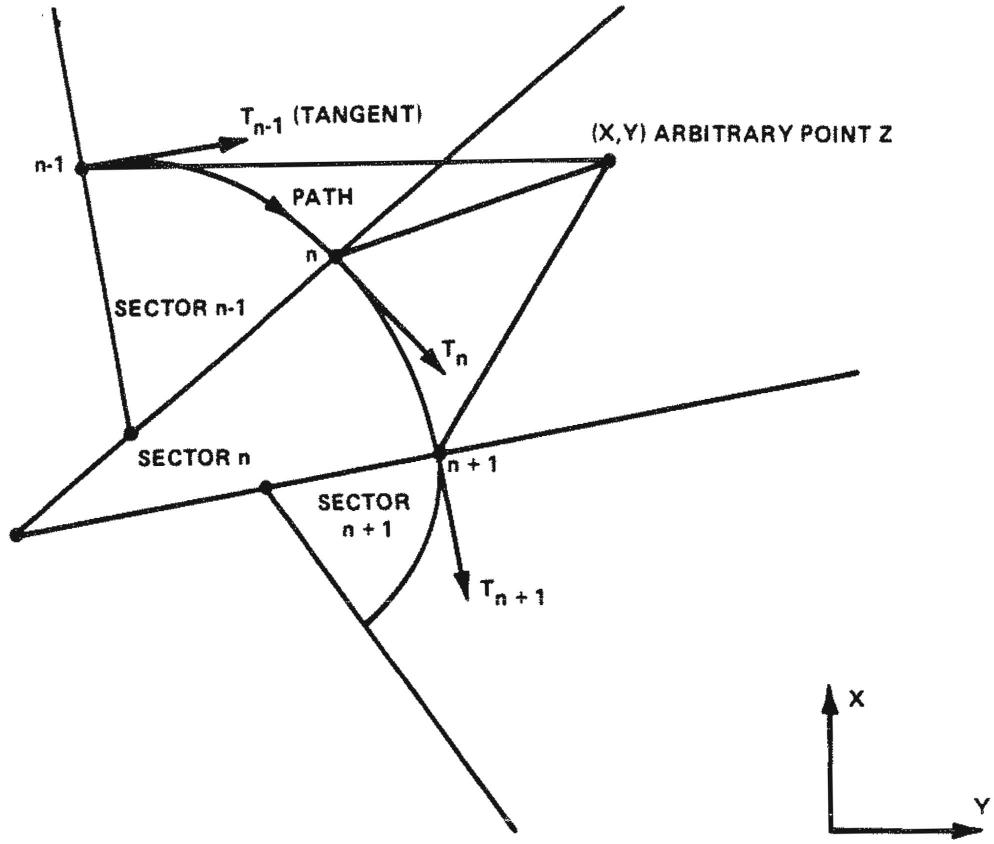

Figure 19. Determination of sector containing arbitrary point.

If the dot product $Z_n \cdot T_n$ is zero, the point Z is on the boundary line defined by the normal N_n to the path.

The above fact gives a simple rule for determining the sector containing the point Z: Find the value of n such that $Z_n \cdot T_n$ is positive for point n and negative for the next point $n+1$. (Recall that Z was evaluated relative to the point n). Explicitly, the dot products are:

$$Z_n \cdot T_n = \left[X - X_n\right] \times U_n + \left[Y - Y_n\right] \times Y_n \quad for\ n=1\ to\ N \tag{56}$$

Regardless of the complexity of the path, if the correct n has been determined, the point z is reasonably close to the path (a small fraction of the radius of curvature); if the next position of z is relatively close to the current position, the proper sector can be determined by testing the dot product for values of $n-1$, n, and $n+1$.

Emergency-Maneuver Control Option

A subroutine called DRIV2 was added to HVOSM by MCI to provide simulation of driver emergency maneuvering. The algorithm was originally developed[21] to simulate the driver recovery maneuver subsequent to remount of a pavement/shoulder-dropoff edge from a tire/pavement-edge srubbing condition. The DRIV2 model is used to accelerate and decelerate changes in the front-wheel steer angle based on user inputs describing driver characteristics.

Subroutine VPOS, which determines the position, orientation, and velocity of the vehicle wheels, calls DRIV2. After t_{PRB} (driver perception/reaction time) seconds have elapsed in the simulation run, DRIV2 executes the equations that follow to accelerate the front-wheel steer velocity to PSIDM (maximum front-wheel steer velocity).

The front-wheel steer velocity at time t is:

$$\dot{\psi}_F = 0.5\,\dot{\psi}_{F_{max}} \left[1 - \cos\left((t - t_{PRB})\,\frac{2\,\ddot{\psi}_{F_{max}}}{\dot{\psi}_{F_{max}}}\right)\right] \tag{57}$$

where: $\dot{\psi}_{F_{max}}$ = maximum front-wheel steer velocity

t_{PRB} = driver perception/reaction time

$\ddot{\psi}_{F_{max}}$ = maximum front-wheel steer acceleration and deceleration

The front-wheel steer velocity remains at $\dot{\psi}_{F_{max}}$ until either: (1) the comfort factor (CMFCG) exceeds the maximum driver discomfort level (PMAX) or (2) the front-wheel steer angle (ψ_F) exceeds the input value for the maximum front-wheel steer angle (PSIMAX). If either (1) or (2) is true, the front-wheel displacement velocity is decelerated back to zero by the relationship:

$$\dot{\psi}_F = \dot{\psi}_{F\,max} - 0.5\,\dot{\psi}_{F\,max}\left[1 - \cos\left((t - t_i)\quad \frac{2\,\ddot{\psi}_{F\,max}}{\dot{\psi}_{F\,max}}\right)\right] \tag{58}$$

where: t_i = initial time of deceleration.

Once the front-wheel steer velocity is decelerated to zero, the front-wheel steer angle will remain constant.

TERRAIN-TABLE ANGLED BOUNDARY SPECIFICATIONS

The angled boundary specifications available through the terrain-table option were modified by MCI to relax the restrictions of the original formulation.[15] This modification allows the user to exercise control over the X' and Y' ranges in which a specific angled boundary occurs, up to a maximum of eight angled boundaries per terrain table. As a result, the angled boundaries may be used, for example, to approximate a curved boundary in the X',Y' plane.

The terrain-table angled boundary option is executed in subroutine INTRP5, where the following interpolation scheme is employed:

1. The highest-numbered terrain table applicable to the wheel is determined by sequentially testing if the wheel is located within the X' and Y' bounds of each table.

2. The particular grid segment within which the wheel is located is determined and the corner points labeled.

3. The angled boundaries are scanned, and the first angled boundary is chosen that passes through the grid segment in which the wheel is located.

When in effect, the terrain-table angled boundary option performs additional tests to determine if the ground-contact coordinates are within the range of a given angled boundary. If they are, the modified program proceeds with the interpolation procedure. If not, the modified program ignores the particular angled boundary and continues the scan of other angled boundaries.

Section 4
HVOSM VERIFICATION

PURPOSE

Prior to application of HVOSM in the analytical study of roadside features, a series of full-scale tests was performed to provide data for evaluating the validity of the modified computer program. The test program included two groups of tests. The first group was performed on flat, rigid pavement to better enable checking that the vehicle characteristics in general were satisfactorily represented by the simulation model input data set. The second group of tests consisted of maneuvers performed on various natural roadside terrains to assess the predictive capability of HVOSM employing the deformable-soil model.

All of the tests were performed on the Calspan Vehicle Experimental Research Facility (VERF) and, with the exception of one test site deemed too hazardous, all tests were performed by a driver in the vehicle.

The HVOSM input data sets used to simulate each of the full-scale tests for verifying the model are listed in card-image format in Appendix A.

TEST VEHICLE AND INSTRUMENTATION

The vehicle used for the full-scale tests was a 1979 Volkswagen Rabbit automobile equipped with a manual transmission. This car, which has front-wheel drive and independent suspensions for both the front and rear wheels, was selected as representative of the small, lightweight class of automobiles which accident data analyses indicate have a high frequency of rollover. In addition, much of the data on the physical properties of the vehicle needed for input to HVOSM were available.

Before preparing the vehicle for test, the "as received" total weight and weight distribution on the front and rear wheels were measured to facilitate accounting for the effect on the vehicle inertial properties of added weight of the instrumentation and other equipment. The total weight of the car before installation of test equipment was 2,030 lb (921 kg), and the total vehicle center of gravity (C.G.) was 30.72 in. (78.03 cm) aft of the front-wheel center.

Preparations of the vehicle for test included the installation of a roll bar, a double shoulder-harness and lap-belt restraint system, and a driver-side window safety net to protect the driver in the event of an inadvertent rollover; installation of instrumentation and recording equipment; and hydraulic brake system modification, which permitted braking of only the rear wheels to aid in inducing skids. A new set of Goodyear Polysteel P155/80R13 radial tires was also installed. Tire force data for this type of tire were available from tests performed on the Calspan Tire Research Facility (TIRF) as part of another research project.

Instrumentation installed in the vehicle included three accelerometers, mounted close to the vehicle center of gravity, to measure the sprung-mass longitudinal, lateral, and vertical linear accelerations; three rate gyroscopes to measure the angular velocities about the vehicle yaw, pitch, and roll axes; a tachometer generator, mounted on one of the rear wheels, for measurement of the vehicle speed; and a string potentiometer, connected to the steering wheel shaft and calibrated to provide a direct measure of the steer angle of the front wheels.

For the driver-controlled tests, the signals from the transducers were amplified and recorded on a seven-channel FM magnetic tape recorder aboard the vehicle. To enable recording the data from the eight transducers on the seven-channel tape recorder, a relay activated by a "time zero" switch was used. As the vehicle was accelerated to the desired speed on the approach to the test site, the output from the tachometer generator was recorded on the data channel normally used to record the pitch angular rate. Upon driver closing of either of two paralleled "time zero" switches (one on the dashboard and the other operated by the brake pedal), the relay disconnected the circuit from the tachometer generator, and the amplified signal from the pitch rate gyro was subsequently recorded on that channel. Activation of the switch produced a spike on all data traces for identification of "time zero" for each test and also fired a flash bulb installed on the roof of the vehicle for time correlation of high-frame-speed photographic films of the tests.

For the tests performed without a driver, the VERF tow system was used to guide and accelerate the vehicle on the short approach to the test site, and the speed upon release of the tow cable was determined using equipment which accurately measures the time interval for the vehicle to traverse a known distance. A hydraulic accumulator system was installed in the vehicle to apply the brakes on the rear wheels and simultaneously cause the front wheels to rapidly steer to a large angle by means of a hydraulic actuator connected to the steering system linkage. Steering and braking were initiated at "time zero" when an electrical plug attached to a tether line trailing the vehicle was disconnected shortly after the car was released from the guide rail and tow cable. The onboard tape recorder was removed from the vehicle for these tests; instead, the signals from the various transducers were transmitted via an umbilical cable to a magnetic tape recorder located in the VERF instrumentation and control building.

The weight of the vehicle after installation of instrumentation and other equipment was 2,230 lb (1,011 kg), and the longitudinal C.G. position was 32.63 in. (82.9 cm) aft of the front-wheel center. The vertical location of the total vehicle C.G. was measured to be 21.3 in. (54.1 cm) above the ground.

Photographs of the test vehicle and some of the onboard instrumentation equipment are presented in Figure 20.

HVOSM INPUTS FOR TEST VEHICLE

Values for the model input parameters describing the physical properties of the Rabbit automobile used in the tests were derived from data and information from several sources.[26,27,28] Much of the data on the characteristics of the vehicle suspension systems were taken directly from the ENSCO report,[26] which contains a complete HVOSM input data set that was used to simulate a Rabbit vehicle having a total weight of 1,800 lb (816 kg). However, since the Rabbit employed in tests of this project was substantially heavier, data from all of the above-cited references were used to estimate the inertial properties of the sprung (including driver) and unsprung masses. Table 32 shows the values of the VW Rabbit test vehicle parameters in the engineering output format of the HVOSM computer program.

As indicated earlier, measured tire test data for the type of tire installed on the vehicle were used to determine the values of the several constants for the tire side and camber force model. In the HVOSM, the tire side-force calculations are based on the small-angle properties of the tires, which are "saturated" at large angles. The side force for small angles is given by

$$F_S' = \left[\frac{A_1}{A_2} \left(F_R'\right)^2 - A_1 F_R' - A_0 \right] \alpha \tag{59}$$

where the parameters A_0, A_1, and A_2 are the coefficients of a parabola used to describe the variation of the small angle cornering stiffness with normal load, F_R', for small slip angles, α.

The side force for the entire range of slip angles, $\left(F_S\right)$, is computed using a nondimensional side-force cubic relationship:

$$\frac{F_S}{(F_S)_{max}} = f(\bar{\beta}) = \bar{\beta} - \frac{1}{3} \bar{\beta} \left|\bar{\beta}\right| + \frac{1}{27} (\bar{\beta})^3 \tag{60}$$

where:

$$\bar{\beta} = \frac{F_S'}{(F_S)_{max}} \tag{61}$$

---

26. Howerter, E.D., Hinch, J.A., and Owings, R.P., "Sensitivity Analysis of Subcompact Vehicle Performance Due to an Impact with a Breakaway Luminaire Support," ENSCO, Inc., Report No. FHWA-83-02, 15 April 1983.
27. Personal communication from Lloyd E. Carlson, Mobility Systems and Equipment Company, to Charles F. McDevitt of FHWA.
28. Riede, P.M., Lefferet, R.L., and Cobb, W.A., "Typical Vehicle Parameters for Dynamic Studies Revised for the 1980's," Society of Automotive Engineers, Inc., Technical Paper No. 840561, March 1984.

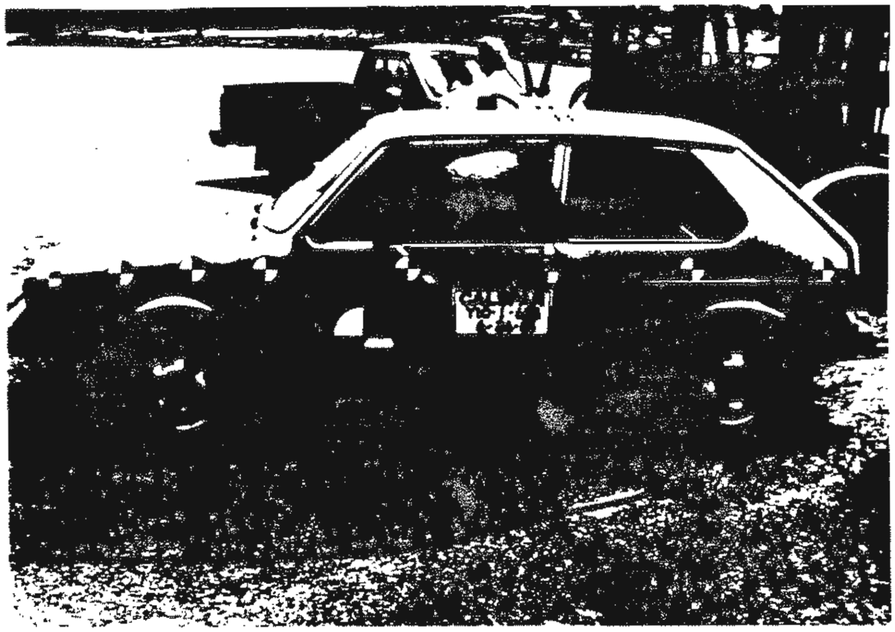

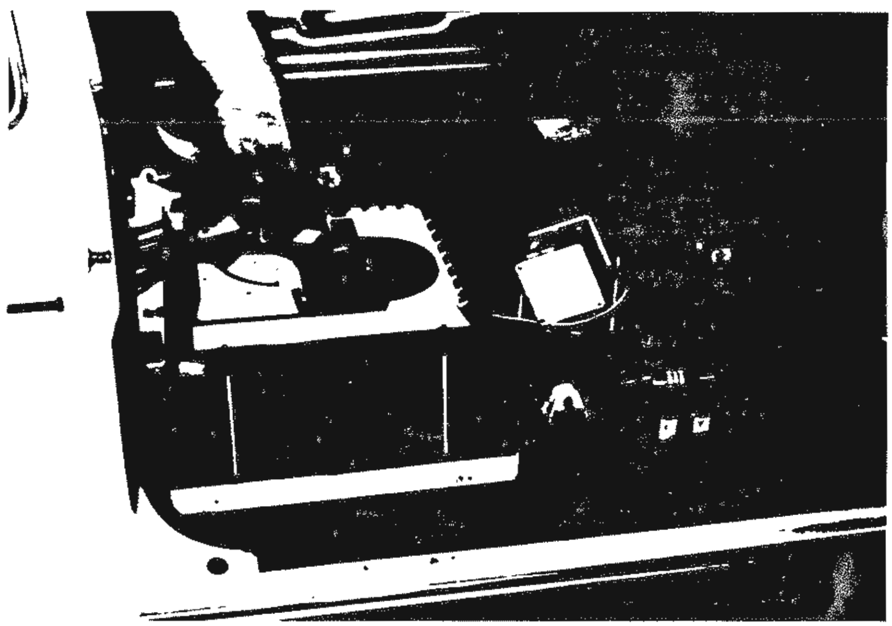

Figure 20. VW test vehicle and instrumentation.

Table 32. HVOSM input parameters for VW Rabbit test vehicle.

SPRUNG MASS	XMS	=	5.023	LB-SEC**2/IN	FRONT WHEEL X LOCATION	A	=	29.600	INCHES
FRONT UNSPRUNG MASS	XMUF	=	.329	LB-SEC**2/IN	REAR WHEEL X LOCATION	B	=	64.900	INCHES
REAR UNSPRUNG MASS	XMUR	=	.316	LB-SEC**2/IN	FRONT WHEEL Z LOCATION	ZF	=	11.893	INCHES
X MOMENT OF INERTIA	XIX	=	2600.000	LB-SEC**2-IN	REAR WHEEL Z LOCATION	ZR	=	11.563	INCHES
Y MOMENT OF INERTIA	XIY	=	8850.001	LB-SEC**2-IN	FRONT WHEEL TRACK	TF	=	54.500	INCHES
Z MOMENT OF INERTIA	XIZ	=	10400.000	LB-SEC**2-IN	REAR WHEEL TRACK	TR	=	53.500	INCHES
XZ PRODUCT OF INERTIA	XIXZ	=	.000	LB-SEC**2-IN	FRONT ROLL AXIS	RHOF	=	.000	NOT USED
FRONT AXLE MOMENT OF INERTIA	XIF	=	.000	NOT USED	REAR ROLL AXIS	RHO	=	.000	NOT USED
REAR AXLE MOMENT OF INERTIA	XIR	=	.000	NOT USED	FRONT SPRING TRACK	TSF	=	.000	NOT USED
GRAVITY	G	=	386.400	IN/SEC**2	REAR SPRING TRACK	TS	=	.000	NOT USED
	X1	=	1.16	INCHES	FRONT AUX ROLL STIFFNESS	RF	=	.00	LB-IN/RAD
ACCELEROMETER 1 POSITION	Y1	=	.00	INCHES	REAR AUX ROLL STIFFNESS	RR	=	84750.01	LB-IN/RAD
	Z1	=	8.00	INCHES	REAR ROLL-STEER COEF.	AKRS	=	.0000	NOT USED
	X2	=	.00	INCHES		AKDS	=	.000	RADIANS
ACCELEROMETER 2 POSITION	Y2	=	.00	INCHES	REAR DEFL-STEER COEFS.	AKDS1	=	.000	RAD/IN
	Z2	=	.00	INCHES		AKDS2	=	.000	RAD/IN**2
						AKDS3	=	.000	RAD/IN**3

STEERING SYSTEM

MOMENT OF INERTIA	XIPS	=	.000	LB-SEC**2-IN
COULOMB FRICTION TORQUE	CPSP	=	.000	LB-IN
FRICTION LAG	EPSP	=	.000	RAD/SEC
ANGULAR STOP RATE	AKPS	=	.000	LB-IN/RAD
ANGULAR STOP POSITION	OMGPS	=	.000	RADIANS
PNEUMATIC TRAIL	XPS	=	.000	INCHES

	FRONT SUSPENSION				REAR SUSPENSION			
SUSPENSION RATE	AKF	=	85.000	LB/IN	AKR	=	73.000	LB/IN
COMPRESSION STOP COEFS.	AKFC	=	303.000	LB/IN	AKRC	=	150.000	LB/IN
	AKFCP	=	902.000	LB/IN**3	AKRCP	=	37.000	LB/IN**3
EXTENSION STOP COEFS.	AKFE	=	2916.000	LB/IN	AKRE	=	1029.000	LB/IN
	AKFEP	=	134265.000	LB/IN**3	AKREP	=	23210.000	LB/IN**3
COMPRESSION STOP LOCATION	OMEGFC	=	-1.620	INCHES	OMEGRC	=	-2.910	INCHES
EXTENSION STOP LOCATION	OMEGFE	=	2.880	INCHES	OMEGRE	=	3.590	INCHES
STOP ENERGY DISSIPATION FACTOR	XLAMF	=	.650		XLAMR	=	.650	
VISCOUS DAMPING COEF.	CF	=	6.080	LB-SEC/IN	CR	=	3.580	LB-SEC/IN
COULOMB FRICTION	CFP	=	15.000	LB	CRP	=	15.000	LB
FRICTION LAG	EPSF	=	.100	IN/SEC	EPSR	=	.100	IN/SEC

Table 32. HVOSM input parameters for VW Rabbit test vehicle. (continued)

FRONT WHEEL CAMBER VS SUSPENSION DEFLECTION		REAR WHEEL CAMBER VS SUSPENSION DEFLECTION		FRONT HALF-TRACK CHANGE VS SUSPENSION DEFLECTION		REAR HALF-TRACK CHANGE VS SUSPENSION DEFLECTION	
DELTAF INCHES	PHIC DEGREES	DELTAR INCHES	PHIRC DEGREES	DELTAF INCHES	DTHF INCHES	DELTAR INCHES	DTHR INCHES
-5.00	-.08	-5.00	.00	-5.00	-.65	-5.00	.00
-4.00	-.33	-4.00	.00	-4.00	-.30	-4.00	.00
-3.00	-.50	-3.00	.00	-3.00	-.10	-3.00	.00
-2.00	-.50	-2.00	.00	-2.00	.05	-2.00	.00
-1.00	-.17	-1.00	.00	-1.00	.05	-1.00	.00
.00	.33	.00	.00	.00	.00	.00	.00
1.00	.83	1.00	.00	1.00	-.20	1.00	.00
2.00	1.83	2.00	.00	2.00	-.45	2.00	.00
3.00	2.58	3.00	.00	3.00	-.80	3.00	.00
4.00	3.50	4.00	.00	4.00	-1.25	4.00	.00
5.00	5.00	5.00	.00	5.00	-1.85	5.00	.00

TIRE DATA

			RF	LF	RR	LR	
TIRE LINEAR SPRING RATE	AKT	=	1099.000	1099.000	1099.000	1099.000	LB/IN
DEFL. FOR INCREASED RATE	SIGT	=	5.000	5.000	5.000	5.000	INCHES
SPRING RATE INCREASING FACTOR	XLAMT	=	10.000	10.000	10.000	10.000	
	A0	=	2542.000	2542.000	2542.000	2542.000	
	A1	=	9.910	9.910	9.910	9.910	
SIDE FORCE COEFFICIENTS	A2	=	2366.000	2366.000	2366.000	2366.000	
	A3	=	.687	.687	.687	.687	
	A4	=	-8184.000	-8184.000	-8184.000	-8184.000	
TIRE OVERLOAD FACTOR	OMEGT	=	.750	.750	.750	.750	
TIRE UNDEFLECTED RADIUS	RW	=	11.313	11.313	11.313	11.313	INCHES
TIRE / GROUND FRICTION COEF.	AMU	=	.800	.800	.800	.800	

1 in. = 2.54 cm
1 lb = 0.4536 kg

and $(F_S)_{max}$ is the maximum (saturated) value of the side force, which, with no braking or traction, is the product of the coefficient of friction, μ, and the normal load.

The usual method of obtaining the parameters A_0, A_1, and A_2 from Equation (59), based only on a least-squares parabolic fit to the cornering-stiffness variation with normal load determined from the test data, did not result in good agreement between the calculated and measured side forces throughout the entire ranges of slip angle and normal load for which test data were obtained. Because it is difficult to determine how much each of the three parameters should be adjusted to achieve a satisfactory analytical fit to the experimental data, a different technique for determining the best values of A_0, A_1, and A_2 was developed.

The experimental data are side force as a function of slip angle for several values of normal load. This side force, F_S, divided by the saturation value, $(F_S)_{max}$, shown by the test data is the left-hand side of Equation (60). For each combination of slip angle and normal load, this cubic equation was solved for the desired root, $\bar{\beta}$. Using $\mu F_R'$ for $(F_S)_{max}$ in Equation (61), all of these values of $\bar{\beta}$ were used to solve a least-squares fit for the coefficients of the second-order Equation (59). (The tire test data indicate that the coefficient of friction varies with the normal load. An average value of 0.96 for μ was used in calculating the values of the tire parameters.) In this way, the resulting values of A_0, A_1, and A_2 are those that minimize the overall difference between the measured and calculated side forces.

The lateral force due to camber at zero slip angle is computed in HVOSM from:

$$(F_S)_{CAMBER} = \left[A_3 F_R' - \frac{A_3}{A_4} (F_R')^2 \right] \left[\phi - \frac{2}{\pi} \phi \left| \phi \right| \right] \tag{62}$$

where the terms in the first bracket are the assumed parabolic variation of the camber stiffness at zero camber angle as a function of normal load. The side force for a given normal load also is assumed to vary parabolically with the camber angle (maximum at 45 degrees of camber) as given by the second bracketed terms. As was the case with cornering stiffness, the determination of the values for A_3 and A_4 based on the slopes of the plots of measured force vs camber angle at zero camber angle also did not yield a good analytical fit to the test data. Therefore, values of the measured side forces for several combinations of camber angle and normal load were all used to compute the coefficients A_3 and A_4 of Equation (62) that provide a least-squares best fit to the test data.

The values of the HVOSM tire-model coefficients and the resulting fits of the slip-angle and camber-angle test data are shown in the carpet plots of Figure 21 and Figure 22, respectively.

TESTS ON PAVED SURFACE

Scope

Two series of tests were performed in which the vehicle was maneuvered on asphalt pavement. The main purpose of these tests was to obtain response data for a single operating environment which would allow checking that, overall, the actual vehicle properties were satisfactorily represented by the model input values before simulating the tests performed on roadside terrains, which involve the added complexity of tire/soil interactions. The vehicle maneuvers executed in these tests were: (1) a sinusoidal steer input and (2) a rapid steer of the front wheels to a large angle, combined with locked rear-wheel braking to produce a spinout. Replicate test runs of each type of maneuver were performed to assure that the measured responses were repeatable and constituted a valid data base with which to compare the results of HVOSM simulations of the tests.

Sinusoidal Steer

In this test, the vehicle was given a nearly sinusoidal steer input of about ± 10 degrees of front-wheel steer angle at a frequency of 0.5 Hz while coasting from an initial speed of 33 mi/h (53.1 km/h) with the transmission in neutral. The predicted vehicle responses are shown in the plots of Figure 23 for comparison with the data measured in the test. The agreement of the model is seen to be quite good. The main differences are the magnitudes of the

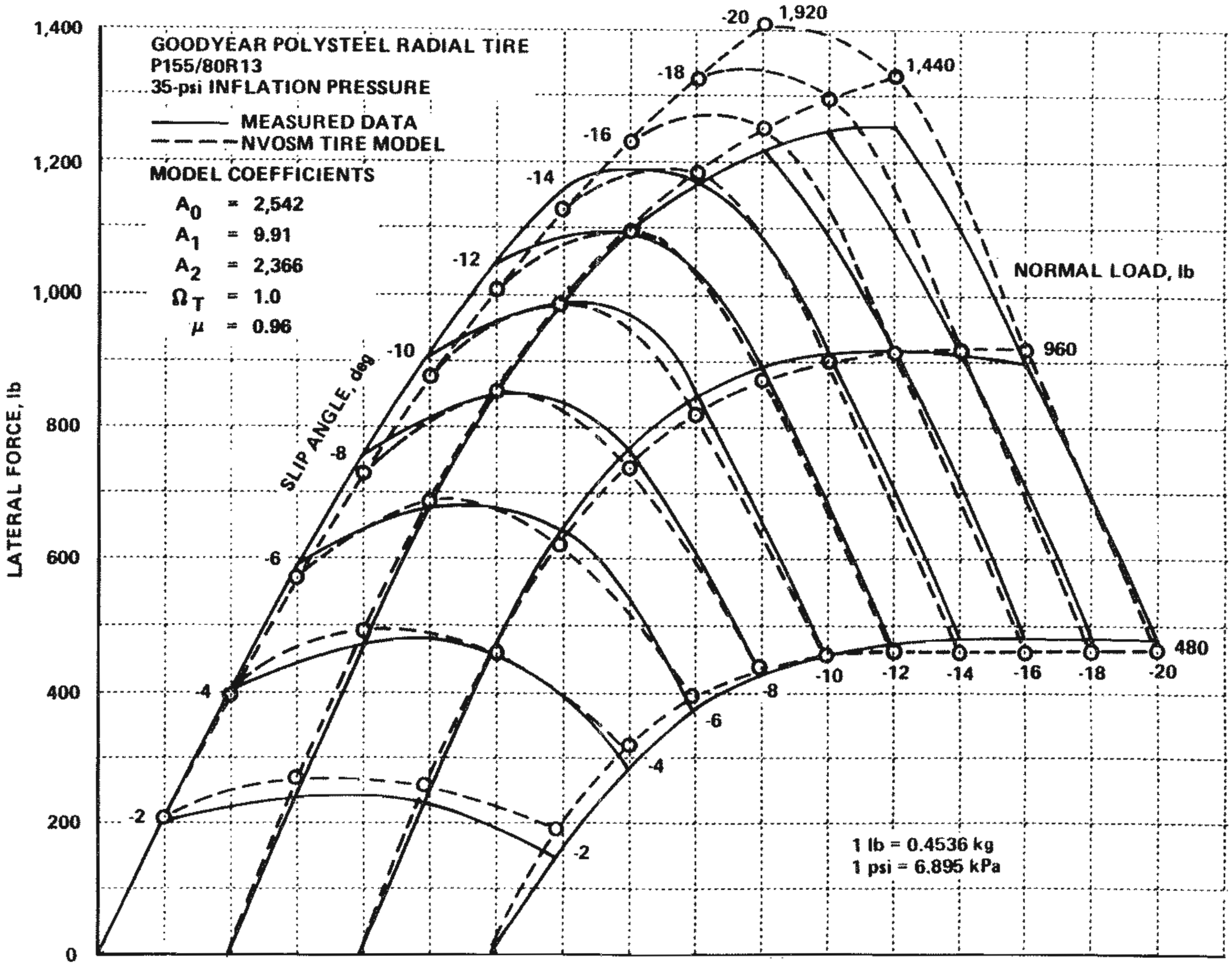

Figure 21. HVOSM fit of measured tire side force vs slip angle data.

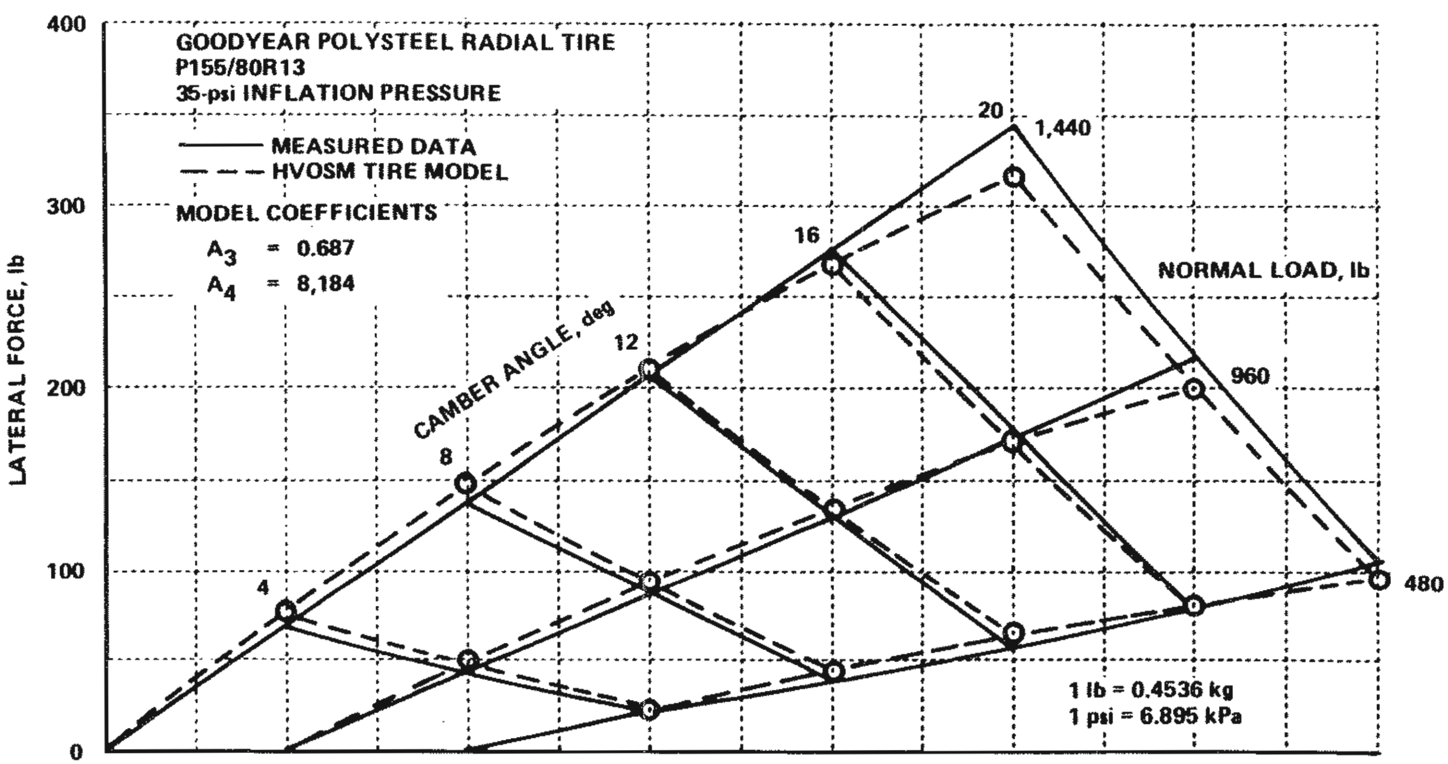

Figure 22. HVOSM fit of measured tire side force vs camber angle data.

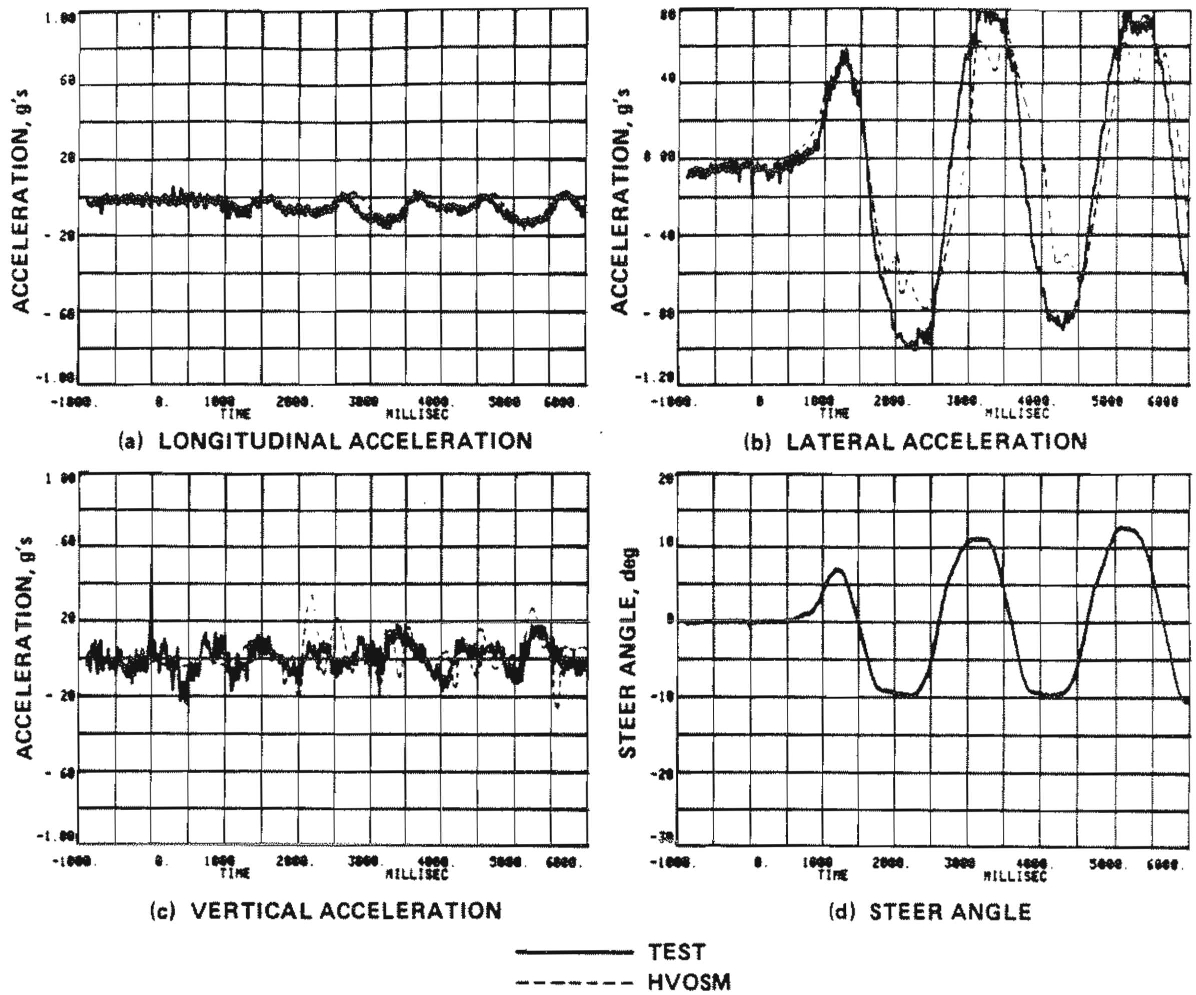

Figure 23. Comparison of HVOSM and measured vehicle responses in sinusoidal-steer test.

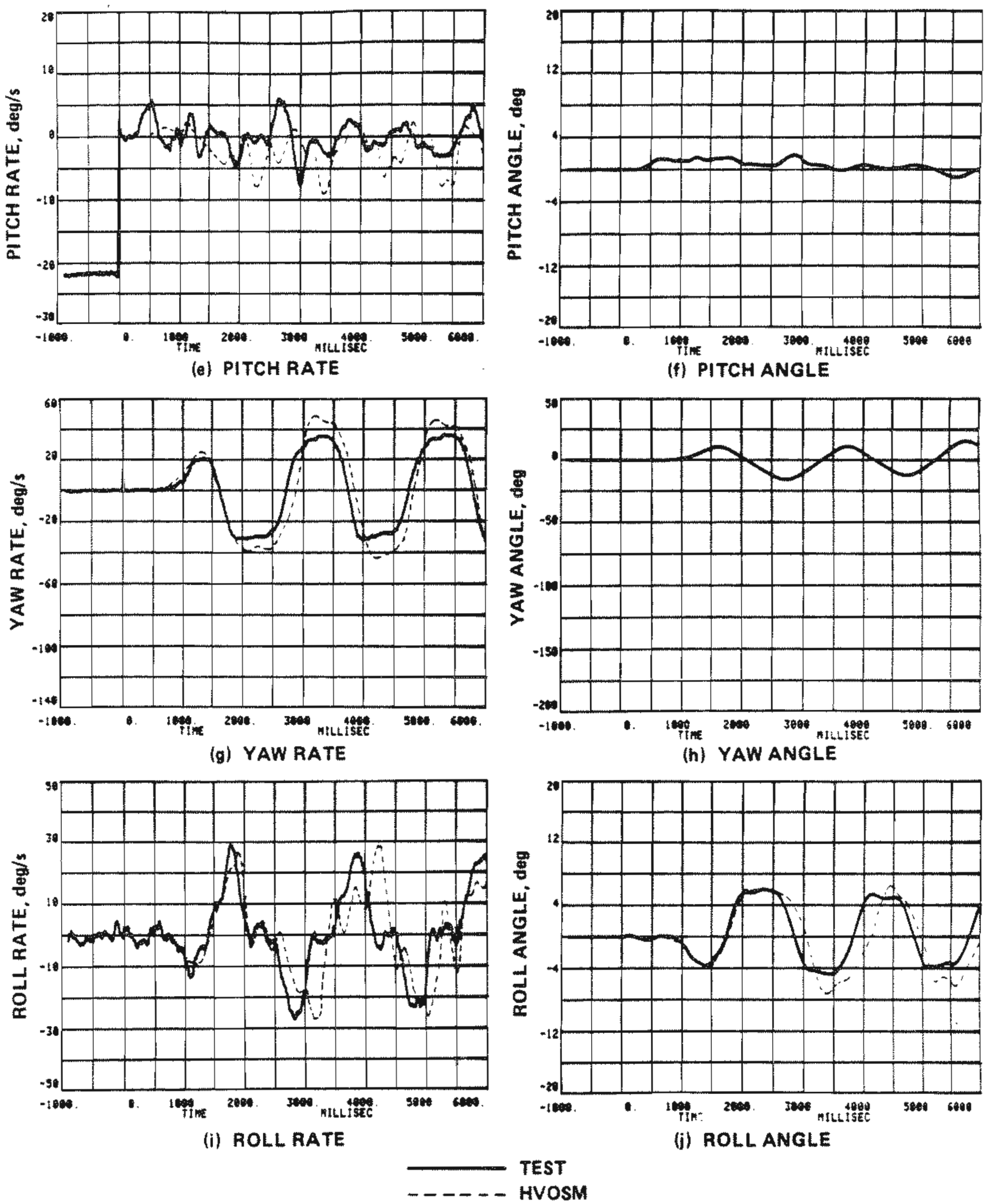

Figure 23. Comparison of HVOSM and measured vehicle responses in sinusoidal-steer test. (continued)

peaks of the lateral-acceleration and yaw-rate responses and an apparent slight phase shift of the roll rate after t = 2.5 seconds. Analysis of the simulation output data shows that the front-wheel suspension deflected sufficiently to contact the jounce bump stops at the times of the lateral-acceleration and yaw-rate peaks. Note that the test measurement of the roll rate is a distorted sine wave with "flat spots" at the zero crossings. These "flat spots" might also be indicative of the suspension's contacting the jounce bump stops in the test, inasmuch as they occur at the same times that the simulation model shows that the stops are engaged. Since data on the actual properties of the bump stops were not available, how well the characteristics are duplicated by the model inputs is not known. Hence, inaccuracies of the bump-stop model could be the main cause of the noted discrepancies.

Plots showing the integrated outputs of the three angular rate gyros recorded in the test are also included in Figure 23. It is noted that these angular displacements do not define the orientation of the vehicle and cannot be directly compared with the pitch, yaw, and roll angle outputs by the HVOSM, which are Euler angles. The roll-angle time history obtained by manually integrating the roll rate predicted by the HVOSM is depicted in part j of Figure 23 for comparison with the test data. As may be seen in this plot, the response of the model lags the test result, and the negative roll-angle peaks are slightly greater following completion of the first cycle of front-wheel steer angle.

Combined Steer and Braking

In this test, the vehicle was caused to skid and spin out on the dry pavement by braking the rear wheels (only) to produce lockup and then rapidly steering the front wheels to a large and constant negative steer angle. Lateral accelerations in excess of 1 g were developed as the vehicle spun about 180 degrees before coming to rest from an initial speed of 35 mi/h (56.3 km/h). Tire marks on the pavement indicate that the left rear wheel lifted off the ground for a short period in at least two of several replicate test runs performed.

Results of the HVOSM simulation of the test are presented in Figure 24 for comparison with the measured data. For the most part, the correlation is excellent; however, it may be seen that peak negative lateral acceleration predicted by the model is substantially less than the 1 g or more recorded in the full-scale test. The value of 0.8 for the tire/pavement friction coefficient assumed for the simulation run was based on skid trailer measurements of the roadway surface made several years earlier. Since a friction coefficient as high as 1.0 or more is indicated by the test data, other simulations in which the coefficient was increased to a maximum value of 1.0 were made to examine the effects of varying this parameter. The most noticeable effect was an increase in the magnitude of the oscillations of the lateral-acceleration and roll-rate responses that may be noted to occur between approximately t = 0.5 second and t = 2 seconds. With a friction coefficient of 1.0, these excursions became very large, and analysis of the run output shows that the right-front suspension deflected sufficiently to contact the jounce bump stop.

The friction coefficient of the tire/pavement suggested by the test results is substantially greater than the range of typical values reported for a dry asphalt surface. However, the difference is too large to be ascribed solely to instrumentation error for the lateral-acceleration data channel. Moreover, the good correlation of the longitudinal acceleration before significant yaw rotation of the vehicle had occurred indicates that the assumption of 0.8 for the coefficient of friction is indeed close to the real value in the test. One plausible explanation is that the actual tire properties are not accurately represented by the model in the high normal-load and slip-angle ranges experienced in the test, and for which no tire test data are available. Analysis of the simulation run shows that, in the time interval between t = 0.75 second and t = 2 seconds, the tires operate at slip angles in the range between approxiamtely 23 degrees to over 100 degrees, and that the right front tire, in particular, is heavily loaded (1,200 to 1,650 lb (544 to 948 kg)). Note that, if the actual side force developed by this tire is higher than predicted, it would be expected to result in not only a higher lateral acceleration but also an increased peak yaw rate (as shown by the test data), since that wheel is basically the pivot for the yaw motion of the vehicle.

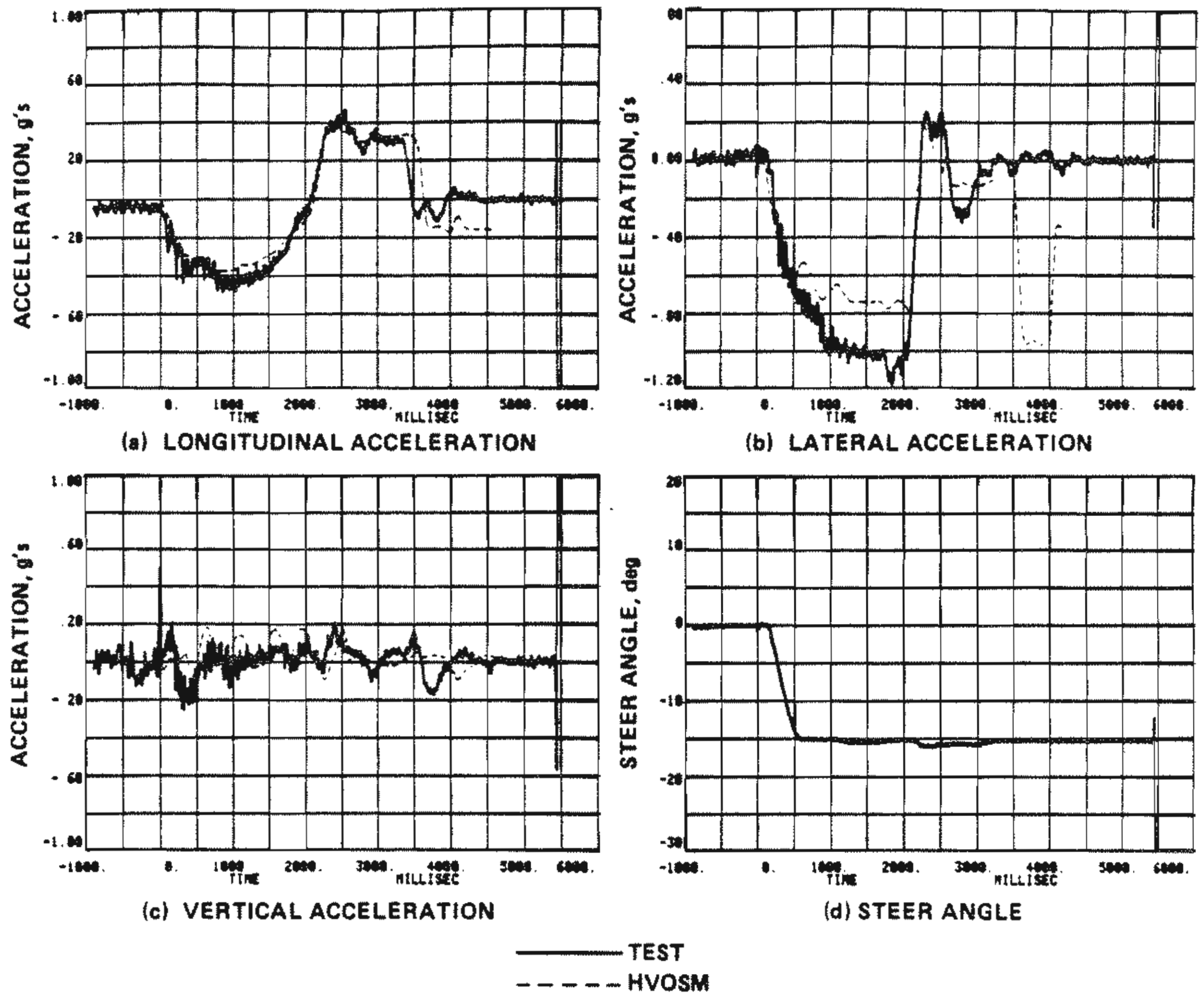

Figure 24. Comparison of HVOSM and measured vehicle responses in combined steer and braking test.

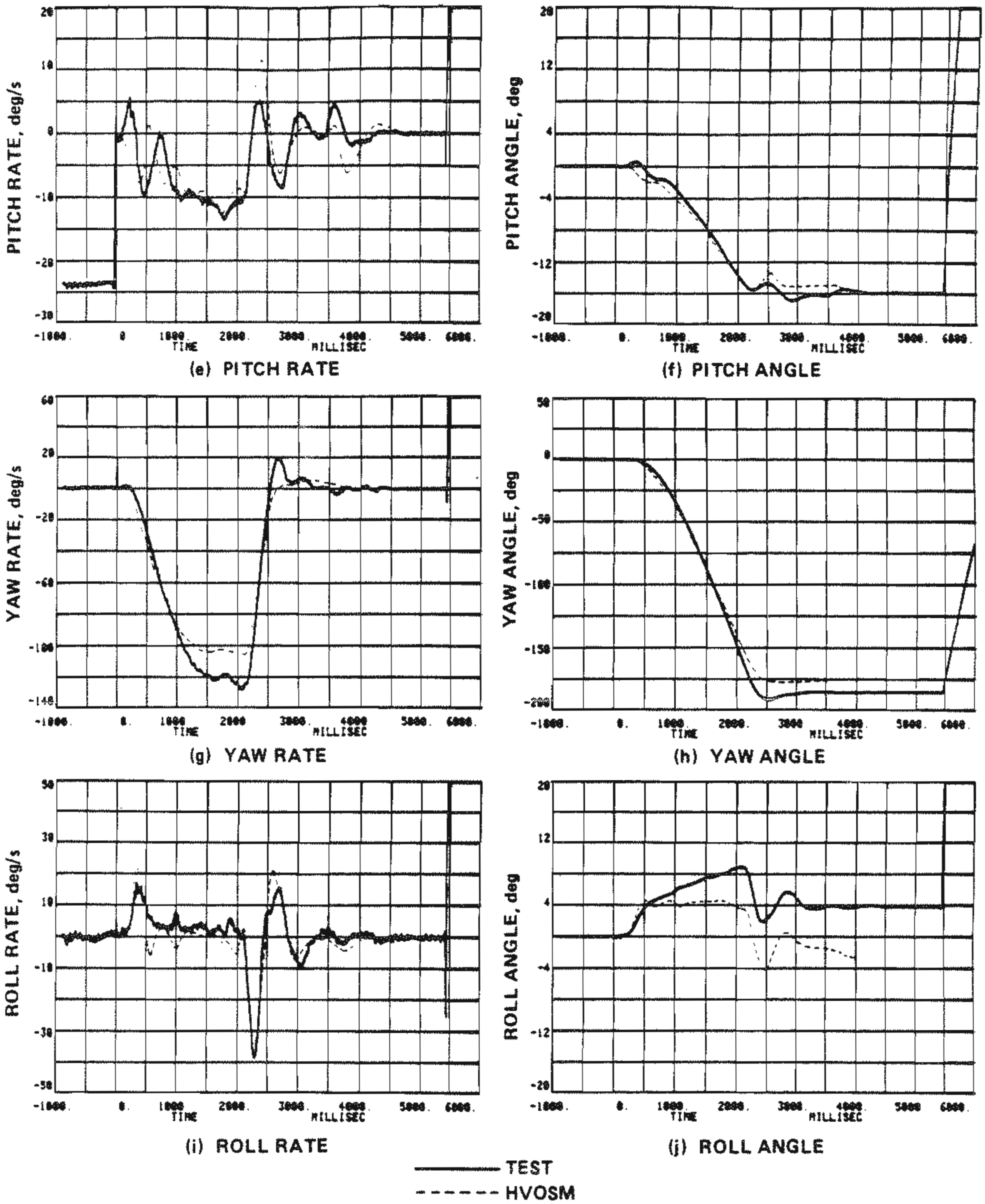

Figure 24. Comparison of HVOSM and measured vehicle responses in combined steer and braking test. (continued)

Another simulation run was made with the auxiliary roll stiffness of the rear suspension reduced to zero. It was thought that this might result in a greater weight transfer to the tires on the right-hand side of the car, particularly the right-front wheel, and thereby increase the side force and, hence, the lateral acceleration and the peak yawing velocity. Although this did occur to some extent, the principal effect again was a greatly increased magnitude of the oscillations of these responses between $t = 0.5$ second and $t = 2$ seconds.

The large negative lateral acceleration pulse evident at about $t = 3.75$ seconds in the simulation results is an anomaly that should be ignored. At that time, the vehicle is moving so slowly that small changes in the direction of the wheel velocity vectors result in large and sudden reversal of the tire slip angles and, hence, of the tire side forces.

The good agreement shown between the simulation and experimental results for both this test and the sinusoidal-steer test provided confidence that the vehicle physical properties were adequately represented by the defined model inputs.

TESTS ON ROADSIDE TERRAIN

Soil Measurements

All of the off-road tests were performed on sod ground consisting primarily of a mixture of coarse rye grass and natural weed cover 4 to 6 in. (10 to 15 cm) in length. Measurements of two samples of the soil underlying the field turf were made to identify and classify the type of soil existing at the test sites. The two soil samples analyzed were taken from beneath the left and right tire tracks made by the vehicle in traversing the ditch embankment described later. The sample from the left track was taken from the lowest part of the ditch, whereas the soil sample from the right track was removed from the steepest part of the sideslope. Although the grass was scuffed and sheared off at the soil surface in some places, the surface was not penetrated by the tires to any significant degree in that test. It is noted, however, that the firmness of the ground varied greatly among and within the individual test sites due to differences in the moisture content of the soils.

The collected soils were analyzed for a variety of physical soil parameters to define the soil characteristics. The parameters selected for measurement included grain-size distribution, moisture content, Atterberg limits (liquid limit, plastic limit, and plasticity index), and the recompacted permeability of the soil. The moisture content of the grass was also measured. The results of these measurements are shown in Table 33.

Table 33. Measured soil properties.

Parameter	ASTM method	Sample	
		Left track	Right track
Grain Size, %	D421, 422		
over 2.0 mm		23	47
0.1-2.0 mm		52	32
less than 0.1 mm		25	21
Moisture Content, %	D2216	45 (64)*	20 (58)*
Liquid Limit	D421, 423	81	47
Plastic Limit	D421, 424	70	32
Plasticity Index	D421, 424	11	15
Recompacted Permeability, cm/sec	D2434	7.7×10^{-9}	1.1×10^{-8}

*Moisture content of grass

Grain size is commonly used as a basis for classifying soils, although such classifications are by no means adequate for all purposes. The four major classification groups are gravel, sand, silt, and clay. The associated ranges of grain sizes are as follows:

Gravel	over 2.0 mm
Sand	2.0-0.06 mm
Silt	0.06-0.005 mm
Clay	less than 0.005 mm

From the measured grain-size distributions shown in Table 33, it appears that the soil is best described as a sandy silt but with substantially more gravel on the sideslope. Based on the permeability data, the soil would be classified more as a clay, but the grain-size analysis does not bear this out.

Motion-Resistance Tests

A series of tests was performed in which the motion-resistance forces developed when the Rabbit test car was pulled over the uneven surface of a sod-covered field were measured. The objective of these tests was to provide data that would allow a gross check of the validity of the HVOSM deformable-soil model as well as determination of the tire/ground coefficient of friction for a typical roadside terrain surface.

For these tests, two steel cables, 58.5 ft (17.8 m) in length, were attached to the center of the front and rear wheels on the right side of the VW Rabbit. A load cell installed on each cable was used to measure the forces developed as the Rabbit was pulled over the surface of the ground at a speed of 10 to 15 mi/h (16.1 to 24.1 km/h) by another vehicle. Tests were also performed with the length of the front-wheel cable reduced to 54 ft (16.5 m) and to 51 ft (15.5 m) so the vehicle would be pulled at different sideslip angles. The conditions and general observations for each of the 11 test runs performed are briefly described below.

Test 1. -- This test was performed in an area where the sod was dry and firm. The cables to the front and rear wheels were each 58.5 ft (17.8 m) in length. No brakes were applied, and very little wheel rotation was observed. Wheel tracks were visible, but no grass roots were torn up. Force data were invalid due to an apparent unknown pre-load on the load cells.

Test 2. -- This was a repeat of the first test except that all wheels were braked. A few surface scuffmarks were observed where grass tufts were uprooted.

Test 3. This test was performed in the same area as the previous tests, but with the front cable shortened to 54 ft (16.5 m), and with the wheels free to rotate. The vehicle moved forward along the initial heading angle until the front cables became disconnected when the load-cell swivel unscrewed from the wheel. No valid data were obtained.

Test 4. -- This test was the same as Test 3, except with braked wheels. The wheel tracks showed occasional scuff marks.

Test 5. -- This test was performed in the same area as the previous tests. The front-cable length was reduced to 51 ft (15.5 m) and all wheels were braked. Some oscillation of the vehicle about the yaw axis was noted. Measurements of the car attitude after the test indicated a slip angle of approximately 40 degrees. No force data were obtained due to inadvertent failure to connect load-cell signal cables to signal-conditioning equipment. However, from observation of the tow cables, it appeared that little force was transmitted by the one attached to the rear wheel.

Test 6. -- This test was a repeat of Test 5. Slight yaw oscillation was again observed, and the rear cable again appeared to carry little or no load. A sideslip angle of approximately 37 degrees was calculated from post-test measurements of the vehicle position. The tires scrubbed the grass without leaving ruts.

Test 7. -- The conditions for this test were the same as for Tests 5 and 6 (i.e., a tow cable 51 ft (15.5 m) in length was attached to the front wheel, and all wheels were braked) except that a location in the field was selected where the ground surface was more uneven and where there were local areas where the sod was moist and less firm. The car driver (who applied the brakes for all of the locked-wheel braking tests) noted that the ride was distinctly more rough than in the earlier tests. The tires produced scuff marks on the more firm ground but made ruts up to 3 in. (7.6 cm) in depth and 10 to 15 ft (3 to 4.6 m) in length in an area where the ground was very soft.

Test 8. -- For this test, the Rabbit was towed broadside (front-wheel and rear-wheel tow cables each 58.5 ft (17.8 m) in length and with all wheels braked) in the same general area of the field as in Test 7. The wheel tracks showed more scuffing of the ground by the front tires than by the rear tires, which tended to "skip" over the surface. Both the front and the rear wheels plowed up the sod surface for a distance of 10 to 15 ft (3 to 4.6 m) in two spots where the soil was quite soft.

Test 9. -- The car was towed longitudinally without brakes over a sod ground surface that was very wet and soft, so as to be easily penetrated by the thumb. Very slight ruts less than 1 in. (2.5 cm) in depth were created by the rolling tires.

Test 10. -- This test was the same as Test 9 except that it was performed with locked-wheel braking. The sod was uprooted by the tires, creating ruts 2 in. (5.1 cm) or more in depth in the softest ground.

Test 11. -- The car was pulled broadside, with the wheels locked, over the same soft sod area as in Tests 9 and 10. Wider ruts than in Test 10, but of about the same depth, were produced by the tires. However, variations in the depth of the ruts, particularly those made by the front wheels, gave the track a lumpy appearance and probably were caused by variations in the firmness of the soil along the vehicle path.

Data obtained from the motion resistance tests are summarized in Table 34. Listed initially in the table are the minimum, maximum, and average forces measured in the individual tow cables attached to front and rear wheels; from the sum of the cable forces, the corresponding value of the effective friction coefficient was calculated. An example data record is presented in Figure 25, which shows the forces measured when the car was pulled broadside in Test 8. The variation of the forces about the mean value when the car was moving at a constant speed may be attributed to contact of the tires with local irregularities of the ground surface.

The data of Table 34 indicate that the average friction coefficient of automobile tires sliding on sod ground is typically about 0.5, which is the same as that reported by the Texas Transportation Institute[29] but less than

29. Ross, Hayes E., Jr. and Post, Edward R., "Comparisons of Full-Scale Embankment Tests With Computer Simulations--Volume 1, Test Results and Comparisons," Texas Transportation Institute, Research Report No. 140-7, December 1972.

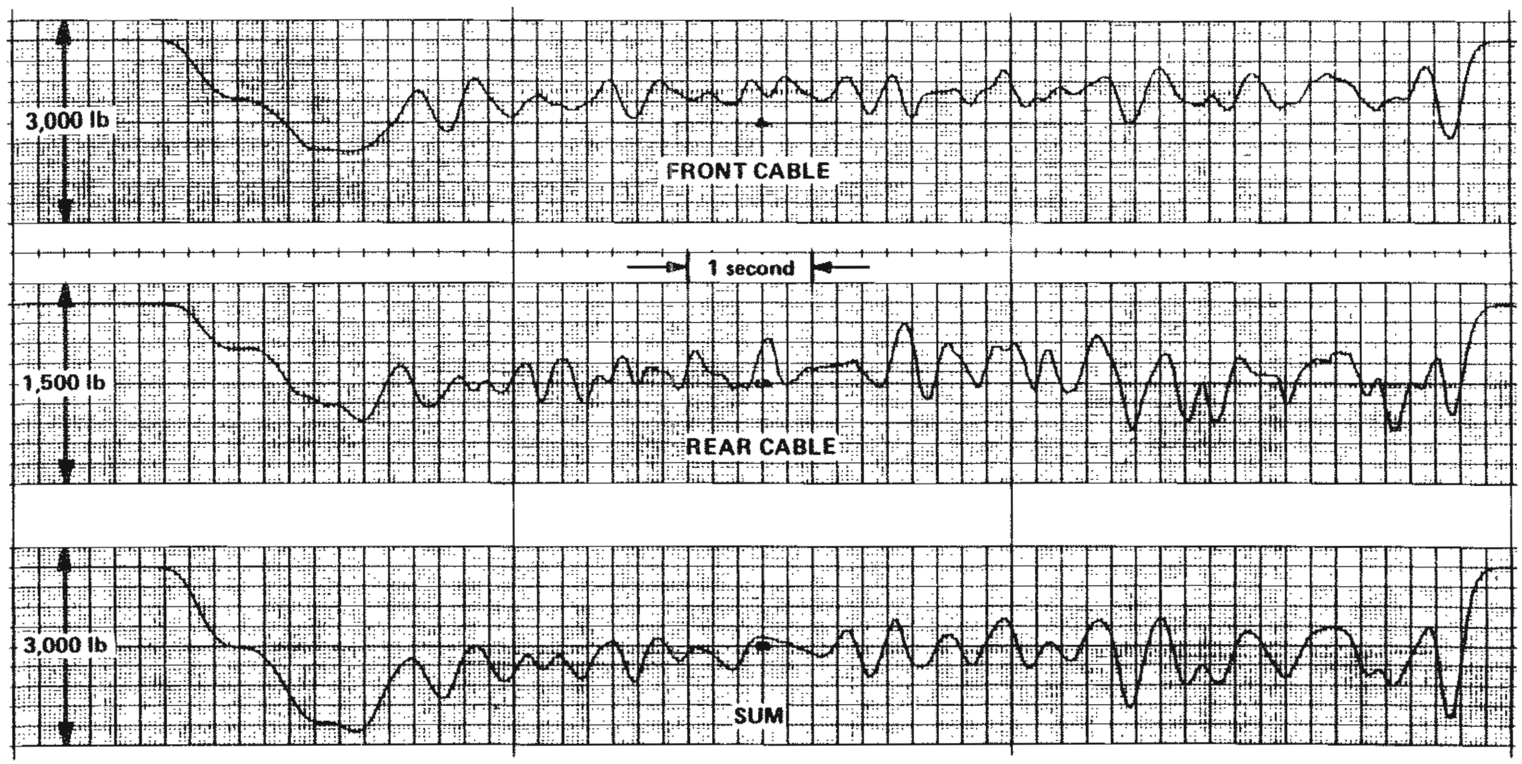

Figure 25. Cable forces measured in broadside pull test no. 8.

Table 34. Summary of forces measured in tests of VW Rabbit pulled over sod.

Test*	Sideslip angle, degrees	Front-cable force, lb			Rear-cable‡ force, lb			Sum of cable forces, lb			Effective frict. coef.		
		Min.	Max.	Ave.	Min.	Max.	Ave.	Min.	Max.	Ave.	Min.	Max.	Ave.
2	90	540	800	640	320	530	390	870	1,280	1,030	0.36	0.53	0.43
4	57	760	1,060	890	140	400	190	970	1,340	1,100	0.40	0.56	0.46
6	39	930	1,480	1,090	0	0	0	930	1,480	1,090	0.39	0.61	0.45
7	39	210	2,700	1,200	0	20	0	210	2,720	1,200	0.09	1.13	0.50
8	90	400	1,210	760	150	940	500	780	2,150	1,290	0.32	0.89	0.54
9**	0	220	300	260	230	420	310	490	720	550	0.20	0.30	0.23
10	0	380	1,110	650	230	900	520	850	1,510	1,210	0.35	0.63	0.50
11	90	490	1,090	800	420	860	560	1,010	1,930	1,370	0.42	0.80	0.57

1 lb = 4.448 N

* Tests 2, 4, and 6 were all performed in same area on firm dry sod. Tests 7 and 8 were performed at two different locations having small localized areas where the ground was moist and less firm. Tests 9, 10, and 11 were all performed in the same area on wet, soft sod that could be easily penetrated by the thumb.

‡ Cable attached to the left front of the vehicle for the longitudinal-pull tests (Tests 9 and 10)

**Test with no wheel braking

half the value measured in similar tests performed at the General Motors Proving Ground[30]. It may be noted that the data from the three tests at 90° sideslip angle (Tests 2, 8, and 11) show a slight trend of increased motion resistance with decreased firmness of the soil.

Tests 2, 4, and 6, which were performed with the car pulled at different sideslip angles on the same ground, show that the motion resistance was not affected by the sideslip angle. In view of the fact that the tires slid over firm sod ground without creating any ruts in these tests, measurement of an essentially constant average resistance force would be expected. It may be noted that no force was measured in the cable to the rear wheel in Test 6 (or Test 7) when the sideslip angle was approximately 40 degrees. Since the resultant pull force must pass through the vehicle C.G., this angle is equal to the angle between the longitudinal axis and the line from the C.G. to the cable attachment point at the front-wheel center. Calculations show that, with the vehicle oriented at that angle, the rear cable, 51 ft (15.5 m) in length, is slack and, thus, would carry no load.

Tests 9, 10, and 11 were performed on a small area of a field where the ground (sod) was wet and soft. Although the sinkage of the tires generally was quite small and variable along the wheel paths, the data from these tests show that higher forces were developed when the car was pulled broadside and allow at least a gross check of the validity of the HVOSM deformable-soil model.

Using soil parameter values given by Bekker[17] for unplowed sod, the computed sinkage of the front and rear tires--0.71 in. (1.8 cm) and 0.46 in. (1.2 cm), respectively--compares favorably with the 1-in. (2.5 cm) or less depth of the ruts produced by the rolling tires observed in Test 9. However, the average motion resistance measured in that test (550 lb (2,446 N)) is substantially greater than the 310 lb (1,379 N) computed by the model. Since Bekker's analysis treats only the resistance due to compaction of the soil, other factors such as friction of the running gear, losses due to deflection

30. Stonex, K.A., "Roadside Design for Safety," Paper presented at the 39th Annual Meeting of the Highway Research Board, March 1960.

of the tire carcass, and bulldozing resistance can account for at least part of the difference between the analytical and test results.

For the 90-degree sideslip angle of Test 11, the lateral force due to plowing of the soil by the sidewall of the tires calculated using the HVOSM deformable-soil model is 441 lb (1,962 N). However, the force in the contact patch due to the tires sliding on the ground must be added to this value in order to make a direct comparison with the total force measured in the test. If it is assumed that the sliding friction force in the tire/ground horizontal contact patch is the difference between the forces measured in the longitudinal pull tests with the wheels locked (Test 10) and those measured with the wheels free to roll (Test 9), the resulting total force would be 441 + 660 = 1,101 lb (4,897 N), compared to the average force of 1,370 lb (6,094 N) measured in the test.

It is also of interest to note that the 131-lb (583-N) increase of the motion resistance predicted by the model for the 90-degree change of the sideslip angle is close to the 160-lb (712-N) increase of the average force indicated by the data measured in Tests 10 and 11. This finding supports the assumption made in formulating the model that the motion-resistance force is proportional to the projection of the vertical tire/soil interface area in the direction of motion.

The results discussed above show that the forces predicted by the deformable-soil model are reasonable for the conditions of the tests but, clearly, are too limited for drawing any firm conclusions regarding the general validity of the model.

Skid on Level Turf

In the first of the tests performed on roadside terrains, the vehicle was maneuvered into a spinning skid on basically level ground. Although the tests were performed following two days of rain showers, the sod surface was quite firm, so rutting by the tires was quite minimal. However, in one of the preliminary runs made to allow the driver to practice the maneuvers required to achieve the desired high angle of departure from the roadway at the preselected location, a rut approximately 3 ft (0.9 m) in length, 1 ft (0.3 m) in width, and 3 in. (7.6 cm) in depth was created by the right-front tire. Blades of grass that were noted to be caught between the wheel rim and the tire bead gave evidence that high side forces were developed by that tire in particular.

Results of the HVOSM simulation of a test in which the vehicle departed from the roadway at 33.5 mi/h (53.9/h) at an angle of 16.8 degrees, as determined from tire-track measurements, are shown in Figure 26 for comparison with the vehicle responses recorded in the test. It may be noted from the steer-angle time history that the driver had not yet completed the right-turn maneuver at "time zero," when rear-wheel braking (only) was applied as the vehicle passed by a marker cone set at the edge of the roadway. Shortly thereafter, the front wheels were rapidly turned to a large left steer angle, which caused the vehicle to skid and spin counterclockwise as it came to a stop.

The test records show considerable high-frequency "hash," particularly for the accelerometer data, which is probably mostly due to sprung-mass structural vibrations that occurred as the vehicle traversed the irregular surface of the field. For the simulation, measurements of the elevation of the ground at grid points spaced 10 ft (3.05 m) and 4 ft (1.22 m) apart in directions parallel and perpendicular to the roadway, respectively, were used to describe the profile of the ground surface.

The plots of Figure 26 show that the dynamic responses of the vehicle were closely predicted by the HVOSM, which used values of the soil parameters given by Bekker[17] for unplowed sod. There was little rutting of the ground observed after the test, although the grass was scuffed and roots torn up in some places. In like manner, the sinkage of the tires in the simulation run was small (generally, between 0.1 and 0.7 in. (0.3 and 1.8 cm)), depending on the wheel load) and exceeded 1 in. (2.5 cm) only briefly for the right-front wheel, which was the most heavily loaded.

Comparison of the time histories of the yaw angle obtained by integrating the output of the yaw date gyro shows that the HVOSM accurately predicted the approximately 175-degree change of the heading angle measured in the test.

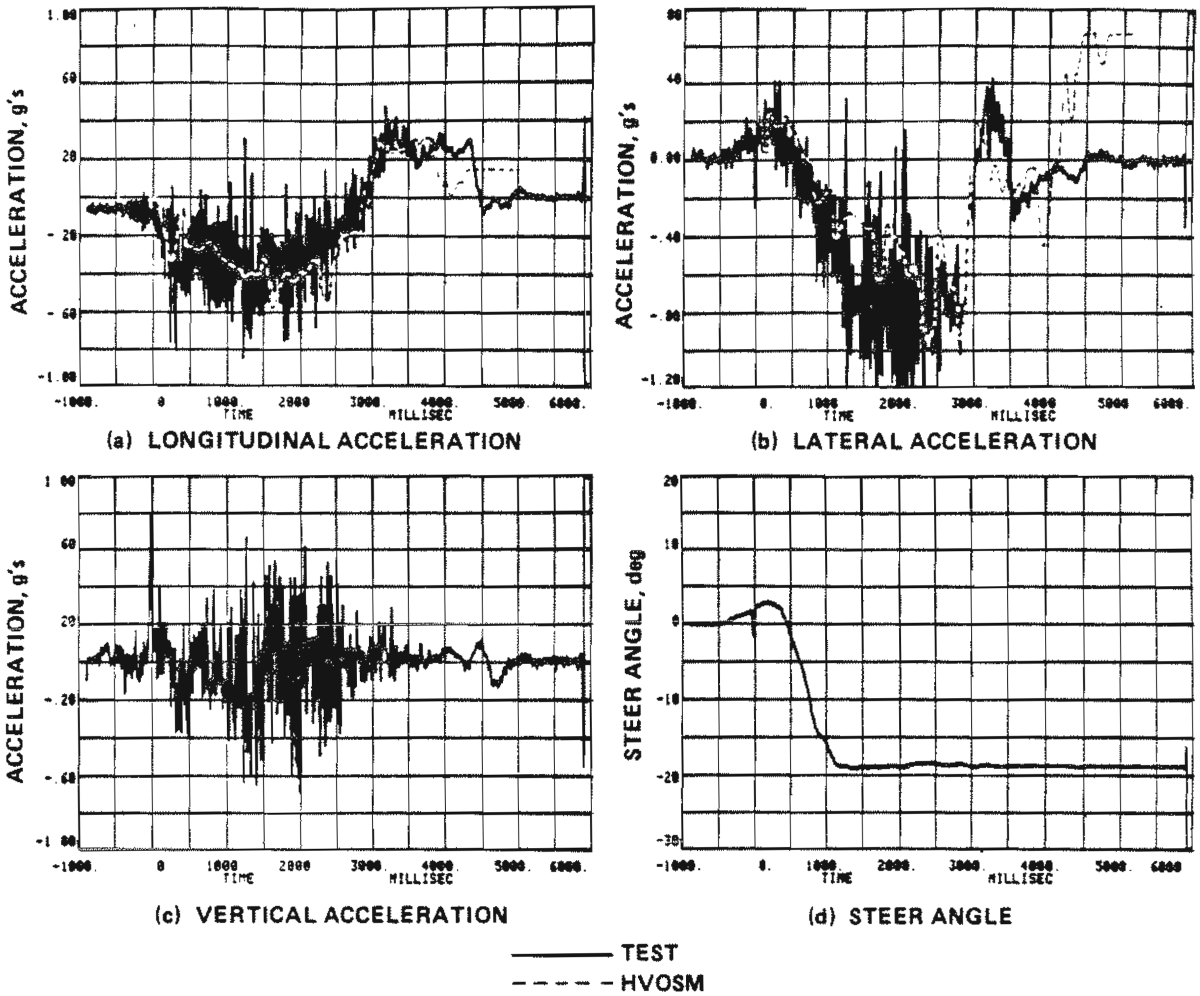

Figure 26. Comparison of HVOSM and measured vehicle responses in level-turf skid test.

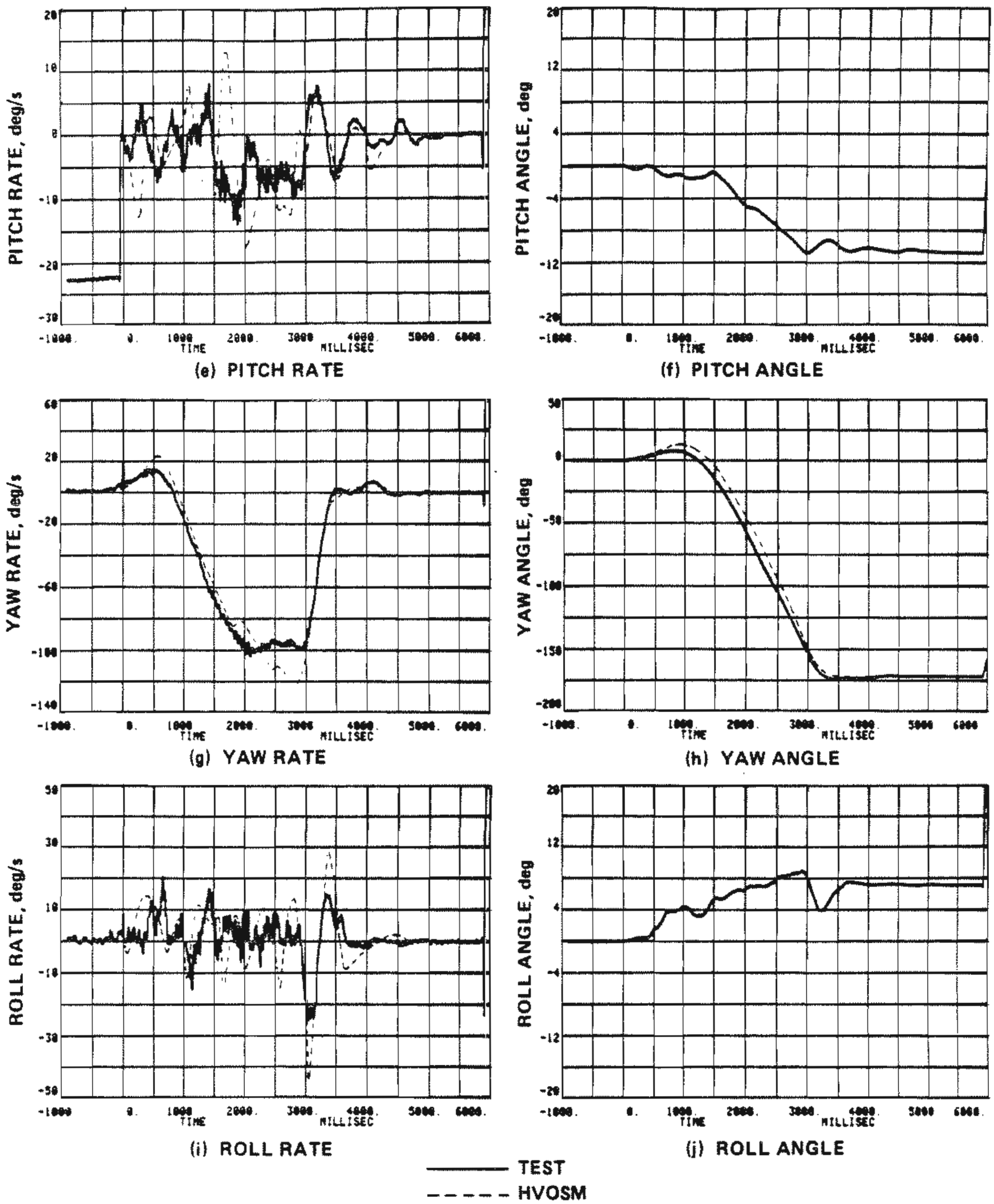

Figure 26. Comparison of HVOSM and measured vehicle responses in level-turf skid test. (continued)

The predicted coordinates of the final rest position of the vehicle were X' = 95.7 ft (29.2 m) and Y' = 20.9 ft (6.4 m), which also is very close to the measured location of approximately X' = 96 ft (29.3 m) and Y' = 19 ft (5.8 m).

Traversal of Fill Transition

In this test, the vehicle was driven over the end transition of a fill embankment to level ground. Since the vertical alignment of the roadway at this site had a slight down grade, the height and slope of the embankment varied with distance along the road. At the point of vehicle departure from the roadway, the embankment was about 3 ft (0.91 m) in height and had an average sideslope ratio of approximately 5:1. The measured profile of the ground surface at several stations along the roadway is illustrated in Figure 27. The grass-covered slope was dry and firm, but the sod at the toe of the embankment was saturated and, hence, quite soft.

For this test, the driver accelerated the car while in the left-hand lane of the two-lane road on the approach to the test site. Shortly after the car passed over a raised railroad grade crossing, the driver executed a sharp right steer maneuver, so the car departed from the right side of the road at a speed of 35 mi/h (56.3 km/h) at an angle of appropximately 18 degrees as determined from tire marks in sand that had been lightly spinkled on the road. Rear-wheel braking signalling "time zero" was applied while the car was still in the right turn. At t = 0.6 second, a large left steer of the front wheels was initiated to induce a counterclockwise spinout on the roadside turf. As may be seen in the post-test photograph of Figure 28, large ruts of varying length and as much as 3 in. (7.6 cm) in depth were created by the skidding tires.

Difficulty was encountered in early attempts to simulate this test, which showed that the yaw angular velocity increased to such a high positive value in the first 0.5 second of the simulation that the vehicle ultimately became unstable and spun out in a clockwise skid. Because the car was in a hard-cornering maneuver (0.4 g lateral acceleration) at "time zero" just prior to departing from the roadway, and also because of disturbances resulting from crossing of the railroad track located about 120 ft (36.6 m) upstream, some of

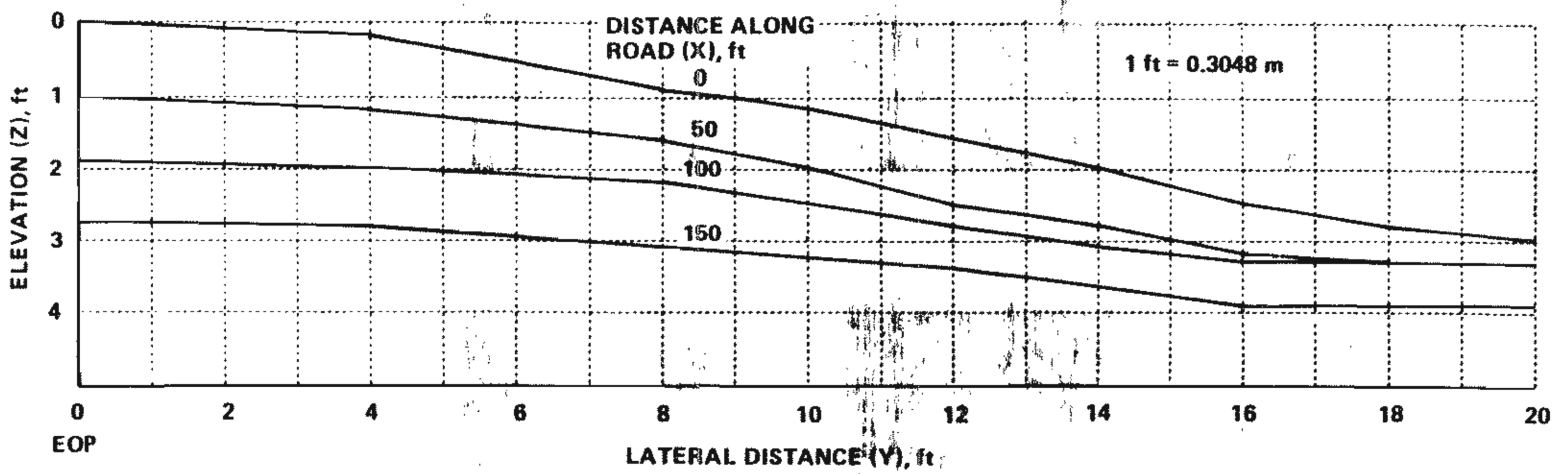

Figure 27. Fill-transition cross sections.

Figure 28. Ruts produced by tires in fill-transition test.

the initial conditions needed for input to the model (e.g., pitch and roll angles, suspension deflections and velocities, and lateral and vertical velocities of the sprung mass) were not accurately known. However, about 20 short-duration runs in which these parameters were varied showed little effect on the yaw response.

Realizing that what was needed to stabilize the vehicle in the turn off the roadway was more side force from the rear tires to balance the yaw moment of the steered front wheels, it was thought that perhaps the braking of the rear wheels was the key to the problem, since those tires had minimal capability to generate side forces when the wheels became locked up. Therefore, a simulation run was made in which lockup of the rear wheels was delayed by 0.2 second from the time of lockup in the earlier simulations. It was found that early clockwise spinout of the vehicle was avoided, and the yaw response time history agreed fairly well with that measured in the full-scale test. In that simulation run, lockup of the left and right rear wheels occurred at t = 0.45 second and t = 0.35 second, respectively, which appear to be reasonable for the time to decelerate the wheels to zero angular velocity from the initial value of approximately 55 rad/second (3,200 degrees/second) for the 35-mi/h (56.3 km/h) speed of the vehicle.

Results of the HVOSM simulation of the test are shown for comparison with the measured responses in Figure 29. These plots all show that, in general, the dynamics of the vehicle were predicted quite well by the model. The main discrepancies are seen to be that the model predicted substantially lower lateral accelerations between t = 1.75 seconds and t = 3.5 seconds, and a smaller change of heading angle as a result of the more rapid decrease of the yaw velocity after t = 3.0 seconds. It is of interest to note that the model predicted the "spikes" evident in the pitch-rate and roll-rate traces at t = 1.5 seconds, although they occur about 0.2 second earlier in the simulation, and the subsequent oscillations are of smaller magnitude.

The measured and predicted wheel paths are depicted in Figure 30, where it may be seen that, except for the final heading angle, the trajectory and final rest position of the test vehicle were quite accurately matched by the simulation model.

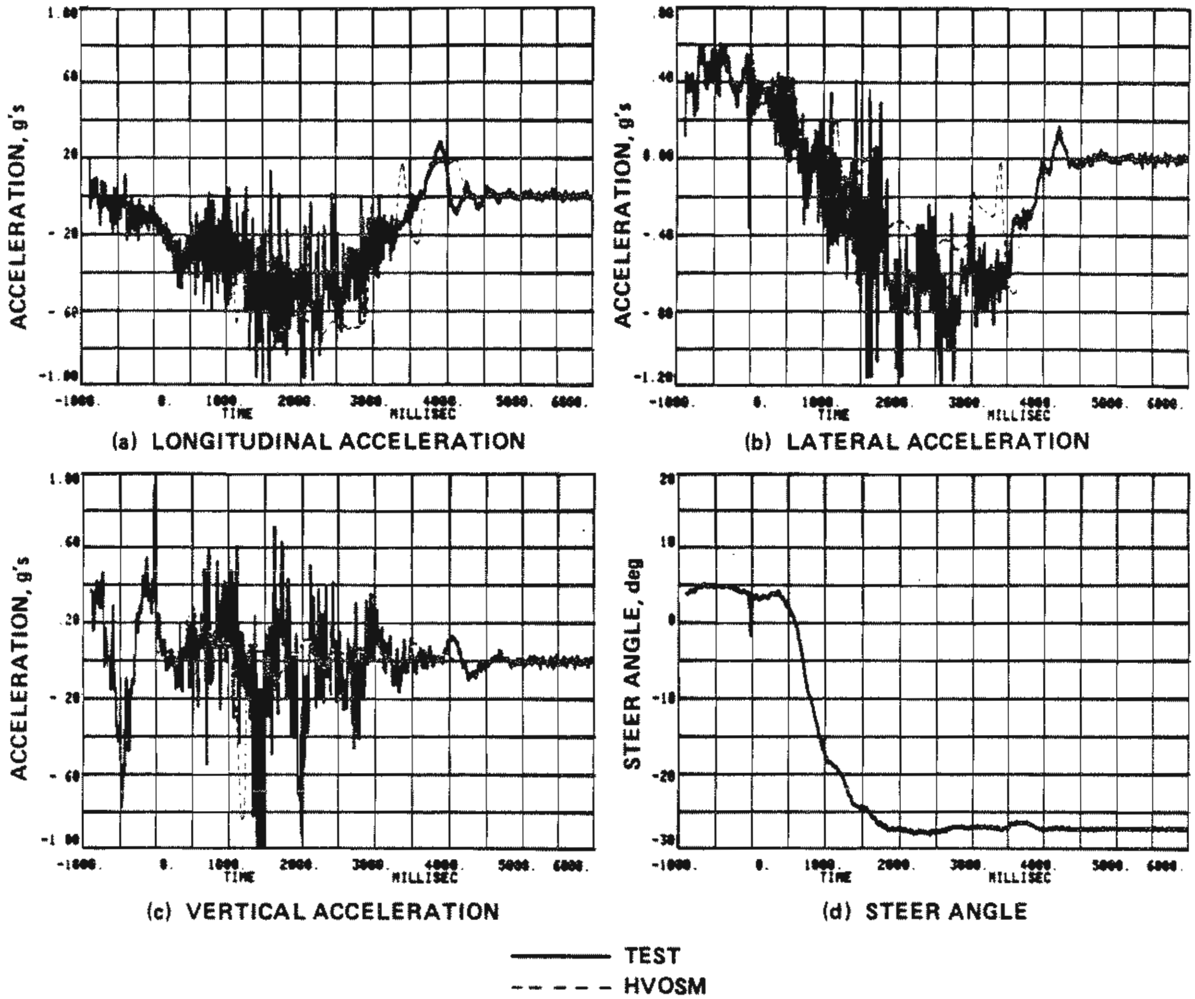

Figure 29. Comparison of HVOSM and measured vehicle responses in fill-transition test.

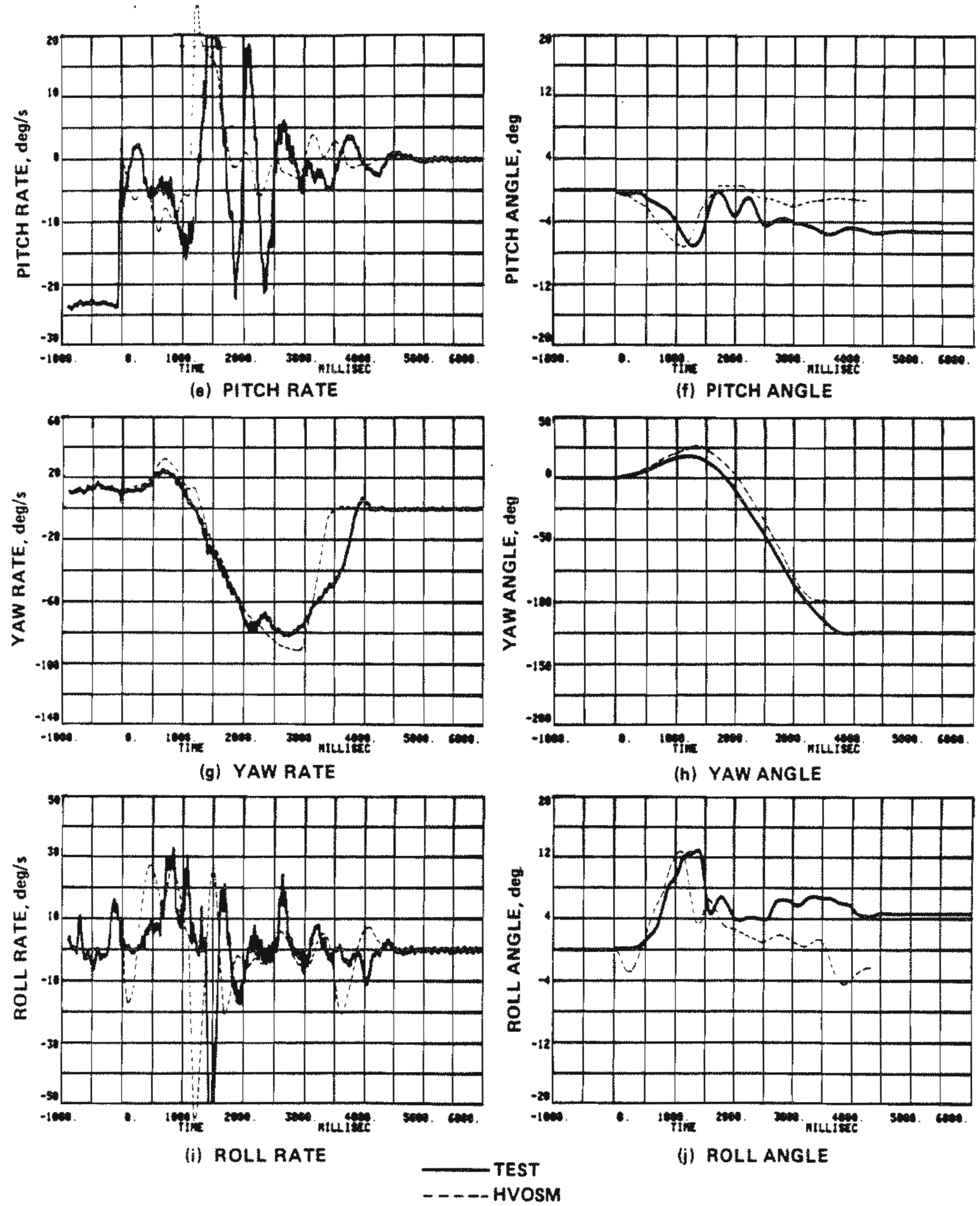

Figure 29. Comparison of HVOSM and measured vehicle responses in fill-transition test. (continued)

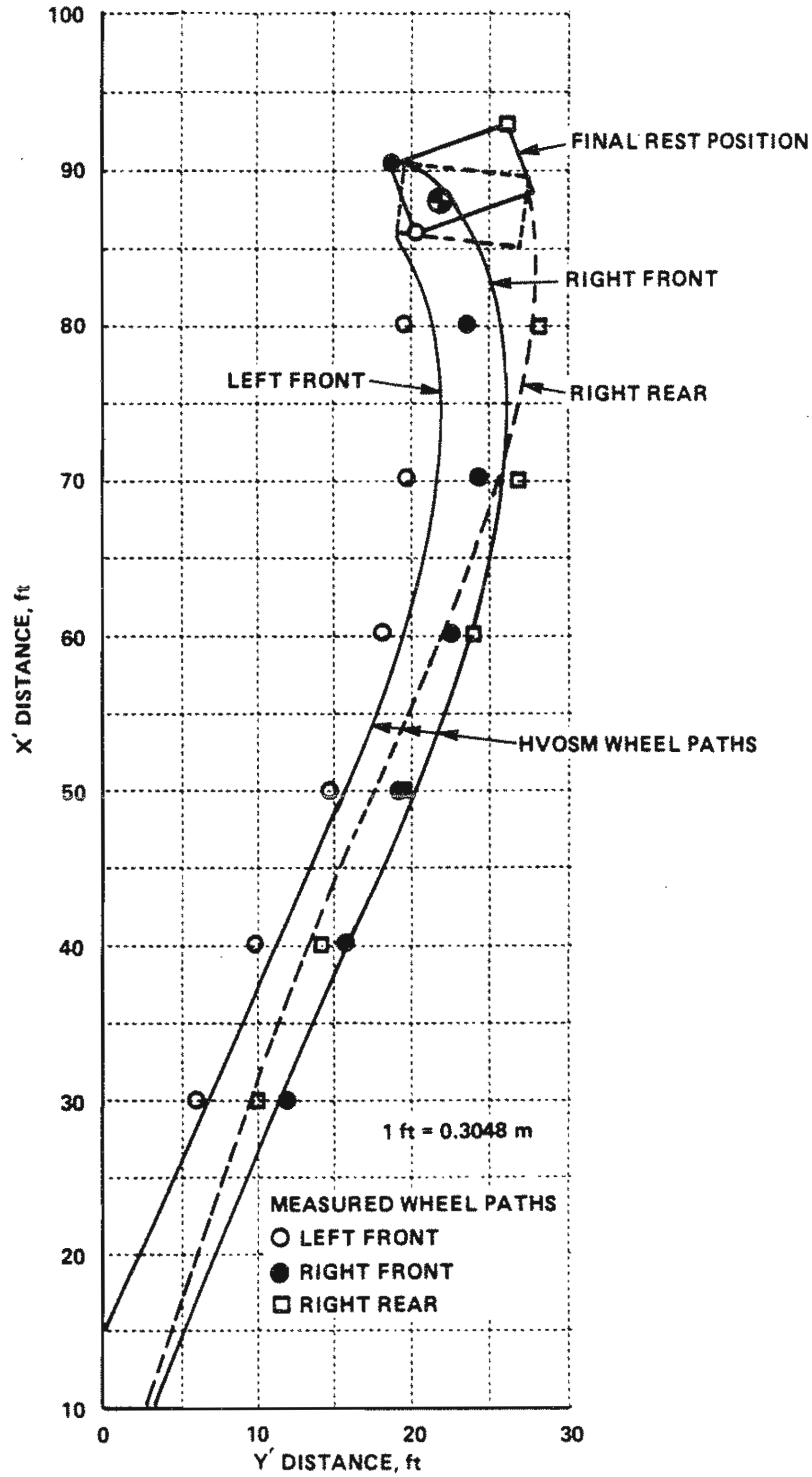

Figure 30. Wheel paths in fill-transition test.

Traversal of Ditch Embankment

The last full-scale test was performed at a site adjacent to the Calspan VERF skid pad that included a 3-ft (0.9-m) deep drainage ditch that widened into a large curved hollow or swale. The slope of the embankment forming the side of the ditch and the hollow traversed by the vehicle was variable, with a maximum value of about 3:1. The slope of the terrain is illustrated in the sketch of Figure 31.

Since the test site was deemed too hazardous to use a driver, the VERF tow and rail guidance system was used to accelerate the vehicle on the approach to the site. The approach path was such that the entry into the ditch was essentially end-on, so the wheels on the left side of the vehicle traveled along the bottom of the ditch while those on the right side remained higher on the embankment. (See Figure 31.) Just before the left-front wheel reached the bottom of the ditch, a remotely activated system aboard the vehicle rapidly turned the front wheels to a large, right steer angle and applied brakes to the rear wheels. The vehicle subsequently climbed back up the side of the ditch (or hollow) about 70 ft (21.3 m) further downstream and spun out as it came to rest. Due to the horizontal curvature of the embankment as well as the turning of the vehicle, the embankment traversed on exit from the ditch was more like a longitudinal slope than a side slope with respect to the vehicle path.

Two nearly identical tests of the vehicle traversing the ditch embankment were performed. In the first test, the speed upon entering the ditch was 39.4 mi/h (63.4 km/h). The car did not roll over and did not appear to have sustained any damage. However, review of the recorded data indicated that the onboard system to steer the front wheels and apply brakes to the rear wheels did not function as intended. The data trace for the steer angle showed that steering was initiated about 0.6 second later than desired and was highly oscillatory, with peaks that exceeded the known maximum steer angle to which the wheels could be turned. In addition, no roll angular velocity data were obtained, due to a faulty rate gyro.

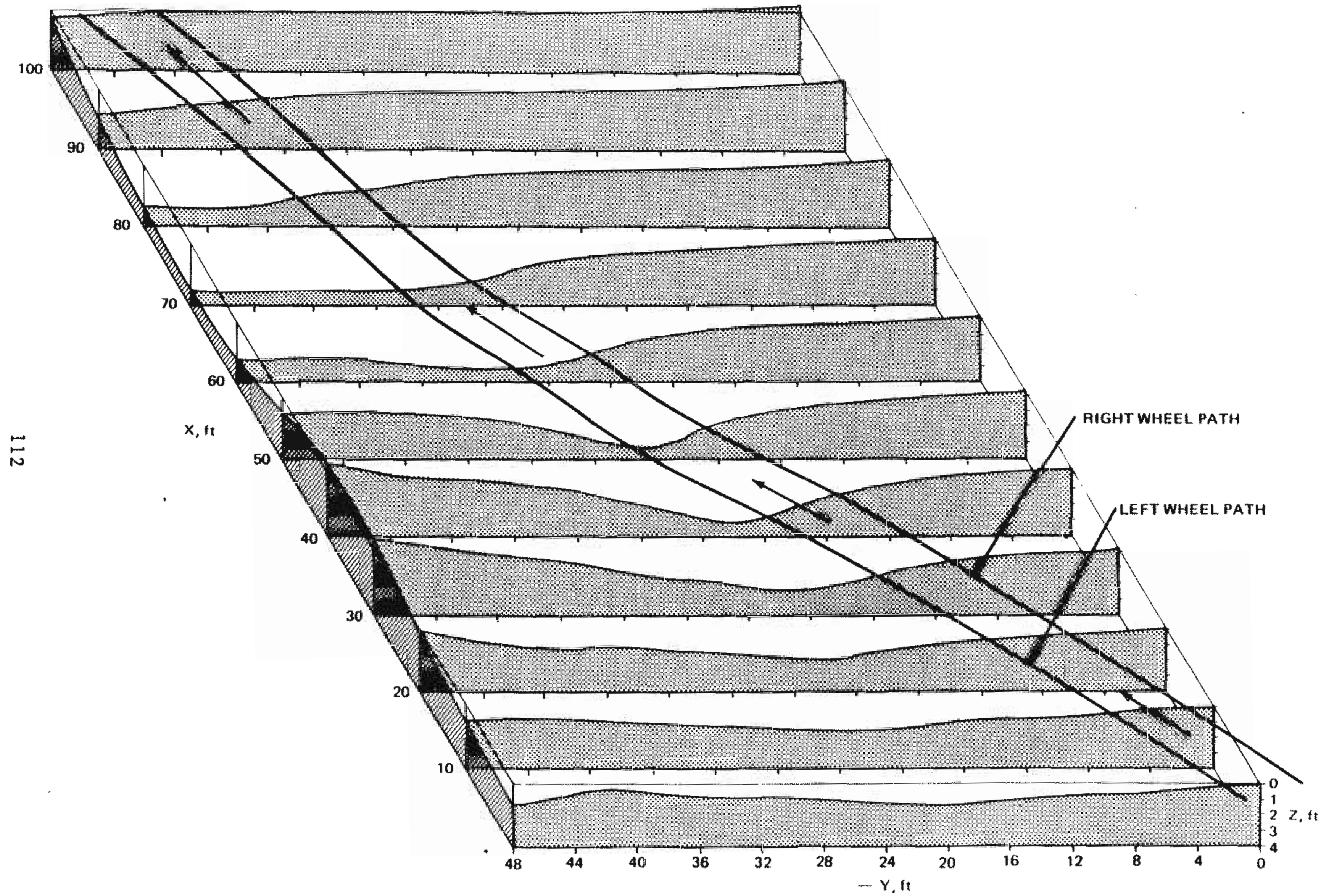

Figure 31. Scale drawing of ditch-embankment test site showing path of vehicle.

After identifying and correcting the source of these problems, a second, replicate test was performed. The vehicle speed in this test was 42.26 mi/h (68.0 km/h), and the front wheels were rapidly steered 17.5 degrees to the right just before the left wheel encountered the bottom of the ditch. Although the response of the car was quite violent, the car remained upright during passage through the ditch and in the subsequent spinout while coming to rest. Sequential photographs of the test are displayed in Figure 32.

Results of the HVOSM simulation of the test are shown for comparison with measured responses in Figure 33. The agreement between the model and test results is, in general, deemed quite good, except for the yaw response. It may be noted that the predicted yaw rate is lower than that measured in the test from about $t = 1$ second to $t = 2.1$ seconds and then continues to increase to a much higher peak value. As a result, the total change of vehicle heading angle shown by the simulation model is substantially greater than observed in the test.

From analysis of the output data from this and other simulation runs made in an attempt to account for the different yaw behavior of the simulated vehicle, it appears that the discrepancy is most likely mainly due to inaccuracy of the plow forces calculated by the deformable-soil model for the very large tire normal forces produced in traversing the terrain feature. The left-front tire, in particular, was heavily loaded at $t = 0.25$ second (8,230 lb) and again at $t = 0.8$ second (6,622 lb), which resulted in the close match of the x and z acceleration "spikes" of the test data. In contrast to the negligible sinkage of the tires in the test, the simulation shows sinkages of the tire of 4.4 in. (11.2 cm) and 3.8 in. (9.7 cm), respectively, at these times, which, in turn, resulted in very high soil plow forces. Although the lateral component of the plow force produces a positive yaw moment, this is more than offset by the counter moment of the much larger circumferential tire plow force, so the net effect is to reduce the yaw angular velocity.

Because of the differences between the simulated and measured yaw responses, the path of the simulated vehicle is also different from the actual trajectory. This is shown in Figure 34, where it may be noted that, although the distance traveled in coming to rest is predicted well by the model, the path of the simulated vehicle curves too sharply to the right.

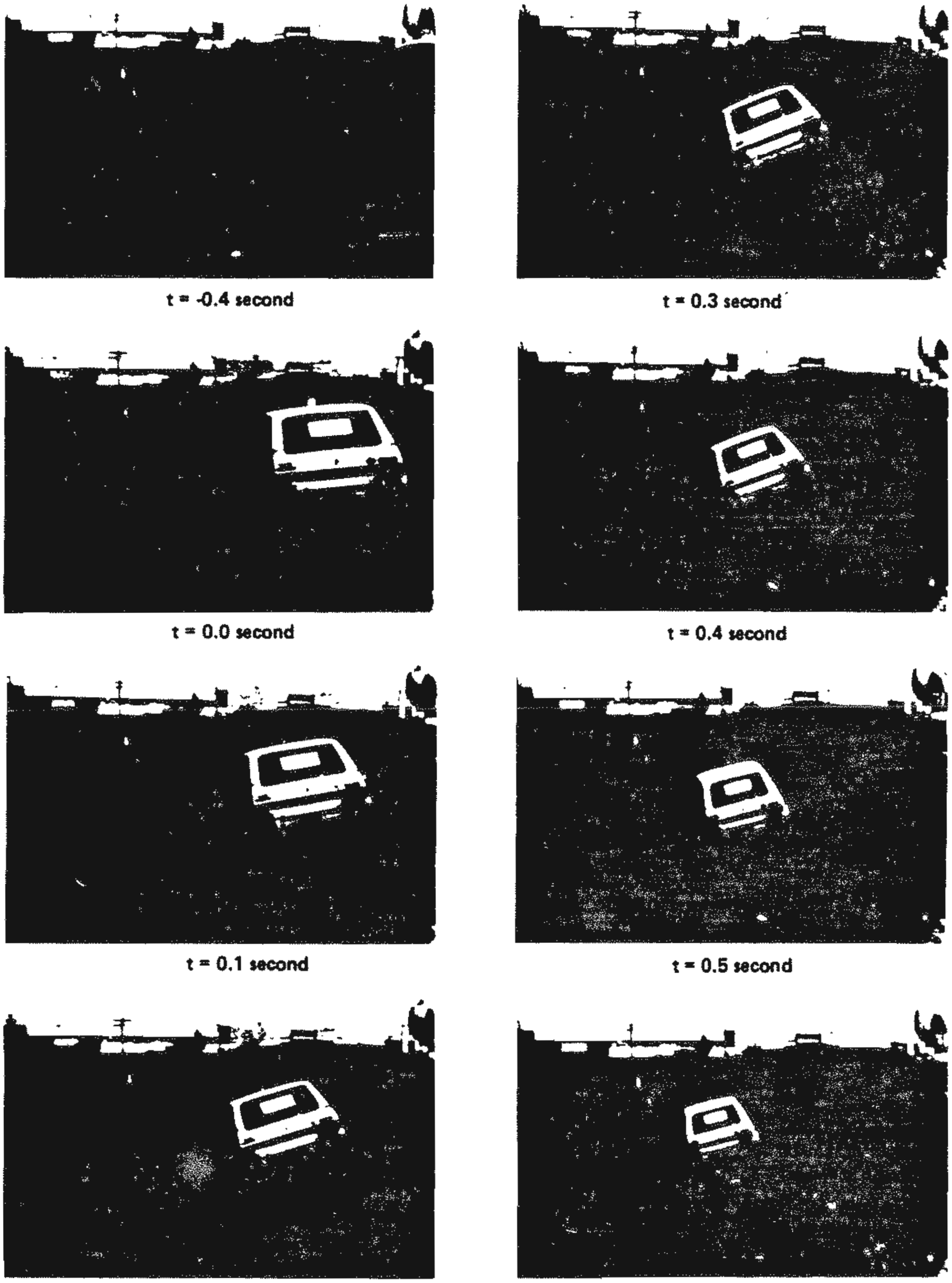

t = -0.4 second

t = 0.3 second

t = 0.0 second

t = 0.4 second

t = 0.1 second

t = 0.5 second

t = 0.2 second

t = 0.75 second

Figure 32. Sequence photographs of ditch-embankment test.

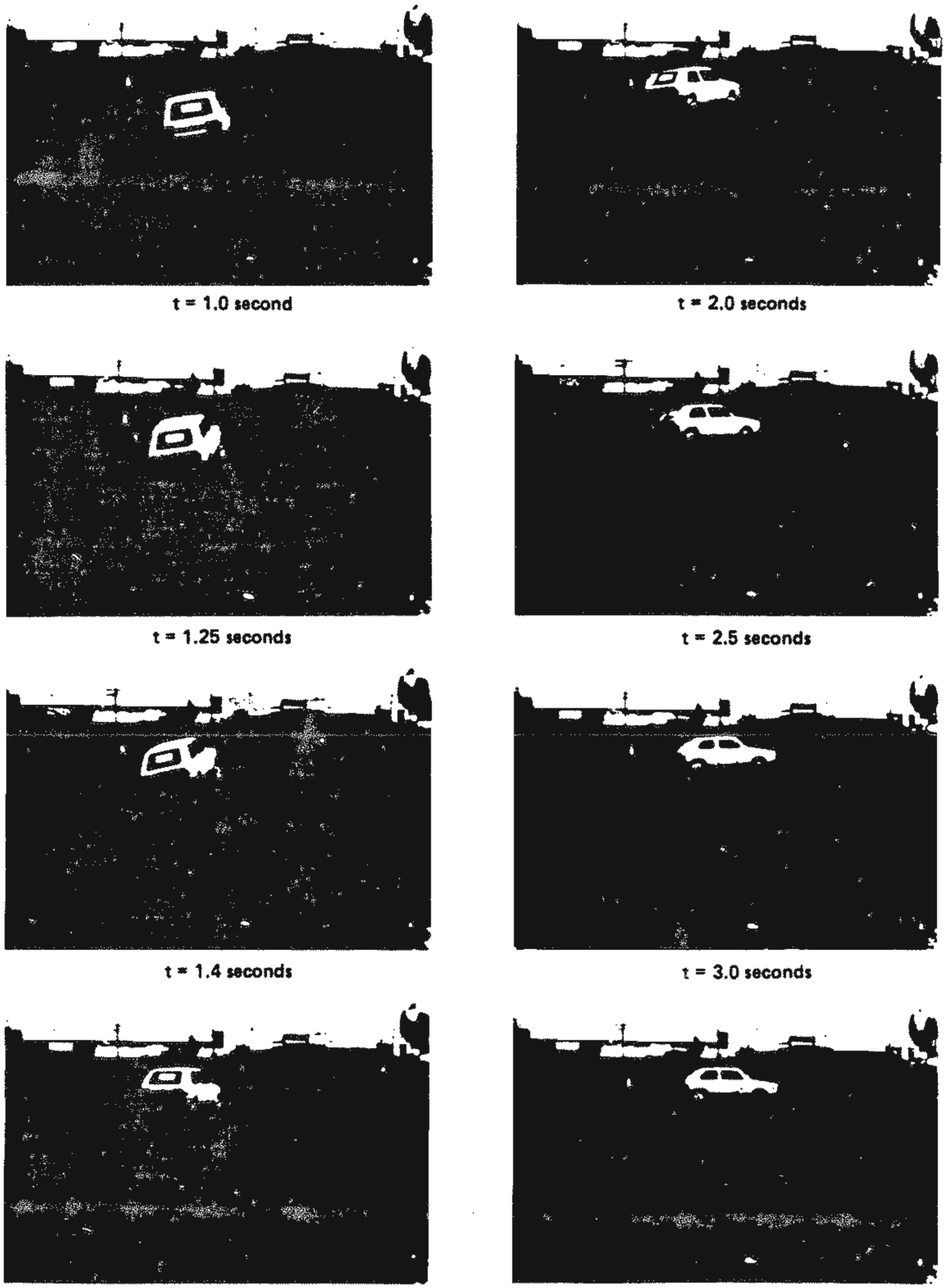

t = 1.0 second

t = 2.0 seconds

t = 1.25 seconds

t = 2.5 seconds

t = 1.4 seconds

t = 3.0 seconds

t = 1.6 seconds

t = 3.5 seconds

Figure 32. Sequence photographs of ditch-embankment test. (continued)

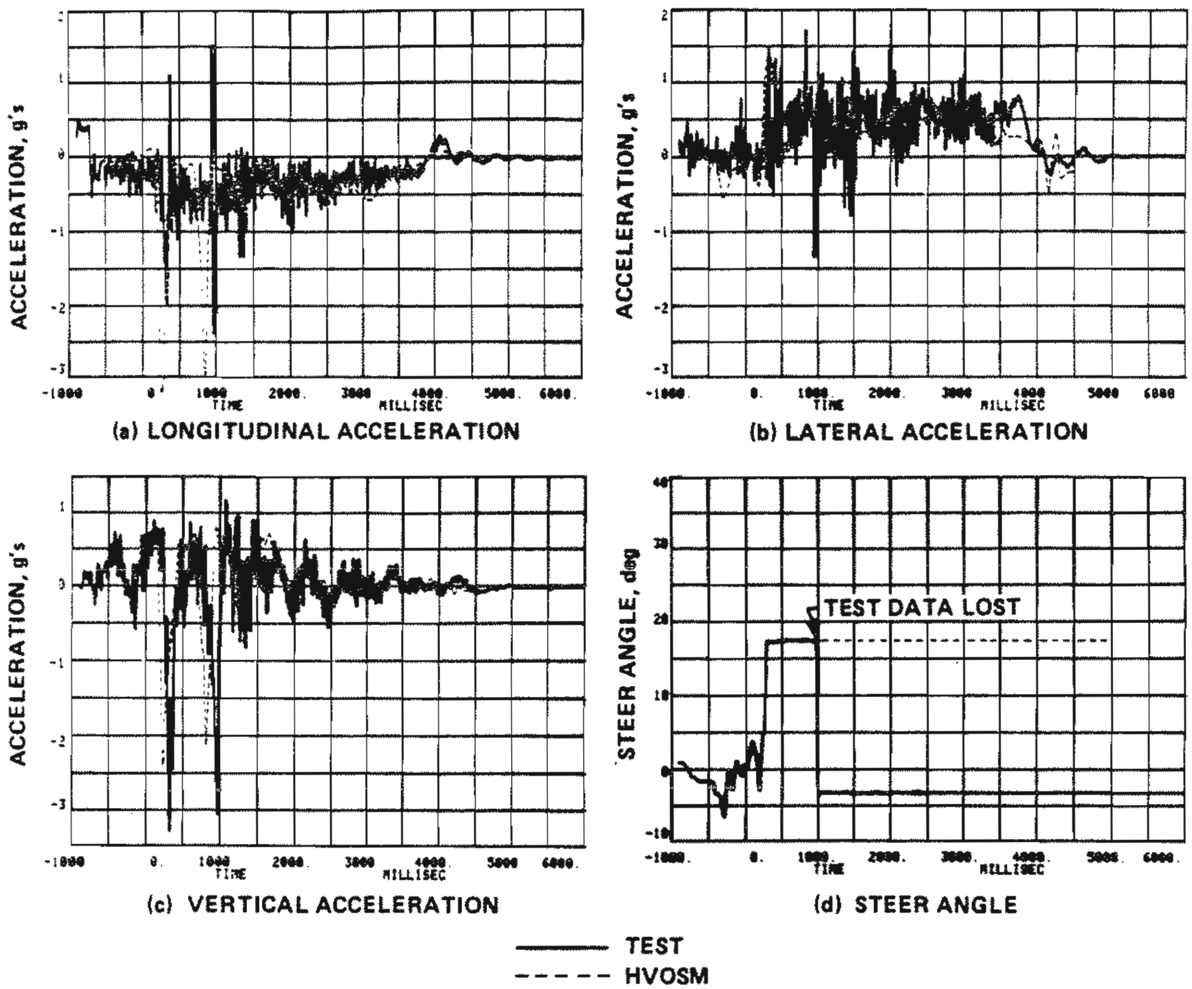

Figure 33. Comparison of HVOSM and measured vehicle responses in ditch-embankment test.

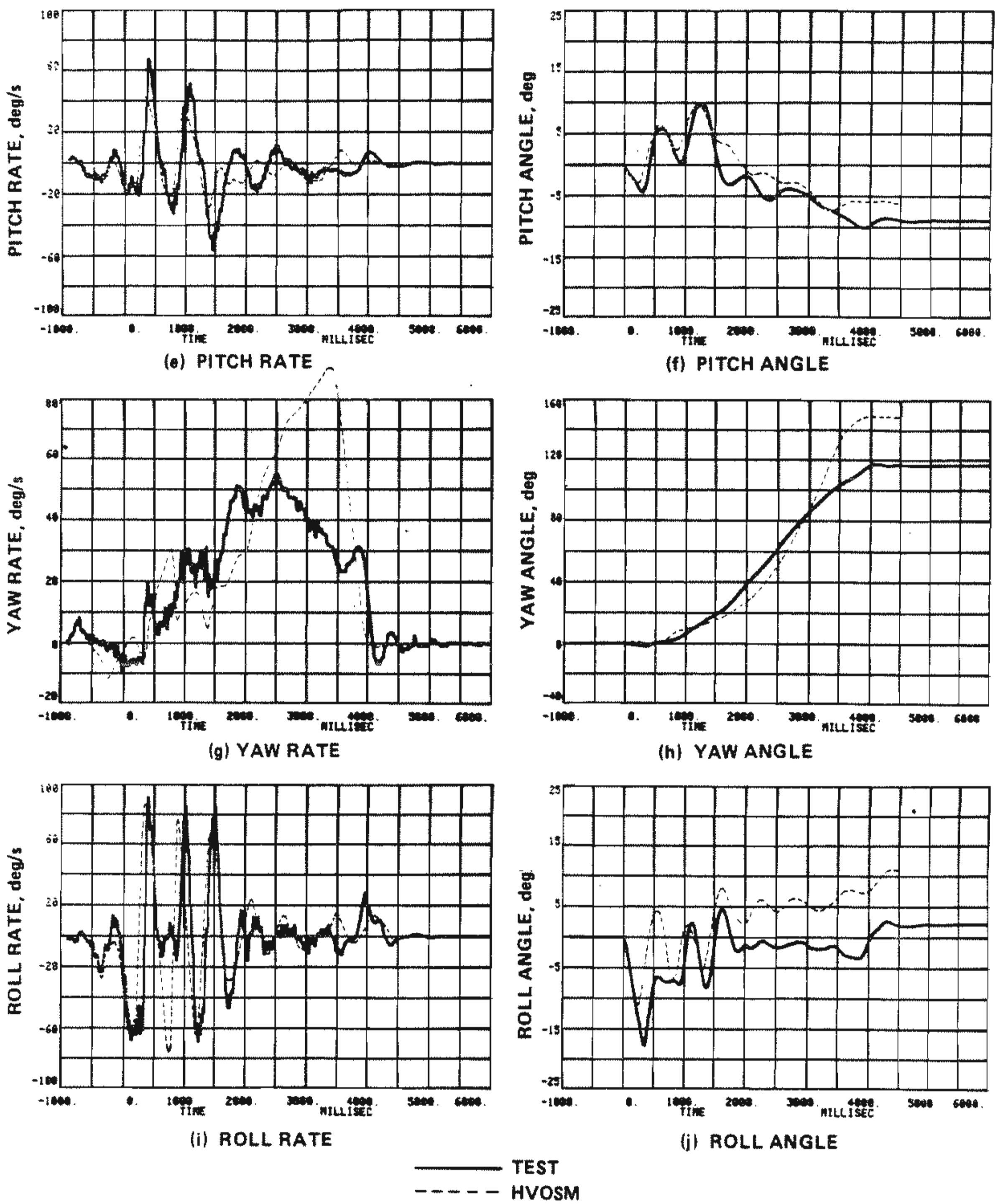

Figure 33. Comparison of HVOSM and measured vehicle responses in ditch-embankment test. (continued)

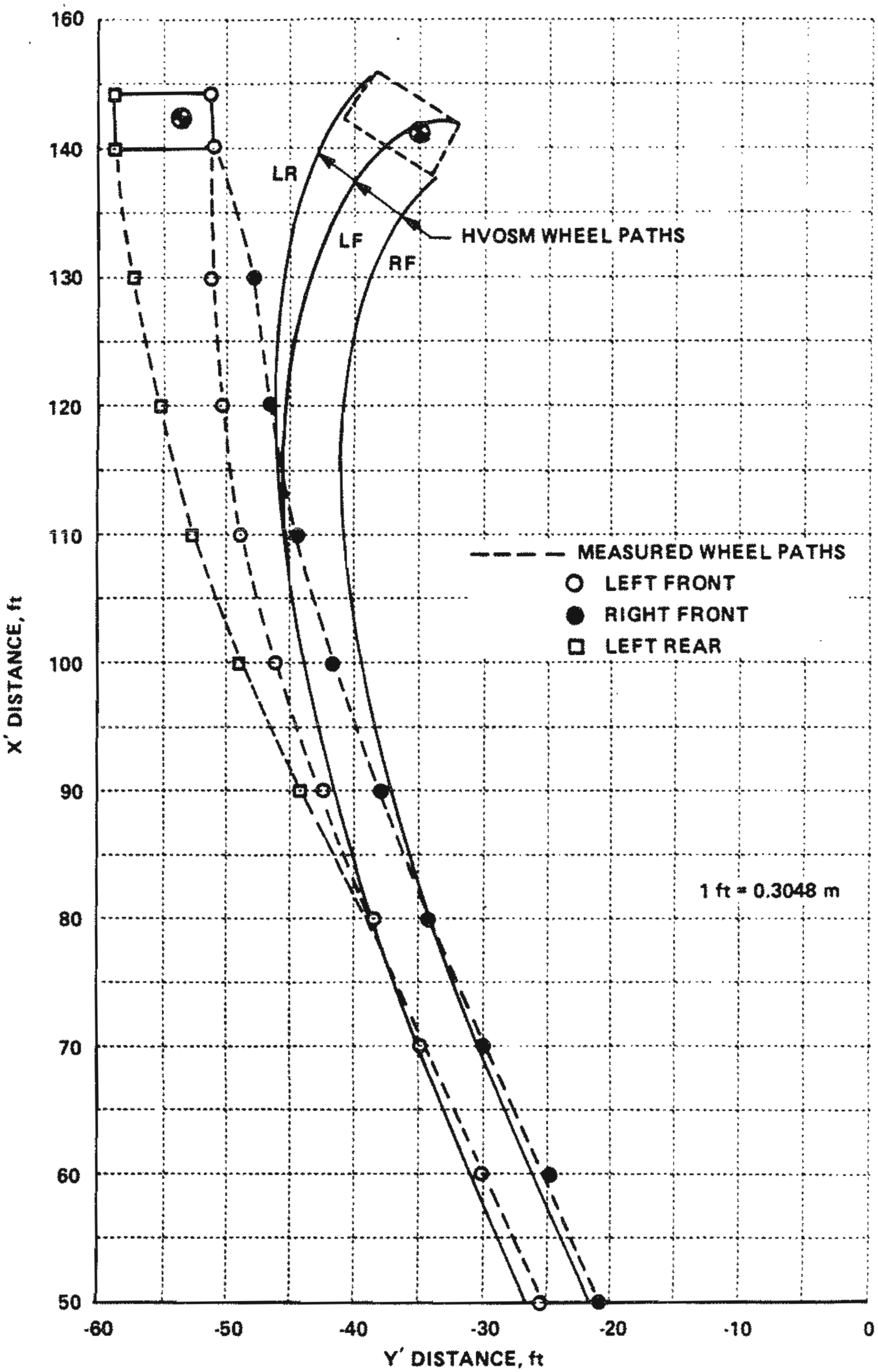

Figure 34. Measured and simulated vehicle trajectories in ditch-embankment test.

To examine the effect of the deformable-soil model, a simulation of the test was made in which the ground was considered rigid. In that run, the shape of the yaw rate response more closely matched that of the test, and the predicted vehicle trajectory up to the final rest position in the test was also better. However, the magnitude of the yaw rate was too large, so the agreement with the test data for the time history of the yaw angle was not as good. Moreover, the two "spikes" in the x acceleration data were not evidenced in this run, and the distance traveled by the vehicle before coming to rest was much greater. Hence, based on these observations, it may be concluded that, despite any shortcomings of the deformable-soil model, the results are nevertheless better than if the tire/soil-interaction effects are neglected altogether.

SUMMARY

The described verification effort allowed assessment of the capability of the modified HVOSM to simulate the responses of a vehicle for a variety of off-the-road environmental conditions. Evaluation of the comparisons presented for all of the full-scale tests performed shows that the HVOSM yielded results that are in reasonable agreement with the experimentally measured responses. As might be expected, the correlation appears to be best for the less-severe operating conditions and tends to decrease as the conditions become more severe and exceed the limits of the underlying assumptions and approximations inherent in the model.

On the whole, the deformable-soil model of the modified HVOSM computer program improved the accuracy of the simulations of the tests on the various roadside terrains, thereby providing some evidence of model validity. However, this study did not thoroughly establish the extent to which the model accounts for all of the various real-world conditions that contribute to vehicle rollover. A more extensive and rigorous validation of the analytical approach might be obtained through direct measurements of the sinkage and motion resistance forces of tires operating on soil for various tire loads, sideslip angles from 0 to 90 degrees, and soil conditions.

Section 5

SIMULATION ANALYSIS OF ROADSIDE FEATURES

APPROACH

The HVOSM computer program was used for investigating the tendency of vehicles to overturn during encounters with different roadside terrain features. Sideslopes and fill embankments were the primary features addressed in the study, but a few simulations of ditch configurations were also made. As indicated by the findings of the accident data analyses summarized in Section 2, those features are indicated to be most frequently involved in rollover accidents that occur off the highway.

Vehicle roll response is affected by a number of factors, including the geometry of the terrain; firmness of the ground; physical characteristics of the vehicle; driver control actions; and the initial conditions of vehicle road departure, such as speed, path angle, position and orientation of the sprung and unsprung masses, and the yaw, pitch, and roll angular rates of rotation. The roadside cross section for all simulations included a rigid shoulder, 8 ft (2.44 m) in width and having a friction coefficient, μ, of 0.6. The ground surface beyond the shoulder was assumed to be deformable, with characteristics defined by the soil constants for sod given by Bekker (1969).[17]

The results of accident studies show that the kinematics of vehicles at the time of departure from the roadway are highly variable and are virtually without limit with regard to the number of combinations of the many factors involved (speed, path angle, orientation, angular velocities, etc.), each of which varies over a wide range. For this reason, the selection of "typical" conditions is somewhat arbitrary. Two sets of departure conditions were considered in this study, as shown in Table 35.

Table 35. Departure conditions considered.

Variable	Departure No. 1	Departure No. 2
Speed, mi/h	60	45
Path Angle, degrees	15	25
Sideslip Angle, degrees	0	30

60 mi/h = 96.5 km/h; 45 mi/h = 72.4 km/h

These departure conditions are illustrated in Figure 35. Departure No. 1 is one of the test conditions recommended for evaluating the safety performance of highway appurtenances.[31] Data from Viner (1985)[10] and Southwest Research Institute[32] show that 60 mi/h (96.5 km/h) is approximately the 85th percentile estimated impact speed and that 40 to 50 percent of the departures occur at path angles of 15 degrees or less. For this departure, the vehicle was also assumed to be oriented at a 15-degree yaw angle, so it was tracking with zero sideslip, which the available data indicate is the case in about 50 percent of the encroachments.

For the second departure condition, the vehicle left the roadway at a lower speed and higher angle while skidding at a 30-degree sideslip angle. This departure was selected as an example of an out-of-control pre-crash condition. The 45 mi/h (72.4 km/h) speed is the average departure speed reported by Southwest Research Institute,[32] and the data of both Viner (1985)[10] and Southwest Research Institute[32] indicate that, in over half of the cases examined in which the vehicles were not tracking when they left the roadway (i.e., more than 25 percent of <u>all</u> of the accidents), they were skidding at a sideslip angle of 30 degrees or more. The forward and lateral components of the vehicle velocity vector for this departure condition are 39 mi/h (62.7 km/h) and 22.5 mi/h (36.2 km/h), respectively.

All simulation runs started with the vehicle on the roadway in static equilibrium and positioned so that the wheel closest to the shoulder was

---

31. Michie, Jarvis D., "Recommended Procedures for the Safety Performance Evaluation of Highway Appurtenances," National Cooperative Highway Research Program, Report No. 230, March 1981.
32. "Analysis of Investigative Accidents," Southwest Research Institute, Contract No. DOT-FH-11-9523, October 1983.

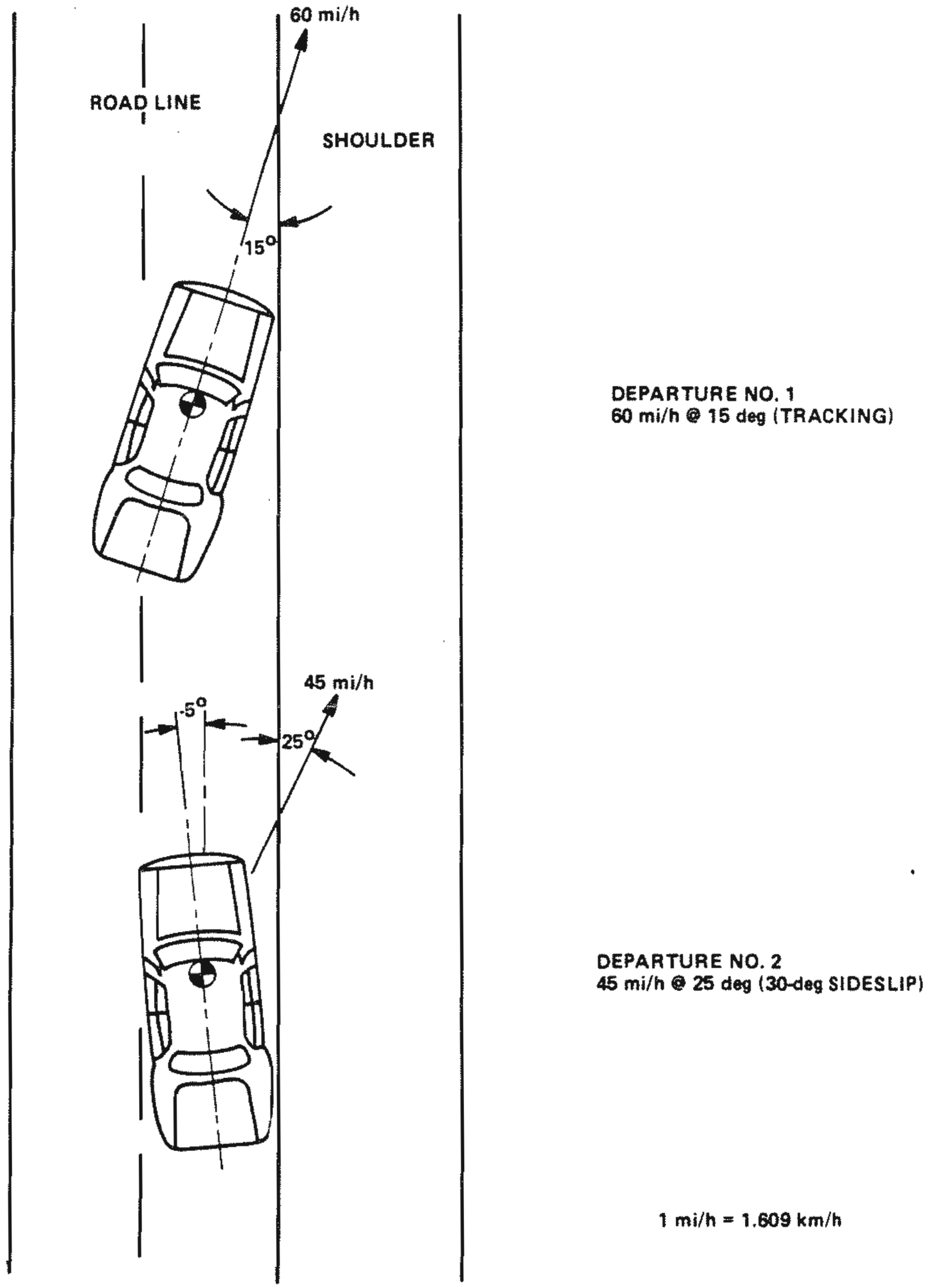

Figure 35. Simulated roadway departure conditions.

within a few inches of the pavement edge. A value of 0.8 for the friction coefficient of the pavement was assumed. Steer control to simulate a driver's attempt to maneuver the vehicle back to the road was also input to the model. The steer maneuver consisted of a linear increase of the front-wheel steer angle to 10 degrees in 1 second, beginning 0.5 second after the first wheel crossed the edge of the pavement. The steer angle remained constant at the maximum value throughout the remainder of the run. The emergency steer maneuver, although quite severe in terms of the magnitude of the steer angle, is well within the capabilities of drivers and corresponds to only about one-half turn of the steering wheel for vehicles equipped with power steering. For example, it may be noted from the steer-angle time histories measured in the full-scale tests presented in Section 4 that the driver performed steer maneuvers in excess of 10 degrees of front-wheel steer angle in less than 0.5 second, or at more than twice the angular rate used in the simulated return-to-the-road maneuver.

PHYSICAL CHARACTERISTICS OF SIMULATED VEHICLES

Three vehicles were simulated to examine the effect of roadside design variables on rollover causation for vehicles representing different weight classes. The VW Rabbit used in the full-scale tests, which weighed 2,410 lb (1,093 kg) including the driver, was selected as one of the vehicles for the study, inasmuch as an input data set of the physical properties had already been defined. (Refer to Table 32.)

For the second vehicle, the data set developed for the VW Rabbit was modified to reflect a lower total weight based on values of parameters reported by ENSCO, Inc.,[26] for a VW Rabbit weighing only 1,800 lb (816 kg). The values of those parameters affected by the different weights of the two vehicles are shown for comparison in Table 36.

The third vehicle simulated was one representing the large, heavy class of automobiles at the opposite end of the size and weight spectrum. Using

Table 36. Physical characteristics of VW Rabbits of different total weight.

Symbol	Parameter	Total vehicle weight	
		1,800 lb	2,410 lb*
M_s	Sprung mass, lb-sec^2/in.	4.014	5.593
I_x	Sprung-mass roll moment of inertia, lb-sec^2-in.	1,932	2,600
I_y	Sprung-mass pitch moment of inertia, lb-sec^2-in.	7,231	8,850
I_z	Sprung-mass yaw moment of inertia, lb-sec^2-in.	7,976	10,400
a	Sprung-mass C.G. location aft of front axle, in.	32.7	31.49
b	Sprung-mass C.G. location forward of rear axle, in.	61.8	63.01
Z_c'	Sprung-mass static C.G. height above ground, in.	(-)21.1	(-)22.49
Z_f	Sprung-mass static C.G. height above front axle, in.	10.307	11.893
Z_r	Sprung-mass static C.G. height above rear axle, in.	10.087	11.563

*Weight of test vehicle plus 180-lb driver

1 lb = 0.454 kg
1 in. = 2.54 cm

data and information from a number of sources,[33,34,35,36] typical values for the characteristics of a vehicle weighing 4,450 lb (2,081 kg) and having a 121-in. (307.3-cm) wheelbase were defined and are shown in Table 37. The tire properties are those determined from tire test measuremements of a HR78-15 tire, which is a type often used on large-size cars. The static stability ratio, T/2h, is 1.44. Hence, among three cars considered in the study, this vehicle is indicated to provide the greatest resistance to rollover.

---

33. Personal communication from Robert J. Keenan, Johns Hopkins University Applied Research Laboratory, IHVHP computer program input data listing for 1976 Ford LTD vehicle, 25 September 1984.
34. Basso, G.L., "Functional Derivation of Vehicle Parameters for Dynamics Studies," National Research Council Canada, Report No. LTR-ST 747, September 1974.
35. Rasmussen, R.E. et al., "Typical Vehicle Parameters for Dynamics Studies," General Motors Corporation, Report No. A-2542, April 1970.
36. "U.S. and Foreign Passenger Car Specifications, 1973-1982," Motor Vehicle Manufacturers Association.

Table 37. Physical characteristics of simulated 4,450-lb (2,018-kg) automobile.

SPRUNG MASS	XMS	=	9.860 LB-SEC**2/IN	FRONT WHEEL X LOCATION	A	=	52.100 INCHES
FRONT UNSPRUNG MASS	XMUF	=	.635 LB-SEC**2/IN	REAR WHEEL X LOCATION	B	=	68.900 INCHES
REAR UNSPRUNG MASS	XMUR	=	1.022 LB-SEC**2/IN	FRONT WHEEL Z LOCATION	ZF	=	10.800 INCHES
X MOMENT OF INERTIA	XIX	=	5000.000 LB-SEC**2-IN	REAR WHEEL Z LOCATION	ZR	=	10.660 INCHES
Y MOMENT OF INERTIA	XIY	=	31000.000 LB-SEC**2-IN	FRONT WHEEL TRACK	TF	=	64.100 INCHES
Z MOMENT OF INERTIA	XIZ	=	35000.000 LB-SEC**2-IN	REAR WHEEL TRACK	TR	=	64.300 INCHES
XZ PRODUCT OF INERTIA	XIXZ	=	.000 LB-SEC**2-IN	FRONT ROLL AXIS	RHOF	=	.000 NOT USED
FRONT AXLE MOMENT OF INERTIA	XIF	=	.000 NOT USED	REAR ROLL AXIS	RHO	=	.000 INCHES
REAR AXLE MOMENT OF INERTIA	XIR	=	750.000 LB-SEC**2-IN	FRONT SPRING TRACK	TSF	=	.000 NOT USED
GRAVITY	G	=	386.400 IN/SEC**2	REAR SPRING TRACK	TS	=	45.500 INCHES
	X1	=	.00 INCHES	FRONT AUX ROLL STIFFNESS	RF	=	230000.00 LB-IN/RAD
ACCELEROMETER 1 POSITION	Y1	=	.00 INCHES	REAR AUX ROLL STIFFNESS	RR	=	.00 LB-IN/RAD
	Z1	=	.00 INCHES	REAR ROLL-STEER COEF.	AKRS	=	.0330 RAD/RAD
	X2	=	.00 INCHES		AKDS	=	.000 NOT USED
ACCELEROMETER 2 POSITION	Y2	=	.00 INCHES	REAR DEFL-STEER COEFS.	AKDS1	=	.000 NOT USED
	Z2	=	.00 INCHES		AKDS2	=	.000 NOT USED
					AKDS3	=	.000 NOT USED

S T E E R I N G S Y S T E M			
MOMENT OF INERTIA	XIPS	=	.000 LB-SEC**2-IN
COULOMB FRICTION TORQUE	CPSP	=	.000 LB-IN
FRICTION LAG	EPSP	=	.000 RAD/SEC
ANGULAR STOP RATE	AKPS	=	.000 LB-IN/RAD
ANGULAR STOP POSITION	OMGPS	=	.000 RADIANS
PNEUMATIC TRAIL	XPS	=	.000 INCHES

	FRONT SUSPENSION			REAR SUSPENSION		
SUSPENSION RATE	AKF	=	120.000 LB/IN	AKR	=	115.000 LB/IN
COMPRESSION STOP COEFS.	AKFC	=	189.000 LB/IN	AKRC	=	324.000 LB/IN
	AKFCP	=	600.000 LB/IN**3	AKRCP	=	600.000 LB/IN**3
EXTENSION STOP COEFS.	AKFE	=	588.000 LB/IN	AKRE	=	864.000 LB/IN
	AKFEP	=	600.000 LB/IN**3	AKREP	=	600.000 LB/IN**3
COMPRESSION STOP LOCATION	OMEGFC	=	-3.000 INCHES	OMEGRC	=	-3.500 INCHES
EXTENSION STOP LOCATION	OMEGFE	=	3.000 INCHES	OMEGRE	=	4.000 INCHES
STOP ENERGY DISSIPATION FACTOR	XLAMF	=	.650	XLAMR	=	.650
VISCOUS DAMPING COEF.	CF	=	6.850 LB-SEC/IN	CR	=	7.480 LB-SEC/IN
COULOMB FRICTION	CFP	=	160.000 LB	CRP	=	55.000 LB
FRICTION LAG	EPSF	=	.100 IN/SEC	EPSR	=	.100 IN/SEC

Table 37. Physical characteristics of simulated 4,450-lb (2,018-kg) automobile. (continued)

FRONT WHEEL CAMBER VS SUSPENSION DEFLECTION		REAR WHEEL CAMBER VS SUSPENSION DEFLECTION		FRONT HALF-TRACK CHANGE VS SUSPENSION DEFLECTION		REAR HALF-TRACK CHANGE VS SUSPENSION DEFLECTION	
DELTAF	PHIC	DELTAR	PHIRC	DELTAF	DTHF	DELTAR	DTHR
INCHES	DEGREES	NOT USED	NOT USED	INCHES	INCHES	NOT USED	NOT USED
-3.00	-.43	-3.00	.00	-3.00	.00	-3.00	.00
-2.00	-.95	-2.00	.00	-2.00	.00	-2.00	.00
-1.00	-1.22	-1.00	.00	-1.00	.00	-1.00	.00
.00	-1.26	.00	.00	.00	.00	.00	.00
1.00	-.98	1.00	.00	1.00	.00	1.00	.00
2.00	-.41	2.00	.00	2.00	.00	2.00	.00
3.00	.00	3.00	.00	3.00	.00	3.00	.00

T I R E D A T A

			RF	LF	RR	LR	
TIRE LINEAR SPRING RATE	AKT	=	1360.000	1360.000	1360.000	1360.000	LB/IN
DEFL. FOR INCREASED RATE	SIGT	=	6.000	6.000	6.000	6.000	INCHES
SPRING RATE INCREASING FACTOR	XLAMT	=	10.000	10.000	10.000	10.000	
	A0	=	2318.000	2318.000	2318.000	2318.000	
	A1	=	9.600	9.600	9.600	9.600	
SIDE FORCE COEFFICIENTS	A2	=	3775.000	3775.000	3775.000	3775.000	
	A3	=	.387	.387	.387	.387	
	A4	=	-3365.000	-3365.000	-3365.000	-3365.000	
TIRE OVERLOAD FACTOR	OMEGT	=	.750	.750	.750	.750	
TIRE UNDEFLECTED RADIUS	RW	=	13.980	13.980	13.980	13.980	INCHES
TIRE / GROUND FRICTION COEF.	AMU	=	.800	.800	.800	.800	

SIDESLOPES

The slope of the ground on fill sections is recognized as an important roadside cross-section variable for which little data showing the effect of different values of the sideslope on the propensity of vehicles to roll over currently exist. Simulations of the responses of different vehicles traversing only the sideslope region of fill embankments having slope ratios of 2:1, 3:1, and 4:1 were performed. The effect of different rounding of the transition from the shoulder to the sideslope was also examined. The roundings considered were 4 ft (1.22 m) and the profiles defined by the equations given by AASHTO[37] for a 60-mi/h (96.6-km/h) departure, which are herein referred to as "optimum" roundings. The roadside terrain configurations simulated are illustrated in Figure 36.

The maximum roll angles of the vehicles operating on sideslopes having a surface friction coefficient of 0.6 are shown in Tables 38 and 39 for cross sections with 4-ft (1.22-m) and optimum rounding at the shoulder, respectively. Also listed in Tables 38 and 39 are the values of the roll angle expressed as a percentage of the critical roll angle of each vehicle. The critical roll angle is the angle at which the vehicle, considered as a rigid body, would become statically unstable and is equal to $\tan^{-1}(T/2h)$.

The tabulated results show that, as one would expect, the amount of vehicle roll decreases as the steepness of the sideslope decreases. In comparing the results obtained for the two different departure conditions, it may be seen that the tendency to produce rollover was greater for the non-tracking departure condition. No rollovers occurred in any of the simulations of the tracking departure, although each of the vehicles came very close to overturning on the 2:1 sideslope with 4-ft (1.22-m) rounding. The importance of rounding, particularly of steep sideslopes, is evidenced by the increased roll stability of the vehicles in the simulations of configurations with optimum rounding. Indeed, vehicles that otherwise rolled over on 2:1 and 3:1 slopes with 4-ft rounding at the shoulder were prevented from overturning when optimum rounding was used. The lateral distance at which the vehicle roll is

---

37. "Guide for Selecting, Locating, and Designing Traffic Barriers," American Association of State Highway and Transportation Officials, 1977.

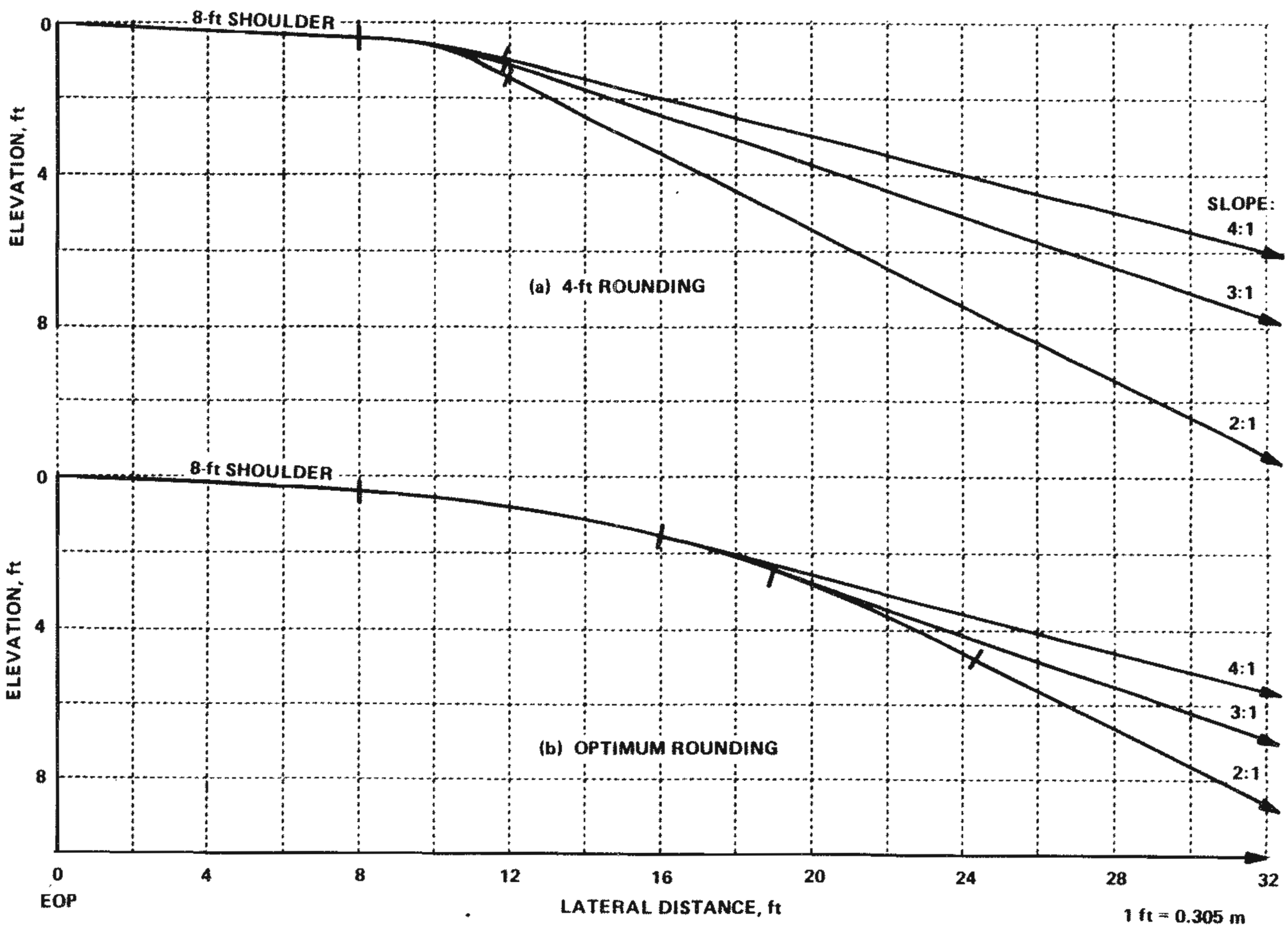

Figure 36. Ground contours of simulated sideslopes.

Table 38. Maximum vehicle roll on sideslopes with 4-ft (1.22-m) rounding (μ = 0.6)

Car weight, lb	Departure, mi/h @ degrees	Roll angle, degrees	% critical roll	Lateral distance @ max. roll, ft
2:1 Slope				
1,800	60 @ 15	43.2	80.2	21.6
2,410	60 @ 15	46.2	89.2	22.8
4,450	60 @ 15	42.4	76.8	22.1
1,800	45 @ 25	Rollover	100.0	19.0
2,410	45 @ 25	Rollover	100.0	18.0
4,450	45 @ 25	37.8	68.5	18.4
3:1 Slope				
1,800	60 @ 15	24.6	45.6	18.0
2,410	60 @ 15	26.4	51.0	19.2
4,450	60 @ 15	24.7	44.8	17.3
1,800	45 @ 25	26.5	49.2	16.4
2,400	45 @ 25	Rollover	100.0	25.2
4,450	45 @ 25	25.1	45.5	22.6
4:1 Slope				
1,800	60 @ 15	17.8	33.0	33.0
2,410	60 @ 15	19.6	37.8	29.0
4,450	60 @ 15	19.6	35.5	39.7
1,800	45 @ 25	19.7	36.6	15.3
2,410	45 @ 25	23.8	45.9	16.8
4,450	45 @ 25	20.0	36.2	20.9

1 lb = 0.454 kg
1 ft = 0.305 m
1 mi/h = 1.609 km/h

Table 39. Maximum vehicle roll on sideslopes with optimum rounding ($\mu = 0.6$)

Car weight, lb	Departure, mi/h @ degrees	Roll angle, degrees	% critical roll	Lateral distance @ max. roll, ft
2:1 Slope				
2,410	60 @ 15	32.8	63.3	48.3
4,450	60 @ 15	32.7	59.2	35.0
2,410	45 @ 25	29.8	57.5	27.2
4,450	45 @ 25	30.4	55.1	27.[illegible]
3:1 Slope				
2,410	60 @ 15	24.8	47.9	28.5
4,450	60 @ 15	25.1	45.5	29.3
2,410	45 @ 25	25.2	48.7	21.0
4,450	45 @ 25	23.7	42.9	24.0
4:1 Slope				
2,410	60 @ 15	19.6	37.8	34.9
4,450	60 @ 15	20.2	36.6	27.9
2,410	45 @ 25	20.0	38.6	20.4
4,450	45 @ 25	19.6	35.5	22.3

1 lb = 0.454 kg
1 ft = 0.305 m
1 mi/h = 1.609 km/h

maximum is somewhat larger for sideslopes with optimum rounding but usually is within 30 ft (9.14 m) of the edge of the pavement.

It may be noted that vehicle rollover was produced in three simulation runs, all involving the small, lightweight cars. Thus, the finding of accident data showing that small cars have a greater propensity to roll over than the large, heavy class of automobiles is also indicated by the simulation results. In the runs in which the vehicle did not overturn on the 2:1 and 3:1 slopes, all of the cars spun out on the sideslopes and did not follow a trajectory that would allow return to the roadway. Spinout was also produced on the 4:1 slope but occurred after the vehicle had started to return to (was on a path back toward) the road. The 4,450-lb (2,018 kg) car had less of a tendency to spin out and returned to the road without loss of directional stability in the nontracking departure on the 4:1 slope.

It had been expected that use of the deformable-soil model incorporated in HVOSM would have produced more rollovers in this series of simulations. However, analysis of the detailed output of the simulations provides insight on some of the complex interactions of various factors that influence the roll dynamics.

Responses of the 2,410-lb (1,093-kg) car traversing the 3:1 sideslope with 4-ft (1.22-m) rounding for both departure conditions are depicted in Figures 37, 38, and 39. In the case of the departure at 45 mi/h (72.4 km/h) and 25 degrees, the negative lateral acceleration is high initially, because the vehicle is moving at a large sideslip angle. As the vehicle starts to roll, the lateral acceleration decreases due to the component of gravity acting along the vehicle lateral axis and because of the decreased load on the tires after they cross the shoulder/sideslope rounding. At t = 0.75 second, both left wheels have lifted off the ground, and the vehicle is rolling at a high angular velocity. Subsequently, the load on the leading tires (particularly, the right-front) increases due to the weight transfer and, since the sideslip angle is large, high side forces are produced that are reflected by the sharp increase of lateral acceleration. Although the suspension forces increase to reduce the roll rate for a short time, the high angular momentum and the effect of the sustained large side forces are sufficient to cause the

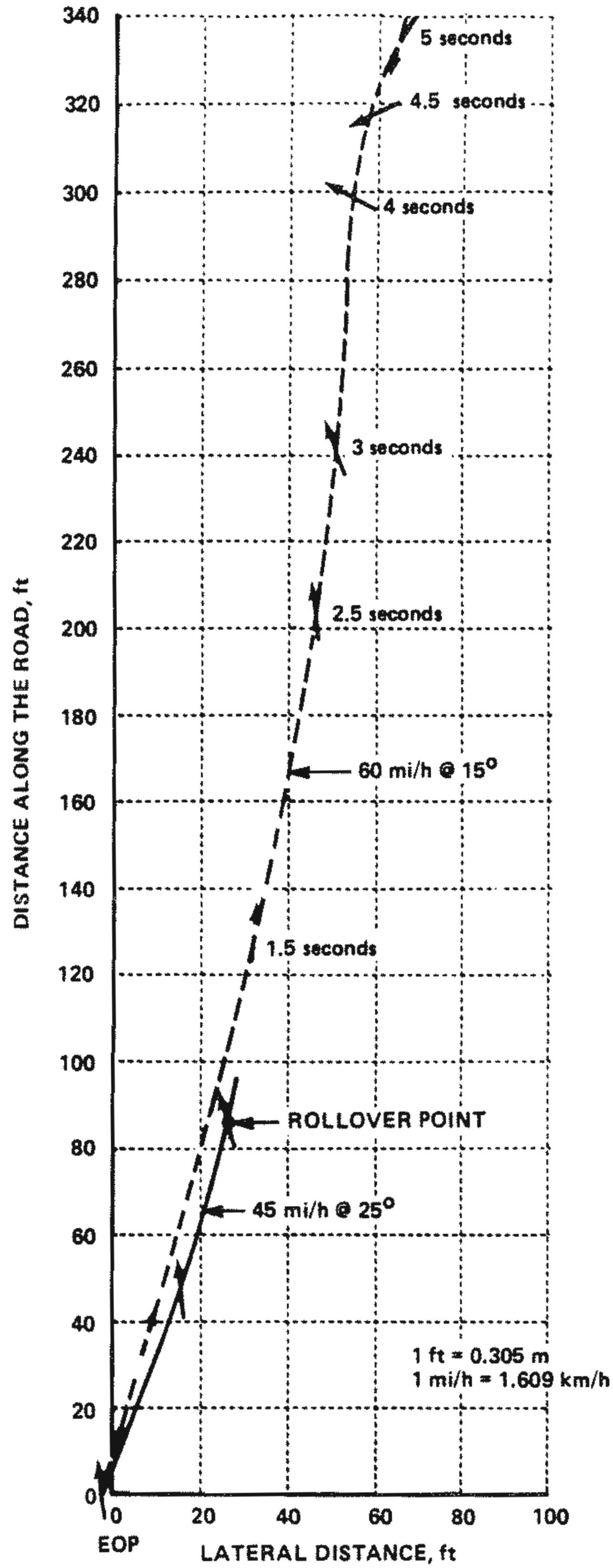

Figure 37. Trajectories of 2,410-lb (1,093-kg) vehicle on 3:1 sideslope.

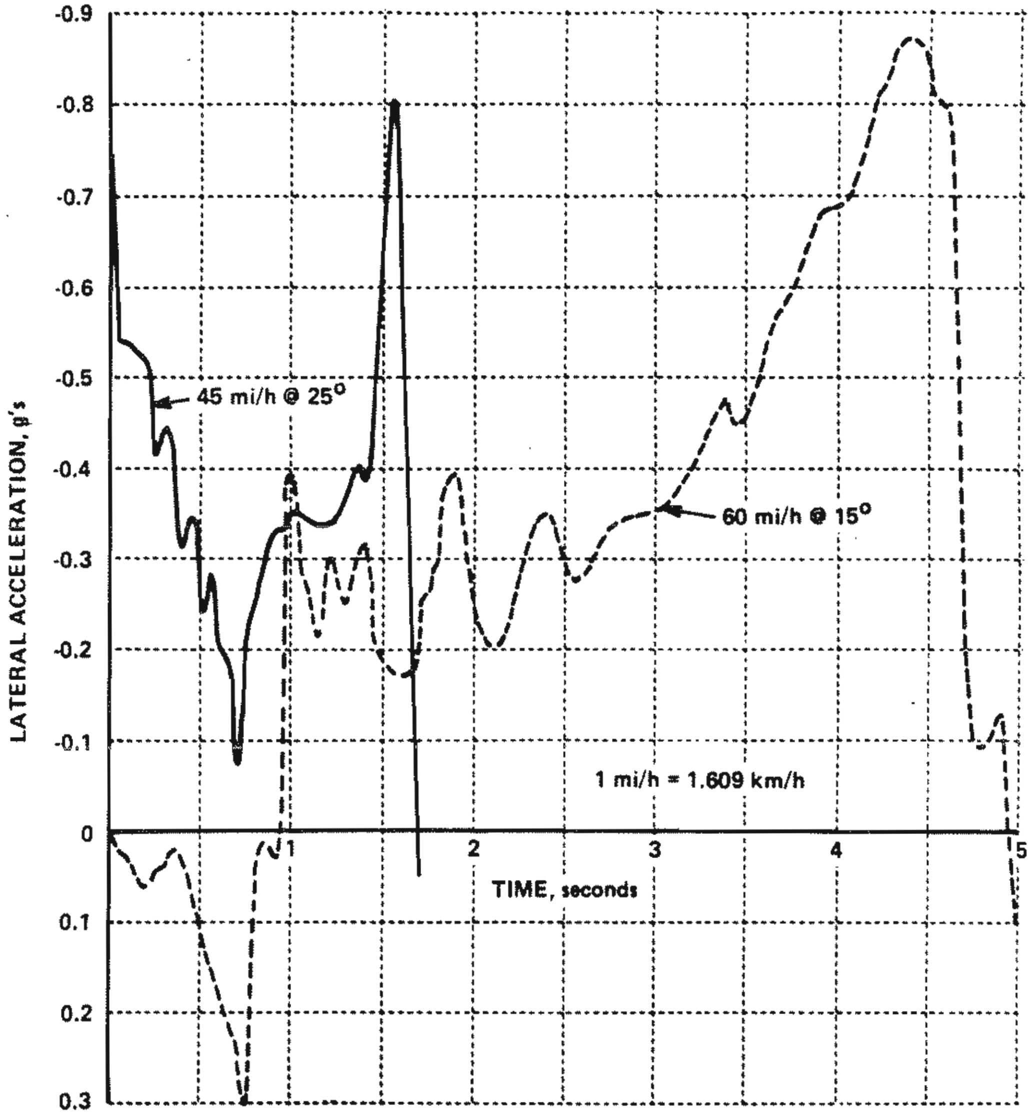

Figure 38. Lateral accelerations of 2,410-lb (1,093 kg) vehicle on 3:1 sideslope.

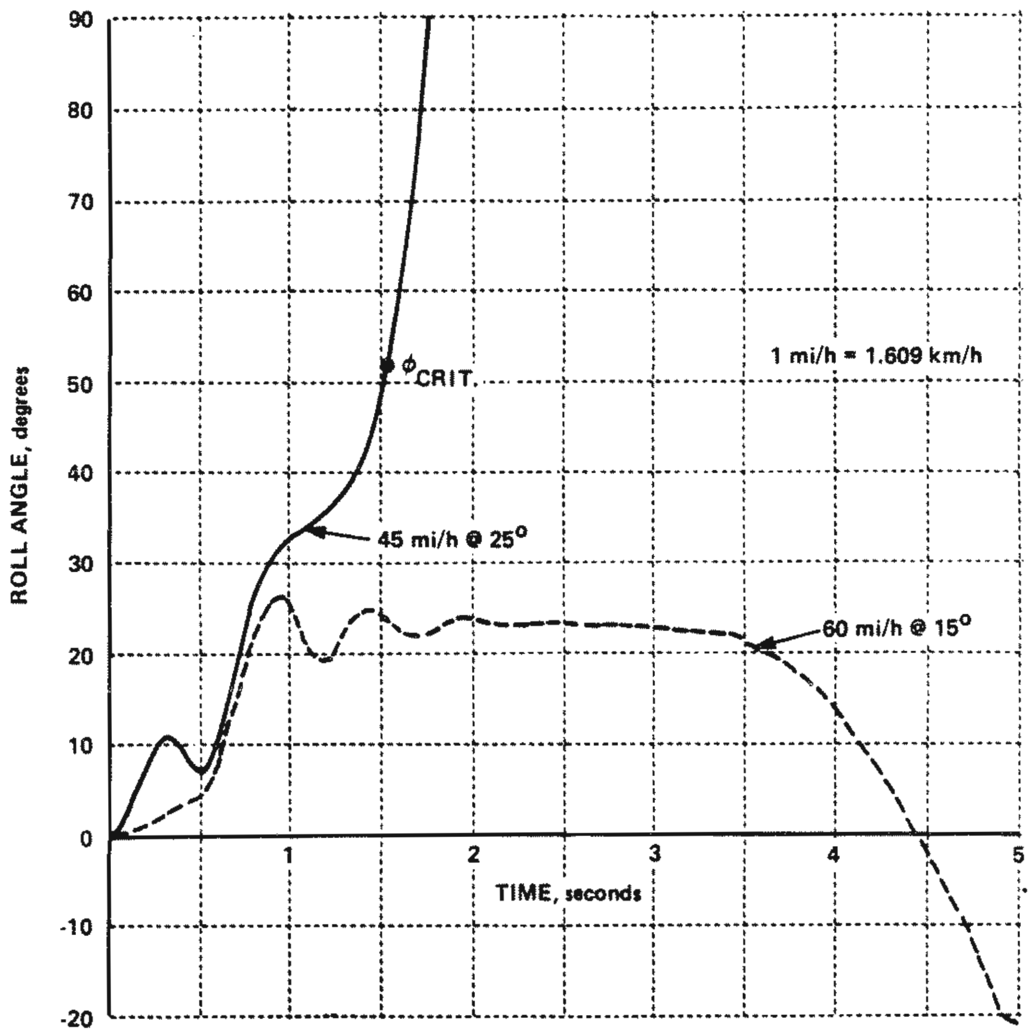

Figure 39. Roll of 2,410-lb (1,093-kg) vehicle on 3:1 sideslope.

vehicle to continue to roll beyond the critical roll angle. Also, it is noted that, because the vehicle yaw angle is small, vehicle roll due to the angle of the sideslope is maximum.

In the case of the departure at 60 mi/h (96.5 km/h) and 15 degrees, the lateral acceleration is positive initially due to the increasing gravitational component as the vehicle rolls and, since the sideslip angle is small and the tires become lightly loaded, the tires do not generate much side force. At $t = 0.8$ second, the right-front tire recontacts the sideslope, and the wheel is forced upward against the jounce travel stop, which decreases the roll rate and limits the maximum roll angle to a subcritical value. As the vehicle turns in response to the steering of the front wheels, the tire side forces increase to produce a net lateral acceleration of about -0.3 g, and the roll angle remains nearly constant at approximately 23 degrees. Thus, the roll angle is only 5 or 6 degrees more than the angle of the sideslope when the vehicle has yawed so that the vehicle heading is nearly perpendicular to the crossslope.

Subsequently, the yaw rate continues to increase and, as shown in Figure 37, the vehicle ultimately spins out. During the spinout, the left-rear tire lifts off the ground, but the side forces developed by the other tires (particularly, the right-front), although high because the vehicle is moving at high slip angles, are insufficient to produce rollover. The increase of the negative lateral acceleration and the reduction of the roll angle beginning at about $t = 3$ seconds result from the reduced effect of the sideslope angle as the yaw angle approaches 90 degrees. Note that, when the vehicle is sliding broadside (between $t = 4$ seconds and $t = 4.5$ seconds), it is pointing nearly straight up the sideslope (at a pitch angle of about 18 degrees), so the slope does not contribute to the vehicle roll. As the rotation continues beyond 90 degrees of yaw angle, the vehicle continues to roll in the counterclockwise direction, and the roll angle becomes negative because the tire side forces decrease and the gravitational moment now assists the negative roll. The vehicle speed also reduces rapidly during the spinout and is only about 28 mi/h (45 km/h) when it is skidding broadside.

An important factor affecting the vehicle roll behavior evidenced by the simulation results, which perhaps before has not been fully recognized, is the jacking effect associated with independent suspensions. The jacking force is a function of the tire-force components acting along the vehicle's lateral and vertical axes and the rate of change of the camber and the half-track change of the wheel with suspension deflection (i.e., $\frac{d\phi_i}{d\delta_i}$ and $\frac{d\Delta TH_i}{d\delta_i}$, respectively). For the vehicles simulated in this study, both $\frac{d\phi_i}{d\delta_i}$ and (for the Rabbit) $\frac{d\Delta TH_i}{d\delta_i}$ of the front suspension vary with suspension deflection, and the characteristics are such that, for given values of the tire-force components, the jacking force increases as the wheel moves in the rebound direction. Since positive jacking forces tend to raise the vehicle C.G. and also resist upward (jounce) motion of the wheel, the roll-moment contribution of the tire lateral forces is higher and, hence, increases the likelihood of rollover. Moreoever, it is noted that the adverse jacking effect tends to be progressive, since, by acting to force the wheel downward, the tire normal load is increased, which, in turn, increases the side force that gave rise to the jacking force in the first place.

From the above discussion, it is clear that vehicle rollover is a dynamic phenomenon that involves complex interactions of many vehicle, environmental, and operational factors whose effects are nonindependent and time-varying.

To better assess the degree to which the rollover hazard is affected by the steepness of the sideslope, additional simulations were performed to determine rollover threshold conditions for each sideslope. The primary independent variable for these simulations was the coefficient of friction of the ground surface beyond the shoulder, which was varied to identify the minimum value necessary to produce vehicle rollover on each sideslope. It was recognized that the resulting values of ground friction coefficient might be unrealistic in terms of representing the value for actual roadside terrain, but the approach was viewed as a simple way to obtain the increases of tire side forces that were necessary to cause vehicle rollover. In this manner, differences of the minimum friction coefficient would serve as a metric indicative of how much the potential for causing rollover differs for various sideslopes.

Over 100 computer runs were made in seeking the rollover threshold values of the ground friction coefficient for the different combinations of vehicles, departure conditions, and sideslopes. In view of the greater roll stability of the vehicles on the sideslope with optimum rounding at the shoulder, only configurations with 4-ft (1.22-m) rounding were simulated. A 5:1 sideslope was included in the simulation run matrix to better verify trends in the results.

The critical ground friction coefficients resulting in rollover of the 1,800-lb (816-kg) car for both departure conditions are given in Table 40 and also are depicted in the plots of Figure 40. For the skidding departures, these data show a consistent trend of increased friction required for rollover as the steepness of the sideslope is decreased. Note that the relationship is linear with the angle of the slope and, hence, is nonlinear with respect to the sideslope ratio. As noted in Table 40, for values of the friction coefficient 0.05 less than critical, the vehicle returned to the road on the 4:1 and 5:1 sideslopes but went into a spinning skid on the steeper slopes. Extrapolation of the curve shows that rollover on flat terrain would be expected for a friction coefficient of about 1.5. However, in a simulation of flat terrain with a friction coefficient of 1.5, the car also quickly returned to the roadway after encroaching about 12 ft (3.7 m) from the edge of the pavement, and the maximum roll angle was 11 degrees. Figure 41 shows the path and yaw attitude of the vehicle in traversals of the 2:1 and 5:1 sideslopes with friction coefficients equal to as well as 0.05 less than the rollover threshold values.

In contrast, the results for the tracking departure show that the friction coefficients required for rollover are nearly the same for all sideslopes and range between 0.9 and 1.0. Although the results do not exhibit a consistent pattern, they seem to indicate a trend of somewhat lower threshold values with decreasing sideslope, which is contrary to what one would normally expect.

The path and yaw attitude of the vehicle in traversals of the 2:1 and 5:1 sideslopes with friction coefficients equal to and 0.05 less than the rollover threshold values are illustrated in Figure 42, where it may be seen that

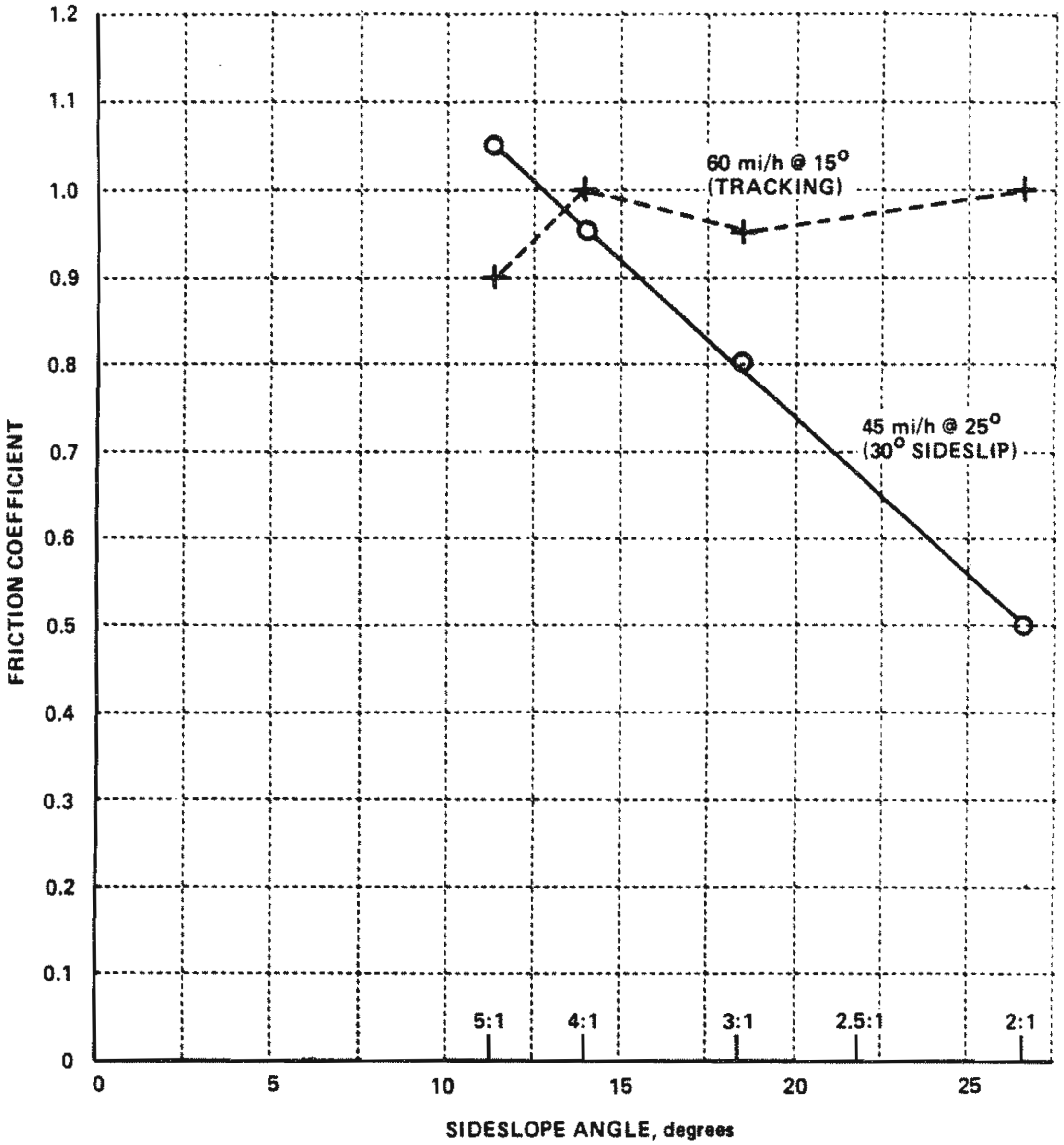

Figure 40. Friction-coefficient threshold for rollover of 1,800-lb (816-kg) car.

Table 40. Threshold of ground friction coefficient for rollover of 1,800-lb (816-kg) car.

Sideslope ratio	Friction coefficient	Maximum roll angle, degrees	Comments
45-mi/h and 25-degree (30-degree Sideslip) Departure			
2:1	0.45	45.2	Car spins out and slides down sideslope.
2:1	0.50	Rollover	Rollover 25.6 ft from EOP.
3:1	0.75	32.1	Car begins return to road, stops on sideslope; maximum lateral distance 26.2 ft from EOP.
3:1	0.80	Rollover	Rollover 21.5 ft from EOP.
4:1	0.90	24.7	Car returns to road at high angle; maximum lateral distance 19.3 ft from EOP.
4:1	0.95	Rollover	Rollover 18.3 ft from EOP.
5:1	1.0	24.3	Car returns to road at high angle; maximum lateral distance 16.6 ft from EOP.
5:1	1.05	Rollover	Rollover 12.6 ft from EOP on return path to road.
60-mi/h and 15-degree (Tracking) Departure			
2:1	0.95	43.5	Car spins out on sideslope.
2:1	1.0	Rollover	Rollover 50.7 ft from EOP.
3:1	0.90	24.9	Car begins return to road, spins out.
3:1	0.95	Rollover	Rollover 27.9 ft from EOP on return path to road.
4:1	0.95	20.8	Car begins return to road, spins out.
4:1	1.0	Rollover	Rollover 14.6 ft from EOP on return path to road.
5:1	0.85	16.8	Car begins return to road, spins out.
5:1	0.90	Rollover	Rollover 16.2 ft from EOP on return path to road.

1 mi/h = 1.609 km/h
1 ft = 0.3048 m

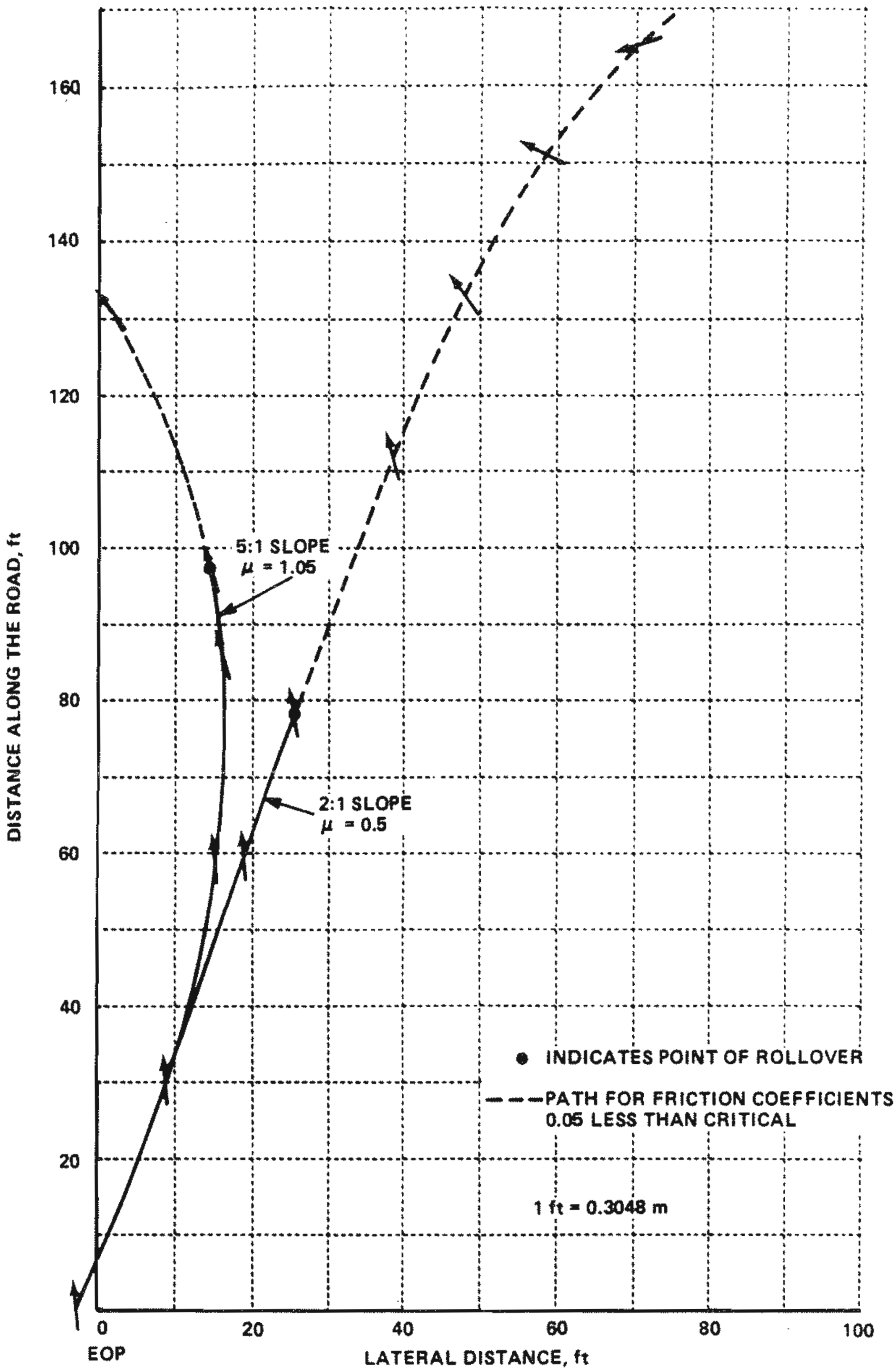

Figure 41. Trajectories of 1,800-lb (816-kg) car on 2:1 and 5:1 slopes for sideslipping departure.

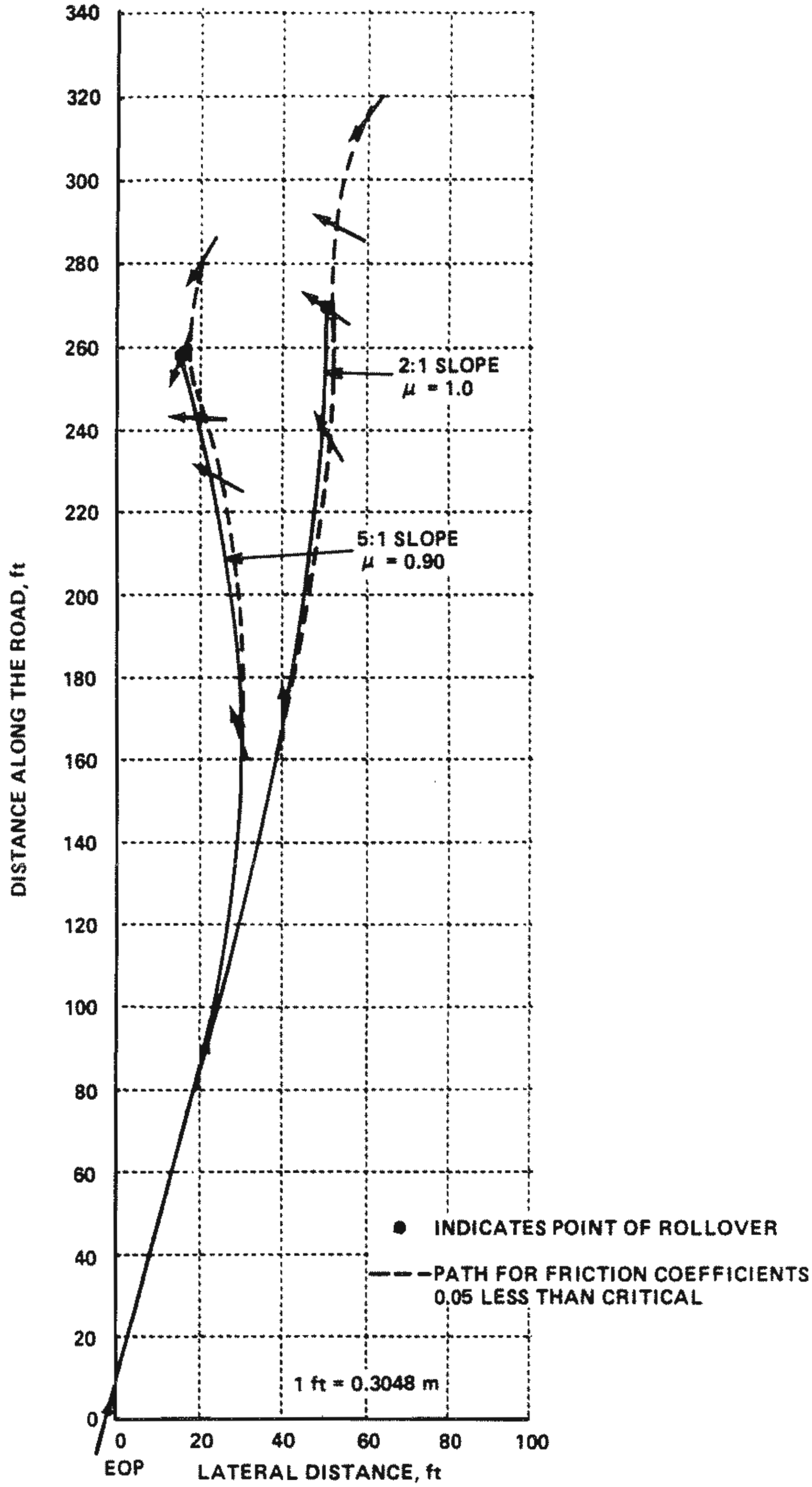

Figure 42. Trajectories of 1,800-lb (816-kg) car on 2:1 and 5:1 slopes for tracking departure.

the yaw and sideslip angles of the vehicle at the time of rollover are much greater for the shallower sideslope. The roll responses of the vehicle when rollover was induced on the various sideslopes are shown for comparison in Figure 43. Note that, although the vehicle initially rolls to a higher angle as the steepness of the sideslope is increased, the time at which the tires develop sufficient side force to overturn the vehicle is nearly the same for all slopes, and the roll angle subsequently increases very rapidly.

The reason for the difference in the relationship between the sideslope and the friction coefficient needed to produce rollover for the two different departure conditions is not clear. In the case of the sideslipping departure, the car is nearly broadside to the slope, so the inclination of the slope contributes to the vehicle roll; hence, the magnitude of the tire side forces needed to trip the vehicle is reduced as the steepness of the slope is increased. For the tracking departure, the interactions of factors affecting the roll dynamics are much more complex, but it appears that the yaw velocity achieved by the vehicle during spinout is a primary factor influencing whether the lateral accelerations developed are high enough and sustained for a sufficiently long period to induce rollover.

The rollover threshold values of ground friction coefficient determined from HVOSM simulations of the 2,410-lb (1,093-kg) automobile are listed in Table 41, and the variation with sideslope angle for the two roadway departure conditions is shown by the plots of Figure 44. These results exhibit trends similar to those for the 1,800-lb (816-kg) car, but the critical friction coefficients are substantially lower for the 2,410-lb vehicle. As was the case for the lighter car, the results for skidding departure at 45 mi/h (72.4 km/h) and 25 degrees show a consistent, and essentially linear, trend of increasing friction coefficient required to produce rollover with decreasing angle of the sideslope. For lower values of the friction coefficient, the vehicle returned to the road on the 5:1 slope but spun out on the steeper slopes.

The results for the (tracking) departure at 60 mi/h (96.5 km/h) and 15 degrees again show little difference in the minimum friction coefficient to produce rollover on the different sideslopes. However, the simulations of the

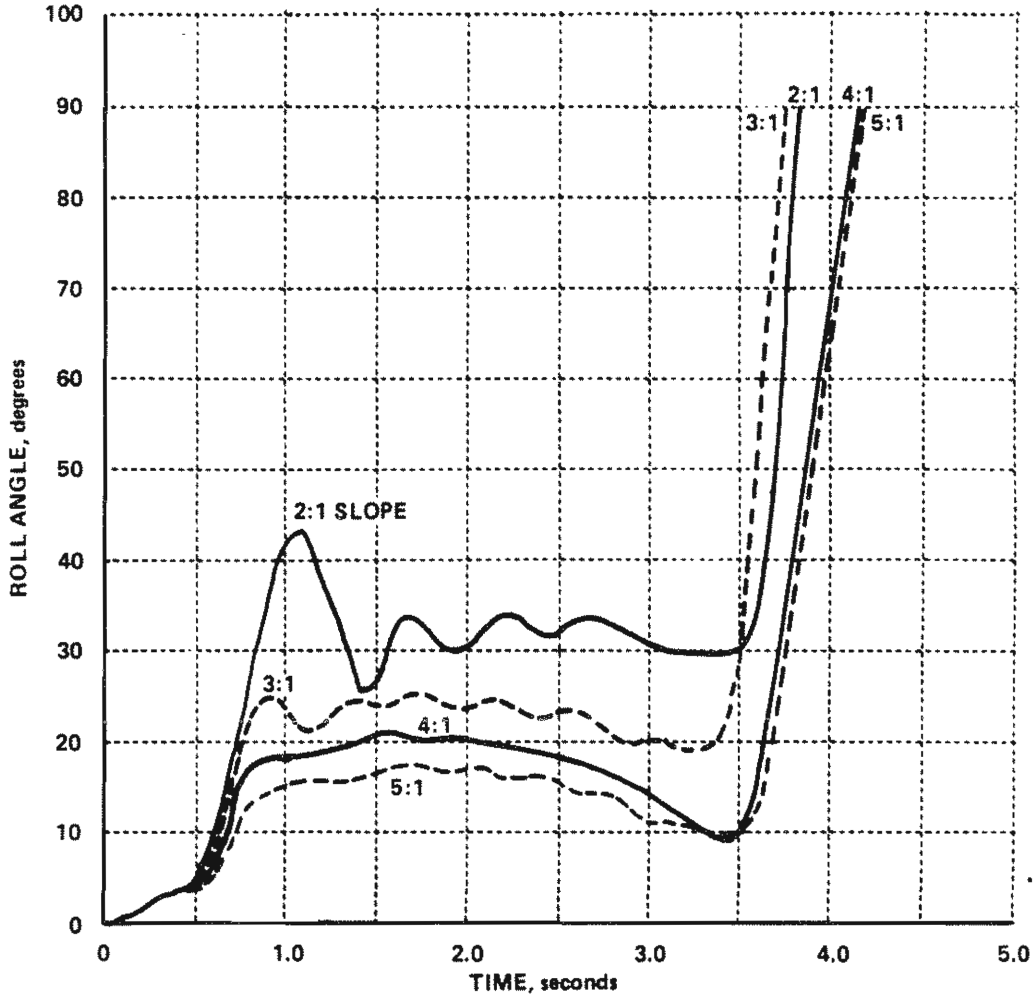

Figure 43. Comparison of rollover responses of 1,800-lb (816-kg) car for tracking departure on various sideslopes.

Table 41. Threshold of ground friction coefficient for rollover of 2,410-lb (1,093-kg) car.

Sideslope ratio	Friction coefficient	Maximum roll angle, degrees	Comments
45-mi/h and 25-degree (30-degree Sideslip) Departure			
2:1	0.30	49.6	Car spins out and slides down sideslope.
2:1	0.35	Rollover	Rollover 21.3 ft from EOP.
3:1	0.50	29.2	Car spins out and backs down sideslope.
3:1	0.55	Rollover	Rollover 39.3 ft from EOP.
4:1	0.70	26.8	Car begins return to road and spins out on sideslope.
4:1	0.75	Rollover	Rollover 21.2 ft from EOP.
5:1	0.75	22.8	Car returns to road; maximum lateral distance 20.2 ft from EOP.
5:1	0.80	Rollover	Rollover 19.0 ft from EOP.
60-mi/h and 15-degree (Tracking) Departure			
2:1	0.75	46.4	Car slides on return path to road.
2:1	0.80	Rollover	Rollover 76.1 ft from EOP on return path to road.
2:1	1.25	46.8	Car on stable return path to road.
2:1	1.30	Rollover	Rollover 55.1 from EOP.
3:1	0.65	26.5	Car spins out on sideslope.
3:1	0.70	Rollover	Rollover 46.4 ft from EOP.
4:1	0.70	17.9	Car begins return to road, spins out.
4:1	0.75	Rollover	Rollover 30.2 ft from EOP on return path to road.
5:1	0.75	18.0	Car begins return to road, spins out.
5:1	0.80	Rollover	Rollover 16.5 ft from EOP on return path to road.

1 mi/h = 1.609 km/h
1 ft = 0.3048 m

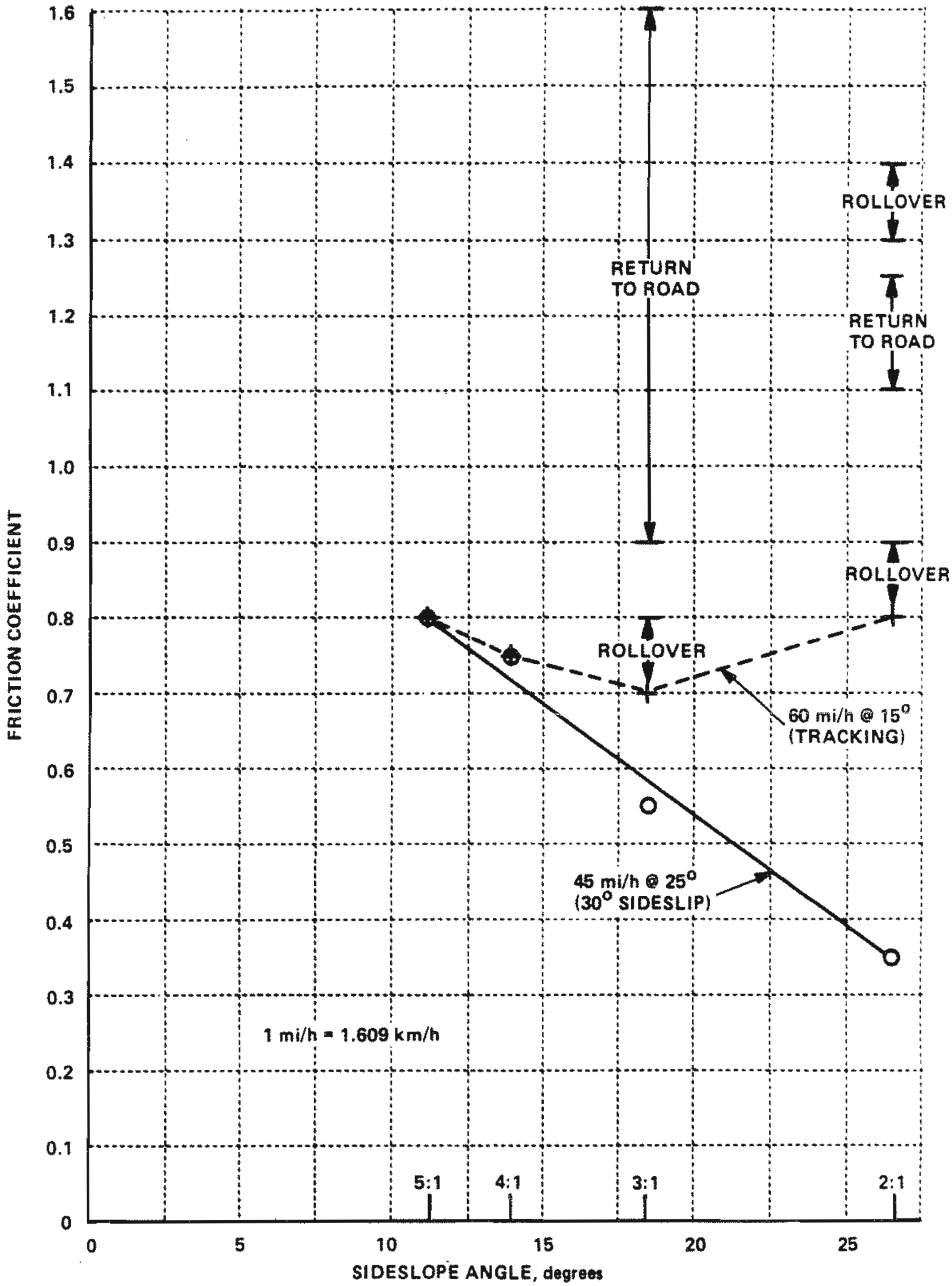

Figure 44. Friction-coefficient threshold for rollover of 2,410-lb (1,093-kg) car.

2:1 and 3:1 sideslopes, for which the friction coefficient was varied over a wide range (between 0.6 and 1.7), show some unexpected findings that further illustrate the complexity of the rollover phenomena. In the case of the 2:1 sideslope, spinout of the vehicle occurred for values of friction coefficient of 0.75 and lower. The car rolled over in runs performed with friction coefficients of 0.8 and 0.9 but followed a stable return path toward the road for coefficients in the range between 1.1 and 1.25. Further increases of the friction coefficient to 1.3 and 1.4 again resulted in rollover of the vehicle.

The responses of the car on the 3:1 sideslope were similar, in that rollover occurred only for the narrow range of friction coefficients between 0.7 and 0.8. Below this range, the car spun out on the slope; for higher values (up to 1.7), it was steered on a stable trajectory back to the road without rolling over.

The results of the simulations of the two small cars indicate that the propensity to roll over is greater for the heavier one, since lower values of the friction coefficient were found to be needed to produce rollover. Two reasons were identified that could possibly explain the difference in the behavior of these vehicles, which, it will be recalled, were identical except for those parameters affected by the different weights and weight distributions of the sprung mass. First, as may be noted in Table 36, the elevation of the sprung-mass center of gravity was higher for the 2,410-lb (1,093-kg) car. As a result, the value of the static rollover stability factor for the total vehicle ($\frac{T}{2h}$) was lower (1.27, compared to 1.37 for the 1,800-lb (816-kg) vehicle). Second, because of the higher loads on the tires (particularly, those of the front) of the 2,410-lb car, the tires produce deeper ruts in the soil. Hence, the soil plow forces not only are larger, but, since they contribute a higher percentage of the total side forces developed, a proportionately lower contribution of the tire "contact patch" forces (and, thus, a lower friction coefficient) is needed to cause rollover.

Twenty-four simulation runs of the 4,450-lb (2,018-kg) car traversing 2:1 and 3:1 sideslopes were executed. It was found that rollover occurred on the 2:1 sideslope for the sideslipping departure condition if the friction coefficient was 0.8 or higher. However, the vehicle otherwise did not roll over, even for values of the friction coefficient as high as 1.6. For the tracking departure, the vehicle spun out on the slope for friction coefficients up to 1.2 and returned to the load with further increases of the coefficient.

On the 3:1 sideslope, the sideslipping departure resulted in the vehicle returning to the road for friction coefficients of 0.8 or more. (Recall that, with a value of 0.6, the car spun out). For the tracking departure, spinout occurred for values of the friction coefficient up to 1.0; for higher values, the car returned to the road. Since it appeared that rollover of the large, heavy car could not be achieved on the 3:1 sideslope by changing the ground friction coefficient, it was deemed that additional simulations of shallower slopes would not be worthwhile.

The reason why the 4,450-lb (2,018-kg) car did not roll over at some value within the wide range of friction coefficients used in the simulations is not clear. For the one case in which the vehicle did overturn, it may be noted that a higher value of the coefficient than was needed to produce rollover of either of the smaller, lighter cars was required. In view of the inherently greater roll stability of the large car, as indicated by the higher value of $\frac{T}{2h} = 1.44$, such a finding is not altogether unexpected. Moreover, although the tire normal loads of the heavy car were higher, the larger diameter and tread width of the tires resulted in soil sinkages and plow forces that were comparable to those for the lighter cars. Therefore, a larger friction coefficient for the contact patch was needed to develop the increased lateral accelerations required to induce rollover.

An interesting observation noted in analyzing the results of all of the simulation runs is that, when the vehicles did not roll over, the maximum roll angles were always much less than the critical roll angle, particularly for the shallower slopes, and changed only slightly with changes of the friction coefficient. For example, in the case of the sideslipping departure of the 1,800-lb (816-kg) car on a 4:1 sideslope, the maximum roll angles were only 19.7 degrees (37% of the critical roll angle) and 24.7 degrees (46% of critical roll) for values of the friction coefficient of 0.6 and 0.9, respectively. Yet, a further small increase in the coefficient to 0.95 suddenly produced a very large change of the roll response that resulted in rollover. This suggests that, when unknown combinations of a host of other variables (e.g., speed, orientation, linear and angular velocities, suspension deflections and velocities, and driver control inputs) are such as to create nearly threshold conditions for rollover, nonuniformities of real-world terrains which may cause only small variations of the effective friction coefficient can spell the difference between whether a vehicle safely traverses a sideslope or is triggered into a rollover.

FILL EMBANKMENTS

The simulations of vehicles traversing fill embankments were aimed at verifying the current AASHTO criteria for determining the need for protective barrier systems on roadway fill sections. These barrier-warranting criteria are shown in Figure 45, taken from AASHTO.[37] Of primary interest was that portion of the curve for fill heights less than about 17 ft (5.2 m), where, depending on the height, unrounded slopes as steep as 1½:1 are permissible without barrier protection.

Embankments with 2:1, 3:1, and 4:1 slopes and varying in height from 3 ft (0.9 m) to 17.5 ft (5.3 m) were considered. The cross sections all included 4-ft (1.2-m) rounding of the shoulder/sideslope juncture except for one embankment, for which optimum rounding to the 2:1 slope was used. Rounding of the toe was provided based on the rate of 0.3 ft (0.09 m) per degree change of slope recommended by DeLeys (1975)[38] for avoiding bumper impact with the ground. The resulting nominal toe roundings were thus 8 ft (2.4 m), 6 ft (1.8 m), and 4 ft (1.2 m) for the 2:1, 3:1, and 4:1 slopes, respectively. A value of 0.6 for the friction coefficient of the ground was used in all of the simulation runs.

The results of the simulated traversals of the various embankment configurations are summarized in Table 42. Note that the vehicle was not steered in several of the runs, because the earlier study of sideslopes had shown that, with the assumed steer maneuver, the car would either return to

---

38. DeLeys, N.J., "Safety Aspects of Roadside Cross-Section Design," Report No. FHWA-RD-75-41, February 1975.

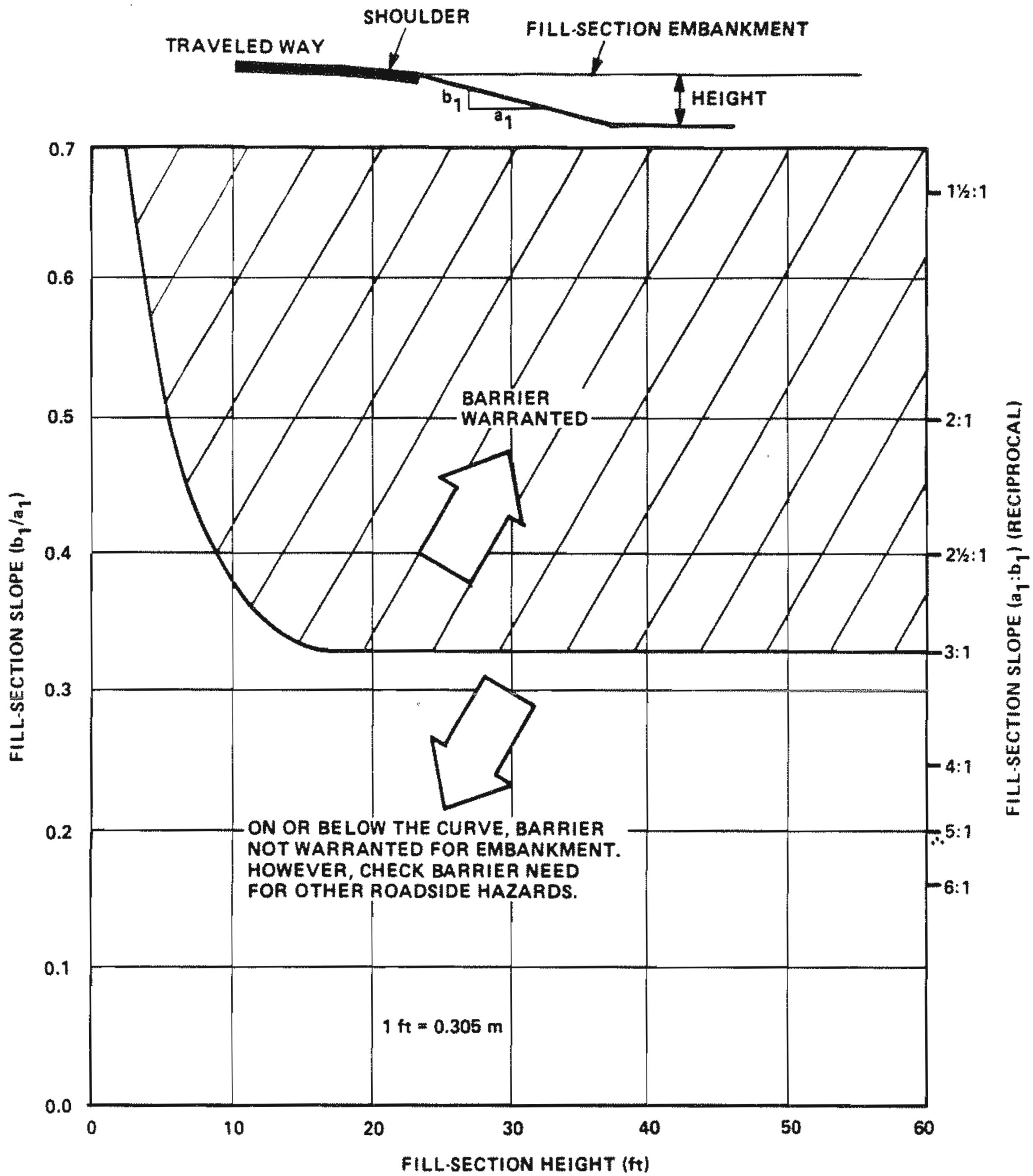

Figure 45. Warrants for fill-section embankments. [37]

Table 42. Summary of fill-embankment simulations.

Vehicle weight, lb	Departure, mi/h @ degrees	Side-slope ratio	Fill height, ft	Toe dist. from EOP, ft	Max. roll, degrees	Max. lat. encroach., ft	Comments
1,800	60 @ 15	2:1	3.2	15.4	26.8/-13.0	35.4	Airborne after crossing rounding at shoulder, impacts beyond toe rounding. Returns to road during spinout.
1,800	45 @ 25	2:1	3.2	15.4	Rollover	18.9	Rollover on toe rounding.
2,410	45 @ 25	2:1	3.2	15.4	Rollover	17.9	Rollover on toe rounding.
1,800	60 @ 15*	2:1	5.5	20.0	37.6/-18.5	>140	Car airborne after crossing rounding at shoulder, impacts on toe rounding, spins out on flat.
1,800	60 @ 15	2:1	5.5	20.0	38.4/-16.5	41.9	Same as above, except steer causes car to return to road during spinout.
1,800	45 @ 25*	2:1	5.5	20.0	Rollover	23.5	Rollover on toe rounding.
2,410	45 @ 25	2:1‡	6.5	27.9	29.9	29.9	Returns to road, no spinout.
4,450	60 @ 15	2:1‡	6.5	27.9	28.3	39.3	Returns to road, no spinout.
1,800	60 @ 15	2:1	10.0	29.0	Rollover	40.9	Rollover during spinout after recrossing toe on return path to road.
1,800	60 @ 15	3:1	3.0	17.5	22.5/-12.1	32.9	Car begins return to road, spins out on flat.
1,800	45 @ 25	3:1	3.0	17.5	26.6/-1.4	22.3	Car returns to road, very stable, LF wheel does not go beyond toe rounding.
1,800	60 @ 15	3:1	5.0	23.5	24.6	33.5	Car returns to road in spin at high yaw and sideslip angles.
1,800	45 @ 25	3:1	5.0	23.5	26.3	26.5	Stable return to road. Left-side wheels do not go beyond toe rouning.
2,410	45 @ 25	3:1	5.0	23.5	Rollover	25.2	Rollover on toe rounding.

Table 42. Summary of fill-embankment simulations. (continued)

Vehicle weight, lb	Departure, mi/h @ degrees	Side-slope ratio	Fill height, ft	Toe dist. from EOP, ft	Max. roll, degrees	Max. lat. encroach., ft	Comments
1,800	60 @ 15	3:1	10.0	38.5	24.5	41.9	Stable return to road. Left-side wheels do not go beyond toe rounding.
1,800	45 @ 25	3:1	10.0	38.5	26.3	35.6	Car stable on return path to road, remains on sideslope.
1,800	60 @ 15*	3:1	17.0	59.5	23.5/-6.2	> 136	Car stable on slight curved path away from road.
1,800	45 @ 25*	3:1	17.0	59.5	26.3/-13.5	41.6	Car spins out on sideslope.
1,800	60 @ 15*	4:1	17.0	76.0	17.0/-5.8	> 133	Car stable on slightly curved path away from road.
1,800	45 @ 25*	4:1	17.0	76.0	19.6/-9.9	27.8	Car begins return to road, spins out.

1 mi/h = 1.609 km/h
1 ft = 0.3048 m
1 lb = 0.454 kg

Notes: * simulations with zero steer input
ǂ simulations with optimum shoulder/sideslope rounding

the road or spin out on the slope before reaching the toe of the embankment. As may be seen from Table 42, rollover of the vehicles occurred for the nontracking departure on the 2:1 embankment with a height of only 3.2 ft (0.98 m), which is the minimum fill-section height possible with the assumed roundings at the shoulder and toe. As would be expected, the vehicle also rolled over when the height of the embankment was increased to 5.5 ft (1.68 m), which is about the maximum height allowed by the current criteria before a barrier is warranted. Note, however, that rollover was avoided when the transition from the shoulder to the sideslope was more gradual, as provided by the optimum rounding.

The vehicle also did not overturn on these embankments for the case of the tracking departure. In traversal of the 5.5-ft (1.68-m) embankment with no vehicle steer input, the vehicle impacted on the toe rounding after having been completely airborne for a short time. The high tire loads when the right-front wheel impacted the ground resulted in a yawing moment that caused the vehicle to subsequently go out of control in a clockwise spin on the flat surface at the bottom of the embankment. In another simulation, identical except that the vehicle was steered, the positive yaw moment upon impact was countered by the negative moment produced by the steered wheels when the car was on the flat and the vehicle followed a return path to the road while in a rapid counterclockwise spin. Although the vehicle did not roll over in either instance, the responses were quite violet, as evidenced by the high acceleration levels and by the large change of roll angle (approximately 55 degrees) that occurred in less than 0.35 second when the car impacted the toe region.

Rollover was also induced after the vehicle had successfully negotiated the 10ft(3.0m)-high embankment with a 2:1 slope while tracking. In this instance, rollover was precipitated by the high lateral acceleration developed while in a rapid spin as the vehicle was moving back up the embankment. It is of interest to note that the rollover was uphill, since the car was facing nearly backward (-148-degree yaw angle) when the critical roll angle (approximately 54 degrees) was reached. According to Calspan accident investigators, such a response, in which the direction of roll was toward the roadway as the vehicle was traveling up a sideslope, has been found to be not uncommon in rollover accidents.

Roll stability was maintained in all of the simulations of the 1,800-lb (816-kg) car traversing the embankments with a 3:1 front slope, and the maximum roll angle was essentially independent of the height of the embankment. For the sideslipping departure condition, the car returned to the road except in the one simulation of the 17ft(5.2m)-high embankment in which the vehicle was not steered and resulted in a spinout on the slope. Spinout also occurred in the tracking departure on the 3ft(0.9m)-high and 5ft(1.5m)-high embankments. Note that the vehicle did not encroach much beyond the toe of the embankment in many of the runs.

The 2,410-lb (1,093-kg) small car rolled over in the case of the skidding departure on the 5ft(1.5m)-high, 3:1 embankment. As discussed in the preceding subsection, that car was found to overturn more readily than the one weighing only 1,800 lb (816 kg).

The results of this study of embankments show that fill sections with a front slope of 2:1 are hazardous, regardless of the height of the embankment. It also appears that a 3:1 embankment slope is marginally safe, since rollover of one of the small cars was shown to occur on embankments 5 ft (1.5 m) or more in height. This is evidenced further by the results of recent full-scale tests of a 15ft(4.6m)-high embankment for which the steepness of the main portion of the sideslope was nominally 3:1.[39] In those tests, a pickup truck, a van, and a minisize automobile weighing 1,938 lb (879 kg) were each remotely controlled so as to depart from the right side of the roadway at 50 mi/h (80.5 km/h) and at a 15-degree angle (tracking). Approximately 1 second after leaving the road, a left-steer control input was initiated to maneuver the vehicle back toward the road. Both the pickup truck and the van successfully traversed the embankment and followed a stable return path to the road; the maximum roll angle of each vehicle was approximately 23 degrees. However, in the test with the small automobile, the rear of the vehicle began to slide around (counterclockwise yaw) shortly after the left-steer maneuver was begun. As the vehicle continued down the embankment, the tires on the right side

---

39. Buth, C.E. and Campise, W.L., "Performance Limits of Longitudinal Barrier Systems, Volume IV - Appendix C, Details of Embankment Traversal Tests," Texas Transportation Institute, Contract No. DTFH61-82-C-00051, May 1985.

began to plow into the sod ground, and the vehicle subsequently rolled over near the bottom of the embankment.

In view of all of these findings, it may be concluded that roadside barriers are warranted on embankments having a front slope steeper than 3:1 and 3 ft (0.9 m) or more in height to protect against rollover of small, lightweight vehicles. Note that this criterion would also be more consistent with the existing AASHTO criteria for the preferred design of ditches. (The AASHTO guidelines for preferred ditch sections[37] indicate that, for ditches having zero backslope (i.e., with a cross section like that of an embankment), the front slope should be no steeper than 3:1.)

DITCHES

Among the important factors that need to be considered in the design of ditches that can be safely traversed are the steepness of the front and back slopes and the depth and shape of the bottom of the ditch. Thus, compared to fill embankments, ditches involve at least two additional geometric variables. Criteria for combinations of front and back slopes that provide acceptable cross sections for ditches with various shapes of the bottom are defined by AASHTO[37] and are depicted in Figure 46.

Because of the short time that was available for investigating the effects of ditch design variables on vehicle rollover tendencies, only a few simulations of three selected ditch configurations could be executed and evaluated. Two of these ditches had combinations of front and back slopes that were within the envelopes for preferred cross sections. One was a 17ft(5.2m)-deep vee ditch with front and back slopes of 4:1 and 6:1, respectively; the other was a 3ft(0.9m)-deep round bottom ditch with an 8-ft (2.4-m) rounding between 4:1 front and back slopes. The third ditch considered was also a vee shape with a 3:1 front slope and a 4:1 back slope which, as may be seen from Figure 46, is a slope combination that is outside the boundary for preferred ditch cross sections. However, this shape is regarded as probably fairly representative of ditches often found along many types of roadways. A ditch depth of 3 ft (0.9 m) was also chosen to ensure that the vehicle would encounter the back slope for the nontracking departure condition. The

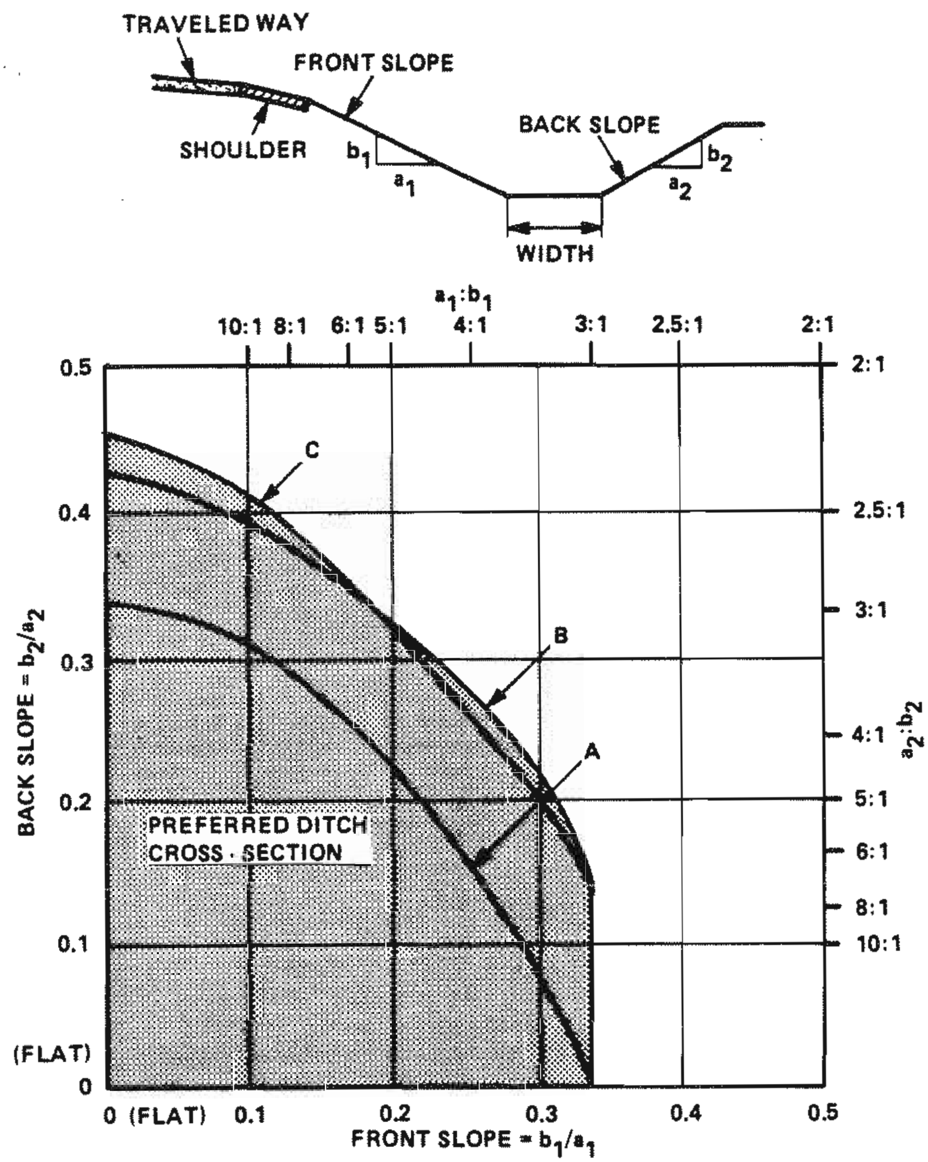

CURVE-A ENVELOPE
- VEE DITCH
- ROUND DITCH, BOTTOM WIDTH < 8 ft
- TRAPEZOIDAL DITCH, BOTTOM WIDTH < 4 ft
- ROUNDED TRAPEZOIDAL DITCH, BOTTOM WIDTH < 4 ft

CURVE-B ENVELOPE
- TRAPEZOIDAL DITCH, BOTTOM WIDTH = 4 ft TO 8 ft
- ROUND DITCH, BOTTOM WIDTH = 8 ft TO 12 ft

CURVE-C ENVELOPE
- TRAPEZOIDAL DITCH, WIDTH > 8 ft
- ROUND DITCH, WIDTH > 12 ft
- ROUNDED TRAPEZOIDAL DITCH, WIDTH > 4 ft

1 ft = 0.3048 m

Figure 46. Envelopes of front and back slope combinations for preferred ditch sections.[37]

roadside terrain for each ditch configuration included an 8ft(2.4m)-wide shoulder with 4-ft (1.2-m) rounding tangent to the front slope.

The responses of the simulated, 1,800-lb (816-kg) small car in traversing the various ditches are summarized in Table 43. Because of the larger lateral distance from the edge of the road to the bottom of the 17ft(5.2m)-deep vee ditch, only the 60-mi/h (96.5-km/h) at 15-degree tracking departure was simulated. The car easily traversed the ditch and, as may be seen, the maximum roll angle was in the counterclockwise direction. From a comparison with a similar simulation of a 17ft(5.2m)-high fill embankment having a 4:1 sideslope (refer to Table 42), it may be noted that the effect of the change from zero to a 6:1 back slope was to increase the maximum negative roll angle from -5.8 degrees to -23.7 degrees.

Table 43. Summary of ditch simulations.

Departure, mi/h @ degrees	Slopes, front/back	Depth, ft	℄ Dist. from EOP, ft	Bottom rounding, ft	Max. roll, deg	Max. Lat. encroach., ft	Comments
Vee Ditches							
60 @ 15*	4:1/6:1	17.0	76.0	0	17.0/-23.7	>133	Car stable on slightly curved path away from road.
60 @ 15	3:1/4:1	3.0	17.5	0	Rollover(-)	21.0	Severe impact with back slope caused "flip"-type rollover.
45 @ 25	3:1/4:1	3.0	17.5	0	48.8/-22.2	20.4	Airborne after impacting backslope. Sprung-mass right-front corner impact with back slope prevented rollover.
Round Bottom Ditch							
60 @ 15	4:1/4:1	3.0	20.0	8	20.9/-11.6	28.1	Car returned to road, very stable.
45 @ 25	4:1/4:1	3.0	20.0	8	19.6	22.5	Car returned to road, did not contact back slope.

1 mi/h = 1.609 km/h
1 ft = 0.3048 m

*Simulation with zero steer input.

The vehicle responses in the simulation of the other vee ditch with steeper front and back slopes were very violent and resulted in overturning of the car in the case of the tracking departure. The very large radial tire forces developed when the right-front wheel impacted the back slope caused a "flip" type of rollover in the counterclockwise direction. The vehicle also nearly rolled over (attained 90% of the critical roll angle) in the nontracking departure from the road. In this instance, however, note that the maximum roll was in the clockwise direction, because of the high lateral forces that were generated by the tires prior to and upon impact with the back slope. As noted in the table, forces resulting from contact of the right end of the front bumper with the back slope prevented the vehicle from rolling over.

From the responses of the vehicles observed in the few simulations of ditches performed in this study, it appears that the existing guidelines for the design of preferred ditch sections, which are primarily based on vehicle linear acceleration limit criteria for avoiding injuries to occupants, provide for designs that also are safe from the standpoint of offering low vehicle rollover potential.

Section 6

CONCLUSIONS AND RECOMMENDATIONS

Based on the findings of this study, the following conclusions and recommendations are made:

1. The sideslope of a fill embankment should be no steeper than 3:1, and preferably flatter, to reduce the likelihood of rollover. Results of tests and computer simulations show that 3:1 slopes are marginally safe for traversal by small, lightweight automobiles, which are known, from the preponderance of evidence from accident data analyses, to be more likely to roll over than large, heavy vehicles. The slopes should also be firm and smooth to minimize the likelihood of the vehicle's tires digging into the ground or striking a surface irregularity which could trip the vehicle into a rollover.

It is recommended, therefore, that consideration be given to revising the current AASHTO design criteria for barrier warrants on sideslopes and embankments so as to indicate that safety barriers are warranted for all slopes steeper than 3:1, for fill heights greater than 3 ft (0.9 m). This would make the criteria for barrier placement on embankments more consistent with the AASHTO criteria for the design of ditches shown in Figure 46. (Note that, for ditches having zero backslope (i.e., with a cross section like that of an embankment), the front slope should be no steeper than 3:1.). The simulations of this study were limited to fill heights of 3 ft (0.9 m) or greater in order to accommodate the roundings of the slope breaks.

2. Current AASHTO criteria for the design of preferred ditch sections, which limit the front slope to no steeper than 3:1, appear to define ditch configurations that are relatively safe with respect to vehicle rollover potential. However, because of the small difference between two of the criteria applicable to different ranges of ditch bottom width (see Figure 46, curves B and C), it is recommended that those criteria be replaced by a single faired curve that follows curve C of Figure 46 for front slopes steeper than

5:1 and that follows curve B of Figure 46 for shallower front slopes to provide a greater margin of safety.

3. All slope breaks of roadside terrain should be rounded as much as possible to reduce the potential for vehicles to be caused to roll over due to tripping on sag vertical curves. The need for adequate rounding of crest vertical curves, such as the break line of shoulder and side slopes, also cannot be overemphasized. Such roundings not only afford drivers greater opportunity to maintain or regain control of their vehicle but also decrease the likelihood of rollover by preventing the vehicle from achieving large values of angular momentum about the roll axis.

4. The modified HVOSM has been demonstrated to be capable of predicting the response of vehicles operating on off-road terrains with reasonable accuracy. The development and incorporation of the deformable-soil model in HVOSM is considered an important improvement, since it allows simulation of the effects of tire sinkage in soil, which has been identified as one of the leading causes of rollover. This model improved the accuracy of the predictions of vehicle dynamic responses during traversals of roadside terrain features, but evidence of the validity of the model is still very limited. It is recommended, therefore, that tests be performed to measure the sinkage and motion-resistance forces of tires in soft soil for various tire loads and for sideslip angles from zero to 90 degrees, which would provide data needed for a more extensive and rigorous validation of the analytical approach.

5. The relatively few simulations that resulted in vehicle rollover in this study point to the dynamic nature of the rollover phenomenon, which is sensitive to the complex interactions of many factors whose effects are nonindependent. Adequate vehicle parametric data for the severe operating regime associated with the rollover response are generally lacking. Among the most important of these are definitive data for tire properties under the high tire load and large slip and camber angle conditions that prevail in most rollover events. To alleviate this deficiency of the model data base, it is strongly recommended that a test program be conducted to determine typical

force characteristics of tires for slip and camber angles ranging up to 90 degrees and for loads including extreme overload.

6. Ultimately, the vehicle rollover potential associated with roadside features is reflected by real-world accident experience. From the literature review performed as a part of this study, it is apparent that the existing accident data base lacks the comprehensive and detailed information necessary to define the conditions that lead to rollover for the different vehicle types. For example, data contained in accident files such as NASS and FARS usually provide little or no information regarding the geometrics of the accident site (e.g., steepness of slopes, embankment height, and roundings), whether the vehicles were tripped by a surface irregularity or as a result of tire ruts in soft soil, where rollovers were initiated with respect to the terrain feature (sideslope, backslope, toe of embankment, etc.), vehicle trajectory, etc.

To alleviate such shortcomings of the existing accident data base, it is recommended that a data-collection effort be made that is specifically directed toward providing the information necessary to evaluate, using statistical analysis techniques, the suitability of roadside-feature design criteria for the current and projected mix of vehicle types.

Appendix A
INPUT DATA FOR HVOSM VERIFICATION

The HVOSM input data sets for simulating the full-scale tests performed for verifying the computer model are presented in Tables 44 through 48.

Table 44. HVOSM inputs for sinusoidal-steer test.

RABBIT SINUSOIDAL STEER TEST #5									0 100
0.0	6.0	0.010	0.050	70.0	1.0	0.010			0 101
1.0									0 102
1.0									0 103
0.0	0.0	0.0	0.0	1.0	1.0	0.0			0 104
1979 VW RABBIT 2 DOOR TEST VEHICLE									0 200
5.593	0.3287	0.3157	2600.0	8850.0	10400.	0.0			0 201
31.49	63.01	54.5	53.5					386.4	0 202
3.05	0.0	8.00				11.893	11.563		0 203
85.0	303.6	902.1	2916.1	134265.	0.65	-1.62	2.88		0 204
73.0	150.6	37.3	1029.3	23210.6	0.65	-2.91	3.59		0 205
6.08	15.0	0.1	3.58	15.0	0.1				0 206
0.0	84750.0		0.0	0.0	0.0	0.0			0 207
-5.0	5.0	1.0	1.	0.0					0 209
-0.08	-0.33	-0.50	-0.50	-0.17	0.33	0.83	1.83	2.58	1 209
3.50	5.00								2 209
0.0	0.0	0.0	0.0	0.0	0.0	0.0	0.0	0.0	3 209
0.0	0.0								4 209
-0.65	-0.30	-0.10	0.05	0.05	0.00	-0.20	-0.45	-0.80	5 209
-1.25	-1.85								6 209
GOODYEAR POLYSTEEL RADIAL P155/80R13									0 300
1.0	1.0	1.0	1.0						0 301
1099.0	5.0	10.0	2542.	9.91	2366.	0.687	-8184.	0.75	1 301
0.80				11.313					0 302
APPROX. SINE STEER AT 0.5 HZ.									0 400
0.0	6.0	0.2	1.0						0 401
0.0	0.0	0.0	0.47	1.16	4.31	7.09	3.61	-3.77	1 401
-8.88	-9.47	-9.67	-7.96	-0.48	7.22	10.98	11.26	8.70	2 401
0.21	-8.25	-9.36	-9.62	-8.29	-1.55	6.66	12.19	12.76	3 401
10.35	2.67	-6.96	-10.53						4 401
33.0 MPH									0 600
0.0	0.0	0.0	0.0	0.0	0.0	0.0			0 601
0.0	0.0	-22.492	580.8	0.0	0.0				0 602
0.0	0.0	0.0	0.0	0.0	0.0	0.0			0 603
									09999

Table 45. HVOSM inputs for combined steer and braking test.

Rabbit Forward Skid Test #10									0	100
0.0	5.0	0.010	0.050	70.0	1.0	0.010			0	101
1.0									0	102
1.0									0	103
0.0	0.0	0.0	0.0	1.0	1.0	1.0			0	104
1979 VW RABBIT 2 DOOR TEST VEHICLE									0	200
5.593	0.3287	0.3157	2600.0	8850.0	10400.	0.0			0	201
31.49	63.01	54.5	53.5					386.4	0	202
3.05	0.0	8.0				11.893	11.563		0	203
85.0	303.6	902.1	2916.1	134265.	0.65	-1.62	2.88		0	204
73.0	150.6	37.3	1029.3	23210.6	0.65	-2.91	3.59		0	205
6.08	15.0	0.1	3.58	15.0	0.1				0	206
0.0	84750.0		0.0	0.0	0.0	0.0			0	207
-5.0	5.0	1.0	1.	0.0					0	209
-0.08	-0.33	-0.50	-0.50	-0.17	0.33	0.83	1.83	2.58	1	209
3.50	5.00								2	209
0.0	0.0	0.0	0.0	0.0	0.0	0.0	0.0	0.0	3	209
0.0	0.0								4	209
-0.65	-0.30	-0.10	0.05	0.05	0.00	-0.20	-0.45	-0.80	5	209
-1.25	-1.85								6	209
GOODYEAR POLYSTEEL RADIAL P155/80R13									0	300
1.0	1.0	1.0	1.0						0	301
1099.0	5.0	10.0	2542.	9.91	2366.	0.687	-8184.	0.75	1	301
0.80				11.313					0	302
LEFT STEER AND LOCKED REAR WHEEL BRAKING									0	400
0.0	3.5	0.1	1.0	0.0	1.0				0	401
0.0	0.0	-2.75	-6.75	-10.75	-14.07	-15.11	-15.11	-15.07	1	401
-15.07	-15.09	-15.15	-15.45	-15.53	-15.45	-15.49	-15.45	-15.35	2	401
-15.15	-15.19	-15.15	-15.15	-15.45	-16.05	-16.05	-15.75	-15.75	3	401
-15.65	-15.65	-15.69	-15.75	-15.55	-15.35	-15.25	-15.25	-15.25	4	401
0.0	-100.0	-300.0	-500.0	-500.0	-500.0	-500.0	-500.0	-500.0	5	401
-500.0	-500.0	-500.0	-500.0	-500.0	-500.0	-500.0	-500.0	-500.0	6	401
-500.0	-500.0	-500.0	-500.0	-500.0	-500.0	-500.0	-500.0	-500.0	7	401
-500.0	-500.0	-500.0	-500.0	-500.0	-500.0	-500.0	-500.0	-500.0	8	401
35.0 MPH									0	600
0.0	0.0	0.0	0.0	0.0	0.0	0.0	0.0		0	601
0.0	0.0	-22.642	628.0	0.0	0.0				0	602
0.0	0.0	0.0	0.0	0.0	0.0	0.0	0.0		0	603
										9999

Table 46. HVOSM inputs for level-turf skid test.

RABBIT SKID ON LEVEL TURF-TEST #18									0 100
0.0	6.0	0.010	0.050	70.0	1.0	0.010			0 101
1.0									0 102
1.0									0 103
0.0	0.0	0.0	0.0	1.0	1.0	1.0			0 104
1979 VW RABBIT 2 DOOR TEST VEHICLE									0 200
5.593	0.3287	0.3157	2600.0	8850.0	10400.	0.0			0 201
31.49	63.01	54.5	53.5					386.4	0 202
3.05	0.0	8.0				11.893	11.563		0 203
85.0	303.0	902.0	2916.0	134265.	0.65	-1.62	2.88		0 204
73.0	150.0	37.0	1029.0	23210.	0.65	-2.91	3.59		0 205
6.08	15.0	0.1	3.58	15.0	0.1				0 206
0.0	84750.0		0.0	0.0	0.0	0.0			0 207
-5.0	5.0	1.0	1.	0.0					0 209
-0.08	-0.33	-0.50	-0.50	-0.17	0.33	0.83	1.83	2.58	1 209
3.50	5.00								2 209
0.0	0.0	0.0	0.0	0.0	0.0	0.0	0.0	0.0	3 209
0.0	0.0								4 209
-0.65	-0.30	-0.10	0.05	0.05	0.00	-0.20	-0.45	-0.80	5 209
-1.25	-1.85								6 209
GOODYEAR POLYSTEEL RADIAL P155/80R13									0 300
1.0	1.0	1.0	1.0						0 301
1099.0	5.0	10.0	2542.	9.91	2366.	0.687	-8184.	0.75	1 301
0.80				11.313					0 302
LEFT STEER AND LOCKED REAR WHEEL BRAKING									0 400
0.0	3.0	0.1	1.0	0.0	1.0				0 401
2.0	2.84	3.03	2.42	1.15	-1.39	-4.30	-7.30	-11.76	1 401
-14.70	-15.69	-17.85	-18.79	-19.0	-19.03	-18.88	-18.89	-19.00	2 401
-18.87	-18.82	-18.92	-18.62	-18.45	-18.41	-18.34	-18.43	-18.72	3 401
-18.78	-18.80	-18.80	-18.80						4 401
0.0	-100.0	-300.0	-500.0	-500.0	-500.0	-500.0	-500.0	-500.0	5 401
-500.0	-500.0	-500.0	-500.0	-500.0	-500.0	-500.0	-500.0	-500.0	6 401
-500.0	-500.0	-500.0	-500.0	-500.0	-500.0	-500.0	-500.0	-500.0	7 401
-500.0	-500.0	-500.0	-500.0						8 401

Table 46. HVOSM inputs for level-turf skid test. (continued)

LEVEL GROUND,BEKKER DATA SET #16 FOR SOD									500
0.0	1800.0	120.0	0.0	624.0	48.0	0.0	0.0		501
0.0	2.2	4.8	7.6	9.6	10.2	10.8	11.5	11.6	1 501
11.8	11.3	11.8	10.8	8.5					2 501
0.0	2.2	4.6	7.2	9.0	9.7	12.1	11.5	12.7	3 501
12.2	10.9	12.5	11.3	10.1					4 501
0.5	1.8	3.6	7.3	9.6	10.8	13.2	12.1	13.2	5 501
13.2	11.3	11.8	12.0	11.3					6 501
0.4	1.9	4.0	7.9	9.1	11.0	12.0	11.8	12.5	7 501
12.7	12.0	11.0	10.2	11.2					8 501
0.2	1.9	3.5	7.2	10.6	10.4	12.5	11.5	12.6	9 501
11.5	11.3	9.8	10.4	10.3					10 501
0.4	1.8	3.2	7.4	8.6	9.7	12.6	10.1	11.8	11 501
11.3	10.4	10.9	10.8	11.0					12 501
-0.5	1.3	3.0	6.2	7.9	8.9	14.9	10.9	10.8	13 501
11.2	11.3	10.3	10.8	10.9					14 501
0.6	1.1	3.1	5.04	7.56	8.4	9.8	10.3	10.8	15 501
11.9	11.9	12.1	11.8	11.6					16 501
0.4	0.8	2.5	5.3	6.5	8.2	9.2	9.8	11.0	17 501
11.4	11.4	12.0	10.9	11.9					18 501
0.36	1.0	1.8	4.8	7.1	7.7	8.8	9.5	10.7	19 501
10.3	12.0	11.9	11.3	12.4					20 501
0.5	1.8	3.5	5.3	7.2	7.8	9.0	9.1	10.4	21 501
10.0	11.8	11.5	10.9	11.0					22 501
1.6	3.2	4.6	6.1	8.2	9.1	9.0	8.3	8.9	23 501
9.8	10.0	11.0	10.6	10.9					24 501
1.9	3.5	6.4	7.1	8.3	8.5	9.0	8.5	7.3	25 501
9.8	10.7	10.3	10.1	11.2					26 501
2.5	4.2	6.8	9.0	9.5	9.1	9.4	10.1	6.6	27 501
9.8	9.8	10.6	10.2	10.8					28 501
3.2	4.7	7.1	10.4	10.4	11.0	10.4	9.6	9.5	29 501
11.3	10.8	10.4	10.4	10.9					30 501
4.3	5.8	7.7	11.9	11.5	12.2	10.1	12.6	11.5	31 501
11.3	11.5	11.0	10.2	12.6					32 501
0.75	0.0	0.0	0.0	0.0	1.0				506
1.0	15.0	64.0	0.95	1.5	6.0	6.0	6.0	6.0	1 506
33.5 MPH,INIT. COND. EST. FROM TEST DATA									0 600
0.0	0.0	16.8	1.0	0.0	3.0	2.0	0.0		0 601
-60.0	0.0	-22.49	589.0	0.0	0.0				0 602
0.0	0.0	0.0	0.0	0.0	0.0	0.0	0.0		0 603
									9999

Table 47. HVOSM inputs for fill-transition test.

RABBIT SKID ON FILL TRANSITION TURF-TEST #22									0 100
0.0	4.5	0.010	0.050	70.0	1.0	0.010			0 101
1.0									0 102
1.0									0 103
0.0	0.0	1.0	1.0	0.0	1.0	1.0			0 104
1979 VW RABBIT 2 DOOR TEST VEHICLE									0 200
5.593	0.3287	0.3157	2600.0	8850.0	10400.	0.0			0 201
31.49	63.01	54.5	53.5					386.4	0 202
3.05	0.0	8.0				11.893	11.563		0 203
85.0	303.0	902.0	2916.0	134265.	0.65	-1.62	2.88		0 204
73.0	150.0	37.0	1029.0	23210.	0.65	-2.91	3.59		0 205
6.08	15.0	0.1	3.58	15.0	0.1				0 206
0.0	84750.0		0.0	0.0	0.0	0.0			0 207
-5.0	5.0	1.0	1.	0.0					0 209
-0.08	-0.33	-0.50	-0.50	-0.17	0.33	0.83	1.83	2.58	1 209
3.50	5.00								2 209
0.0	0.0	0.0	0.0	0.0	0.0	0.0	0.0	0.0	3 209
0.0	0.0								4 209
-0.65	-0.30	-0.10	0.05	0.05	0.00	-0.20	-0.45	-0.80	5 209
-1.25	-1.85								6 209
GOODYEAR POLYSTEEL RADIAL P155/80R13									0 300
1.0	1.0	1.0	1.0						0 301
1099.0	5.0	10.0	2542.	9.91	2366.	0.687	-8184.	0.75	1 301
0.80				11.313					0 302
LEFT STEER AND LOCKED REAR WHEEL BRAKING									0 400
0.0	4.2	0.1	1.0	1.0	1.0				0 401
3.90	3.18	3.50	3.99	3.42	2.07	-0.19	-5.30	-9.96	1 401
-13.79	-17.35	-18.75	-19.71	-22.01	-24.11	-24.59	-25.22	-26.77	2 401
-26.80	-27.23	-27.20	-27.60	-28.09	-27.85	-28.12	-27.83	-27.41	3 401
-27.29	-27.12	-27.26	-27.18	-27.25	-27.27	-27.13	-27.36	-27.22	4 401
-26.72	-26.60	-26.79	-27.17	-27.21	-27.21	-27.21			5 401
-100.0	-150.0	-150.0	-150.0	-150.0	-150.0	-150.0	-150.0	-150.0	6 401
-150.0	-150.0	-150.0	-150.0	-150.0	-150.0	-150.0	-150.0	-150.0	7 401
-150.0	-150.0	-150.0	-150.0	-150.0	-150.0	-150.0	-150.0	-150.0	8 401
-150.0	-150.0	-150.0	-150.0	-150.0	-150.0	-150.0	-150.0	-150.0	9 401
-150.0	-150.0	-150.0	-150.0	-150.0	-150.0	-150.0			10 401
0.0	0.0	0.0	-100.0	-300.0	-500.0	-500.0	-500.0	-500.0	11 401
-500.0	-500.0	-500.0	-500.0	-500.0	-500.0	-500.0	-500.0	-500.0	12 401
-500.0	-500.0	-500.0	-500.0	-500.0	-500.0	-500.0	-500.0	-500.0	13 401
-500.0	-500.0	-500.0	-500.0	-500.0	-500.0	-500.0	-500.0	-500.0	14 401
-500.0	-500.0	-500.0	-500.0	-500.0	-500.0	-500.0			15 401

Table 47. HVOSM inputs for fill-transition test. (continued)

FILL TRANS.									500
-360.0	360.0	360.0	-200.0	0.0	100.0				501
-9.0	-9.0	-9.0							1 501
0.0	0.0	0.0							2 501
7.56	7.56	7.56							3 501
0.0	1800.0	120.0	0.0	624.0	48.0	0.0	0.0		502
0.0	2.28	10.2	19.7	30.5	35.6	34.7	34.0	34.0	1 502
35.4	37.8	38.5	38.9	39.2					2 502
3.0	6.1	11.6	21.5	32.5	36.1	36.8	37.7	37.4	3 502
37.7	38.4	38.0	38.6	39.7					4 502
5.6	8.4	13.9	23.4	33.8	36.6	36.8	37.3	37.9	5 502
40.2	42.5	42.4	40.9	40.3					6 502
7.56	10.2	16.6	26.3	35.6	39.0	38.9	41.9	41.0	7 502
40.6	41.3	43.1	41.4	42.2					8 502
9.6	12.4	17.5	28.3	37.2	38.4	39.5	38.3	38.9	9 502
41.9	42.4	42.7	42.2	41.8					10 502
11.5	14.6	18.8	29.4	38.2	40.0	39.0	37.9	38.4	11 502
39.2	41.0	41.6	43.1	44.2					12 502
13.8	14.6	19.3	29.3	37.9	41.0	40.1	37.6	38.0	13 502
38.3	40.3	42.8	43.1	42.6					14 502
16.7	17.2	22.2	30.8	39.8	41.8	40.1	37.0	37.0	15 502
39.2	41.2	42.7	44.6	45.0					16 502
18.8	19.7	23.6	31.4	38.8	42.5	39.6	38.6	38.3	17 502
39.5	42.5	44.3	44.8	45.4					18 502
21.7	21.7	25.0	32.3	39.8	40.2	40.0	38.8	39.2	19 502
39.2	41.2	42.8	45.0	46.1					20 502
22.8	23.6	25.9	33.7	39.6	39.5	38.4	39.0	39.5	21 502
39.8	40.9	41.6	43.9	46.6					22 502
24.4	24.8	27.1	35.6	41.5	39.5	38.9	39.0	40.3	23 502
40.7	41.4	42.4	46.3	44.6					24 502
27.1	29.2	30.2	37.9	43.2	40.8	42.0	40.0	40.6	25 502
41.0	42.4	44.0	47.0	45.7					26 502
29.3	31.9	35.2	42.2	44.9	44.2	43.4	42.7	43.2	27 502
42.5	43.8	45.7	47.0	46.7					28 502
30.5	34.1	36.0	40.7	44.8	46.1	44.5	44.8	45.0	29 502
45.6	46.7	48.6	48.5	49.1					30 502
32.2	33.6	37.4	40.2	46.2	46.6	48.1	48.0	48.4	31 502
48.7	49.4	49.1	50.4	50.9					32 502
1.0	0.75	0.0	0.0	0.0	1.0				0 506
2.0	15.0	64.0	0.95	1.5	6.0	6.0	6.0	6.0	1 506
35 MPH, INIT. COND. EST. FROM TEST DATA									0 600
-1.0	-1.37	16.0	4.0	0.0	11.0	3.9	0.0		0 601
-90.0	-60.0	-24.74	616.0	-9.0	0.0				0 602
0.5	-0.5	0.0	0.0	0.0	0.0	0.0	0.0		0 603
									9999

Table 48. HVOSM inputs for ditch-embankment test.

RABBIT TRAVERSAL OF DITCH EMBANKMENT TEST #25									0	100
0.0	5.0	0.005	0.025	70.0	1.0	0.010			0	101
1.0									0	102
1.0									0	103
0.0	0.0	1.0	1.0	1.0	0.0	1.0			0	104
1979 VW RABBIT 2 DOOR TEST VEHICLE									0	200
5.023	0.3287	0.3157	2600.0	8850.0	10400.	0.0			0	201
29.60	64.90	54.5	53.5					386.4	0	202
1.16	0.0	8.0				11.893	11.563		0	203
85.0	303.0	902.0	2916.0	134265.	0.65	-1.62	2.88		0	204
73.0	150.0	37.0	1029.0	23210.	0.65	-2.91	3.59		0	205
6.08	15.0	0.1	3.58	15.0	0.1				0	206
0.0	84750.0		0.0	0.0	0.0	0.0			0	207
-5.0	5.0	1.0	1.	0.0					0	209
-0.08	-0.33	-0.50	-0.50	-0.17	0.33	0.83	1.83	2.58	1	209
3.50	5.00								2	209
0.0	0.0	0.0	0.0	0.0	0.0	0.0	0.0	0.0	3	209
0.0	0.0								4	209
-0.65	-0.30	-0.10	0.05	0.05	0.00	-0.20	-0.45	-0.80	5	209
-1.25	-1.85								6	209
GOODYEAR POLYSTEEL RADIAL P155/80R13									0	300
1.0	1.0	1.0	1.0						0	301
1099.0	5.0	10.0	2542.	9.91	2366.	0.687	-8184.	0.75	1	301
0.80				11.313					0	302
RIGHT STEER & LOCKED REAR WHEEL BRAKING									0	400
0.0	2.45	0.05	1.0	0.0	1.0				0	401
-1.7	-1.7	-1.7	-3.2	-3.4	-6.0	-1.0	-1.0	-0.17	1	401
0.41	-0.55	0.15	2.01	3.51	0.60	0.36	6.14	17.29	2	401
17.45	17.45	17.45	17.45	17.45	17.45	17.45	17.45	17.45	3	401
17.45	17.45	17.45	17.45	17.45	17.45	17.45	17.45	17.45	4	401
17.45	17.45	17.45	17.45	17.45	17.45	17.45	17.45	17.45	5	401
17.45	17.45	17.45	17.45	17.45					6	401
0.0	0.0	0.0	0.0	0.0	0.0	0.0	0.0	0.0	7	401
0.0	0.0	0.0	0.0	0.0	0.0	0.0	0.0	0.0	8	401
0.0	0.0	0.0	0.0	0.0	0.0	0.0	0.0	0.0	9	401
0.0	0.0	0.0	0.0	0.0	0.0	0.0	0.0	0.0	10	401
0.0	0.0	0.0	0.0	0.0	0.0	0.0	0.0	0.0	11	401
0.0	-100.0	-250.0	-250.0	-250.0					12	401

Table 48. HVOSM inputs for ditch-embankment test. (continued)

DITCH & CURVED EMBANKMENT-SITE 3									500
0.0	1200.0	120.0	-192.0	0.0	48.0	0.0	0.0		501
12.4	8.6	7.3	2.4	0.0					1 501
11.4	8.4	7.6	1.6	0.8					2 501
12.2	8.0	4.6	1.6	-0.8					3 501
19.9	9.2	4.0	0.2	-2.0					4 501
18.1	6.5	2.5	-1.1	-3.0					5 501
10.2	5.4	2.2	-1.0	-3.5					6 501
6.2	2.5	1.8	-1.0	-3.7					7 501
5.3	3.2	0.8	-0.8	-4.4					8 501
3.5	3.5	1.9	-1.7	-5.0					9 501
2.6	1.1	-0.2	-3.0	-5.8					10 501
0.5	-0.7	-1.3	-3.4	-6.7					11 501
0.0	1200	120.0	-600.0	-192.0	24.0	0.0	0.0		502
15.7	13.9	8.5	6.4	3.8	5.8	6.2	8.6	10.0	1 502
9.1	9.8	12.0	13.4	14.4	15.5	14.9	15.0	12.4	2 502
10.6	11.9	11.0	10.1	9.0	10.9	12.5	13.4	15.2	3 502
14.9	16.8	16.8	17.4	18.8	18.5	17.6	15.4	11.4	4 502
-3.2	0.8	5.4	7.9	11.8	13.0	14.6	12.4	13.4	5 502
16.2	16.7	18.1	19.6	21.1	22.0	20.5	15.2	12.2	6 502
-9.4	-9.1	-7.1	-3.5	-0.7	2.5	4.9	7.2	10.2	7 502
14.9	18.1	20.0	22.7	26.3	28.0	27.5	24.7	19.9	8 502
-6.7	-6.5	-3.1	1.2	3.8	5.0	5.2	8.9	10.0	9 502
13.3	19.2	24.2	28.6	33.7	37.8	34.1	26.4	18.1	10 502
6.8	5.9	6.2	9.1	11.2	12.7	13.9	16.1	17.8	11 502
22.1	27.7	33.5	37.1	37.3	30.7	22.1	15.1	10.2	12 502
28.3	28.7	28.7	28.4	30.2	31.9	32.9	35.5	37.2	13 502
38.3	38.9	34.8	30.2	21.6	14.6	11.4	8.5	6.2	14 502
34.6	35.8	35.9	36.6	36.1	35.6	36.4	36.0	35.5	15 502
33.1	29.0	23.9	16.2	12.4	10.3	7.7	6.2	5.3	16 502
31.3	30.8	31.0	32.8	34.1	31.6	26.5	22.4	21.4	17 502
16.8	13.3	10.1	8.2	6.2	5.6	4.9	4.2	3.5	18 502
24.1	21.6	18.5	16.4	14.6	12.0	10.2	8.2	6.7	19 502
5.5	4.3	4.6	3.5	4.0	3.4	2.9	2.3	2.6	20 502
8.8	7.2	4.7	2.4	2.0	1.6	1.7	1.8	0.5	21 502
1.4	0.8	0.6	1.0	0.7	0.4	-0.5	-1.0	0.5	22 502
1200.0	1800.0	120.0	-576.0	0.0	48.0	0.0	0.0		503
7.2	2.4	1.6	1.8	1.4	0.6	0.7	-0.5	0.5	1 503
-0.7	-1.3	-3.4	-6.7						2 503
2.4	0.6	0.0	1.6	2.2	1.1	-0.4	-1.0	-0.2	3 503
-1.3	-3.6	-3.8	-7.6						4 503
2.2	1.2	0.7	0.1	0.1	-1.1	-2.0	-2.4	-3.7	5 503
-4.8	-5.3	-6.7	-8.3						6 503
2.0	2.5	2.6	1.7	-0.2	-1.3	-0.4	-1.1	-4.6	7 503
-9.0	-9.8	-8.8	-8.5						8 503
0.5	1.6	1.9	2.4	-0.1	-1.0	-1.4	-4.8	-9.8	9 503
-9.4	-10.4	-9.8	-9.1						10 503
3.6	3.5	4.2	3.6	2.2	0.5	-1.2	-2.8	-6.2	11 503
-9.7	-10.3	-10.7	-10.0						12 503

Table 48. HVOSM inputs for ditch-embankment test. (continued)

600.0	1800.0	120.0	-1200.0	-576.0	48.0	0.0	0.0			504
32.8	33.4	33.7	32.9	32.4	29.0	25.0	14.8	10.2	1	504
10.2	8.8	8.4	6.8	5.9					2	504
33.2	38.3	34.8	33.1	32.9	32.5	30.7	28.2	28.0	3	504
29.2	28.4	29.2	30.6	28.7					4	504
25.1	28.1	30.4	31.3	32.5	32.8	34.0	32.4	30.5	5	504
31.6	33.6	34.9	36.1	35.8					6	504
32.4	33.6	34.1	34.8	35.0	35.8	36.1	37.0	36.4	7	504
35.9	35.4	33.4	31.3	30.8					8	504
30.6	29.5	30.4	30.0	30.5	29.2	29.0	29.6	29.8	9	504
29.8	28.3	26.4	24.5	21.6					10	504
24.8	24.2	24.1	26.1	24.7	22.7	21.9	20.9	20.7	11	504
20.0	15.9	13.1	10.4	7.2					12	504
19.8	19.3	19.9	20.2	18.4	18.7	17.4	17.5	16.4	13	504
15.4	13.8	7.7	3.8	2.4					14	504
12.6	15.5	16.3	16.2	15.7	14.5	14.2	13.9	12.2	15	504
11.5	8.9	6.5	4.3	2.2					16	504
0.5	7.2	11.3	13.9	14.3	13.2	11.9	11.0	11.3	17	504
10.0	8.5	6.7	4.1	2.0					18	504
-7.7	-3.1	6.1	8.4	10.3	12.4	10.0	7.9	7.8	19	504
5.6	4.1	3.4	2.3	0.5					20	504
-7.7	-7.7	-3.5	1.1	6.2	8.4	7.7	8.4	7.0	21	504
5.2	4.7	3.1	3.1	3.6					22	504
0.75	0.75	0.75	0.75	0.0	4.0				0	506
1.0	15.0	64.0	0.95	1.5	6.0	6.0	6.0	6.0	1	506
2.0	15.0	64.0	0.95	1.5	6.0	6.0	6.0	6.0	2	506
3.0	15.0	64.0	0.95	1.5	6.0	6.0	6.0	6.0	3	506
4.0	15.0	64.0	0.95	1.5	6.0	6.0	6.0	6.0	4	506
42.26 MPH AT -23.75 DEG. DEPARTURE									0	600
0.0	0.0	-23.75	0.0	0.0	0.0	-1.7	0.0		0	601
0.0	0.0	-22.49	743.8	0.0	0.0				0	602
0.0	0.0	0.0	0.0	0.0	0.0	0.0	0.0		0	603
										9999

Appendix B

HVOSM INPUT DESCRIPTION

Input to the HVOSM is supplied in 80-column punched-card formats. Each input card must contain a three-digit number in columns 78 through 80. The first of these digits represents the data-block number, and the remaining two digits represent the card number within the data block. Data blocks are categorized and numbered as follows:

Data-Block Number	Data Content
1	Simulation-control data
2	Vehicle data
3	Tire data
4	Vehicle-control data
5	Terrain/environmental data
6	Initial conditions

Each data block may contain a title card, with the last two digits of the card number being 00. (For example, the title card for vehicle data is numbered 200.) Title cards may contain alphanumeric information, which is printed on each output page.

Data are entered on individual data cards and on table cards in nine fields of eight columns each (9F8.0 format). Any data not supplied defaults to 0.0. The format for table entry consists of a table information card containing information on the number of entries, the beginning and end values, the number of tables, etc., depending on the particular table being read. Immediately following this card are the table data cards, each containing the same card number in columns 78 through 80 as the table information card. Table data cards must also contain a table sequence number in column 76 (columns 75 and 76 if a two-digit number) which must always be larger than the sequence number on the previous table data card. The last card in the input data deck must be numbered 9999 in columns 77 through 80.

A description of the data required follows in the form of a chart for each card. Plots of functions simulated and/or the geometry involved are included following card charts as necessary for clarity, as are discussions of the use of cards for given tables.

RUN TITLE									100

Program Variable	Analytical Variable	Description	Input Units
HED	-	RUN TITLE CARD This card may contain up to 72 characters of alphanumeric information describing a run and is printed on each output page.	

T0	T1	DTCOMP	DTPRNT	THMAX	UVWMIN	PQRMIN			101

Program Variable	Analytical Variable	Description	Input Units
T0		Initial simulation time	s
T1		Final simulation time	s
DTCOMP		Normal vehicle integration time step	s
DTPRNT		Output print time interval (multiple of DTCOMP)	s
THMAX		Value of pitch angle (θ_t') at which space-fixed axes are indexed (usually, 70 deg)	deg
UVWMIN PQRMIN		Values of resultant linear and angular velocities for simulation stop test. If both vehicle velocities are less than input values, run is terminated.	in./s rad/s

ISUS	INDCRB	NCRBSL	DELTC		DELTB				102

Program Variable	Analytical Variable	Description	Input Units
ISUS		Suspension option indicator = 0, independent front, solid rear axles = 1, independent front and rear axles = 2, solid front and rear axles	-
INDCRB		Curb impact indicator = 0, no curb input = 1, curb input supplied (provides steer degree of freedom and radial-spring tire model) = -1, no curb input supplied (provides steer degree of freedom with point-contact tire model)	-
NCRBSL		Number of curb slopes supplied if INDCRB = 1 $2 \leq$ NCRBSL ≤ 7	-
DELTC	Δt_c	Integration time step for curb impacts Note: Barrier Option has been disabled; field 5 should be blank.	s
DELTB	$(\Delta t)_B$	Vehicle integration time step for use during sprung-mass ground contacts Note: If INDCRB = -1, initial conditions for front-wheel steer angle (PSIFIO, (PSIFDO) must be supplied on card 601.	s

MODE	BBAR	EM	AAA	HMAX	HMIN	BETA			103

Program Variable	Analytical Variable	Description	Input Units
MODE		Numerical integration mode indicator = 0, variable Adams-Moulton = 1, Runge-Kutta = 2, fixed Adams-Moulton Note: The following variables are required only when MODE = 0.	
EBAR	$\bar{E}$	Upper bound on truncation error estimate	
EM	M	Constant from which lower bound on truncation error estimate is computed	
AAA	α	Positive number used to prevent unnecessary reduction in variable step size	
HMAX	h_{max}	Positive upper bound on magnitude of variable step size	
HMIN	h_{min}	Positive lower bound on magnitude of variable step size	
BETA	β	Positive number between zero and one used to increase or decrease step size	

NPAGE(4)	NPAGE(6)	NPAGE(7)	NPAGE(8)	NPAGE(9)	NPAGE(10)	NPAGE(14)	NPAGE(17)		104
1 2 3 4 5 6 7 8	9 10 11 12 13 14 15 16	17 18 19 20 21 22 23 24	25 26 27 28 29 30 31 32	33 34 35 36 37 38 39 40	41 42 43 44 45 46 47 48	49 50 51 52 53 54 55 56	57 58 59 60 61 62 63 64	65 66 67 68 69 70 71 72	73 74 75 76 77 78 79 80

Program Variable	Analytical Variable	Description	Input Units
		Note: The NPAGE array is used to control output printed from a run. If an array element is non-zero, the group of output data corresponding to that element is printed. The output corresponding to the elements read on card 104 are user-controlled. If an output is desired, a non-zero number must be read in the appropriate field. The output groups corresponding to these elements are:	
NPAGE(4)		Angular accelerations; suspension accelerations for independent suspensions; or displacements, velocities, and accelerations of roll center and axle angle for solid axles	
NPAGE(6)		Inclination (camber) angle of wheels with respect to ground; steer angle of wheels; and camber angle of wheels with respect to vehicle	
NPAGE(7)		Longitudinal and lateral velocities of tire contact point with respect to vehicle	
NPAGE(8)		Elevation of ground contact point of tires	
NPAGE(9)		Total suspension forces and suspension anti-pitch forces	
NPAGE(10)		Suspension damping forces and change in suspension spring forces from equilibrium	
NPAGE(14)		Components of tire forces along inertial axes, tire sinkage and circumferential and side plow force	
NPAGE(17)		Comfort factor, friction demand, terrain friction coefficient	

VEHICLE	DESCRIPTION TITLE								200

Program Variable	Analytical Variable	Description	Input Units
VHED	-	VEHICLE DESCRIPTION TITLE This card may contain up to 72 characters of alphanumeric information describing the simulated vehicle. Note that only the first 40 characters are printed on each output page.	

XMS	XMUF	XMUR	XIX	XIY	XIZ	XIXZ	XIR	XIF	201

Program Variable	Analytical Variable	Description	Input Units
XMS	M_S	Sprung mass	lb-s^2/in.
XMUF	M_{uF}	Total front unsprung mass	lb-s^2/in.
XMUR	M_{uR}	Total rear unsprung mass	lb-s^2/in.
XIX	I_X	Mass moment of inertia of sprung mass about vehicle X-axis	lb-s^2-in.
XIY	I_Y	Mass moment of inertia of sprung mass about vehicle Y-axis	lb-s^2-in.
XIZ	I_Z	Mass moment of inertia of sprung mass about vehicle Z-axis	lb-s^2-in.
XIXZ	I_{XZ}	Mass product of inertia of sprung mass in vehicle X-Z plane	lb-s^2-in.
XIR	I_R	Mass moment of inertia of solid-axle rear unsprung mass about a line parallel to vehicle X-axis and through rear unsprung-mass C.G. Required only if ISUS = 0 or 2.	lb-s^2-in.
XIF	I_F	Mass moment of inertia of solid-axle front unsprung mass about a line parallel to vehicle X-axis and through front unsprung-mass C.G. Required only if ISUS = 2.	lb-s^2-in.

A	B	TF	TR	RHO	TS	RHOF	TSF	G	202
1 2 3 4 5 6 7 8	9 10 11 12 13 14 15 16	17 18 19 20 21 22 23 24	25 26 27 28 29 30 31 32	33 34 35 36 37 38 39 40	41 42 43 44 45 46 47 48	49 50 51 52 53 54 55 56	57 58 59 60 61 62 63 64	65 66 67 68 69 70 71 72	73 74 75 76 77 78 79 80

Program Variable	Analytical Variable	Description	Input Units
A	a	Horizontal distance from sprung-mass C.G. to centerline of front wheels	in.
B	b	Horizontal distance from sprung-mass C.G. to centerline of rear wheels	in.
TF	T_F	Front wheel track	in.
TR	T_R	Rear wheel track	in.
RHO	ρ	Vertical distance between rear-axle C.G. and rear-axle roll center, positive for roll center above C.G.	in.
TS	T_S	Distance between rear spring mounts for solid rear axle	in.
		Note: RHO and TS required only if ISUS = 0 or 2.	
RHOF	ρ_F	Vertical distance between front-axle C.G. and front-axle roll center, positive for roll center above C.G.	in.
TSF	T_{SF}	Distance between front spring mounts for solid front axle	in.
		Note: RHOF and TSF required only if ISUS = 2.	
G	g	Gravitational acceleration	in./s^2
		Note: If G is not supplied, a default value of 386.4 in/s^2 is assumed.	

X1	Y1	Z1	X2	Y2	Z2	ZF	ZR		203
1 2 3 4 5 6 7 8	9 10 11 12 13 14 15 16	17 18 19 20 21 22 23 24	25 26 27 28 29 30 31 32	33 34 35 36 37 38 39 40	41 42 43 44 45 46 47 48	49 50 51 52 53 54 55 56	57 58 59 60 61 62 63 64	65 66 67 68 69 70 71 72	73 74 75 76 77 78 79 80

Program Variable	Analytical Variable	Description	Input Units
X1	X_1	Coordinates of first accelerometer position with respect to sprung-mass C.G.	in.
Y1	Y_1		
Z1	Z_1		
X2	X_2	Coordinates of second accelerometer position with respect to sprung-mass C.G.	in.
Y2	Y_2		
Z2	Z_2		
ZF	Z_F	Static vertical distance between front-wheel C.G. (or front-axle roll center if ISUS = 2) and sprung-mass C.G.	in.
ZR	Z_R	Static vertical distance between rear-axle roll center (or rear-wheel C.G.) and sprung-mass C.G. Note: If ZF and ZR are not supplied, they will automatically be calculated within the program to ensure initial vertical equilibrium of the vehicle on flat, level terrain at 0.0 elevation.	in.

AKF	AKFC	AKFCP	AKFE	AKFEP	XLAMF	OMEGFC	OMEGFE		204

Program Variable	Analytical Variable	Description	Input Units
AKF	K_F	Linear front-suspension load/deflection rate	lb/in.
AKFC	K_{FC}	Linear coefficient of front-suspension compression (jounce) bumper term	lb/in.
AKFCP	K'_{FC}	Cubic coefficient of front-suspension compression (jounce) bumper term	lb/in.^{3}
AKFE	K_{FE}	Linear coefficient of front-suspension extension (rebound) bumper term	lb/in.
AKFEP	K'_{FE}	Cubic coefficient of front-suspension extension (rebound) bumper term	lb/in.^{3}
XLAMF	λ_F	Ratio of conserved to total absorbed energy in front-suspension bumpers	-
OMEGFC	Ω_{FC}	Front-suspension deflection at which compression bumper is contacted (Note: should be negative)	in.
OMEGFE	Ω_{FE}	Front-suspension deflection at which extension bumper is contacted (Note: should be positive)	in.
		Note: All suspension parameters are effective at the wheel for independent front suspension or at the spring position for solid front axle.	

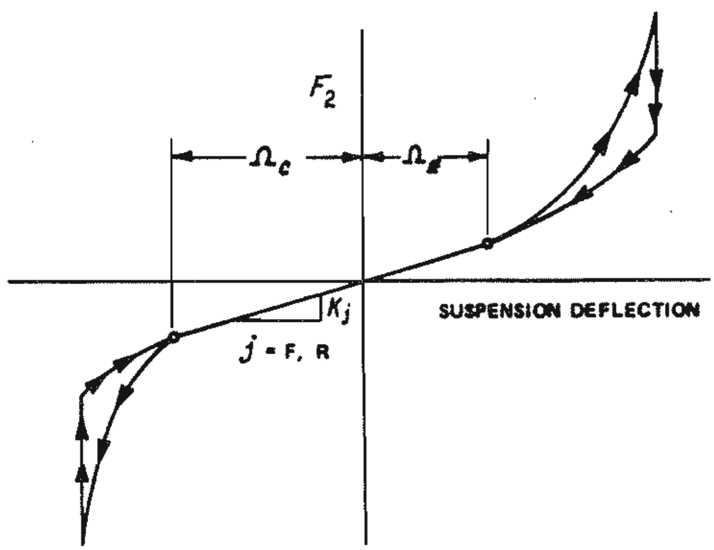

GENERAL FORM OF SIMULATED SUSPENSION BUMPER CHARACTERISTICS

AKR	AKRC	AKRCP	AKRE	AKREP	XLAMR	OMEGRC	OMEGRE		205

Program Variable	Analytical Variable	Description	Input Units
AKR	K_R	Linear rear-suspension load/deflection rate	lb/in.
AKRC	K_{RC}	Linear coefficient of rear-suspension compression (jounce) bumper term	lb/in.
AKRCP	K'_{RC}	Cubic coefficient of rear-suspension compression (jounce) bumper term	lb/in.^{3}
ARKE	K_{RE}	Linear coefficient of rear-suspension extension (rebound) bumper term	lb/in.
AKREP	K'_{RE}	Cubic coefficient of rear-suspension extension (rebound) bumper term	lb/in.^{3}
XLAMR	λ_R	Ratio of conserved to total absorbed energy in rear-suspension bumpers	-
OMEGRC	Ω_{RC}	Rear-suspension deflection at which compression bumper is contacted (Note: should be negative)	in.
OMEGRE	Ω_{RE}	Rear-suspension deflection at which extension bumper is contacted (Note: should be positive)	in.
		Note: All suspension parameters are effective at the wheel for independent rear suspension or at the spring position for solid rear axle.	

CF	CFP	EPSF	CR	CRP	EPSR				206

Program Variable	Analytical Variable	Description	Input Units
CF	C_F	Front-suspension viscous damping coefficient per side	lb-s/in.
CFP	C'_F	Front-suspension coulomb friction per side	lb
EPSF	ϵ_F	Front-suspension friction null band	in./s
CR	C_R	Rear-suspension viscous damping coefficient per side	lb-s/in.
CRP	C'_R	Rear-suspension coulomb friction per side	lb
EPSR	ϵ_R	Rear-suspension friction null band	in./s
		Note: All suspension parameters are effective at the wheel for independent suspension or at the spring position for solid axle.	

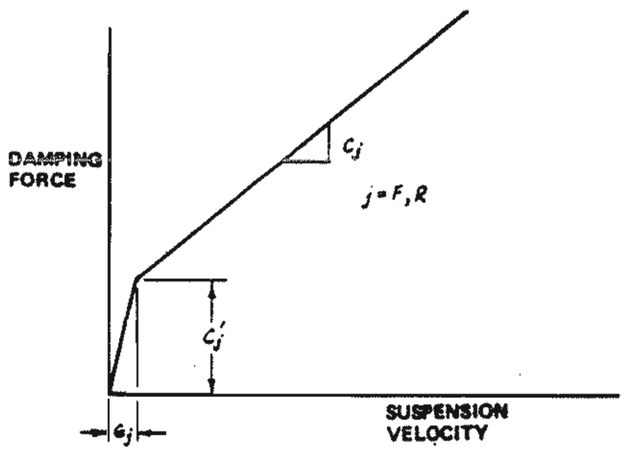

RF	RR	AKRS	AKDS	AKDS1	AKDS2	AKDS3			207

Program Variable	Analytical Variable	Description	Input Units
RF	R_F	Auxiliary roll stiffness of front suspension	lb-in./rad
RR	R_R	Auxiliary roll stiffness of rear suspension	lb-in./rad
AKRS	K_{RS}	Rear-axle roll-steer coefficient Note: AKRS is required only if ISUS = 0 or 2.	deg/deg
AKDS	$K_{\delta s}$	Coefficients for cubic representation of rear-wheel steer angle as a function of wheel displacement. These coefficients are required only when ISUS = 1	rad
AKDS1	$K_{\delta s1}$		rad/in.
AKDS2	$K_{\delta s2}$		rad/in.^{2}
AKDS3	$K_{\delta s3}$		rad/in.^{3}

XIPS	CPSP	OMGPS	AKPS	EPSPS	XPS				208

Program Variable	Analytical Variable	Description	Input Units
XIPS	I_ψ	Steering-system steer moment of inertia about wheel steering axis	lb-s^2-in.
CPSP	C'_ψ	Steering-system coulomb friction torque, effective at wheel steering axis	lb-in.
OMGPS	Ω_ψ	Front-wheel steer angle at which steering limit stops are engaged	rad
AKPS	K_ψ	Stiffness of steering limit stops, effective at front-wheel steering axis	lb-in./rad
EPSPS	ϵ_ψ	Friction lag in steering system	rad/sec
XPS	PT	Front-wheel pneumatic trail	in.
		Note: This card must be furnished if INDCRB (Card 102) is either 1.0 or -1.0.	

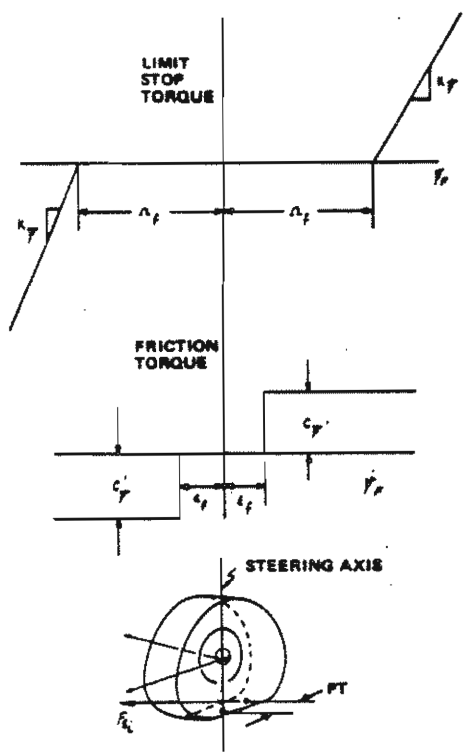

DELB	DELE	DDEL	NDTHF	NDTHR					209

Program Variable	Analytical Variable	Description	Input Units
		Note: The parameters on card 209 apply to four tables defining camber and half-track changes as a function of wheel displacement. Card 209 and subsequent table cards are not required if ISUS = 2.	
DELB		Beginning value of wheel displacement for tables	in.
DELE		End value of wheel displacement for tables	in.
DDEL		Increment value of wheel displacement for tables	in.
NDTHF		Indicator for front half-track change table. Table is supplied if NDTHF ≠ 0.	
NDTHR		Indicator for rear half-track change table. Table is supplied if NDTHR ≠ 0.	
		Following card 209 are up to four tables containing (DELE-DELB)/DDEL +1 entries in the order:	
		PHIC(I) Right-front wheel camber	deg
		PHIRC(I) Right-rear wheel camber (required if ISUS = 1)	deg
		DTHF(I) Front half-track change (required if NDTHF ≠ 0)	in.
		DTHR(I) Rear half-track change (required if ISUS = 1) and NDTHR ≠ 0)	in.
		Table entries are read in fields of eight and must contain 209 in columns 78 through 80. A table sequence number must also be supplied in column 76, and the sequence number must increase with each card. Each new table must start on a new card. A maximum of 50 entries is allowed for each table.	

-5.0	5.0	1.0	1.0	1.0					209
PHIC(1)	PHIC(2)	...				...		PHIC(9)	1 209
PHIC(10)	PHIC(11)								2 209
PHIRC(1)	PHIRC(2)	...				...		PHIRC(9)	3 209
PHIRC(10)	PHIRC(11)								4 209
DTHF(1)	DTHF(2)	...				...		DTHF(9)	5 209
DTHF(10)	DTHF(11)								6 209
DTHR(1)	DTHR(2)	...				...		DTHR(9)	7 209
DTHR(10)	DTHR(12)								8 209

CAMBER TABLE
(DEFINED FOR RIGHT-FRONT (OR RIGHT-REAR) WHEEL)

δ	ϕ_c
DELB	PHIC(1)
DELB+DDEL	PHIC(2)
⋮	⋮
DELB+nDDEL	PHIC(n+1)
⋮	⋮
DELE	PHIC$\left(\frac{\text{DELE-DELB}}{\text{DDEL}}+1\right)$

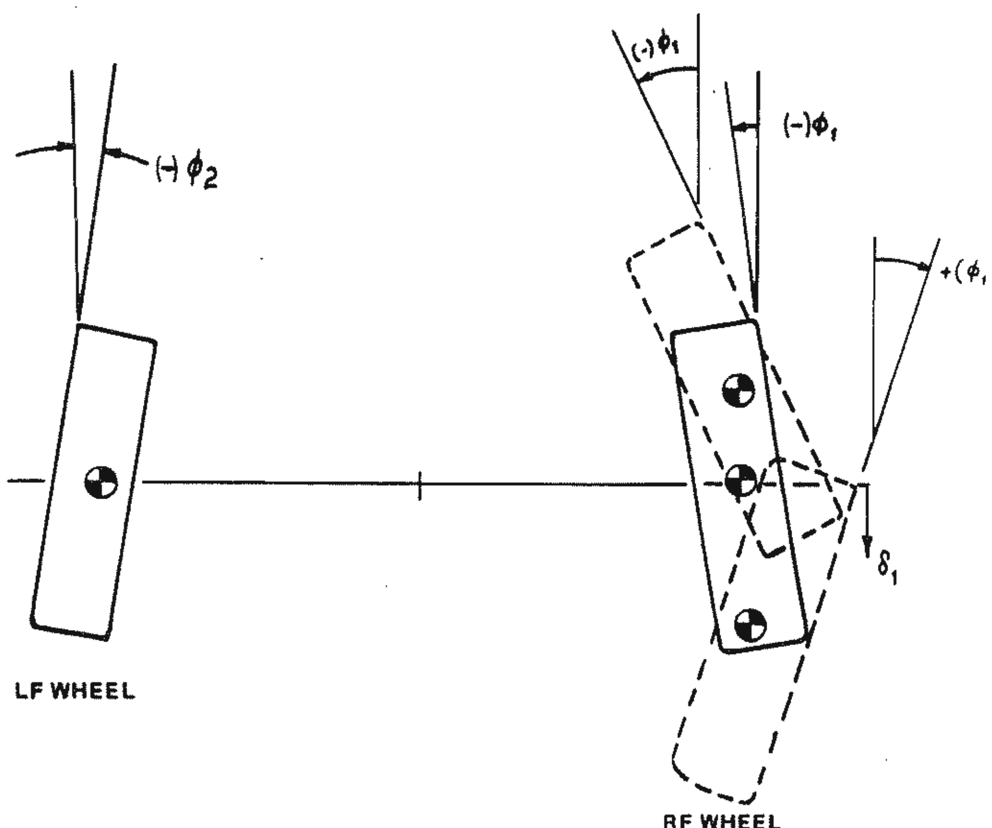

POSITIVE CAMBER – WHEEL LEANS OUT AT TOP
NEGATIVE CAMBER – WHEEL LEANS IN AT TOP

DAPFB	DAPFE	DDAPF							210

Program Variable	Analytical Variable	Description	Input Units
DAPFB		Beginning suspension deflection for front anti-pitch coefficient table	in.
DAPFE		Ending suspension deflection for front anti-pitch coefficient table	in.
DDAPF		Incremental deflection for front anti-pitch coefficient table	in.
		Following card 210 is a table containing (DAPFE-DAPFB)/DDAPF + 1 entries of front anti-pitch coefficient, APF(I)	lb/lb-ft
		Note: Table entries are read in nine fields of eight columns. A monotonically increasing table sequence number must be in column 76, and card number 210 must be in columns 78 through 80. A maximum of 21 entries is allowed. Example:	

-5.0	5.0	1.0							210
APF(1)	APF(2)	APF(3)	...				APF(8)	APF(9)	1 210
APF(10)	APF(11)								2 210

DAPRB	DAPRE	DDAPR							211

Program Variable	Analytical Variable	Description	Input Units
DAPRB		Beginning suspension deflection for rear anti-pitch coefficient table	in.
DAPRE		Ending suspension deflection for rear anti-pitch coefficient table	in.
DDAPR		Incremental deflection for rear anti-pitch coefficient table	in.
		Following card 211 is a table containing (DAPRE-DAPRB)/ DDAPR + 1 entries of rear anti-pitch coefficient, APR(I) Note: Table entries are read in nine fields of eight columns. A monotonically increasing table sequence number must be in column 76, and card number 211 must be in columns 78 through 80. A maximum of 21 entries is allowed. Example:	lb/lb-ft

-5.0 APR(1)	5.0 APR(2)	5.0 APR(3)							211 1 211

NHARPT	EPSHP	AMUGHP	INDKST	AKCNST	PHIHP				215

Program Variable	Analytical Variable	Description	Input Units
		<u>Sprung-mass/ground-contact option</u>	
NHARPT	--	Number of points on sprung mass to be checked for ground interference, maximum 39	--
EPSHP		Velocity-null band for ground-contact point friction-force calculations	in./s
AMUGHP	μ_{HP}	Nominal point/ground-friction coefficient. Note: The effective coefficient is the product of μ_{HP} and AMUG for the terrain (see card 506).	--
INDKST	--	Indicator for constant stiffness for all points If INDKST = 1, all points have same stiffness If INDKST = 0, the stiffness for each point must be input on card(s) 217	--
AKCNST	--	Constant omnidirectional stiffness of vehicle structural points, must be input if INDKST = 1	lb/in.
PHIHP		Vehicle roll or pitch angle at which option is enabled, input positive, test is made on absolute value. Note: DELTB > 0.0 (card 102, field 6) is required for sprung-mass/ground-contact option	deg

XSTIO(I)	YSTIO(I)	ZSTIO(I)	XSTIO (I+1)	YSTIO (I+1)	ZSTIO (I+1)	XSTIO (I+2)	YSTIO (I+2)	ZSTIO (I+2)	N 216

Program Variable	Analytical Variable	Description	Input Units
		Sprung-mass/ground-contact option	
XSTIO(I) YSTIO(I) ZSTIO(I) XSTIO(I+1) YSTIO(I+1) ZSTIO(I+1) XSTIO(I+2) YSTIO(I+2) ZSTIO(I+2)		X, Y, and Z positions of vehicle structural points with respect to vehicle axis system. Input three sets per card up to a maximum NHARPT.	in. in. in.
N		Card sequence number, right-justified in columns 75 and 76, beginning at 0	

AKST(I)	AKST (I+1)	AKST (I+2)	AKST (I+3)	AKST (I+4)	AKST (I+5)				N 217

Program Variable	Analytical Variable	Description	Input Units
		Sprung-mass/ground-contact option	
AKST(I) AKST(I+1) AKST(I+2) AKST(I+3) AKST(I+4) AKST(I+5)		Omnidirectional stiffness for each individual point, must be input if INDKST = 0 (card 215, field 4). Six values per card up to a maximum NHARPT	lb/in.
N		Card sequence number starting at 0.	

TIRE DESCRIPTION		TITLE							300

Program Variable	Analytical Variable	Description	Input Units
THED	-	TIRE TITLE This card may contain up to 72 characters of alphanumeric information describing the simulated vehicle tires. Note that only the first 40 characters are printed on each output page.	

ITIR(1)	ITIR(2)	ITIR(3)	ITIR(4)	RWHJE	DRWHJ				301

Program Variable	Analytical Variable	Description	Input Units
ITIR(1)		Indicator identifying set of tire data to be used for RF tire	-
ITIR(2)		Indicator identifying set of tire data to be used for LF tire	-
ITIR(3)		Indicator identifying set of tire data to be used for RR tire	-
ITIR(4)		Indicator identifying set of tire data to be used for LR tire	-
RWHJE		Final deflection (R_w-h'_j) of the force (F'_j) versus deflection characteristic of radial-spring tire model	in.
DRWHJ		Increment of deflection of the force/deflection characteristics of radial-spring tire model. Note: RWHJE and DRWHJ must be supplied only if INDCRB = 1. The force corresponding to the deflection values is computed automatically in subroutine WHEEL for each set of tire properties. The number of force entries is limited to 35. Therefore, $\frac{\text{RWHJE}}{\text{DRWHJ}} + 1 \leq 35$	in.

AKT(1)	SIGT(1)	XLAMT(1)	AO(1)	A1(1)	A2(1)	A3(1)	A4(1)	OMEGT(1)	1 301

Program Variable	Analytical Variable	Description	Input Units
AKT(1)	K_{T_1}	Tire load/deflection rate in quasi-linear range	lb/in.
SIGT(1)	σ_{T_1}	Tire deflection at which load deflection rate increases	in.
XLAMT(1)	λ_{T_1}	Multiplier of K_T used to obtain tire stiffness at large deflections	-
AO(1)	A_{0_1}	Constants for parabola describing small-angle cornering-stiffness variation with tire normal load. (See sketch on following page.)	
A1(1)	A_{1_1}		
A2(1)	A_{2_1}		
A3(1)	A_{3_1}	Constants for parabola describing small-angle camber-stiffness variation with tire normal load. (See sketch on following page.)	
A4(1)	A_{4_1}		
OMEGT(1)	Ω_{T_1}	Multiplier of A_2 at which tire side-force characteristic variation with load is abandoned	
		Note: This card represents the first partial set of tire data and is required. If more than one tire data set is indicated by two or more different entries for ITIR on card 301, subsequent data follow this card with the same format and the tire data set number replacing 1 in column 76. For example, card 301 below indicates two different tire data sets, with the first used for the front tires and the second used for the rear tires of the vehicle.	

1.0	1.0	2.0	2.0						301
AKT(1)	SIGT(1)	XLAMT(1)	AO(1)	A1(1)	A2(1)	A3(1)	A4(1)	OMEGT(1)	1 301
AKT(2)	SIGT(2)	XLAMT(2)	AO(2)	A1(2)	A2(2)	A3(2)	A4(2)	OMEGT(2)	2 301

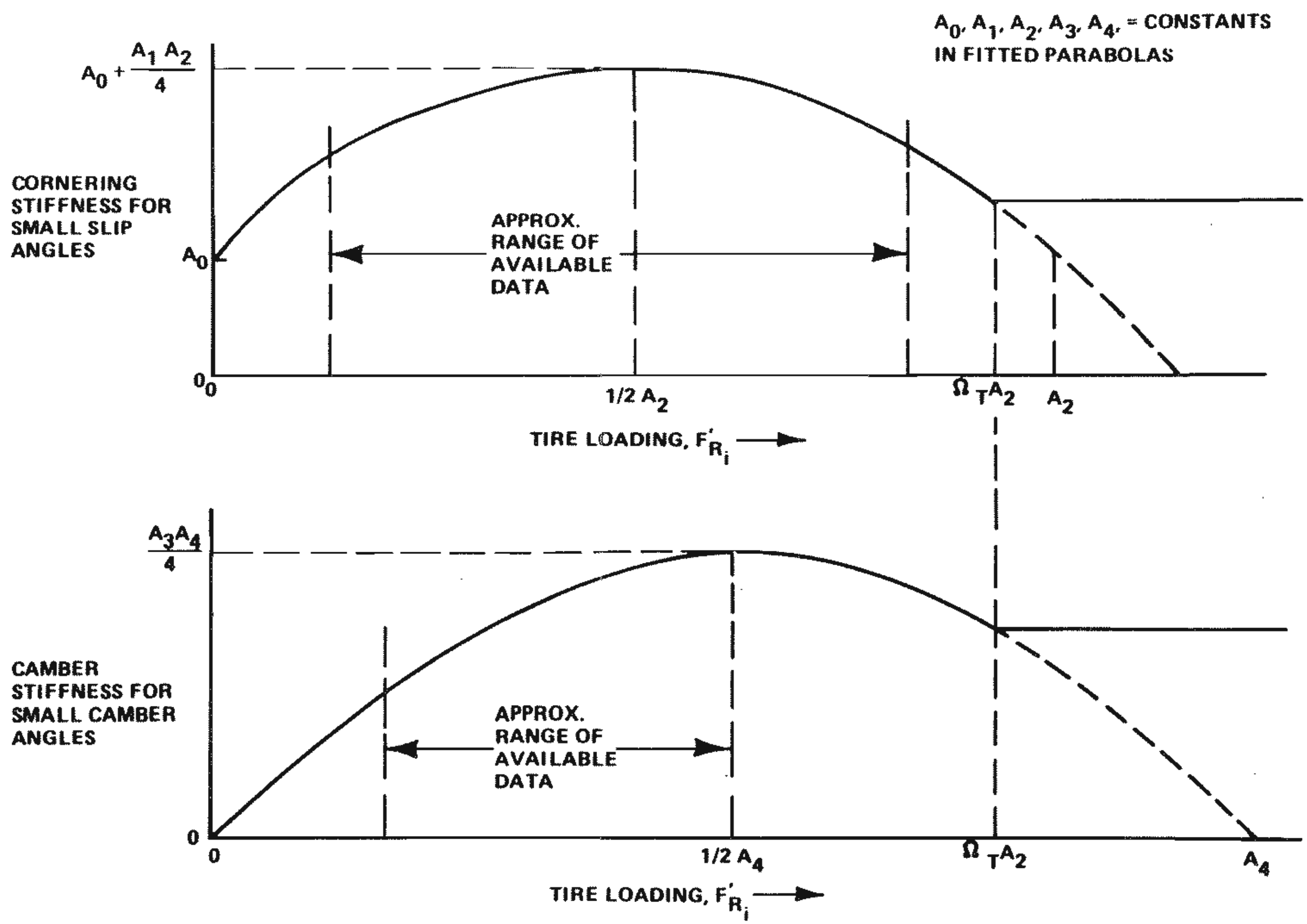

Simulated variation of small-angle cornering and camber stiffness with loading normal to tire/terrain contact patch.

AMU(1)	AMU(2)	AMU(3)	AMU(4)	RW(1)	RW(2)	RW(3)	RW(4)		302

Program Variable	Analytical Variable	Description	Input Units
AMU(1)	μ_1	Nominal friction coefficient between tire and ground. The four values correspond to the four tire data sets. At least one, and at most the same number as the number of data sets being used, is required.	
AMU(2)	μ_2		
AMU(3)	μ_3		
AMU(4)	μ_4		
RW(1)	R_{W_1}	Undeflected tire radius. The four values correspond to the four tire data sets. At least one, and at most the same number as the number of data sets being used, is required.	in.
RW(2)	R_{W_2}		in.
RW(3)	R_{W_3}		in.
RW(4)	R_{W_4}	For example, if, as in the example of card 301, two tire data sets are being used:	in.

AMU(1)	AMU(2)			RW(1)	RW(2)				302

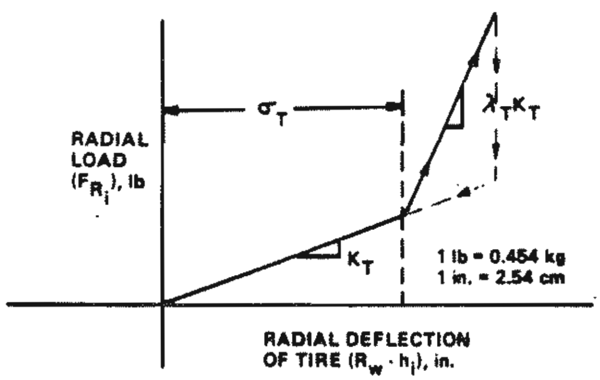

VEHICLE	CONTROL	DESCRIPTION	TITLE						400

Program Variable	Analytical Variable	Description	Input Units
CHED	-	VEHICLE CONTROL TITLE This card may contain up to 72 characters of alphanumeric information describing vehicle control inputs. Note that only the first 40 characters are printed on each output page.	-

TB	TE	TINCR	NTBL1	NTBL2	NTBL3				401

Program Variable	Analytical Variable	Description	Input Units
TB		Initial time for driver control input tables	s
TE		Final time for driver control input tables	s
TINCR		Increment of time for driver control input tables	s
NTBL1		Indicator for steer angle (ψ_f) table; read ψ_F table only if NTBL1 $\neq$ = 0.0	
NTBL2		Indicator for front-wheel torque (TQ_F) table; read TQ_F table only if NTBL2 $\neq$ 0.0	
NTBL3		Indicator for rear-wheel torque (TQ_R) table; read TQ_R table only if NTBL3 $\neq$ 0.0	
		Note: TE must be >TB, and the number of entries in each table (TE-TB)/TINCR +1 must be $\leq$ 50. If TB $\neq$ TO (control inputs starting in the middle of a run), the first three values in the input tables must be zero control inputs between TO and TB. Also, if TE < T1 (control inputs ending in the middle of a run), the control inputs between TE and T1 are determined by quadratic interpolation of the last three values in the control table. Hence, if zero control inputs are desired between TE and T1, the last three entries in the tables must be zero. Any (or all) of the three tables that are to be input must appear in the order:	
		PSIF - front-wheel steer table	deg
		TQF - front-wheel torque table (each wheel)	lb-ft
		TQR - rear-wheel torque table (each wheel)	lb-ft
		Note: Each table card must contain 401 in columns 78 through 80 and must also contain an increasing table sequence number in column 76. For example, if PSIF and TQR are to be read from t = 0.0 to t = 1.0 second, in increments of 0.1 second:	

0.0	1.0	0.1	1.0	0.0	1.0				401
PSIF(1)	PSIF(2)	...				...	PSIF(8)	PSIF(9)	1 401
PSIF(10)	PSIF(11)								2 401
TQR(1)	TQR(2)	...				...	TQR(8)	TQR(9)	3 401
TQR(10)	TQR(11)								4 401

IPATH	IWAGN	IFILT	TIL	TI	TAUF	ITDOPT			402

Program Variable	Analytical Variable	Description	Input Units
		Driver model path-following option	
IPATH		Driver model path-generator option indicator = 0, no path data to be supplied = 1, user will supply path data on card 403, 404	
IWAGN		Driver model wagon-tongue steer option indicator = 0, no wagon-tongue steer data to be used = 1, wagon-tonque steer data to be supplied on card 405 = -1, DRIV2 emergency steer response model option, additional card 402 required	
IFILT		Driver model neuro-muscular filter option indicator = 0, no filter data to be supplied = 1, filter data to be supplied as follows:	
TIL		Time-constant lag of neuro-muscular filter	s
TI		Time lead of neuro-muscular filter	s
TAUF		Net time delay of neuro-muscular filter	s
ITDOPT		Variable-torque path-following option indicator, set = 1.0 for VTPF	
		Note: If ITDOPT = 1, IWAGN must equal 1, and alternate definition of card 405 using VTPF inputs is used.	

PSIA	PSIDM	PSIDDM	TPRB	PMAX	PSIMAX	IDUMP			1 402

Program Variable	Analytical Variable	Description	Input Units
		DRIV2 - Emergency-maneuver driver control option inputs (card must be supplied if IWAGN = -1)	
PSIA	ψ_F	Initial front-wheel steer angle	deg
PSIDM*	$\dot{\psi}_F$	Maximum front-wheel steer velocity	deg/s
PSIDDM*	$\ddot{\psi}_F$	Maximum front-wheel steer acceleration and deceleration	deg/s^2
TPRB	t_{PRB}	Time at which emergency-maneuver driver control algorithm is to begin	s
PMAX**		Maximum driver discomfort level at which deceleration of steering system is to begin	g's
PSIMAX		Maximum front-wheel steer angle, input as positive value	deg
		After TPRB seconds have elapsed in the simulation run, DRIV2 accelerates the front-wheel steer velocity to PSIDM.	
		The velocity remains at PSIDM until either (1) the comfort factor exceeds PMAX or (2) the front-wheel steer angle exceeds PSIMAX. If either (1) or (2) is true, the front-wheel steer velocity is decelerated back to zero.	
IDUMP		If IDUMP > 0, subroutine DRIV2 intermediate variables are printed on unit 49.	
		*Note: Algebraic sign of these variables determines the direction of initial response.	
		**Note: For accel limit to work, must set NPAGE(17) = 1 (i.e., card 104, field 8) Also: PMAX = -SIGN(PSIDM) * ABS(PMAX)	

KLI	NPTS	XINIT	YINIT	PSA	DELL				403

Program Variable	Analytical Variable	Description	Input Units
		Driver model path-generator option inputs (must be supplied if IPATH = 1)	
KLI		Number of curvature descriptors to follow on card(s) 404, maximum of 8	--
NPTS		Number of points to be generated from the path descriptors, maximum of 100	--
XINIT		Initial X space-fixed coordinate of path	in.
YINIT		Initial Y space-fixed coordinate of path	in.
PSA		Initial path heading with respect to space-fixed coordinate axes	rad
DELL		Distance between generated path points	in.

DI(I)	RLI(I)	DI(I+1)	RLI(I+1)	DI(I+2)	RLI(I+2)	DI(I+3)	RLI(I+3)		N 404

Program Variable	Analytical Variable	Description	Input Units
		Driver model path-generator path descriptors (must be supplied if KLI > 0 (card 403, field 1))	
DI(I)		Degree of curvature of path where degree = 5729.6/radius in inches (1 in. = 2.54 cm)	deg
RLI(I)		Distance along path at which degree is effective	in.
		Note: A constant and/or spiral path may be generated by the use of DI(I) and RLI(I). RLI(I) should be a multiple of DELL. If DI(I) does not equal DI(I+1), the curvature will be spiraled between the two descriptors.	
N		Sequence No., initial value 0	

TPRB	DPRB	PLGTH	PMIN	PMAX	PSIFD	PGAIN	QGAIN		405

Program Variable	Analytical Variable	Description	Input Units
		Driver model wagon-tongue steer option inputs (must be supplied if IWAGN = 1 (card 402, field 2))	
TPRB		Initial probe sample time	s
DPRB		Time between probe samples	s
PLGTH		Length of probe from vehicle C.G. extending along vehicle-fixed longitudinal (X) axis	in.
PMIN		Error correction null band. If error of probe from path is $\leq$ PMIN, no corrective steer will be applied.	in.
PMAX		Maximum acceptable comfort factor above which driver model will only reduce front-wheel steer angle.	g's
PSIFD		Maximum front-wheel steer velocity. Corrective steer response will be limited to $\leq$ PSIFD	deg/s
PGAIN		Steer correction factor. Error is multiplied by PGAIN to determine corrective steer.	rad/in.
QGAIN		Steer velocity damping term. Limits velocity with which front-wheel steer angle can change.	rad-s/in.
		Note: If ITDOPT = 1 (card 402, field 7), see alternate definition of card 405 inputs on following page.	

TPRB	DPRB	PLGTH	PMIN	PMAX	KTQR1	KTQR2	TMAX	TDPSIO	405

Program Variable	Analytical Variable	Description	Input Units
		Variable-torque path-following (VTPF) option inputs (must be supplied if ITDOPT = 1 (card 402, field 7))	
TPRB		Initial probe sample time	s
DPRB		Time between probe samples	s
PLGTH		Length of probe from vehicle C.G. extending along vehicle-fixed longitudinal (X) axis	in.
PMIN		Error correction null band. If error of probe from desired path is ≤ PMIN, no corrective torque will be applied.	in.
PMAX		Maximum acceptable driver discomfort factor above which driver model will only reduce front-wheel steering torque	g's
KTQR1		Torque correction factor. Error is multiplied by KTQR1 to determine corrective torque applied to front-wheel steering system	lb-in./in.
KTQR2		Torque correction damping factor. Limits resultant change in corrective torque applied to front-wheel steering system	lb-in.-s/in.
TMAX		Maximum corrective torque which can be applied to front-wheel steering system	lb-in.
TDPSIO		Initial corrective torque to be applied to front-wheel steering system	lb-in
		Note: VTPF is used in conjunction with the tire sidewall contact option model. See input IADDT, card 516, field 8.	

TERRAIN	DESCRIPTI	ON TITLE							500

Program Variable	Analytical Variable	Description	Input Units
GHED	-	TERRAIN TITLE This card may contain up to 72 characters of alphanumeric information describing the simulated vehicle's environment (curbs, terrain tables). Note that only the first 40 characters are printed on each output page.	-

Cards 501 through 505 are employed for input of terrain tables. These tables include a maximum of four constant-increment tables and one variable-increment table, which must be the highest-numbered table in use. The constant-increment tables are all read under the same format, Table 1 being read on cards 501, etc. The variable-increment table is read with a slightly different format on cards numbered one greater than the highest-numbered constant-increment table.

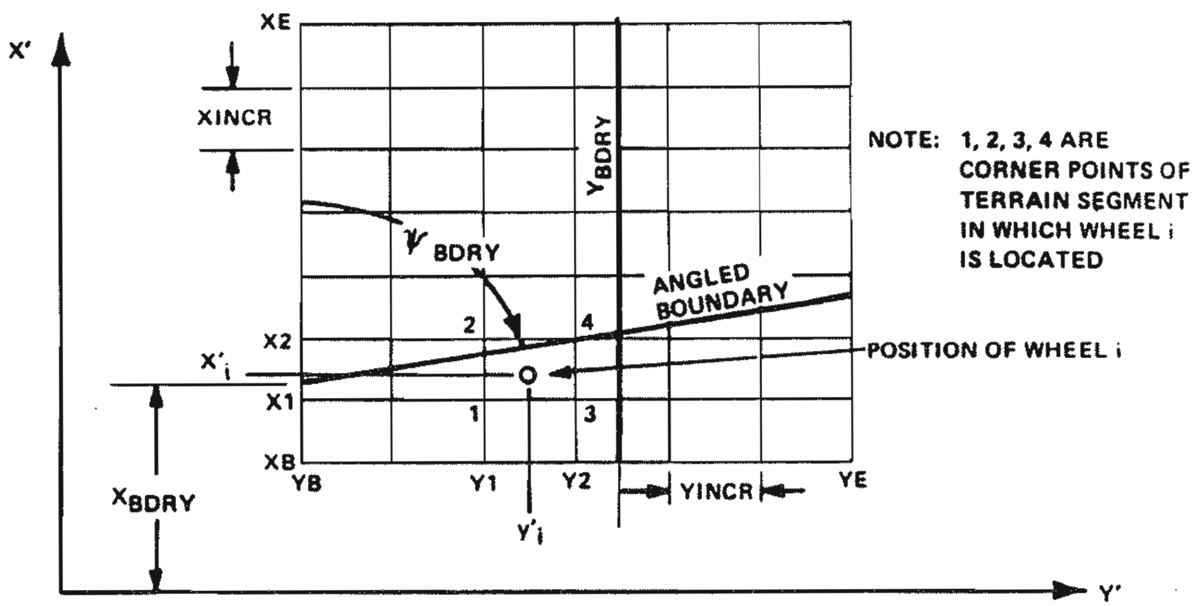

TERRAIN TABLE GRID

XB(I)	XE(I)	XINCR(I)	YB(I)	YE(I)	YINCR(I)	NBX(I)	NBY(I)		50I

Program Variable	Analytical Variable	Description	Input Units
		Constant-increment terrain tables	
		Note: The constant-increment terrain table number replaces the letter I in the card number. Thus, constant-increment Table 1 becomes card 501, etc.	
XB(I)		Initial X' value of terrain Table I	in.
XE(I)		Final X' value of terrain Table I (XE(I) > XB (I))	in.
XINCR(I)		Increment of X' between terrain-table entries	in.
YB(I)		Initial Y' value of terrain Table I	in.
YE(I)		Final Y' value of terrain Table I (YE(I) > YB(I))	in.
YINCR(I)		Increment of Y' between terrain-table entries	in.
NBX(I)		Number of angled boundaries for Table I ($0 \leq NBX \leq 8$)	
NBY(I)		Number of Y' boundaries for Table I ($0 \leq NBY \leq 8$)	
		Card 50I contains the control information for terrain Table I. The remainder of the data is contained on cards numbered 50I, with an increasing table sequence number contained in column 76.	
		If NBX(I) ≠ 0, the following two cards are required containing:	
XBDRY PSBDRO	X_{BDRY} ψ_{BDRY}	XBDRY - XB intercept of angled boundaries PSBDRO - angled boundaries' angle from X' axis	in. deg
XBDRY(J,I) PSBDRO(J,I)		J = 1, NBX(I) J = 1, NBX(I)	1 50I 2 50I
		If NBY(I) ≠ 0, the following card is required containing:	
YBDRY	Y_{BDRY}	YBDRY - the location of the Y' boundaries	in.
YBDRY(J,I)		J = 1, NBY(I)	n 50I
		where n is the largest sequence number yet supplied. Note: $0 \leq NBX(I) \leq 8$ $0 \leq NBY(I) \leq 8$ No boundary cards need be supplied if boundaries are not required for Table I.	

Following the boundary cards, or card 50I if no boundary cards are used, are the terrain-elevation cards. These cards contain the elevation of the terrain (Z'_G) at each grid point within Table I. NX x NY entries must be supplied, where:

$$NX = [(XE(I)-XB(I))/XINCR(I)] + 1$$
$$NY = [(YE(I)-YB(I))/YINCR(I)] + 1$$

and NX $\leq$ 21, NY $\leq$ 21. Entries are made with the Y' coordinate varying most rapidly and must contain card number 50I in columns 78 through 80 and an increasing sequence number in column 76.

ZGP(1,J)		J = 1,NY	Elevation for y' values at XB(I)	s	50I
ZGP(2,J)		J = 1,NY	Elevation for y' values at XB(I) + XINCR(I)	s	50I
:				:	:
:				:	:
ZGP(NX,J)		J = 1,NY	Elevation for y' grid points at XE(I)	s	50I
1–8	9–16	17–32	33–72	73–76	77–80

where s in column 76 represents the table sequence number, which must increase with each card.

XB(I)	XE(I)	NX(I)	YB(I)	YE(I)	NY(I)	NBX(I)	NBY(I)	1.0	50I
1 2 3 4 5 6 7 8	9 10 11 12 13 14 15 16	17 18 19 20 21 22 23 24	25 26 27 28 29 30 31 32	33 34 35 36 37 38 39 40	41 42 43 44 45 46 47 48	49 50 51 52 53 54 55 56	57 58 59 60 61 62 63 64	65 66 67 68 69 70 71 72	73 74 75 76 77 78 79 80

Program Variable	Analytical Variable	Description	Input Units
		<u>Variable-increment terrain table</u>	
		Note: The variable-increment terrain table number replaces the letter I in the card number. Thus, if the variable-increment table is Table Number 3, it is read on cards 503.	
XB(I)		Initial X' value of terrain Table I	in.
XE(I)		Final X' value of terrain Table I (XE(I) > XB(I))	in.
NX(I)		Number of X' grid points to be supplied	
YB(I)		Initial Y' value of terrain Table I	in.
YE(I)		Final Y' value of terrain Table I (YE(I) > YB(I))	in.
NY(I)		Number of Y' grid points to be supplied	
NBX(I)		Number of angled boundaries for Table I (0 ≤ NBX ≤ 8)	
NBY(I)		Number of Y' boundaries for Table I (0 ≤ NBY ≤ 8)	
		Note: 1.0 must appear in columns 65 through 72.	
		Card 50I contains the control information for terrain Table I. The remainder of the data is contained on cards numbered 50I, with an increasing table sequence number contained in column 76.	
		If NBX(I) ≠ 0, the following two cards are required containing:	
XBDRY PSBDRO	X_{BDRY} ψ_{BDRY}	XBDRY - XB intercept of angled boundaries PSDBDRO - angled boundaries' angle from X' axis	in. deg
XBDRY(J,I) PSBDRO(J,I)		J = 1, NBX(I) J = 1, NBX(I)	1 50I 2 50I
		If NBY(I) ≠ 0, the following card is required containing:	
YBDRY	Y_{BDRY}	YBDRY - the location of the Y' boundaries	in.
YBDRY(J,I)		J = 1, NBY(I)	n 50I
		where n is the largest sequence number yet supplied. Note: 0 ≤ NBX(I) ≤ 8 0 ≤ NBY(I) ≤ 8 No boundary cards need be supplied if boundaries are not required for Table I.	

Following the boundary cards, or card 50I if no boundary cards are used, are the terrain-elevation cards. These cards contain the elevation of the terrain (Z'_G) at each grid point within Table I. NX x NY entries must be supplied, where NX and NY are read in fields 3 and 6 on card 50I and NX $\leq$ 21, NY $\leq$ 21. Entries are made with the Y' coordinate varying most rapidly and must contain card number 50I in columns 78 through 80 and an increasing sequence number in column 76.

ZGP(1,J)		J = 1,NY	Elevation for y' values at XB(I)	s	50I
ZGP(2,J)		J = 1,NY	Elevation for y' values at XXZGP5(2)	s	50I
:				:	:
:				:	:
ZGP(NX,J)		J = 1,NY	Elevation for y' grid points at XE(I)	s	50I

where s in column 76 represents the table sequence number, which must increase with each card.

Following the elevation entries are two tables containing the Y' and X' grid locations for the variable increment table:

YYZGP5(N)		N = 1,NY(I)		s	50I
XXZGP5(N)		N = 1,NX(I)		s	50I

TERRAIN TABLE EXAMPLE

Consider three terrain tables as shown in the sketch:

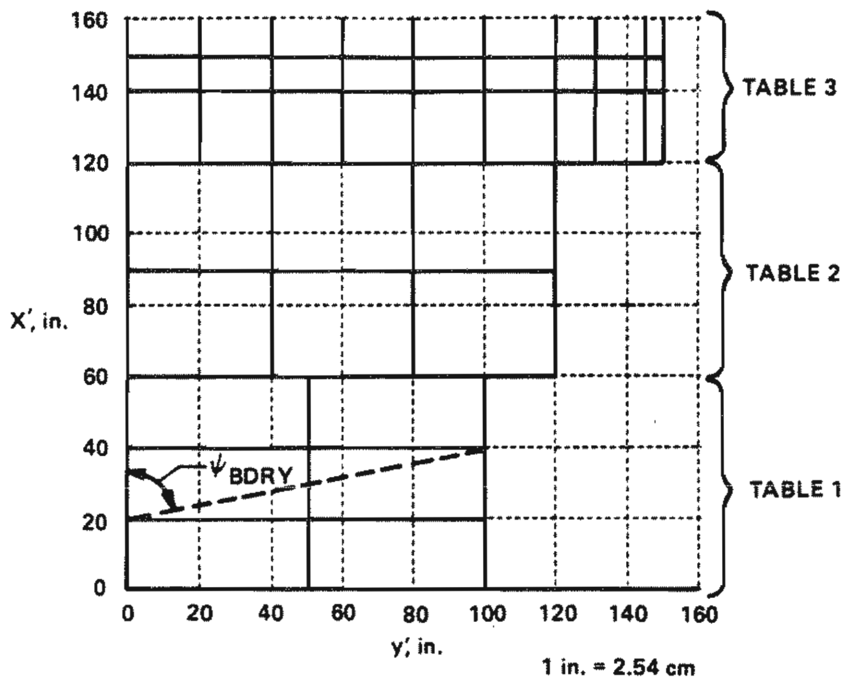

Let table 1 have a X' increment of 20 in. and a Y' increment of 50 in.; let table 2 have an X' increment of 30 in. and a Y' increment of 40 in. Table 3 is a variable-increment table containing elevations at Y' = 0, 20, 40, 60, 80, 100, 120, 130, 145, and 150 in. and X' = 120, 140, 150, and 160 in. Also, let table 1 contain an angled boundary with an X' intercept of 20 in. and ψ_{BDRY} = arctan $(\frac{100}{20})$ = 78.7 degrees.

Let the elevations for each grid point be as given in the following tables:

Table 1

Y', in.

		0.0	50.0	100.0
X', in.	0.0	0.0	0.0	0.0
	20.0	1.0	2.0	1.0
	40.0	2.0	3.0	2.0
	60.0	4.0	4.0	4.0

1 in. = 2.54 cm

Table 2

Y', in.

		0.0	40.0	80.0	120.0
X', in.	60.0	4.0	4.0	4.0	4.0
	90.0	4.0	5.0	6.0	4.0
	120.0	3.0	4.0	5.0	5.0

Table 3

Y', in.

		0.0	20.0	40.0	60.0	80.0	100.0	120.0	130.0	145.0	150.0
X', in.	120.0	3.0	3.5	4.0	4.5	5.0	5.0	5.0	6.0	3.0	3.5
	140.0	3.0	3.0	3.5	4.0	4.0	4.5	4.0	3.5	2.5	2.0
	150.0	1.0	2.0	2.0	2.5	2.5	2.5	2.5	2.0	1.0	0.5
	160.0	0.0	0.0	0.0	0.0	0.0	0.0	0.0	0.0	0.0	0.0

0.0	60.0	20.0	0.0	100.0	50.0	1.0	0.0		501
20.0									1 501
78.7									2 501
0.0	0.0	0.0							3 501
1.0	2.0	1.0							4 501
2.0	3.0	2.0							5 501
4.0	4.0	4.0							6 501
60.0	120.0	30.0	0.0	120.0	40.0	0.0	0.0		502
4.0	4.0	4.0	4.0						1 502
4.0	5.0	6.0	4.0						2 502
3.0	4.0	5.0	5.0						3 502
120.0	160.0	4.0	0.0	150.0	10.0	0.0	0.0	1.0	503
3.0	3.5	4.0	4.5	5.0	5.0	5.0	6.0	3.0	1 503
3.5									2 503
3.0	3.0	3.5	4.0	4.0	4.5	4.0	3.5	2.5	3 503
2.0									4 503
1.0	2.0	2.0	2.5	2.5	2.5	2.5	2.0	1.0	5 503
0.5									6 503
0.0	0.0	0.0	0.0	0.0	0.0	0.0	0.0	0.0	7 503
0.0									8 503
0.0	20.0	40.0	60.0	80.0	100.0	120.0	130.0	145.0	9 503
150.0									10 503
120.0	140.0	150.0	160.0						11 503

AMUG(1)	AMUG(2)	AMUG(3)	AMUG(4)	AMUG(5)	ISINK				506

Program Variable	Analytical Variable	Description	Input Units
AMUG(1) AMUG(2) AMUG(3) AMUG(4) AMUG(5)	μ_{a_1} μ_{a_2} μ_{a_3} μ_{a_4} μ_{a_5}	Terrain table friction multipliers. These factors are a multiple of the nominal tire-ground friction coefficient (card 302) that change that value when a tire is within a given terrain table.	--
ISINK		Number of terrain tables for which deformable soil option is in effect ISINK ≤ 5 If ≥ 1, additional card(s) 506 must be supplied. See below.	

J	KC(J)	KPHI(J)	N(J)	PTPLOW	TRB(1)	TRB(2)	TRB(3)	TRB(4)	NSEQ 506

Program Variable	Analytical Variable	Description	Input Units
		<u>Deformable soil terrain table option inputs</u> (must be supplied if ISINK > 0, card 506, field 6)	
J		Terrain table no. for which deformable soil descriptors are to be used	
KC(J)	k_c	Modulus of soil deformation due to cohesive ingredients of soil for Table J	lb/in.$^{N+2}$
KPHI(J)	k_ϕ	Modulus of soil deformation due to frictional ingredients of soil for Table J	lb/in.$^{N+2}$
N(J)	n	Exponent of soil deformation	--
PTPLOW		Pneumatic trail for soil-induced moments	in.
TRB(I)	t_w	Tire tread width for wheel I, where I =: 1 for RF, 2 for LF, 3 for RR, 4 for LR	in.
		Note: KC, KPHI, N are soil constants as defined by Bekker.[17]	
NSEQ		Sequence number, beginning with 1, up to value of ISINK. Enter in column 76	

YCN(1)	YCN(2)	YCN(3)	YCN(4)	YCN(5)	YCN(6)	(YCN(7)	AMUC		507

Program Variable	Analytical Variable	Description	Input Units
		<u>Curb Option Inputs</u> (must be supplied if NCRBSL (card 102, field 3) > 0	
YCN(I)	Y'_{CN}	Lateral positions of first through seventh slope changes defining a curb Note 1: The first and last curb slope definitions are for the terrain preceding and following the curb. The radial-spring tire model is only used on curb faces number I+1 up to NCRBSL-1. Note 2: Only as many curb slope change positions as indicated by NCRBSL need be supplied. Note 3: Terrain table definitions may be used in addition to the curb option. The terrain tables will be ignored only for each tire within one wheel radius of the second and second-last curb-face definition.	in.
AMUC	μ_c	Curb friction coefficient multiplier. This value is a multiple of the nominal tire-ground friction coefficient (card 302) that changes that value when in contact with the curb.	--

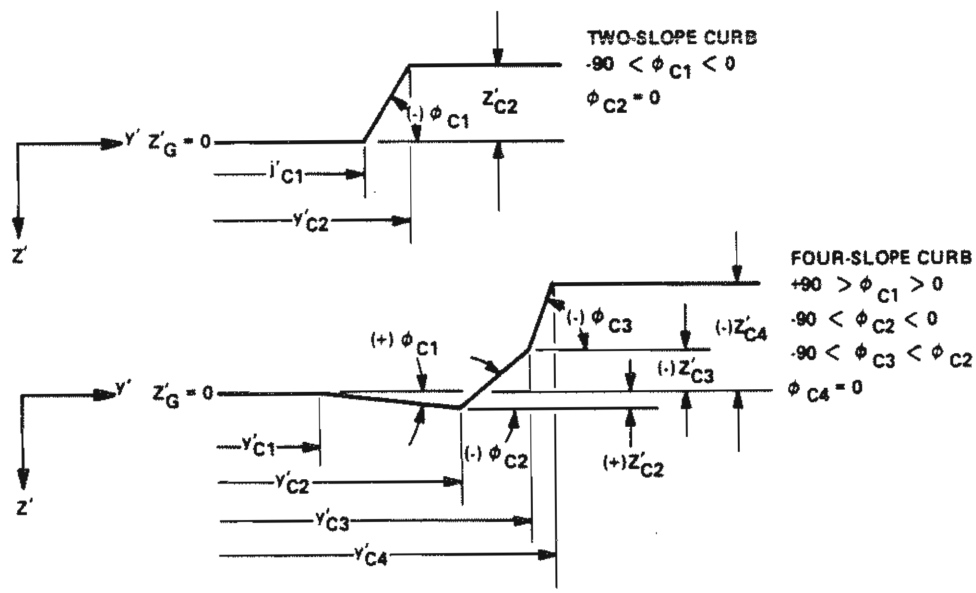

ZCN(1)	ZCN(2)	ZCN(3)	ZCN(4)	ZCN(5)	ZCN(6)	ZCN(7)			508

Program Variable	Analytical Variable	Description	Input Units
ZCN(I)	Z'_{CI}	Curb elevation at YCN(1) through YCN(7), respectively. (See notes on card 507.)	in.

PHICU(1)	PHICU(2)	PHICU(3)	PHICU(4)	PHICU(5)	PHICU(6)	PHICU(7)			509

Program Variable	Analytical Variable	Description	Input Units
PHICU(I)	ϕ_{CI}	First through seventh curb slope angles	deg

XBERO (1,I)	XEERO (1,I)	XBERO (2,I)	XEERO (2,I)	XBERO (3,I)	XEERO (3,I)	XBERO (4,I)	XEERO (4,I)	I	NSEQ 514

Program Variable	Analytical Variable	Description	Input Units
		Terrain table angled-boundary specification	
XBERO(J,I)		Beginning of X range for angled boundary J, terrain Table I	in.
XEERO(J,I)		Ending of X range for angled boundary J, terrain Table I	in.
		where $1 \leq J \leq 8$ $1 \leq I \leq 5$	
I		No. of terrain table containing boundaries	
NSEQ		Card sequence No.: $0 \leq NSEQ \leq 9$	

YBERO (1,I)	YEERO (1,I)	YBERO (2,I)	YEERO (2,I)	YBERO (3,I)	YEERO (3,I)	YBERO (4,I)	YEERO (4,I)	I	NSEQ 515

Program Variable	Analytical Variable	Description	Input Units
		Terrain table angled-boundary specification	
YBERO(J,I)		Beginning of Y range for angled boundary J, terrain Table I	in.
YEERO(J,I)		Ending of Y range for angled boundary J, terrain Table I	in.
		where $1 \leq J \leq 8$ $1 \leq I \leq 5$	
I		No. of terrain table containing boundaries	
NSEQ		Card sequence No.: $0 \leq NSEQ \leq 9$	
		Note: Either or both cards 514 and 515 may be used.	

NSW	DIWS	DIWI	ISWOPT	DUM(1)	DUM(2)	DUM(3)	IADDT	DUM(4)	516

Program Variable	Analytical Variable	Description	Input Units
		Tire-sidewall contact model option inputs (ISWOPT)	
NSW		Number of sidewall springs per radial vector (maximum of 6)	
DIWS		Radial-spring sweep extent (default = 104 degrees)	deg
DIWI		Radial-spring sweep interval (default = 4 degrees)	deg
		Note: DIWS must be a multiple of DIWI.	
ISWOPT		Sidewall contact model option indicator = 0, model not used = 1, option enabled If = 1, sidewall point definition must be supplied on card 517	
DUM(1)		Maximum sidewall-spring-induced moment which can act on front-wheel steering system	lb-in.
DUM(2)		Elevation of top of curb (simple step curb representation), used for additive torque option. This is separate from the multiple slope curb option on cards 507-509.	in.
DUM(3)		Initial elevation of front tire, additive torque option	in.
IADDT		Additive torque option indicator =: 1 for RF, 2 for LF. Permits the simulation of tire sidewall spring/curb scrubbing, where driver model will abandon path following and add torque to front-wheel steering system at DUM(4) rate	
DUM(4)		Percentage of existing torque to be added to front-wheel steering system per sampling time (DPRB, card 405, field 2 for VTPF option)	%

ZSW(I)	YSW(I)	SWKST(I)	WSIGT(I)	SWMU(I)					N 517

Program Variable	Analytical Variable	Description	Input Units
		<u>Tire-sidewall contact model option inputs (ISWOPT)</u>	
ZSW(I)		Tire radius at which sidewall spring is located on each radial vector for spring I	in.
YSW(I)		Distance from wheel centerline to sidewall point I	in.
SWKST(I)		Sidewall point I load deflection rate	lb/in.
WSIGT(I)		Sidewall point I deflection at which saturation occurs	in.
SWMU(I)		Sidewall point I friction coefficient multiplier	--
N		Card sequence number, beginning with 0 in column 76.	
		Note: This card represents the first set of tire sidewall point definitions. If NSW >1 (card 516, field 1), additional cards must be supplied with the same format as this card except that the sequence number must be increased by one for each additional card.	

INITIAL	CONDITION	DESCRIPTION	TITLE						600

Program Variable	Analytical Variable	Description	Input Units
SHED	-	INITIAL CONDITION TITLE This card may contain up to 72 characters of alphanumeric information describing the initial conditions for the run. Note that only the first 40 characters are printed on each output page.	-

PHIO	THETAO	PSIO	PO	QO	RO	PSIFIO	PHIFDO		601

Program Variable	Analytical Variable	Description	Input Units
PHIO	ϕ_O	Initial vehicle vehicle roll angle (Euler angles*)	deg
THETAO	θ_O	Initial vehicle pitch angle (Euler angles*)	deg
PSIO	ψ_O	Initial vehicle yaw angle (Euler angles*)	deg
PO	P_O	Initial vehicle angular velocity about X axis	deg/s
QO	Q_O	Initial vehicle angular velocity about Y axis	deg/s
RO	R_O	Initial vehicle angular velocity about Z axis	deg/s
PSIFIO	ψ_{fO}	Initial front-wheel steer angle	deg
PSIFDO	$\dot{\psi}_{fO}$	Initial front-wheel steer angular velocity	deg/s
		*Rotation sequence is yaw, pitch, roll	

XCOP	YCOP	ZCOP	UO	VO	WO				602

Program Variable	Analytical Variable	Description	Input Units
XCOP	X'_{co}	Initial X' coordinate of sprung-mass C.G. from space axes	in.
YCOP	Y'_{co}	Initial Y' coordinate of sprung-mass C.G. from space axes	in.
ZCOP	Z'_{co}	Initial Z' coordinate of sprung-mass C.G. from space axes	in.
UO	U_o	Initial longitudinal velocity of vehicle C.G. (along vehicle X axis)	in./s
VO	V_o	Initial lateral velocity of vehicle C.G. (along vehicle Y axis)	in./s
WO	W_o	Initial vertical velocity of vehicle C.G. (along vehicle Z axis)	in./s

DEL10	DEL20	DEL30	PHIRO	DEL10D	DEL20D	DEL30D	PHIROD		603

Program Variable	Analytical Variable	Description	Input Units
DEL10	δ_{10}	Initial RF-wheel displacement from equilibrium	in.
DEL20	δ_{20}	Initial LF-wheel displacement from equilibrium	in.
DEL30	δ_{30}	Initial rear roll-center displacement from equilibrum	in.
PHIRO	ϕ_{R_o}	Initial rear-axle roll angle with respect to vehicle	deg
DEL10D	$\dot{\delta}_{10}$	Initial RF-wheel deflection velocity	in./s
DEL20D	$\dot{\delta}_{20}$	Initial LF-wheel deflection velocity	in./s
DEL30D	$\dot{\delta}_{30}$	Initial rear roll-center displacement velocity	in./s
PHIROD	$\dot{\phi}_{R_o}$	Initial rear-axle roll angular velocity	deg/s
		Note: This form of card 603 is used only when ISUS = 0.	

DEL10	DEL20	DEL30	DEL40	DEL10D	DEL20D	DEL30D	DEL40D		603

Program Variable	Analytical Variable	Description	Input Units
DEL10	δ_{10}	Initial RF-wheel displacement from equilibrium	in.
DEL20	δ_{20}	Initial LF-wheel displacement from equilibrium	in.
DEL30	δ_{30}	Initial RR-wheel displacement from equilibrium	in.
DEL40	δ_{40}	Initial LR-wheel displacement from equilibrium	in.
DEL10D	$\dot{\delta}_{10}$	Initial RF-wheel deflection velocity	in./s
DEL20D	$\dot{\delta}_{20}$	Initial LF-wheel deflection velocity	in./s
DEL30D	$\dot{\delta}_{30}$	Initial RR-wheel deflection velocity	in./s
DEL40D	$\dot{\delta}_{40}$	Initial LR-wheel deflection velocity	in./s
		Note: This form of card 603 is used only when ISUS = 1.	

DEL10	PHIFO	DEL30	PHIRO	DEL10D	PHIFOD	DEL30D	PHIROD		603

Program Variable	Analytical Variable	Description	Input Units
DEL10	δ_{10}	Initial front roll-center displacement from equilibrium	in.
PHIFO	ϕ_{F_0}	Initial front-axle roll angle relative to vehicle	deg
DEL30	δ_{30}	Initial rear roll-center displacement from equilibrium	in.
PHIRO	ϕ_{R_0}	Initial rear-axle roll angle relative to vehicle	deg
DEL10D	$\dot{\delta}_{10}$	Initial front roll-center deflection velocity	in./s
PHIFOD	$\dot{\phi}_{F_0}$	Initial front-axle angular velocity	deg/s
DEL30D	$\dot{\delta}_{30}$	Initial rear roll-center deflection velocity	in/s
PHIROD	$\dot{\phi}_{R_0}$	Initial rear-axle angular velocity	deg/s
		Note: This form of card 603 is used only when ISUS = 2.	

									9999

Program Variable	Analytical Variable	Description	Input Units
		This card signifies the end of a data set and must be supplied.	

Appendix C

FUNCTIONAL DESCRIPTION OF HVOSM EXTENSIONS

SCOPE

This appendix provides a functional description of the additions and modifications contained in this version of HVOSM. For the new options (deformable-soil model and sprung-mass ground contact model), a full description of input, intermediate, and output program variables is given. For existing routines that have been modified or extended, the input program variables and, where applicable, the output program variables are defined. All input program variables have the input card number and the location on that card listed next to them. Wherever it exists, the analytical variable (symbology) representing a program variable is also given.

DEFORMABLE SOIL-MODEL

The vehicle response due to one or more wheels leaving the pavement and sinking into soft soil is simulated by the deformable-soil model option in subroutine SINKF. Subroutine SINKF is called by subroutine TIRFRC (tire force).

Inputs for the deformable-soil model are entered on the 506 card series. Entry of ISINK ≥ 1 on card 506 and the inclusion of additional 506 cards (one for each terrain table with soft soil) are necessary to enable the deformable-soil model. The input variables, intermediate variables, and output variables for the deformable-soil model are described in Table 49, Table 50, and Table 51, respectively.

Table 49. Input variables for deformable-soil model.

Program variable	Analytical variable	Card	Field	Description	Units
AMUG(J)	μ_a	506	1-5	Terrain-table friction multipliers	-
ISINK		506	6	Number of terrain tables for which deformable-soil model is in effect	-
	If ISINK ≥ 1, values for the following input variables must be supplied on ISINK number of supplementary 506 cards				
J	j	506	1	Terrain-table number for which deformable-soil model is in effect	-
KC(J)	K_c	506	2	Modulus of soil deformation due to cohesive components of the soil for table J	$lb/in.^{N+2}$
KPHI(J)	K_ϕ	506	3	Modulus of soil deformation due to frictional components of the soil for table J	$lb/in.^{N+2}$
N(J)	n	506	4	Exponent of the soil deformation	-
PTPLOW		506	5	Pneumatic trail for soil-induced moments	in.
TRB(I)	t_w	506	6	Tire tread width for wheel I	in.

Values for K_c, K_ϕ, and n for different types of soils are given by Bekker.[17]

Table 50. Intermediate variables for deformable-soil model.

Program variable	Analytical variable	Description	Units
I	i	Tire number	
FRCP(I)	F'_{R_i}	Tire force perpendicular to the tire/terrain-contact plane.	lb
HI(I)	h_i	Tire rolling radius	in.
SLPANG(I)	α_i	Tire I sideslip angle	rad
VG(I)	v_{G_i}	Contact-point lateral velocity in the direction parallel to the tire/terrain-contact plane	in./s
UG(I)	u_{G_i}	Wheel center forward velocity in the direction parallel to the tire/terrain-contact plane	in./s
PSIIP(I)	ψ'_i	Steer angle of wheels in tire/terrain-contact plane	rad
RW	R_w	Undeflected tire radius	in.
[HI(I)-ZSINK(I)]	δ_Z	Tire deflection	in.
THET1	θ_Z	One-half the angle subtended by the chord Z	rad
THET2	θ_{δ_Z}	One-half the angle subtended by the chord δ_Z	rad
AS	A_s	Area of tire side in contact with soil	in.^{2}
AF	A_f	Front area of tire in contact with soil	in.^{2}
AP	A_p	Projected tire/soil-interface area for a sideslipping tire	in.^{2}
MR(I)	F_{MR_i}	Motion-resistance force	lb
FS(I)	F_{S_i}	Tire side force in plane of the tire/terrain-contact patch perpendicular to the line of intersection of the wheel plane and the ground plane.	lb

Table 51. Output variables for deformable-soil model.

Program variable	Analytical variable	Description	Units
ZSINK(I)	z_i	Tire sinkage for wheel I	in.
FPLOWX(I)	$F_{PLOW_{x_i}}$	Tire circumferential plow force for wheel I	lb
FPLOWY(I)	$F_{PLOW_{y_i}}$	Tire side plow force for wheel I	lb

SPRUNG-MASS GROUND CONTACT MODEL

The sprung-mass ground contact model (contact-point) option is incorporated into subroutine SFORCE (sprung-mass impact force) to allow the vehicle sprung mass to react to contacts with the local terrain. The resultant moments and friction forces at each body point are computed in subroutine RESFRC.

Inputs for this model are supplied on cards 102, 215, 216, and 217. Inclusion of cards 215 and 216 and an entry of NHARPT > 0 (card 215) are required to call the sprung-mass ground contact model into effect.

The input variables, intermediate variables, and output variables for the sprung-mass ground contact model are described in Table 52, Table 53, and Table 54, respectively.

Table 52. Input variables for sprung-mass ground contact model.

Program variable	Analytical variable	Card	Field	Description	Units
DELTB		102	6	Vehicle integration time step for use during point/ground contacts	s
NHARPT		215	1	Number of structural omnidirectional points, maximum of 39	-
EPSHP	ϵ_{HP}	215	2	Friction null band of point/ground contact point calculations	in./s
AMUGHP	μ_{HP}	215	3	Nominal point/ground friction coefficient. Note: The effective coefficient is the product of μ_{HP} and AMUG for the terrain (see card 506).	-
INDKST		215	4	Indicator for constant stiffness for all points If INDKST = 1, all points have same stiffness If INDKST = 0, the stiffness for each point must be input on card(s) 217	-
AKCNST		215	5	Constant omnidirectional stiffness of vehicle structural points, must be input if INDKST = 1	lb/in.
PHIHP	ϕ_{HP}	215	6	Roll or pitch angle at which point option calculators are to begin, input positive, test is made on absolute value.	deg
XSTIO(I)	$x_{ST_{i_o}}$	216	1	X, Y, and Z positions of vehicle structural points with respect to vehicle axis system. Input three sets per card up to a maximum of NHARPT.	in.
YSTIO(I)		216	2		
ZSTIO(I)		216	3		
XSTIO(I+1)		216	4		
YSTIO(I+1)	$y_{ST_{i_o}}$	216	5		
ZSTIO(I+1)		216	6		
XSTIO(I+2)		216	7		
YSTIO(I+2)		216	8		
ZSTIO(I+2)	$z_{ST_{I_o}}$	216	9		
AKST(I)	K_{ST_i}	217	1	Omnidirectional stiffness for each individual point, must be input if INDKST = 0. Six values per card up to a maximum of NHARPT.	lb/in.
AKST(I+1)		217	2		
AKST(I+2)		217	3		
AKST(I+3)		217	4		
AKST(I+4)		217	5		
AKST(I+5)		217	6		

Table 53. Intermediate variables for sprung-mass ground contact model.

Program variable	Analytical variable	Description	Units
XSTI YSTI ZSTI	X_{ST_i} Y_{ST_i} Z_{ST_i}	Vehicle-fixed locations of deflected points calculated in SFORCE	in.
XSTIP YSTIP ZSTIP	$X_{ST_{i}P}$ $Y_{ST_{i}P}$ $Z_{ST_{i}P}$	Spaced-fixed locations of deflected points in ground plane, calculated in SFORCE	in.
XSTIPO YSTIPO ZSTIPO	X_{HP_i} Y_{HP_i} Z_{HP_i}	Space-fixed locations of undeflected points, calculated in SFORCE	in.
FNSTI	F_{NST_i}	Point force normal to local terrain	lb
INDHPT	-	Point option indicator set in BLK02 if input card 215 is supplied	-
INITHP	-	Point initialization flag set equal to 0 in BLK02, equals 1 in SFORCE after initialization	-
FRICF		Resultant friction force for each point calculated in RESFRC	lb
UPT VPT WPT	U'_{ST_i} V'_{ST_i} W'_{ST_i}	Velocity components of the points in space-fixed axes	in./s
ZAPGHP(40)	Z_{GHP_i}	Elevation of terrain at point location, calculated in INTRP5 on a call from SFORCE	in.
THGIHP(40)	θ_{GHP_i}	Pitch angle of terrain at point location, calculated in INTRP5 on a call from SFORCE	rad
PHGIHP(40)	ϕ_{GHP_i}	Camber angle of terrain at point location, calculated in INTRP5 on a call from SFORCE	rad
XMUGHP(40)	μ_{GHP_i}	Resultant friction coefficient of point, calculated in INTRP5 on a call from SFORCE	-

Table 54. Output variables for sprung-mass ground contact model.

Program variable	Analytical variable	Description	Units
DEFHP(I)	$\left(\delta_{HP_i}\right)_{max}$	Point/ground-contact-induced deflection	in.
SFXS SFYS SFZS	ΣF_{XS} ΣF_{YS} ΣF_{ZS}	X, Y, and Z resultant forces of point/ground contact in vehicle-fixed axis system	lb
SNPS SNTS SNPSS	$\Sigma N_{\phi S}$ $\Sigma N_{\theta S}$ $\Sigma N_{\psi S}$	Roll, pitch, and yaw moments resulting from point/ground contact forces in vehicle-fixed coordinate system	lb-in.
FXPSUM FYPSUM FZPSUM	ΣF_{XP} ΣF_{YP} ΣF_{ZP}	X, Y, and Z resultant forces of point/ground contact in space-fixed axis system	lb

TIRE MODEL

The modifications to the HVOSM tire model involving energy dissipation for large radial deflections, normal-load calculation, and side-force saturation for overloaded tires did not result in changes in the tire input or output variables. For a description of tire input information, refer to the charts for cards 300 through 302 in Appendix B.

TIRE-SIDEWALL CONTACT MODEL

A tire sidewall in contact with the curb is modeled in subroutine CRBIMP (curb impact). To initiate the tire-sidewall contact model option, NSW (card 516) must not equal 0, and card(s) 517 (providing tire-sidewall information) must be supplied. Since this option serves to calculate the forces and moments on each wheel that are added to the existing summations in subroutines TIRFRC, UMOMNT, and DAUX, there are no direct output variables.

The variable-torque path-following (VTPF) option up to this point in time has been used only in conjunction with the tire-sidewall contact model to provide driver control during a tire/curb-scrubbing situation. Since the VTPF requires driver-model inputs, the input variable description for this option is included in the subsection entitled Driver Model in this appendix.

The input variables for the tire-sidewall contact model are described in Table 55.

Table 55. Input variables for tire-sidewall contact model.

Program variable	Analytical variable	Card	Field	Description	Units
NSW		516	1	Number of sidewall springs per radial vector (maximum of 6)	
DIWS		516	2	Radial-spring sweep extent (default = 104 degrees)	deg
DIWI		516	3	Radial-spring sweep interval (default = 4 degrees) Note: DIWS must be a multiple of DIWI.	deg
ISWOPT		516	4	Sidewall spring option indicator = 0 option not in effect = 1 option in effect	
DUM(1)		516	5	Maximum sidewall spring-induced moment which can act on front-wheel steering system	lb-in.
DUM(2)		516	6	Elevation of top of curb	in.
DUM(3)		516	7	Initial elevation of front tire	in.
IADDT		516	8	Additive torque option indicator =: 1 for RF, 2 for LF. Permits simulation of tire sidewall spring/curb scrubbing where driver model will abandon path-following mode and add torque to front-wheel steering system at DUM(4) rate.	
DUM(4)		516	9	Percentage of existing torque to be added to front-wheel steering system per sampling time (DPRB, card 405, field 2)	%
ZSW(I)		517	1	Tire radius at which sidewall spring is located for each radial vector for spring I	in.
YSW(I)		517	2	Distance from wheel centerline to sidewall point I	in.
SWKST(I)		517	3	Sidewall point I load deflection rate	lb/in.
WSIGT(I)		517	4	Sidewall point I deflection at which saturation occurs	in.
SWMU(I)		517	5	Sidewall point I friction coefficient multiplier	
N		517	10	Card sequence number, beginning with 0. Note: This card represents the first set of tire sidewall point definition. If NSW > 1, additional cards must be supplied with the same format as this card, except that the sequence number must be increased by one for each additional card.	

DRIVER MODEL

General Discussion

Inputs for vehicle control are entered on the 400 series cards. A driver model has been added that includes a neuro-muscular filter, an emergency-maneuver option for the driver, a path-generating option, a "wagon-tongue" steer option, and a variable-torque path-following option. It is noted that the variable-torque path-following (VTPF) option must be selected in conjunction with the wagon-tongue steer control algorithm; that is, IWAGN = 1 (card 402, field 2) and the alternate definition of card 405 are used. The inputs for the wagon-tongue steer control option are then derived from the VTPF inputs.

Along with the driver-model enhancements, calculation and output of additional data related to the vehicle response were added to subroutine OUTPUT. These are (a) a discomfort factor indicating the net lateral acceleration felt by vehicle occupants and (b) a friction-demand factor indicating the friction demand of each tire.

"Discomfort Factor"

The lateral-acceleration output of HVOSM corresponds to measurements made with a "hard-mounted," or body-fixed, accelerometer oriented laterally on the vehicle. During cornering, the lateral acceleration of the vehicle is directed toward the center of the turn. On a superelevated turn, the component of gravity that acts laterally on the vehicle is also directed toward the turn center. Thus, the lateral-acceleration output is increased by superelevation.

Since the vehicle occupants respond to centrifugal force, their inertial reaction is toward the outside of the turn; therefore, the component of gravity that acts laterally on them in a superelevated turn reduces the magnitude of the disturbance produced by cornering. A corresponding program output has been defined to evaluate occupant discomfort in turns.

The effects of the vehicle roll angle and lateral acceleration on occupants are combined in a discomfort-factor relationship which represents the net lateral disturbance felt by the occupants (i.e., the occupants' reaction to the combined effects of the lateral acceleration and roll angle).

The discomfort factor at the C.G. and at two specified accelerometer positions are calculated in subroutine OUTPUT using these equations:

at C.G.: $CMF_{CG} = -a_{LAT} + \sin \phi'_T$ where ϕ'_T = roll angle
a_{LAT} = lateral acceleration at C.G.

at location 1: $CMF_{A1} = -a_{y_1} + \sin \phi'_T$ where a_{y_1} = lateral acceleration at location 1

at location 2: $CMF_{A2} = -a_{y_2} + \sin \phi'_T$ where a_{y_2} = lateral acceleration at location 2

Friction Demand

The friction demand is defined as the ratio of the side force to the normal load of an individual tire. It is indicative of the friction being utilized by each individual tire. The standard outputs of HVOSM include the side force and normal force for each tire. Coding changes to calculate and print out the friction demand of each tire at each interval of time using the equation

$$ZUDMD_i = F_{S_i}/F'_{R_i}$$

were incorporated into subroutine OUTPUT.

Input Variables

Input variables for the basic driver model are described in Table 56. Input variables for the driver emergency-maneuver option are described in Table 57. Input variables for the model's path-generating option and wagon-tongue steer option are described in Table 58 and Table 59, respectively. Input variables for the variable-torque path-following option are described in Table 60.

Table 56. Input variables for driver model.

Program variable	Analytical variable	Card	Field	Description	Units
IPATH		402	1	Driver-model path-generating option indicator = 0, no path data to be supplied = 1, user will supply path data on card 403, 404	-
IWAGN		402	2	Driver-model wagon-tongue steer option indicator = 0, no wagon tongue steer data to be used = 1, wagon-tongue steer data to be supplied on card 405 = -1, DRIV2 emergency steer response model option, additional card 402 required	
IFILT		402	3	Driver model neuro-muscular filter option indicator = 0, no filter data to be supplied = 1, filter data to be supplied on card 402	
				Driver model filter inputs as follows:	
TIL		402	4	Time constant lag of neuro-muscular filter	s
TI		402	5	Time lead of neuro-muscular filter	s
TAUF		402	6	Net time delay of neuro-muscular filter	s
ITDOPT		402	7	Variable-torque path-following option indicator, set = 1.0 for VTPF Note: Option inputs on card 405.	

Table 57. Input variables for driver emergency-maneuver option.

Program variable	Analytical variable	Card	Field	Description	Units
				(Card 402 must be supplied if IWAGN = -1)	
PSIA	ψ_F	402	1	Initial front-wheel steer angle	deg
PSIDM*	$\dot{\psi}_{F_{max}}$	402	2	Maximum front-wheel steer velocity	deg/s
PSIDDM*	$\ddot{\psi}_{F_{max}}$	402	3	Maximum front-wheel steer acceleration and deceleration	deg/s^2
TPRB		402	4	Time at which driver emergency-maneuver control algorithm is to begin	s
PMAX**		402	5	Maximum driver discomfort level at which deceleration of steering system is to begin	g's
PSIMAX		402	6	Maximum front-wheel steer angle, input as positive value	deg
				After TPRB seconds have elapsed in the simulation run, DRIV2 accelerates the front-wheel steer velocity to PSIDM.	
				The velocity remains at PSIDM until either (1) comfort factor exceeds PMAX or (2) front-wheel steer angle exceeds PSIMAX. If either (1) or (2) is true, front-wheel steer displacement velocity is decelerated back to zero.	
				*Note: Algebraic sign of these variables determines the direction of initial response.	
				**Note: For accel limit to work, must set NPAGE(17) = 1 (i.e., card 104, field 8)	
				Also: PMAX = -SIGN(PSIDM) * ABS(PMAX)	

Table 58. Input variables for driver-model path-generating option.

Program variable	Analytical variable	Card	Field	Description	Units
				(Card 403 must be supplied if IPATH = 1)	
KLI		403	1	Number of curvature descriptors to follow on card(s) 404, maximum of 8	--
NPTS		403	2	Number of points to be generated from path descriptors, maximum of 100	--
XINIT		403	3	Initial X' space-fixed coordinate of path	in.
YINIT		403	4	Initial Y' space-fixed coordinate of path	in.
PSA		403	5	Initial path heading with respect to space-fixed coordinate axes	rad
DELL		403	6	Distance between generated path points	in.
				Driver-model path-generator path descriptors (must be supplied if KLI > 0)	
DI(I)		404	1,3, 5,7	Degree of curvature of path	deg
RLI(I)		404	2,4, 6,8	Distance along path at which degree of curvature is effective	in.
				Note: A constant and/or spiral path may be generated by the use of DI(I) and RLI(I). RLI(I) should be a multiple of DELL. If DI(I) does not equal DI(I+1), the curvature will be spiraled between the two descriptors.	
N				Sequence No., initial value 0	

Table 59. Input variables for driver-model wagon-tongue steer option.

Program variable	Analytical variable	Card	Field	Description	Units
				(Card 405 must be supplied if IWAGN = 1 (card 402, field 2))	
TPRB		405	1	Initial probe sample time	s
DPRB		405	2	Time between probe samples	s
PLGTH		405	3	Length of probe from vehicle C.G. extending along vehicle-fixed longitudinal (X) axis	in.
PMIN		405	4	Error correction null band. If error of probe from path is ≤ PMIN, no corrective steer will be applied.	in.
PMAX		405	5	Maximum acceptable comfort factor above which driver model will only reduce front-wheel steer angle.	g's
PSIFD		405	6	Maximum front-wheel steer velocity. Corrective steer response will be limited to ≤ PSIFD	deg/s
PGAIN		405	7	Steer correction factor. Error is multiplied by PGAIN to determine corrective steer.	rad/in.
QGAIN		405	8	Steer velocity damping term. Limits velocity with which front-wheel steer angle can change.	rad-s/in.
				Note: If ITDOPT = 1 (card 402, field 7), see alternate definition of card 405 inputs on following page.	

Table 60. Input variables for variable-torque path-following option.

Program variable	Analytical variable	Card	Field	Description	Units
				Variable-torque path-following (VTPF) option inputs (must be supplied if ITDOPT = 1 (card 402, field 7))	
TPRB		405	1	Initial probe sample time	s
DPRB		405	2	Time between probe samples	s
PLGTH		405	3	Length of probe from vehicle C.G. extending along vehicle-fixed longitudinal (X) axis	in.
PMIN		405	4	Error correction null band. If error of probe from desired path is $\leq$ PMIN, no corrective torque will be applied.	in.
PMAX		405	5	Maximum acceptable driver discomfort factor above which driver model will only reduce front-wheel steering torque	g's
KTQR1		405	6	Torque correction factor. Error is multiplied by KTQR1 to determine corrective torque applied to front-wheel steering system	lb-in./in.
KTQR2		405	7	Torque correction damping factor. Limits resultant change in corrective torque applied to front-wheel steering system	lb-in.-s/in.
TMAX		405	8	Maximum corrective torque which can be applied to front-wheel steering system	lb-in.
TDPS10		405	9	Initial corrective torque to be applied to front-wheel steering system	lb-in

TERRAIN-TABLE ANGLED BOUNDARY SPECIFICATION

The terrain-table angled boundary option was modified to allow for the specification of up to eight angled boundaries for each terrain table. The user now has control over the X'- and Y'-ranges in which a specific angled boundary occurs. This revision was designed to use the angled boundaries to approximate a curved boundary (such as the separation of a roadway curve from the shoulder) within a terrain table.

The inclusion of card 514 initiates the X'-range angled boundary option. An entry of NBX > 0 (card 50I where I = no. of terrain table) and the completion of cards 1 50I and 2 50I must also be made to define the number of boundaries per table and the angle of each boundary. The Y'-angled boundaries may or may not be specified along with the X'-angled boundaries; they are not required. If selected, the Y'-angled boundary range information is input on card 515. The number of Y'-boundaries and the location of the Y'-boundaries are supplied in the 50I series cards. Separate boundary specifications must be made for each terrain table that contains one or more angled boundaries. The above-mentioned cards may be omitted for tables that do not contain angled boundaries.

Input variables for terrain-table angled boundary specification are described in Table 61.

Table 61. Input variables for terrain-table angled boundary specification.

Program variable	Analytical variable	Card	Field	Description	Units
XBERO(N,I)		514	1,3,5,7	Beginning of X'-range for angled boundary	in.
XEERO(N,I)		514	2,4,6,8	Ending of X'-range for angled boundary	in.
				Note: XEERO > XBERO	
				N = no. of angled boundary $N \leq 8$ I = no. of terrain table $I \leq 5$	
				i.e., maximum of five terrain tables with eight angled boundaries each	
I		514	9	No. of terrain table containing boundary	
NSEQ		514	10	Card sequence no.	
YBERO(N,I)		515	1,3,5,7	Beginning of Y'-range for angled boundary	in.
YEERO(N,I)		515	2,4,6,8	Ending of Y'-range for angled boundary	in.
I		515	9	No. of terrain table containing boundary	
NSEQ		515	10	Card sequence no.	
				Note: YEERO > YBERO	

REFERENCES

1. "1975 Model Year Passenger Car and Truck Accident Investigations Manual," Motor Vehicle Manufacturers Association of the United States, Inc.

2. Evans, Leonard, "Accident Involvement Rate and Car Size," General Motors Research Laboratories, Report No. GMR-4453, August 1, 1983.

3. Huelke, Donald F., Marsh, Joseph C., and Sherman, Harold W., "Analysis of Rollover Factors and Injury Causation," in Proceedings of the 16th Conference of the American Association for Automotive Medicine, October 1972.

4. McGuigan, R. and Bondy, N., "A Descriptive Study of Rollover Crashes," National Highway Traffic Safety Administration, unpublished report, July 1980.

5. Reinfurt, D.W., Li, L.K., and Popkin, C.L., "Rollover and Serious Driver Injury Differences Among Utility Vehicles, Pickup Trucks, and Passenger Car Groups," in Proceedings of the 26th Annual Conference of the American Association for Automotive Medicine, October 1982.

6. Snyder, R.G., McDole, T.L., Ladd, W.M., and Minahan, D.J., "On-Road Crash Experience of Utility Vehicles," University of Michigan Highway Safety Research Institute, Report No. UM-HSRI-80-14, February 1980.

7. Perchonok, K., Ranney, T., Baum, S., Morris, D., and Eppich, J., "Hazardous Effects of Highway Features and Roadside Objects," Calspan Field Services, Inc., Report No. ZR-5564-V-2, September 1978.

8. Malliaris, A.C., Nicholson, R.M., Hedlund, J.H., and Scheiner, S.R., "Problems In Crash Avoidance and In Crash Avoidance Research," Society of Automotive Engineers, Inc., Paper No. 830560, March 1983.

9. Wright, P.H. and Zador, P., "A Study of Fatal Rollover Crashes in Georgia," Insurance Institute for Highway Safety, unnumbered report, November 1980.

10. Personal communication from John G. Viner, FHWA Office of Safety and Traffic Operations R&D, 1985, on tentative findings of FHWA staff study 21T1-554, "Clinical Analysis of Roadside Accidents."

11. Mackay, G.M. and Tampen, I.D., "Field Studies of Rollover Performance," Society of Automotive Engineers, Inc., Paper No. 700417, 1970.

12. Viner, John G., "Implications of Small Cars on Roadside Safety," in Proceedings of the 27th Annual Conference of the American Association of Automotive Medicine, October 1983.

13. Hall, J.W. and Zador, P., "A Survey of Single Vehicle Fatal Rollover Crash Sites in New Mexico," Insurance Institute for Highway Safety, unnumbered report, November 1980.

14. Klein, R.H., Johnson, W.A., and Szostak, H.T., "Influence of Roadway Disturbances on Vehicle Handling," Volumes 1-3, Systems Technology, Inc., Report Nos. DOT HS-802-210,-211,-212, February 1977.

15. Segal, D.J., "Highway-Vehicle-Object Simulation Model--1976, "Volumes 1 through 4, Report No. FHWA-RD-76-162, -163, -164, and -165, February 1976.

16. Bekker, M.G., Off-the-Road Locomotion, University of Michigan Press, Ann Arbor, MI, 1960.

17. Bekker, M.G., Introduction to Terrain-Vehicle Systems, University of Michigan Press, Ann Arbor, MI, 1969.

18. Radt, H.S. and Milliken, W.F., "Motions of Skidding Automobiles," Society of Automotive Engineers, Inc., Paper No. 205A, June 1960.

19. McHenry, R.R., DeLeys, N.J., and Segal, D.J., "Determination of Physical Criteria for Roadside Energy Conversion Systems," Calspan Corporation, Report No. VJ-2251-V-1, Contract No. CPR-11-3988, July 1967.

20. McHenry, R.R., "An Analysis of the Dynamics of Automobiles During Simultaneous Cornering and Ride Motions," Institute of Mechanical Engineers, Paper No. 3, Symposium--Handling of Vehicles under Emergency Conditions, 1969.

21. McHenry, B.G., "Final Report on the Investigation of Pavement/Shoulder Dropoffs," Contract No. DTFH61-80-C-00146, November 1982.

22. McHenry, R.R., McHenry, B.G., and Glennon, J.C., "Follow-up HVOSM Studies of Highway Curb Impacts," Contract No. DOT-FH-11-9575, March 1981.

23. Olson, R.M. et al., "Effect of Curb Geometry and Location on Vehicle Behavior," Transportation Research Board, National Cooperative Highway Research Program, Report No. 150, Washington, 1974.

24. McHenry, R.R. and Deleys, N.J., "Automotive Dynamics--A Computer Simulation of Three-Dimensional Motions for Use in Studies of Braking Systems and of the Driving Task," Calspan Corporation, Report No. VJ-2251-V-7, Contract No. CPR-11-3988, August 1970.

25. Glennon, J.C., McHenry, B.G., and Neuman, T.R., "HVOSM Studies of Highway Cross Slope Design," Contract No. DOT-FH-11-9575, October 1983.

26. Howerter, E.D., Hinch, J.A., and Owings, R.P., "Sensitivity Analysis of Subcompact Vehicle Performance Due to an Impact with a Breakaway Luminaire Support," ENSCO, Inc., Report No. FHWA-83-02, 15 April 1983.

27. Personal communication from Lloyd E. Carlson, Mobility Systems and Equipment Company, to Charles F. McDevitt of FHWA.

28. Riede, P.M., Leffert, R.L., and Cobb, W.A., "Typical Vehicle Parameters for Dynamic Studies Revised for the 1980's," Society of Automotive Engineers, Inc., Technical Paper No. 840561, March 1984.

29. Ross, Hayes E., Jr. and Post, Edward R., "Comparisons of Full-Scale Embankment Tests With Computer Simulations--Volume 1, Test Results and Comparisons," Texas Transportation Institute, Research Report No. 140-7, December 1972.

30. Stonex, K.A., "Roadside Design for Safety," Paper presented at the 39th Annual Meeting of the Highway Research Board, March 1960.

31. Michie, Jarvis D., "Recommended Procedures for the Safety Performance Evaluation of Highway Appurtenances," National Cooperative Highway Research Program, Report No. 230, March 1981.

32. "Analysis of Investigative Accidents," Southwest Research Institute, Contract No. DOT-FH-11-9523, October 1983.

33. Personal communication from Robert J. Keenan, Johns Hopkins University Applied Research Laboratory, IHVHP computer program input data listing for 1976 Ford LTD vehicle, 25 September 1984.

34. Basso, G.L., "Functional Derivation of Vehicle Parameters for Dynamics Studies," National Research Council Canada, Report No. LTR-ST 747, September 1974.

35. Rasmussen, R.E. et al., "Typical Vehicle Parameters for Dynamics Studies," General Motors Corporation, Report No. A-2542, April 1970.

36. "U.S. and Foreign Passenger Car Specifications, 1973-1982," Motor Vehicle Manufacturers Association.

37. "Guide for Selecting, Locating, and Designing Traffic Barriers," American Association of State Highway and Transportation Officials, 1977.

38. DeLeys, N.J., "Safety Aspects of Roadside Cross-Section Design," Report No. FHWA-RD-75-41, February 1975.

39. Buth, C.E. and Campise, W.L., "Performance Limits of Longitudinal Barrier Systems, Volume IV - Appendix C, Details of Embankment Traversal Tests," Texas Transportation Institute, Contract No. DTFH61-82-C-00051, May 1985.